Durham University

Durham E-Theses

A NEW CLASS OF LUMINESCENT ORGANOMETALLICS -DIETHYNYLRHODACYCLOPENTADIENES

MENG GUAN TAY

How to cite:

TAY, MENG GUAN (2010) A NEW CLASS OF LUMINESCENT ORGANOMETALLICS -DIETHYNYLRHODACYCLOPENTADIENES. Doctoral thesis, Durham University.

Use policy

The full-text may be used and/or reproduced, and given to third parties in any format or medium, without prior permission or charge, for personal research or study, educational, or not-for-profit purposes provided that:

- a full bibliographic reference is made to the original source
- a https://etheses.durham.ac.uk/id/eprint/247/ is made to the metadata record in Durham E-Theses
- the full-text is not changed in any way

The full-text must not be sold in any format or medium without the formal permission of the copyright holders.

Please consult the full Durham E-Theses policy for further details.

Academic Support Office, The Palatine Centre, Durham University, Stockton Road, Durham, DH1 3LE
e-mail: e-theses.admin@durham.ac.uk Tel: +44 0191 334 6107
https://etheses.durham.ac.uk

A NEW CLASS OF LUMINESCENT ORGANOMETALLICS - DIETHYNYLRHODACYCLOPENTADIENES

MENG GUAN TAY

Ph.D THESIS **2010**

Declaration

The work described in this thesis was carried out in the Department of Chemistry at Durham University between August 2006 and September 2009, under the supervision of Prof. Todd B. Marder. All the work is my own, unless otherwise stated, and has not been submitted previously for a degree at this or any other university.

Meng Guan Tay

Statement of Copyright

The copyright of this thesis rests with the author. No quotation from it should be published without prior consent and information derived from it should be acknowledged.

To my wife, daughter and son:
For the love, support and fun they give

Acknowledgements

On the rainy and chilly morning of 21st August 2006, my family and I first arrived in the UK at Newcastle Airport. A gentleman and two of my Malaysian seniors met us at the airport and led us to a fully furnished, nice and tidy house located in Belmont. In the first paragraph of my acknowledgements, I would like to express my most sincere thanks to this gentleman, who is my supervisor, Professor Todd B. Marder. A million thanks for his arrangements upon our arrival in Durham, and of course, for his excellent guidance, support and ideas during my entire Ph.D project.

Also thanks to my second supervisor, Dr. Paul J. Low, for his guidance, support and sharing his knowledge as well as his chemistry techniques in his laboratory.

Thanks to all the members of and visitors to the Marder group, past and present: Dr. Richard Ward, Dr. Kittiya Wongkhan, Andrew Crawford, Nim, Jonathan Barnard, Hazmi Tajuddin, Peter Harrisson, Laura Mackay, Dr. Liu Zhi Qiang, Li Qiang, Liu Chao, Dr. Manolo Romero, Dr. Christian Kleeberg, Dr. Bianca Bitterlich and Dr. Marie-Hélène Thibault for giving me most important and essential advice during the research period. Special thanks to Brian Hall for his work for the group, for his help with the glove box and for providing solvents for us. Also thanks to the research group of Li Qiang and Liu Chao in Wuhan University, China, for supplying us with the "P-Olefin ligand".

I also would like to express my special thanks to two important members in the group, Dr. Jonathan Collings and Dr. Andreas Steffen. Thanks to Dr. Jonathan Collings for teaching me chemistry techniques and helping me to check and edit this thesis. Thanks to Dr. Andreas Steffen for his advice, sharing his knowledge and techniques, helping me to

measure the quantum yields and lifetimes for rhodacyclopentadienes, and the excellent developments that he brought to the project.

I wish to thank to the analytical services and technical support units in the Department of Chemistry, Durham University, especially to the NMR service, Dr. Alan Kenwright, Ian McKeag and Catherine Heffernan; and the elemental analysis service, Judith Magee and Jaroslava Dostal. Thanks to Dr. Andrei S. Batsanov for obtaining the molecular structures in this thesis from the single-crystal X-ray diffraction experiments. Also thanks to Dr. Andrew Beeby for allowing use of the photophysical instruments in his laboratory.

Thanks to my wife, Pei Fen; my daughter, Esther Tay; and my new son, Lewis Tay, for their continual family support. Especially to my lovely wife - I knew how tough it was for you to look after Esther and Lewis during the period when I was writing this thesis. Also thanks to my farther, brothers and sister in Malaysia for the support they give.

Thanks to the two Malaysian seniors who picked us up from Newcastle Airport and took us to the house in Belmont, Dr. Wan Khairul and Dr. Abdul Talib, for your help and friendship. Thanks to the Zulkhairi family (Azila, Fatimah, Luqman and Sumayyah) for help and sharing the wonderful working experience. Thanks to my colleague, Azhar and his wife, Lily, for being Esther's good friends and helping us to look after Esther when my wife was giving birth to Lewis in the hospital. *Ribuan terima kasih kepada anda semua! Persahabatan kita tidak akan tamat selepas ini.* (A thousand thanks to all of you! Our friendship never ends after this.)

Last but not least, thanks to Universiti Malaysia Sarawak (UNIMAS) for the Ph.D scholarship. Thanks to all the people who have given their support and shared their

knowledge that I forgot to mention by name in this section. And also to all the people who read this thesis, thank for your time and comments.

Meng Guan Tay

Publications

2,5-Bis(*p*-R-Arylethynyl)-Rhodacyclopentadienes: Unprecedented Intense Fluorescence Denying the Presence of a Heavy Atom**.**

A. Steffen, M. G. Tay, A. S. Batsanov, J. A. K. Howard, A. Beeby, K. Q. Vuong, X.-Z. Sun, M. W. George and T. B. Marder. *Angew*. *Chem*. *Int*. *Ed*., 2010, **49**, 2349.

The Synthesis of Extended Arylene Ethynylene Butadiynes via the Oxidative Homocoupling of (4-ethynylphenylethynyl)arenes

M. R. Al-Haddad, J. C. Collings, R. M. Ward, M. G. Tay, M. D. Green, W. M. Khairul, P. J. Low, A. S. Batsanov, J. A. K. Howard, A. J. Scott, W. Clegg and T. B. Marder. *in preparation*.

Abstract

The main objective in this project is to develop a greater understanding of the unusual photophysical properties of 2,5-bis(arylethynyl)rhodacyclopentadienes. Three distinct and unusual photophysical properties were found in the 2,5-bis(arylethynyl)-rhodacyclopentadienes: (i) long-lived singlet excited states, from which some of them exhibit high-intensity fluorescence with nanosecond lifetimes; (ii) slow intersystem crossing rates (k_Δ values $\approx 10^8$ s^{-1}) compared to typical luminescent organometallic complexes (with k_Δ values $\approx 10^{12}$ s^{-1}); and (iii) no phosphorescence was observed even at 77 K in a rigid glass. Many photophysical experiments such as e.g. low-temperature lifetime measurments, singlet oxygen sensitisation and time-resolved infrared (TRIR) have been carried out in order to investigate further and explain the unusual photophysical properties of this class of organometallic complexes.

Five different types of ligand X on 2,5-bis(*p*-R-arylethynyl)-X-rhodacyclopentadienes [X = 4-[4-(*N*,*N*-di-*n*-hexylamino)phenylethynyl]phenylethynyl- (DHAPEPE-), trimethyl silylethynyl- (TMSE-), methyl- (Me-), η^2-benzoato- and acetylacetonato- (acac-)] have been synthesised and the photophysical properties of the complexes were investigated. The TMSE-rhodacyclopentadienes gave the highest fluorescence quantum yields compared to the other series of rhodacyclopentadienes. Extended phenylene-ethynylene ligands (i.e. DHAPEPE-) did not impart any effects on the λ_{max} values in absorption and emission but the quantum yields were lower than those for the TMSE-rhodacyclopentadienes. η^2-Benzoato- and acac- ligands shifted the λ_{max} values in absorption and emission to lower energy, which implies that they induce smaller energy gaps between the excited and ground states. The emissions from the η^2-benzoato-

rhodacyclopentadienes were quenched (especially for those with R = H and SMe substituents, which have quantum yields of less than 0.01).

The first example of isomeric biphenyl-rhodacyclopentadiene by-product formation was found in the synthesis of acac-rhodacyclopentadienes. The isomeric biphenyl-rhodacyclopentadiene by-product with R = CO_2Me was isolated and its molecular structure was confirmed by X-ray analysis. Its emission spectrum shows two emission bands with λ_{max} values of 394 and 544 nm in degassed toluene solution. The fluorescent emission at 394 nm has a quantum yield of 0.03, whereas the phosphorescent emission at 544 nm has a quantum yield of 0.05. The unusual long lifetime (237.6 μs) of the phosphorescence at room temperature indicates that the transition is from a ligand-centred (LC) $\pi \rightarrow \pi^*$ transition.

In addition, the syntheses of 1,4-bis(*p*-R-phenyl)buta-1,3-diynes and novel 1,12-bis(*p*-R-phenyl)dodaca-1,3,9,11-tetraynes, which serve as the starting materials for the synthesis of the rhodacyclopentadienes, are also reported. Four novel 1,12-bis(*p*-R-phenyl)dodaca-1,3,9,11-tetraynes (where R = H, SMe, CO_2Me and $BMes_2$) have been synthesised and characterised. The formation of homo-coupling products was a major problem which reduced the yields of the 1,3,9,11-dodacatetraynes. The 1,3,9,11-dodacatetraynes were separated from their respective homo-coupling products using column chromatography, and the yields obtained were 30 – 46%.

Abbreviations

ABS = Absorbance

acac = Acetylacetone

Å = Angstrom

Aryl = Aryl

bpy = Bipyridine

$BMes_2$ = Dimesityl boryl

BPEBs = 1,4-Bis(phenyl ethynyl)benzenes

BPETs = 2,5-Bis(phenyl ethynyl)thiophenes

Bu = Butyl

CO_2Me = Carbomethoxy

COD = 1,5-Cyclooctadiene

COE = Cyclooctene

DHAPEPE = 4-[4-(*N*,*N*-di-*n*-hexyl amino)phenylethynyl]phenylethynyl

DCCI = *N*,*N*'-dicyclohexyl carbodiimide

DMAP = 4-(*N*,*N*-dimethyl amino)pyridine

DMF = Dimethylformamide

DBAs = Dehydrobenzo annulenes

ΔE = Energy gap

EML = Emissive layer

ETL = Electron transport layer

ε = Extinction coefficient

EI = Electron impact ionisation

Et_3N = Triethylamine

EM = Emission

EL = Electroluminescence

EPEDHA = 4-(4-ethynylphenyl ethynyl)-*N*,*N*-di-*n*-hexylaniline

ES = Electrospray

FT-IR = Fourier transform infrared

f_v = Frank-Condon factor

GC-MS = Gas chromatography mass spectroscopy

HTL = Hole transport layer

Hex = Hexyl

HOMO = Highest occupied molecular orbital

HPLC = High performance liquid chromatography

IC = Internal conversion

ISC = Intersystem crossing

*i*Pr = Isopropyl

$[Ir(ppy)_3]$ = Tris(2-phenyl pyridine) iridium

k_{IC} = Rate constant of internal conversion

k_f = Rate constant of fluorescence

k_Δ = Rate constant of intersystem crossing

LUMO = Lowest unoccupied molecular orbital

LCDs = Liquid crystal displays

LC = Ligand-centred

LDA = Lithium diisopropylamide

τ = Lifetime

MLCT = Metal-to-ligand charge transfer

MALDI = Matrix-assisted laser desorption ionisation

Me = Methyl

MC = Metal-centred

NBS = *N*-bromosuccinimide

NMe_2 = Dimethylamino

OMe = Methoxy

$^3O_2$, $O_2(^3\Sigma)$ = Triplet oxygen

$^1O_2$ = Singlet oxygen

OLEDs = Organic light emitting diodes

OAc = Acetate

$[Pt(bpy)_3]^{2+}$ = Tris(bipyridine) platinum$^{(II)}$ dication

PtOEP = 2,3,7,8,12,13,17,18-octaethyl-21H,23H-porphine platinum$^{(II)}$

Ph = Phenyl

phen = 1,10-phenanthroline

"P-olefin ligand" =

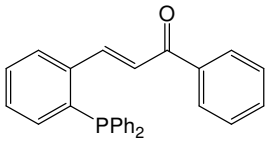

PMe_3 = Trimethylphosphine

PPh_3 = Triphenylphosphine

Φ = Quantum yield

Φ_Δ = Quantum yield of intersystem crossing

$[Rh(phen)_3]^{3+}$ = Tris(1,10-phenanthroline) rhodium$^{(III)}$ trication

$[Rh(bpy)_3]^{3+}$ = Tris(bipyridine) rhodium$^{(III)}$ trication

$[Ru(bpy)_3]^{2+}$ =	Tris(bipyridine) ruthenium$^{(II)}$ dication	TRIR =	Time-resolved infrared
R.T. =	Room temperature	TD-DFT =	Time-dependent Density Functional Theory
SOC =	Spin-orbit coupling		
S_0 =	Ground state	T_1 =	Lowest triplet excited state
S_1 =	Lowest singlet excited state	T_2 =	Second lowest triplet excited state
S_2 =	Second lowest singlet excited state	TBAF =	Tetra-*n*-butyl ammonium fluoride
SMe =	Methylthio	ToF =	Time of flight
$SiMe_3$ =	Trimethylsilyl	TMSA =	Trimethylsilyl acetylene
ToF =	Time of flight	TMSE =	Trimethylsilylethynyl
THF =	Tetrahydrofuran	VR =	Vibrational relaxation

NMR Abbreviations

br =	Broad	NMR =	Nuclear magnetic resonance
d =	Doublet	q =	Quartet
dd =	Doublet of doublets	quint =	Quintet
dt =	Doublet of triplets	s =	Singlet
J =	Coupling constant	t =	Triplet

Table of contents

List of figures

Chapter 1

Chapter 2

Chapter 3

Chapter 4

List of tables

Chapter 1

Chapter 2

Chapter 3

Chapter 1

Introduction

1.1 Molecular photophysics

1.1.1 General terms in photophysical transitions

Luminescence is a process whereby a compound in an excited electronic state returns to its ground state by emission of light. Luminescence can be divided into several different categories depending on how the excited state is formed. Two major processes of interest are: photoluminescence (PL), in which the excited state is formed by absorption of light; and electroluminescence (EL), in which the excitation occurs when an electric field is applied to the material.

A modified Jabłoński diagram which illustrates the photophysical processes in the ground and excited states of a molecule is shown in **Figure 1.1** below.

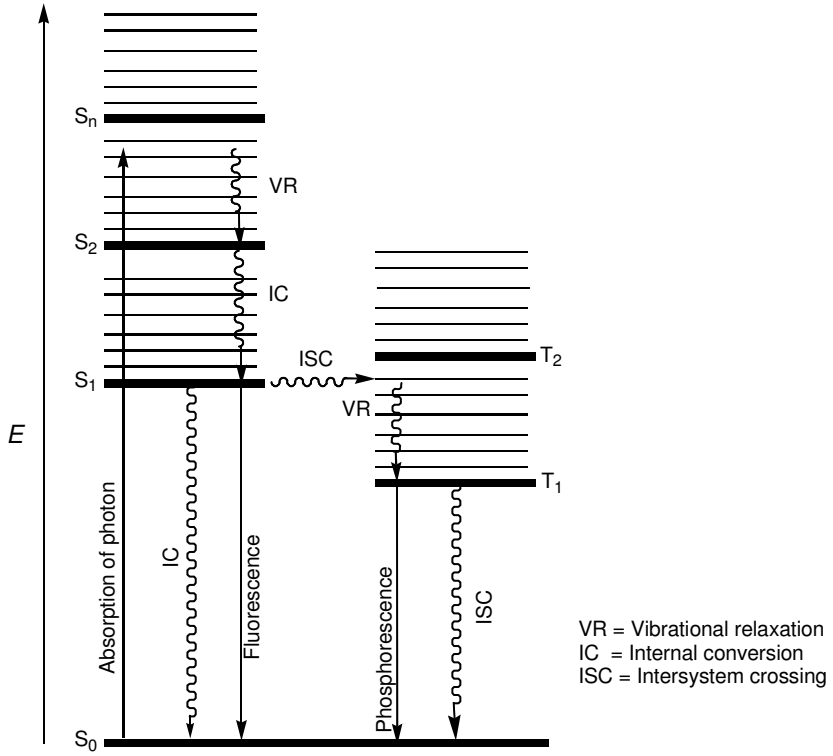

Figure 1.1: Photophysical transitions between electronic states in a single molecule.

The straight arrows in **Figure 1.1** represent various possible radiative transitions, whereas the wavy arrows show the non-radiative transitions between electronic or vibrational states. The singlet ground state is labelled as S_0, and the first, second and higher electronic excited singlet states are represented by S_1, S_2 and S_n, respectively, with n = 3, 4, 5 and so on. A molecule exhibits a singlet state when there is no net electronic spin associated with the state (all of the spins are paired). The triplet states are labelled as T_1 and T_2, where 'T' indicates that there are three possibilities of spin orientation of two unpaired electrons (**Figure 1.2**). The spin multiplicity formula $2S + 1$ gives the number of the states which can arise, where the '*S*' is the total spin quantum number. In the case where all electrons of a molecule are spin-paired, $S = 0$ (because there is no net electronic spin associated with the state), and the spin multiplicity = 1, which represents the singlet state. In contrast, when the molecule has two unpaired spins, $S = 1$, it has to be the spin multiplicity = 3, which implies the triplet state.[1]

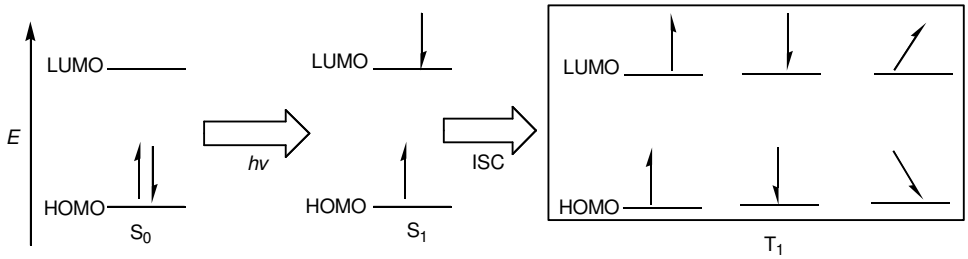

HOMO = Highest occupied molecular orbital; LUMO = Lowest unoccupied molecular orbital

Figure 1.2: General diagram of the electron orientation in the ground (S_0), singlet (S_1) and triplet (T_1) excited states of a molecule for HOMO-LUMO transition.

When a photon is absorbed, the molecule can be excited from the ground state to an energetically higher lying singlet excited state with two spin-paired electrons (**Figure 1.2**). If the molecule is excited to the second singlet excited state ($S_0 \rightarrow S_2$), it rapidly

relaxes to the lowest vibrational level of S_2 via vibrational relaxation (VR). Internal conversion (IC) occurs when the molecule release excess energy from the second singlet excited state to the first singlet excited state ($S_2 \rightarrow S_1$). These processes occur very quickly (10^{-12} s or less) and are generally complete before the emission occurs.[2] Fluorescence results if the molecule returns back to the ground state from the lowest singlet excited state ($S_1 \rightarrow S_0$) by emission of a photon, and fluorescence lifetimes are typically ca. 10^{-9} to 10^{-7} s. Kasha's rule states that the emission generally occurs from the lowest excited state to the ground state.[3] The efficiency of an emission process is measured as the quantum yield, Φ, which is defined as the ratio of photons emitted to photons absorbed of a sample.

Under certain conditions, the molecule in the singlet excited state may undergo a non-radiative process, known as intersystem crossing (ISC), to a triplet state ($S_1 \rightarrow T_1$), in which the molecule has two electrons with parallel spin (**Figure 1.2**). However, in some cases, ISC from higher lying singlet states to higher lying triplet states ($S_n \rightarrow T_n$, where, n = 2, 3, 4 and higher) could also be possible. Similarly, the molecule at the higher vibrational energy levels of T_1 state can release the excess energy via VR to the lowest vibrational energy level of T_1 state. Phosphorescence results if the molecule returns back to the ground state from the lowest T_1 state ($T_1 \rightarrow S_0$). The rate constants for phosphorescence are several orders of magnitude smaller ($10^6 - 10^0$ s^{-1}) than those for fluorescence due to the fact that the transition from T_1 to S_0 is spin-forbidden.[2] As T_1 is often lower in energy than S_1, phosphorescence generally occurs at lower frequency relative to fluorescence.[2]

1.1.2 Non-radiative decay transitions in an excited molecule

Non-radiative decay such as ISC and IC from an excited state to the ground state can significantly reduce the quantum yield of a luminescence process. Typically, non-radiative processes depend on several factors such as the nature of the molecular structure, in particular its molecular rigidity, and the energy gap (ΔE) between the excited states (S_1 or T_1) and S_0.

In general, the more rigid a molecule, the higher is its luminescence efficiency. For example, the Φ_f of the *trans*- (compound **a**) and *cis* (compound **b**) stilbenes are 0.05 and 0.00, respectively. However, the Φ_f of a structurally rigid derivative (compound **c**) is 1.00 (**Figure 1.3**).[4]

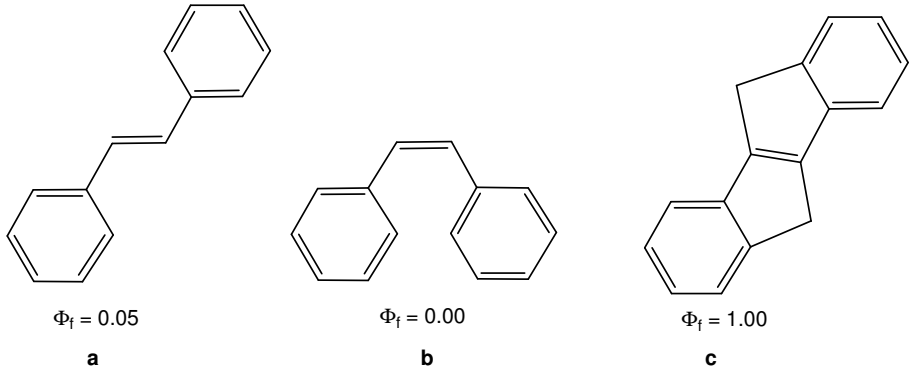

Figure 1.3: Influence of rigidity on the Φ_f in stilbenes.[4]

The non-radiative decay rate constant of an excited molecule can also be estimated by the energy gap law, which expresses the exponential relationship between the non-radiative rate constant of internal conversion (k_{IC}) and the energy gap (ΔE) between the two states (**Eq 1.1**).[4, 5]

$$k_{IC} \sim 10^{13} \exp -\alpha \Delta E \qquad (\mathbf{1.1})$$

where α is a proportionality constant and the 'exp $-\alpha\Delta E$' term is defined as the Frank-Condon factor (f_v), which can determine the overlap between the potential energy curves of two states and the rate of transitions between them. In principle, the overlap between two states is inversely proportional to the ΔE of the two states; the smaller the ΔE, the greater the overlap, consequently, the faster the transitions (i.e. non-radiative decay) between two states. Therefore, **Eq. 1.1** can also be written in the form of **Eq. 1.2**:[4]

$$k_{IC} \sim 10^{13} f_v \qquad (\mathbf{1.2})$$

For a π-conjugated and rigid organic molecule, if ΔE is less than 209 kJ/mol (ca. 2 eV), k_{IC} is about 10^8 s^{-1} or higher, and in this case, the non-radiative process becomes the dominant process, leading to a lower fluorescence quantum yield (Φ_f).[4] For example, the ΔE of S_1 to S_0 for pentacene is about ~209 kJ/mol and the quantum yield of IC (Φ_{IC}) is about 0.75. This is also the reason that non-radiative decay of triplet states occurs very efficiently in aromatic hydrocarbon molecules as the T_1 state is often lower in energy than the S_1 state and k_{IC} becomes dominant.[6]

Furthermore, the largest Frank-Condon factors are usually found in high frequency vibrations.[4] For example, the C-H stretching motion is the highest frequency vibration in an organic molecule; thus, the loss of vibrational energy is expected to be fastest through the C-H vibration mode. Many researchers have studied and calculated the isotope effect by replacing the hydrogen (H) atoms with deuterium (D), which has a lower C-D

vibrational energy (~2200 cm^{-1}). Robinson and Frosch[7] stated that changing benzene to benzene-d_6 can increase Φ_P because there is a large deuterium effect in the benzene case, which can cause the phosphorescence to be more favourable than the non-radiative transition. Another example is naphthalene, which shows an increase in phosphorescence lifetime and quantum yield from ~2 to ~20 sec and from 0.05 to ~0.80, respectively, upon substitution of C-H for C-D.[4]

In general, ISC is always a spin forbidden process. However, ISC in organic molecules can still occur even when a heavy atom such as bromine or iodine is incorporated into the molecule. The probability of ISC increases with increasing atomic number due to greater spin orbit coupling (SOC) effect of the heavy atom.[8] In this context, it is important to note that the rate constant of the ISC from S_1 to T_1 (k_Δ) and the phosphorescence quantum yield (Φ_P) are expected to increase but the Φ_F should decrease. The typical example for demonstrating the heavy atom effect on k_Δ, Φ_F and Φ_P is substituting naphthalene with different halogens as shown in **Table 1.1**.[4] The SOC constants of the respective elements are shown in the last column.[9]

Table 1.1: Summarised data of k_Δ, Φ_F and Φ_P of naphthalene and its halo derivatives,[4] and the SOC constant of the respective element.[9]

Molecule	k_Δ	Φ_F	Φ_P	SOC constant (cm^{-1})
Naphthalene	10^6	0.55	0.05	H = 0.24
1-Fluoronaphthalene	10^6	0.84	0.06	F = 269
1-Chloronaphthalene	10^8	0.06	0.54	Cl = 587
1-Bromonaphthalene	10^9	0.002	0.55	Br = 2460
1-Iodonaphthalene	10^{10}	0.0	0.70	I = 5069

Note: Data for rigid solution at 77 K. Rate constants are approximate.

From **Table 1.1**, the effect of a fluorine (F) substituent on k_Δ and Φ_P is negligible in 1-fluoronaphthalene; however, its Φ_F is higher than that of naphthalene. This is due to that fact that the vibrational frequency of a C-H bond is much higher than that of the C-F bond, thus energy loss is more efficient via the C-H bond than via the C-F bond. On the other hand, chloro (Cl), bromo (Br) and iodo (I) substituted naphthalenes show a decrease in Φ_F, but increase k_Δ and Φ_P, indicating that the SOC of the heavy atom can significantly facilitate ISC, and thus form the triplet excited state.[4]

The heavy atom effect is also present in transition metal compounds, and as a result, many organometallic complexes such as $[Ir(ppy)_3]$,[10, 11] $[Ru(bpy)_3]^{2+}$,[12, 13] and 2,3,7,8,12,13,17,18-octaethyl-21H,23H-porphine platinum$^{(II)}$ (PtOEP)[14, 15] are well known phosphorescent organometallic complexes with fairly high SOC constants for the 2nd and 3rd row transition metals (e.g. SOC constant for Ru = 1042 cm^{-1}, Ir = 3909 and Pt

= 4481 cm^{-1}).[9] Therefore, fluorescence is usually not observed in organometallic complexes.

Apart from the heavy atom effect, ISC in organic molecules still can occur if the transitions involved can generate a spin momentum change such as an n → π* transition (**Figure 1.4.a**, 'n' means nonbonding orbital).[4] As illustrated in **Figure 1.4.a**, a π electron 'jumps' from one p orbital (e.g. p_x orbital) to another p orbital (e.g. p_y orbital) on the oxygen atom. The p_x → p_y orbital jump is a one-centre jump, involving a change in angular momentum, which is similar to a SOC situation, and since the total spin has to be preserved, a spin flip creating a triplet state is allowed.[4] Consequently, the angular momentum change during the n → π* transition leads to a situation in which the formation of a singlet state is forbidden. In **Figure 1.4.b**, a π → π* transition in ethylene is shown. The π electron on the carbon atom cannot find a low-energy orbital in the molecular plane to 'jump' into in order to facilitate a change in angular momentum. Therefore, a one-centre jump spin interaction is not present in the ethylene case, and consequently, no spin flip can occur to form the triplet excited state.

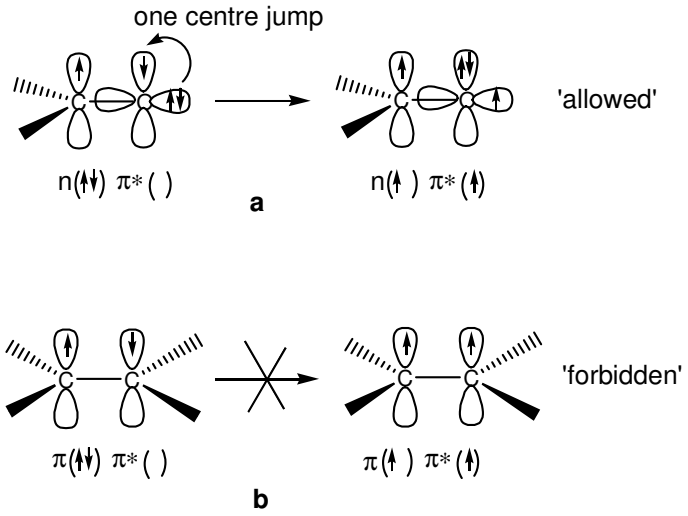

Figure 1.4: Spin-flip cases in (**a**) formaldehyde and (**b**) ethylene, respectively.[4]

Besides the n → π* transition, σ → π* and π → σ* transitions are also known as spin-flip allowed transitions.[4, 8, 16] For example, the triplet excited states of the thiophene trimer (**Figure 1.5**) arise from a nearly pure π → σ* transition.[16]

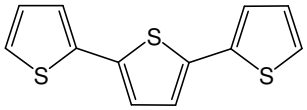

Figure 1.5: The structure of thiophene trimer.[16]

1.1.3 External quenching of excited states

Besides intramolecular processes, the efficiency of fluorescence and phosphorescence can be reduced by external quenching processes. In the presence of external quenchers (e.g. oxygen and halides), the excitation energy in a molecule can be lost through energy transfer and electron transfer processes. There are many mechanisms to describe the quenching processes, but in general, they can be categorised into three mechanisms, (i) 'trivial', (ii) collisional quenching, and (iii) Coulombic interaction.

'Trivial' is when the donor (**D**) emits fluorescence and the acceptor (**A**) absorbs the fluorescence (**Eq. 1.3** and **1.4**).[17]

$$\mathbf{D^*} \rightarrow \mathbf{D} + h\nu \qquad (\mathbf{1.3})$$

$$h\nu + \mathbf{A} \rightarrow \mathbf{A^*} \qquad (\mathbf{1.4})$$

A does not influence the emission ability of **D**, but it reduces the amount of observed photons emitted from **D**, as a result the recorded Φ_F will be less than the real one. Three factors determine how the recorded Φ_F is affected, (i) the concentration of **A**, (ii) the extinction coefficient of **A**, and (iii) the overlap of the emission spectrum of **D*** with the

absorption spectrum of **A**. Φ_F can be decreased dramatically when each of these three factors is maximised.

The second quenching mechanism is called collisional quenching, where the excitation energy of **D*** is lost when it comes into physical contact with **A** in solution. (**Eq. 1.5** and **Figure 1.6**).[4]

$$\mathbf{D^* + A \rightarrow D + A^*} \qquad (\mathbf{1.5})$$

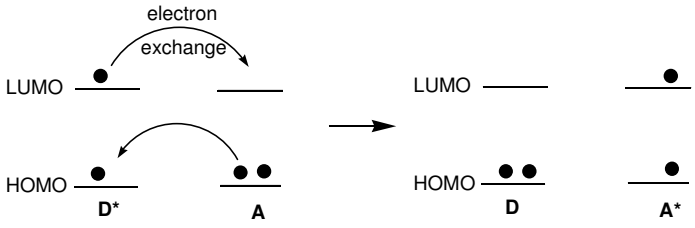

Figure 1.6: Energy transfer by collisional quenching.[4]

In this mechanism, the electron in the lowest unoccupied molecular orbital (LUMO) of **D*** 'jumps' to the LUMO of the ground state **A**, and at the same time, an electron in the highest occupied molecular orbital (HOMO) in **A** 'jumps' to the HOMO of **D***. As a result, the excited state of **D** has been quenched.

The principle of this quenching mechanism can be applied to determine the quantum yield of triplet state formation, Φ_Δ, of a molecule via a singlet oxygen sensitisation experiment.[18, 19] **Figure 1.7** shows how the singlet oxygen ($^1O_2$) is formed when a ground state molecular oxygen physically contacts with a triplet state molecule. By knowing the percentage of $^1O_2$ formation from the weak emission spectrum of $^1O_2$ around 1270 nm (depending on the solvent used[18]), the Φ_{ISC} of a molecule can be determined.

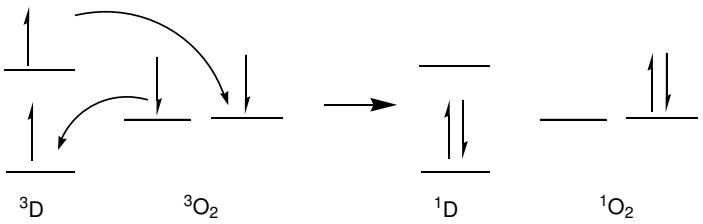

Figure 1.7: Triplet-triplet annihilation and singlet oxygen formation.[4]

The third quenching mechanism is Coulombic interaction or dipole-dipole interaction between **D** and **A**. The principle of this quenching is depicted in **Figure 1.8**.[4]

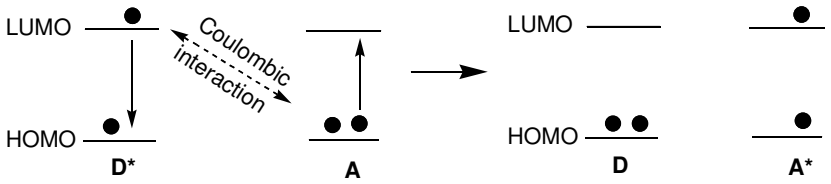

Figure 1.8: Coulombic interaction between **D*** and **A**.[4]

The main distinction between the collisional quenching and the Coulombic interaction is that in the latter, physical contact is not necessary. Förster[20, 21] proposed that the magnitude of interaction is dependent on the magnitude of two dipoles (μ_D and μ_A) and the distance between **D** and **A** (R_{DA}), which can be represented by **Eq 1.6**:

$$\text{Interaction energy } \alpha \frac{\mu_D \mu_A}{R_{DA}^3} \qquad (\mathbf{1.6})$$

Based on **Eq. 1.6**, a significant interaction energy can be caused by the large dipole moment of **D** (μ_D) and **A** (μ_A) and the small separation between **D** and **A**. [20, 21]

Interaction between an excited molecule and a solvent molecule in a polar solvent is a typical quenching example via Coulombic interaction. In general, emission shifts to a lower energy region in polar solvents because of the strong dipole moment interaction between the excited molecules with the polar solvent molecules, which can stabilise the S_1 excited state and result in a red shift in the emission. However, due to the strong dipole moment interactions, the excitation energy can be lost from the excited molecules to solvent molecules thereby reducing the Φ. The reduction of Φ in polar solvent can be explained by **Eq 1.6**; a higher Φ is observed in a non-polar solvent, e.g. hexane, compared to a polar solvent because the dipole moment of non-polar solvent, μ_A, is close to zero, hence, the interaction energy is very small.

1.2 Applications of luminescent materials

1.2.1 Organic light emitting diodes

The main applications for luminescent materials are in display technologies such as organic light emitting diodes (OLEDs)[15, 22-24] and biological labelling agents.[25-27] Compared to other display technologies such as plasma displays and liquid crystal displays (LCDs), OLEDs have unique properties.[22, 28] In addition to being brighter and having longer operational lifetimes, OLEDs can be manufactured in a portable, roll-up form with conformable displays, which display the images on windows, panels, building walls and so on. This unique property is due to the fact that OLED materials can be deposited on a wide range of substrates, ranging from glass and silicon, which are rigid substrates, to incorporation into polymers, which are highly flexible substrates. OLEDs

are thus believed to have greater potential in the application of high performance flat panel displays.[28, 29] A simple general structure of an OLED device is shown in **Figure 1.9**, which consists of three layers, namely cathode, organic layer and anode. When a potential is applied across the device, the organic material is oxidised, forming hole carriers at the anode because its electrons are ejected from the HOMO of the organic material. At the same time, the material near the cathode is reduced, forming electron carriers when an electron is injected into the LUMO of the organic material. The holes and electrons will recombine leading to the emission of light, termed electroluminescence.

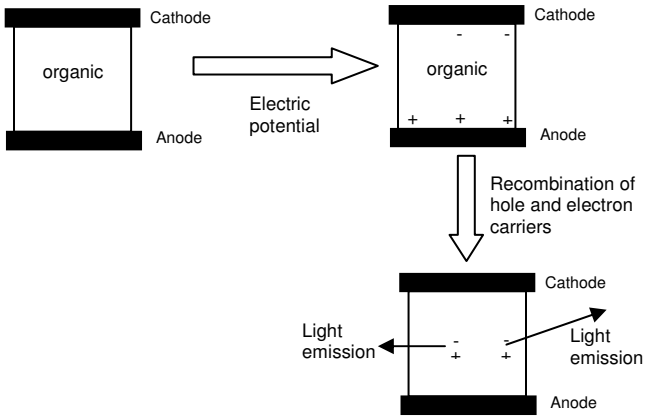

Figure 1.9: Schematic diagram showing how an OLED device emits light.

However, the simple structure OLED device in **Figure 1.9** is often inefficient. The organic material needs to satisfy a number of criteria in order to have a high probability for hole and electron carrier recombination within the layer. Therefore, multilayer OLEDs are designed, and each layer is optimised for its particular role (**Figure 1.10**). The selection of material for each layer is based on the HOMO-LUMO energy gap as well as

their electron and hole transport properties in order to achieve highly efficient light emission from the device.[29, 30]

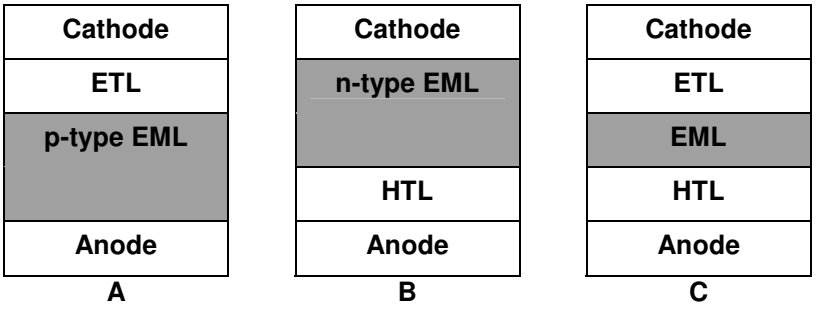

Figure 1.10: Multilayer OLED devices with hole transport layer (HTL) and/or an electron transport layer (ETL) and emissive layer (EML).[30]

Simple fluorescent organic compounds were employed in the EML materials in the early stages of OLED technology.[31] However, in recent times, organometallic complexes have been employed in the OLED devices due to the fact that device efficiency can be improved by up to a factor of four after electron/hole recombination in the emissive layer, according to spin statistics.[32] This is due to the strong SOC of heavy atoms such as 2nd and 3rd row transition metals, which can lead to highly emissive triplet states, and consequently increases the electroluminescence efficiency by up to four times higher than the simple fluorescent organic compounds which are typically singlet state emitters.[32]

1.2.2 Biological labelling and imaging

In biological labelling applications, fluorescent probes enable researchers to observe and detect specific components in bio-molecular assemblies. They have become key research tools for non-invasive diagnostics and for biological imaging. Therefore, the design of an ideal practical probe has become a growing interest. An ideal practical

probe, which is suitable for living cells and is able to be observed by spectroscopic techniques, should be able to fulfil several criteria. The probe should be non-toxic, cell-permeable, emitting in the visible region, having a large Stokes shift to minimise re-absorption by other molecules and a long-lived emission that can allow time-resolved methods to be employed.[33] The output of a fluorescent probe depends on the extinction coefficient (ε) of the absorption and the Φ of the emission. In principle, the higher Φ and ε, the better the fluorescent probe is.

The performance of a fluorescent dye is also dependent on certain external factors such as solvent polarity, the presence and concentration of quenchers, and the pH of the aqueous medium. As discussed in **section 1.1**, polar solvents can cause the emission wavelength of a fluorescent dye to shift to lower energy regions and result in lower Φ than less polar solvents.

In biological cases, proteins are found to be the quenchers due to the charge-transfer interaction between the amino acid and the fluorescent dyes. For example, the fluorescence of (α-*N*-L-alanine)-7-nitro-benz-2-oxa-l,3-diazole (NBDA) is quenched when it binds to immunoglobulins, which is because of the hydrogen bond formation between the proton donor groups in immunoglobulins with the nitro or oxadiazole oxygens in NBDA.[34]

An example of how the pH of the aqueous medium affects the emission efficiency of the fluorescent dye is shown in **Figure 1.11**. The conversion of the prototropic 3'- and 6'-hydroxyl groups of fluorescein to acetate esters can make the colour change from colourless and nonfluorescent (compound **d**) to highly fluorescent (di-anionic fluorescein, compound **g**).[35]

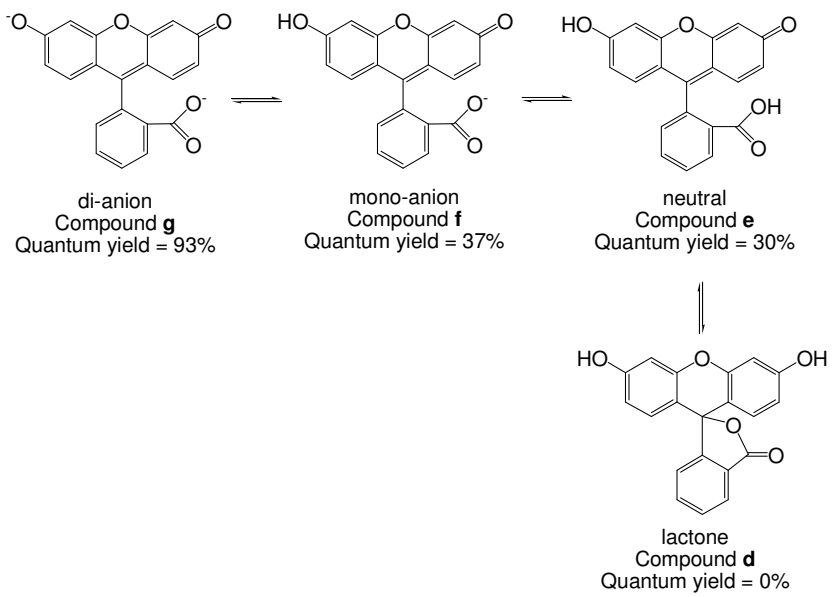

Figure 1.11: Ionisation equilibrium of fluorescein.[35]

Similar to OLED applications, utilisation of fluorescent organic compounds also has several limitations for biological imaging, sensing or labelling applications. Some of the limitations include short fluorescence lifetimes and small Stokes shifts.[26] In order to solve these problems, various metal complexes such as lanthanide (Ln) coordination complexes containing chelating ligands,[27, 33, 36] rhenium and iridium-containing diimine complexes[26, 37, 38] which display intensive and long-lived luminescence, have been developed. For example, Lo et al.[39] synthesised a series of luminescent $Re^{(I)}$ isothiocyanate polypyridine complexes (**Figure 1.12**) to label human serum albumin. The labelled bio-conjugate exhibited an intensive and long-lived yellow emission band in the polyacrylamide gel electrophoresis study. Importantly, this band was not observed when an isothiocyanate-free $Re^{(I)}$ complex was used, which indicates that the yellow band is associated with the Re-labelled protein.

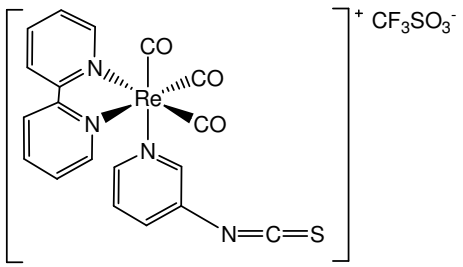

Figure 1.12: Structure of *fac*-[Re(N-N)$(CO)_3$(py-3-NCS)](CF_3SO_3).[39]

Long-lived luminescent Ln complexes with chelating ligands have been developed to be localised within living cells by luminescence microscopy.[27, 33, 40, 41] The function of chelate ligands are (i) to protect the luminescent Ln centre from quenching by water molecules; and (ii) to allow energy transfer to the Ln centre.[36] Parker and Pal[33] reported a luminescent europium (Eu) complex (**Figure 1.13**), where upon changing the pH, the emission maxima shifts. Importantly, the lifetime and emission intensity of this Eu complex were not affected when the pH was changed. The cellular uptake profile (using mouse skin fibroblasts) of the Eu complex was also reported. Two emission maxima were observed at wavelengths of 570 nm (red, from Eu emission) and 450 nm (green, from azathiaxanthone fluorescence) indicating that the complex was localised in the cell nucleus.[33]

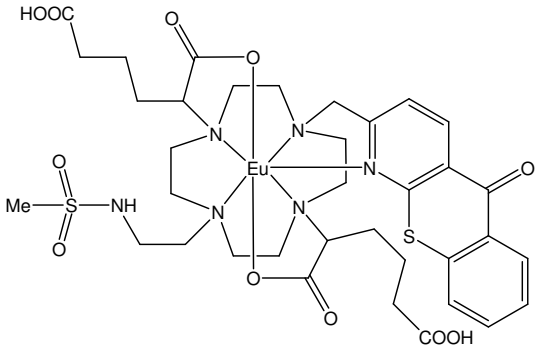

Figure 1.13: The structure of a luminescent Eu complex with a chelating ligand.[33]

Besides being used for displays and labelling purposes as discussed above, luminescent materials are also promising for use in other applications such as photocatalysts for CO_2 reduction,[42, 43] as singlet oxygen sensitisers[44, 45] and for sensor applications.[46, 47]

1.3 Photophysical properties of luminescent organometallics

The photophysical properties of a molecule are mainly dependent on the nature of molecular orbitals, which correspond to the electronic ground state and the lowest excited state.[48] Specifically, the excitations in organometallic complexes that will be discussed here are (i) ligand-centred (LC) $\pi \rightarrow \pi^*$ transitions, (ii) metal-centred (MC) $d \rightarrow d^*$ transitions and (iii) metal-to-ligand charge transfer (MLCT) $d \rightarrow \pi^*$ transitions (**Figure 1.14**).

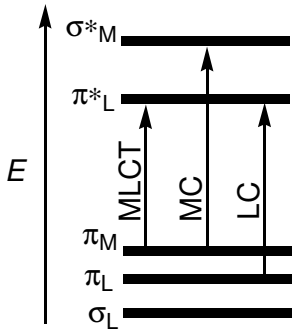

Figure 1.14: The three types of electronic transitions that are discussed in this section.

LC $\pi \rightarrow \pi^*$ transitions are typically found originating from the π-conjugated organic ligands of a metal complex. The HOMO and LUMO are the respective π and π* orbitals of the organic ligands. As a simple example, in the ground state, the electron configuration is π^2 (**Figure 1.15.a**). Upon excitation, one electron is promoted from the π

orbital to the π* orbital and thus giving the electron configuration of $\pi^1\pi^{*1}$, which can be a singlet (**Figure 1.15.b**) or triplet (**Figure 1.15.c**) excited state. Since formation of a singlet excited state is a spin allowed process, it corresponds to a strong absorption band with a large extinction coefficient. However, triplet excited state formation is a spin forbidden process, and it is therefore associated with a small extinction coefficient for absorption.

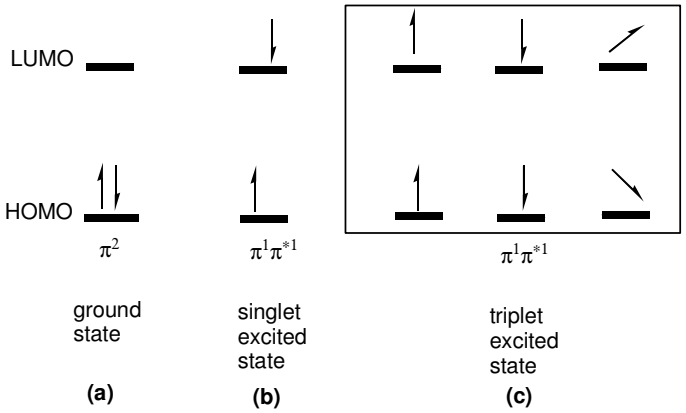

Figure 1.15: (**a**) Ground state, (**b**) singlet excited states and (**c**) triplet excited state of π-conjugated organic ligands in a transition metal complex.[48]

MC d → d* absorptions involve the transition between d-orbitals in a metal. **Figure 1.16** shows the d-orbitals splitting diagram of a transition metal complex with octahedral geometry and with a d^6 configuration. The ΔE value between t_{2g} and e_g orbitals is influenced by the ligands attached to the metal. Based on ligand field theory, strong field ligands such as CO, CN^- and ppy^- split the orbitals greater than weak field ligands such as Br^-, S^{2-}, SCN^-, etc.[49]

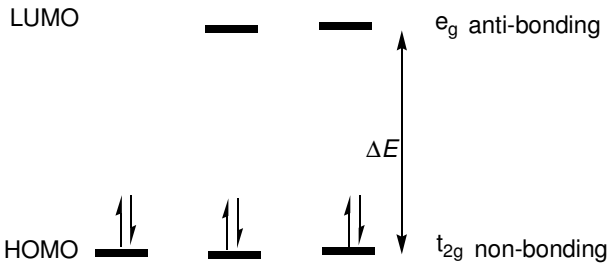

Figure 1.16: Splitting of d-orbitals in a transition metal complex with octahedral geometry (with strong field ligands, large ΔE value).[48]

Upon excitation, the electron configuration can change: $t_{2g}^6 \rightarrow t_{2g}^5 e_g^1$ and $t_{2g}^6 \rightarrow t_{2g}^4 e_g^2$ etc; and as a result, the excited states have longer metal-ligand bond lengths than the ground state because of the occupation of the anti-bonding e_g σ^*-orbitals. Increasing the metal-ligand bond length can increase the overlap between low-lying vibrational wavefunctions of the excited state with the high-energy vibrational wavefunctions of the ground state. An increase of Frank-Condon factor and non-radiative process rate is the result, and emission is quenched.[48]

MLCT transition refers to the transition from a metal d-orbital to a low-lying π^* orbital at the ligand. The transition usually occurs at low energy if the metal ion has a low oxidation number, whereby its d-orbitals are high in energy.[49] In addition, this transition is also represented by a weaker absorption band compared to the LC absorption band in a spectrum.

1.3.1 Tris(bipyridine) ruthenium$^{(II)}$ dication, $[Ru(bpy)_3]^{2+}$

The discovery of the photophysical properties of tris(bipyridine) ruthenium$^{(II)}$ dication, $[Ru(bpy)_3]^{2+}$ (**Figure 1.17**) was an important landmark in modern organometallic photochemistry.[22, 50] This complex has been extensively studied and has played a key role in understanding the photophysics, photochemistry, electroluminescence, and electron and energy transfer mechanisms in organometallic complexes.[12] The HOMO of the d^6 configuration $[Ru(bpy)_3]^{2+}$ complex arises from the t_{2g} orbitals of the Ru centre, whereas the LUMO arises from the π^* of the bpy ligands.[12, 13]

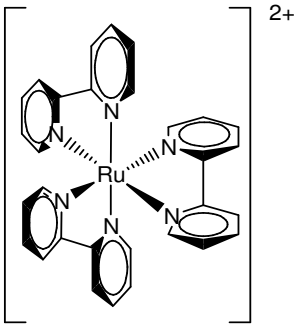

Figure 1.17: Structure of $[Ru(bpy)_3]^{2+}$.

Five electronic transitions are observed in the absorption spectrum of $[Ru(bpy)_3]^{2+}$ at 185, 285, 240, 344 (shoulder) and 450 nm (**Figure 1.18**).[12] The absorption bands at 185 and 285 nm are due to the LC $\pi \rightarrow \pi^*$ transitions,[12, 51] while the other two bands at 240 and 450 nm are believed to be the MLCT $d \rightarrow \pi^*$ transitions. The shoulder at 344 nm may be the MC $\pi_{metal} \rightarrow \sigma^*_{metal}$ (or $d \rightarrow d^*$) transition.[12]

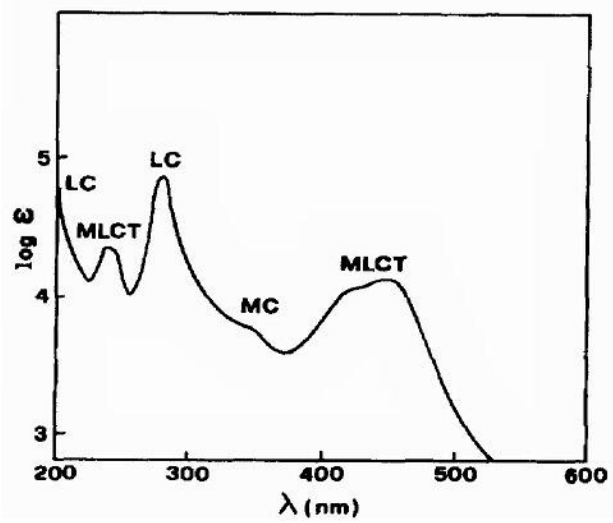

Figure 1.18: Absorption spectrum of $[Ru(bpy)_3]^{2+}$ (Diagram taken from reference 12).

Apart from the above mentioned transitions, Klassen and Crosby observed a shoulder at 550 nm when they recorded the absorption spectrum at 77 K in a rigid ethanol-methanol glass. The authors assigned this absorption feature to the spin-forbidden ^{3}MLCT transition with $\varepsilon \sim 600\ M^{-1}\ cm^{-1}$.[52] The initial excited state species that is produced from the absorption of a photon is generally a singlet state, but because of the extremely fast ISC process that occurs in $[Ru(bpy)_3]^{2+}$, the singlet state lifetime is only ≤ 10 ps[51] and all the singlet states 'cross over' to the triplet excited state.[53, 54] However, by using femtosecond fluorescence spectroscopic technology, Cannizzo et al. were able to determine the lifetime of fluorescence, which is 15 ± 10 fs at the emission λ_{max} of 520 nm.[55] This indicates that the fluorescence in organometallic complexes is very hard to observe due to the present of strong SOC from the metal that generates the extremely fast ISC process. At room temperature, the triplet state λ_{max} emission occurs at 626 nm with a lifetime of 0.9 μs and a quantum yield of 0.062 in argon-purged acetonitrile.[56] The

lifetime and Φ of the triplet state emission is temperature dependent; the higher the temperature, the lower the Φ and the shorter the lifetime. For example, the emission lifetime at 77 K was reported to be about 5 μs with a Φ of 0.40.[12] A summary of the excited state decay of $[Ru(bpy)_3]^{2+}$ at room temperature is shown in **Figure 1.19**.

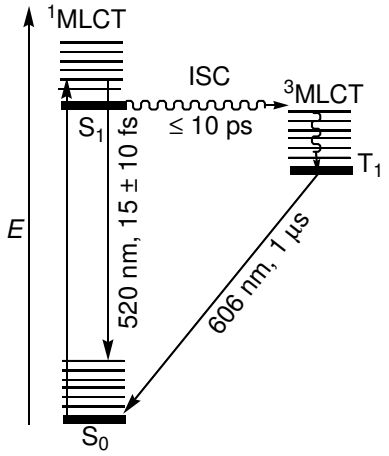

Figure 1.19: Proposed model of the excited state decay in $[Ru(bpy)_3]^{2+}$ at room temperature.

Tuning the emission colour, lifetime and Φ of $[Ru(bpy)_3]^{2+}$ via modification of the ligands has been attempted over the past few decades.[57] Unfortunately, ligand modification in $[Ru(bpy)_3]^{2+}$ to tune the emission colour has proven relatively ineffective, and the emission wavelengths are limited to the orange-red spectral region.[22] For example, changing the ligand bpy to 1,10-phenanthroline (phen) to form $[Ru(phen)_3]^{2+}$ (**Figure 1.20**), which has higher degree of rigidity than the bpy framework, does not improve the Φ.[58] At room temperature, the lifetime and Φ (in ethanol) of $[Ru(phen)_3]^{2+}$ are 340 ns and 0.023, respectively, whereas the lifetime and Φ (in ethanol) of

$[Ru(bpy)_3]^{2+}$ are 870 ns and 0.075, respectively. The emission wavelength of $[Ru(phen)_3]^{2+}$ also shifted to higher energy (587 nm) compared to $[Ru(bpy)_3]^{2+}$.[58]

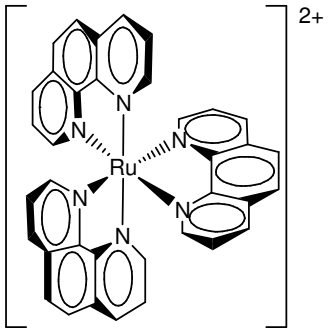

Figure 1.20: Structure of $[Ru(phen)_3]^{2+}$.

1.3.2 Tri(2-phenylpyridine) iridium, $[Ir(ppy)_3]$

Another remarkable luminescent organometallic, which has been extensively studied since the year 2000, is $[Ir(ppy)_3]$ (**Figure 1.21**). Two isomers are found for $[Ir(ppy)_3]$, the facial isomer, *fac*-$[Ir(ppy)_3]$, (**Figure 1.21.a**) and meridional isomer, *mer*-$[Ir(ppy)_3]$ (**Figure 1.21.b**). The photophysical properties of the *fac*-$[Ir(ppy)_3]$ isomer were initially reported by Watts and co-workers[10] in 1985 and were then applied in OLED devices by Baldo et al.[11] in 2000.

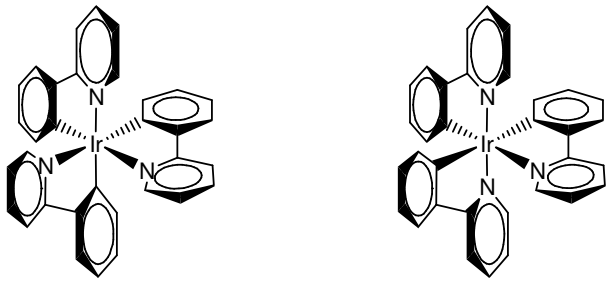

Figure 1.21: Cyclometallated $Ir^{(III)}$ complex; (**a**) *fac*- and (**b**) *mer*-$[Ir(ppy)_3]$.

[Ir(ppy)$_3$] and its derivatives are still the most promising materials for OLED technology because (i) they have high Φ for phosphorescence and relatively short phosphorescence lifetimes, (ii) they are thermally stable, and (iii) the emission colour can be tuned efficiently by changing the ligands.[59] Based on TD-DFT theoretical calculations (with B3LYP functional) from Hay in 2002, the HOMO of *fac*-[Ir(ppy)$_3$] consists of a mixture of phenyl-π from the ppy ligands and d-orbitals from the Ir centre, whereas the LUMO has contributions mainly from the pyridyl π-orbitals in the ppy ligand.[60] Similar to [Ru(bpy)$_3$]$^{2+}$, *fac*-[Ir(ppy)$_3$] also shows MLCT character in the lowest energy excited state.[10] Upon absorption of a photon, an electronic transition occurs from the 5d orbital on the Ir centre to the pyridyl π*-orbitals of the ppy ligand to form a singlet excited MLCT state. Then, with an extremely fast ISC rate that is promoted by the strong SOC from Ir, the initial singlet excited state converts to a triplet excited MLCT state within 100 fs.[61] However, based on the results from femtosecond timescale experiments carried out by Hedley and co-workers, the authors claimed that the ISC timescale is actually < 100 fs. The diagram to illustrate the excited state timescale in *fac*-[Ir(ppy)$_3$] is shown in **Figure 1.22**.[62]

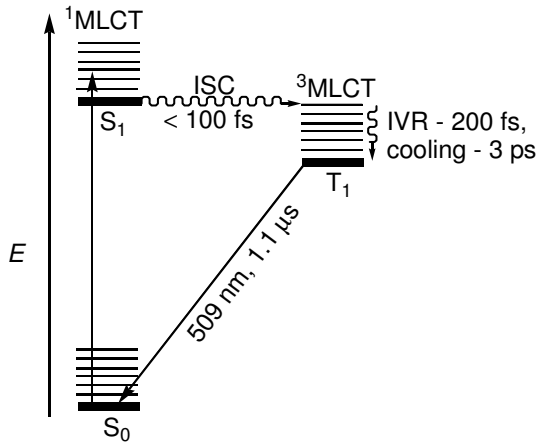

Figure 1.22: Proposed model of the excited state processes that occur in *fac*-[Ir(ppy)$_3$].[62]

The non-radiative relaxation to the lowest vibrational level of the triplet excited state in *fac*-[Ir(ppy)$_3$] is through an IC process known as intramolecular vibrational energy redistribution (IVR), which involves energy transfer from hot vibrational modes to the lower frequency modes.[62] The authors found that about 86% of the non-radiative relaxation within the sub-states is IVR with a timescale of 200 fs and the rest (14%) is a vibrational cooling process such as transferring energy to the solvent molecules.[62] At room temperature, the phosphorescence lifetime for *fac*-[Ir(ppy)$_3$] in a degassed toluene solution is about 1.1 µs and Φ_P = 0.73 with λ_{max} (emission) occurring at 509 nm.[63, 64] However, in air-saturated toluene solution, the phosphorescence lifetime is 23 ns and Φ_P is only 0.01 to 0.02 at room temperature.[64] This indicates that triplet oxygen quenching can significantly affect the phosphorescence efficiency of *fac*-[Ir(ppy)$_3$].

Since the photophysical properties of [Ir(ppy)$_3$] have been extensively studied, many modifications to the ligand have been carried out in order to tune the emission colour as well as to improve the efficiency of phosphorescence. According to You and Park, the

phosphorescence efficiency of [Ir(ppy)$_3$] analogues can be improved by several approaches, which include: (i) isomer control, (ii) substituents on the ligands, (iii) rigidity control, (iv) de-stabilizing a thermal accessible non-emissive state.[59]

As already mentioned, there are two isomers in the cyclometallated Ir$^{(III)}$ complex, namely *fac*-[Ir(ppy)$_3$] (**Figure 1.21.a**) and *mer*-[Ir(ppy)$_3$] (**Figure 1.21.b**). The *mer*-isomer can be synthesised at a lower temperature (about <150 °C) than the *fac*-isomer, which requires >200 °C.[59] Although the *mer*-isomer is easier to synthesise compared to the *fac*-isomer, the Φ_P of the *mer*-isomer is lower than that of the *fac*-isomer. This is because of the self-quenching which occurs in the excited state of the *mer*-isomer due to the bond dissociation in forming the *fac*-isomer, and the longer *trans* Ir-C bond length, which is caused by the strong *trans*-influence of the mutually *trans* C-bound ligands in the *mer*-isomer.

Many researchers have tuned the emission colour by introducing electron donating and electron withdrawing substituents on the ligands of [Ir(ppy)$_3$]. If an electron withdrawing group is located on the pyridyl ring of the ppy ligand (where the LUMO is located), the emission wavelength is shifted to lower energy because the electron withdrawing substituent stabilises the LUMO and reduces the HOMO-LUMO gap. This is why many Ir$^{(III)}$ complexes with electron withdrawing substituents on the pyridyl moiety are known to exhibit yellow, orange and red emission.[65-67] In contrast, blue-shifted emission is observed if an electron withdrawing substituent is introduced at the phenyl moiety of ppy (where the HOMO is located). The common example is replacing hydrogen (H) atoms by electron withdrawing fluorine (F) atoms on the phenyl ring of the ppy ligands.[64, 68-70]

Ono et al. have used different degrees of rigidity in the phenylpyridine (ppy) ligand framework to enhance the phosphorescence efficiency of their Ir complexes (**Figure 1.23**). The carbazole substituted Ir complex (complex **b**) was found to have a higher Φ_P compared to the other two.[71]

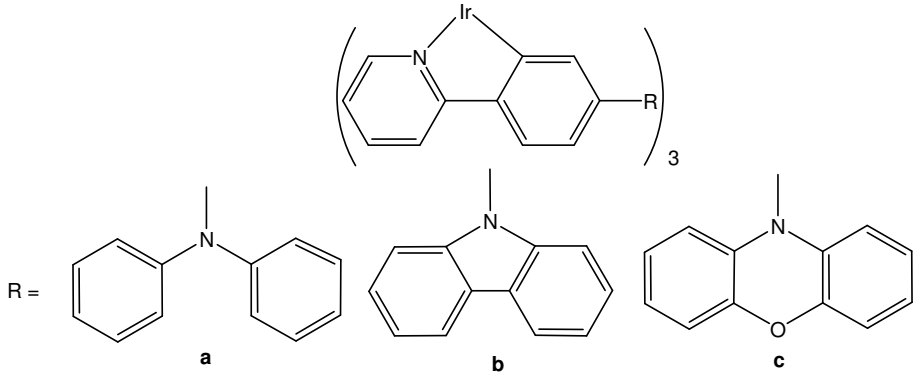

Figure 1.23: $Ir^{(III)}$ complexes with different rigidity of the substituted ppy ligand.[71]

The $Ir(ppy)_3$ analogue complexes have a high energy MC d → d* transitions,[72] which are known as non-emissive transitions. However, because a blue emissive organometallic molecule requires a large energy gap between excited and ground states, the corresponding high-lying excited state can approach the MC d → d* state. A non-radiative transition can result when the excited state energy transfers to the MC d → d* transition state and hence reduces Φ. Nazeeruddin et al. employed basic ligand field theory to tune the emission colours of $[Ir(ppy)_2X_2]^-$ salts, where X = CN^-, NCS^- and NCO^-, to avoid the MC d → d* transition.[73] Based on the frontier molecular orbital (MO) diagram in **Figure 1.24**, the t_{2g} orbitals in $[Ir(ppy)_2(CN)_2]^-$ complex were stabilised by the strong field ligand (CN^-), leading to a larger energy gap between the t_{2g} orbital and the π_{ppy}* orbital without changing the energy level of the π_{ppy}* orbital. Consequently, the $[Ir(ppy)_2(CN)_2]^-$ complex gives a blue-shifted emission spectrum.

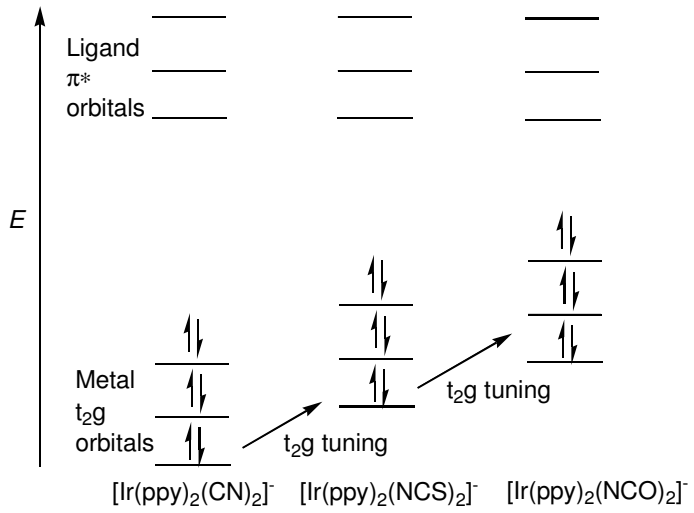

Figure 1.24: Frontier orbital diagram of $[Ir(ppy)_2(CN)_2]^-$, $[Ir(ppy)_2(NCS)_2]^-$ and $[Ir(ppy)_2(NCO)_2]^-$.[73]

1.3.3 Luminescent rhodium complexes

The luminescent properties of rhodium (Rh) complexes also have received considerable attention. So far, three general classes of Rh complexes have been investigated for their luminescent properties: (i) amino complexes and substituted derivatives, (ii) multiply bridged dirhodium complexes, and (iii) polypyridine and related complexes.[74] Similarly to Ru complexes, the photophysical properties of cyclometallated Rh complexes that contain pyridine ligands such as $[Rh(bpy)_3]^{3+}$ (**Figure 1.25.a**) and $[Rh(phen)_3]^{3+}$ (**Figure 1.25.b**) have been widely studied.

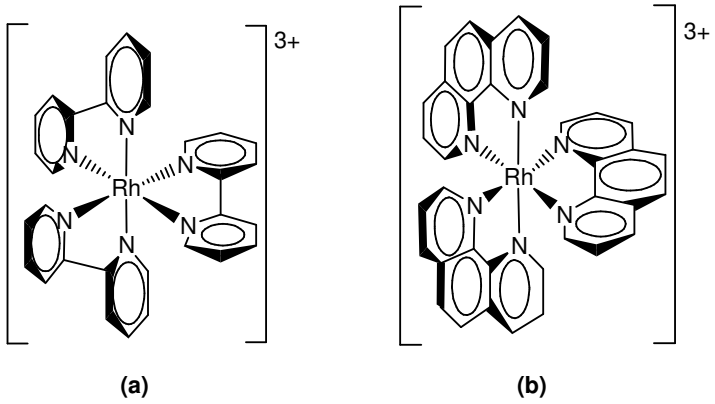

Figure 1.25: Structure of (**a**) $[Rh(bpy)_3]^{3+}$ and (**b**) $[Rh(phen)_3]^{3+}$.

The photophysical behaviour of $[Rh(bpy)_3]^{3+}$ is very different from that of $[Ru(bpy)_3]^{2+}$. The various high intensity bands that are observed below 350 nm in the absorption spectrum of $[Rh(bpy)_3]^{3+}$ are generally assigned to the $^1LC\ \pi \rightarrow \pi^*$ transitions in the bpy ligands, and no MLCT transition band was found in the spectrum.[75] At room temperature, $[Rh(bpy)_3]^{3+}$ is non-emissive in fluid solution. The emission from $[Rh(bpy)_3]^{3+}$ at 448 nm with a lifetime of 2.2 ms was only observed at low temperature (77 K) in a rigid glass. The long-lived millisecond lifetime suggests that the emission belongs to the $^3LC\ \pi \rightarrow \pi^*$ excited state.[75-77] However, Yersin and co-workers[75] found that there is little mixing of MC d → d* character with the lowest triplet states, and this phenomenon is even more obvious in the $[Pt(bpy)_3]^{2+}$ case. In view of this, the authors claimed that $[Pt(bpy)_3]^{2+}$ is the intermediate situation in between $[Ru(bpy)_3]^{2+}$ and $[Rh(bpy)_3]^{3+}$, and a comparison of spectroscopic properties for the bpy ligand, $[Rh(bpy)_3]^{3+}$, $[Pt(bpy)_3]^{2+}$ and $[Ru(bpy)_3]^{2+}$ is shown in **Table 1.2**.[75]

Table 1.2: Summary of the comparison of spectroscopic properties for bpy and its complexes.[75]

Compound	Lowest triplet transition (cm^{-1})	Emission lifetime (μs)	Characterisation of the electronic transition
bpy	23504	4000000[a]	^{3}LC ($\pi \rightarrow \pi^*$)
$[Rh(bpy)_3]^{3+}$	22757	2200[b]	^{3}LC ($\pi \rightarrow \pi^*$) + small MC ($d \rightarrow d^*$) contribution
$[Pt(bpy)_3]^{2+}$	21237	50[a]	^{3}LC ($\pi \rightarrow \pi^*$) + small MLCT contribution
$[Ru(bpy)_3]^{2+}$	17684	5.0[c]	^{3}MLCT ($d \rightarrow \pi^*$)

[a]At 1.3 K, data from reference 77.
[b]At 77 K, data from reference 76.
[c]At 77 K, data from reference 12.

On the other hand, the photophysical properties of $[Rh(phen)_3]^{3+}$ are similar to $[Rh(bpy)_3]^{3+}$.[78] The absorption bands in $[Rh(phen)_3]^{3+}$ are also assigned to the LC $\pi \rightarrow \pi^*$ transition, and similarly, the emission band also belongs to the ^{3}LC $\pi \rightarrow \pi^*$ excited state.[78, 79] Interestingly, the $[Rh(phen)_3]^{3+}$ complex is a typical example wherein the emission is similar to that of the free ligand in terms of energy and structure.[78] However, the shorter lifetime of $[Rh(phen)_3]^{3+}$ (48 ms) compared to that of the free ligand (1.52 s) suggests that the Rh is involved in the transitions.[78] A broad, structureless and weak emission, which is assigned to phosphorescence from the triplet MC $d \rightarrow d^*$ state, has been observed at about 578 nm in MeCN solution at room temperature. This proves that there is very little metal character in the lowest triplet states, which is similar to $[Rh(bpy)_3]^{3+}$.[76, 79, 80] On the other hand, Indelli et al. found that the efficiency of ISC to the ^{3}LC $\pi \rightarrow \pi^*$ state in $[Rh(phen)_3]^{3+}$ is 100%, even at room temperature.[79]

Compared to *fac*-[Ir(ppy)$_3$], reports on the photophysical properties of *fac*-[Rh(ppy)$_3$] (**Figure 1.26**) are very limited. Only Colombo et al., in 1994, compared the photophysical properties of *fac*-[Rh(ppy)$_3$] and *fac*-[Ir(ppy)$_3$].[81]

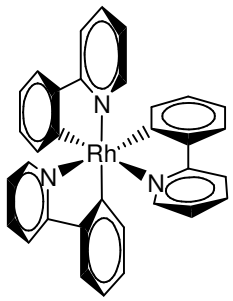

fac-[Rh(ppy)$_3$]

Figure 1.26: Structure of *fac*-[Rh(ppy)$_3$].

The absorption spectra of *fac*-[Ir(ppy)$_3$] and *fac*-[Rh(ppy)$_3$] are nearly identical. The only difference found is a weak broad band in the *fac*-[Ir(ppy)$_3$] spectrum at about 454 nm which corresponds to the spin-forbidden triplet excited state MLCT transition. The reason why this band is observed in the *fac*-[Ir(ppy)$_3$] but not in the *fac*-[Rh(ppy)$_3$] absorption spectrum is because the SOC constant of Ir (SOC for Ir = 3909 cm^{-1}) is larger than that of Rh (SOC for Rh = 1259 cm^{-1}). The larger the SOC constant, the more intense the corresponding ^{3}MLCT bands are. The other two high intensity bands in the higher energy region belong to the spin-allowed ^{1}LC $\pi \rightarrow \pi^*$ transition from the ppy ligands and the ^{1}MLCT d $\rightarrow \pi^*$ transition, respectively.[81]

The emission spectra of *fac*-[Ir(ppy)$_3$] and *fac*-[Rh(ppy)$_3$] are different. At room temperature, *fac*-[Rh(ppy)$_3$] shows a structured emission band, with the structure becoming finer as the temperature is lowered to 9 K, whereas, the *fac*-[Ir(ppy)$_3$] emission spectrum consists of a broad, asymmetric band at room temperature. The structured

emission band in *fac*-[Rh(ppy)$_3$] is assigned to the triplet $\pi \rightarrow \pi^*$ transition. The emission lifetime of *fac*-[Rh(ppy)$_3$] at 77 K was determined to be 45 μs, which was considered a short-lived emission for a triplet $\pi \rightarrow \pi^*$ transition of a Rh^{3+} complex. This is due to the fact that there is considerable mixing of MLCT character into the transition.[81]

1.4 Photophysical properties of main group heterocycle analogues, EC_4

[Ru(bpy)$_3$]$^{2+}$ and [Ir(ppy)$_3$] have a metallacyclopentadiene motif (**Figure 1.27**). Metallacyclopentadienes consist of a five-membered ring system containing a metal atom, for example, in **Figure 1.27**, (**a**) metal 2,2'-biphenyl complex,[82] (**b**) metal bipyridine complex e.g. [Ru(bpy)$_3$]$^{2+}$,[12] (**c**) metal 2-phenylpyridine complex e.g. [Ir(ppy)$_3$],[11] and (**d**) metal diimine complex.[83, 84] Among the metallacyclopentadienes in **Figure 1.27**, the photophysical properties of those with bipyridine ligands have been extensively studied over last few decades. However, complexes of type **e**, which are structurally-related to the rhodacyclopentadienes that we synthesised in this work, are the best known as an intermediate in metal catalysed [2+2+2] cycloaddition (or cyclotrimerisation) reactions of alkynes, but there are no comprehensive reports on their photophysical properties.

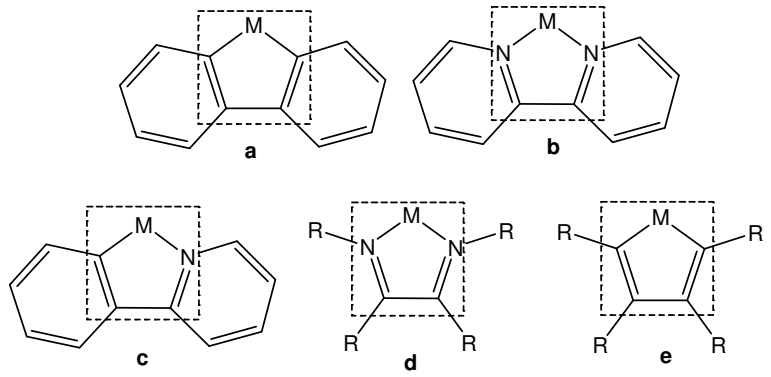

Figure 1.27: Examples of metallacyclopentadiene complexes.

Interestingly, the photophysical properties of the main group heterocyclic analogues (EC_4, E = Si, P and S), which are structurally-related to **e**-type complexes in **Figure 1.27** have been widely investigated. Therefore, due to the structural similarity of EC_4 to rhodacyclopentadienes (RhC_4), the synthesis and photophysical properties of siloles (**Figure 1.28.a**), phospholes (**Figure 1.28.b**) and thiophenes (**Figure 1.28.c**) are discussed in this section.

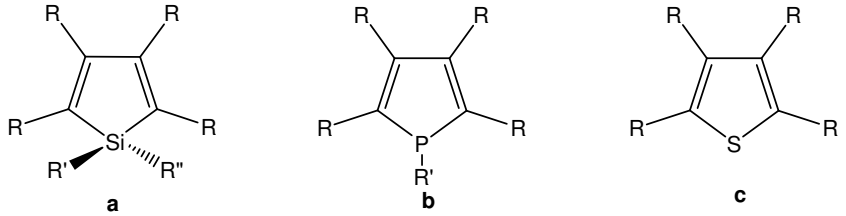

Figure 1.28: The structures of (**a**) siloles, (**b**) phospholes and (**c**) thiophenes.

1.4.1 Siloles

The synthetic methodology for preparing siloles (1-silacyclopentadienes) was first reported in 1959.[85-87] As shown in **Figure 1.29**, siloles posses low-lying LUMO levels, which have contributions from the σ* orbital of the SiR_2 moiety as well as the π* orbital from the butadiene moiety, forming a σ*-π* conjugation interaction.[86-88] The orbital

interaction between silicon and butadiene occurs effectively because of the fixed perpendicular arrangement of the plane of the SiR_2 moiety to the plane of butadiene moiety.[89]

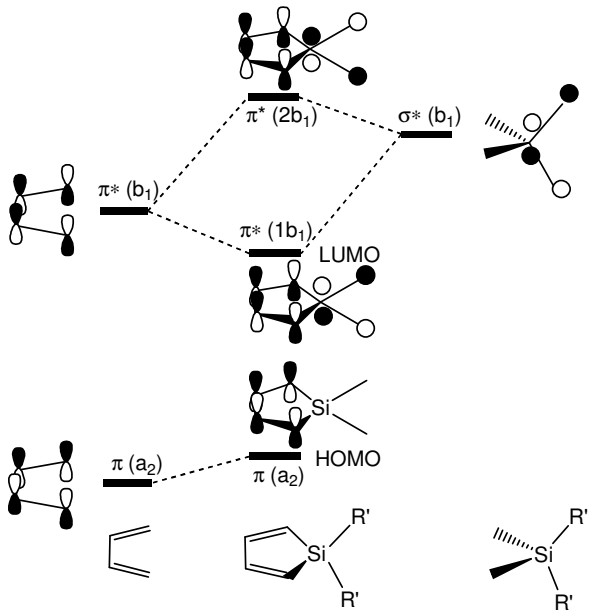

Figure 1.29: Frontier orbital diagram of silole.[88]

A series of blue silole emitters are shown in **Figure 1.30** and were reported by Tang et al. in 2001.[90] All of the siloles shown in **Figure 1.30** exhibit two absorption bands at about 250 and 360 nm, which are assigned to the $\pi \rightarrow \pi^*$ transition of the phenyl groups and the silacyclopentadiene ring, respectively. Changing the methyl group to a phenyl group at the R and R' substituents on the silicon atom can slightly shift the absorption λ_{max} value to lower energy. In other words, the electronic properties on the siloles can be tuned by the electronegativity of the R and R' substituents on the silicon atom. This result is consistent with the findings of Tamao et al., who noted that the more electronegative the R and R' substituents are, the lower the energy of the absorption maxima is.[91]

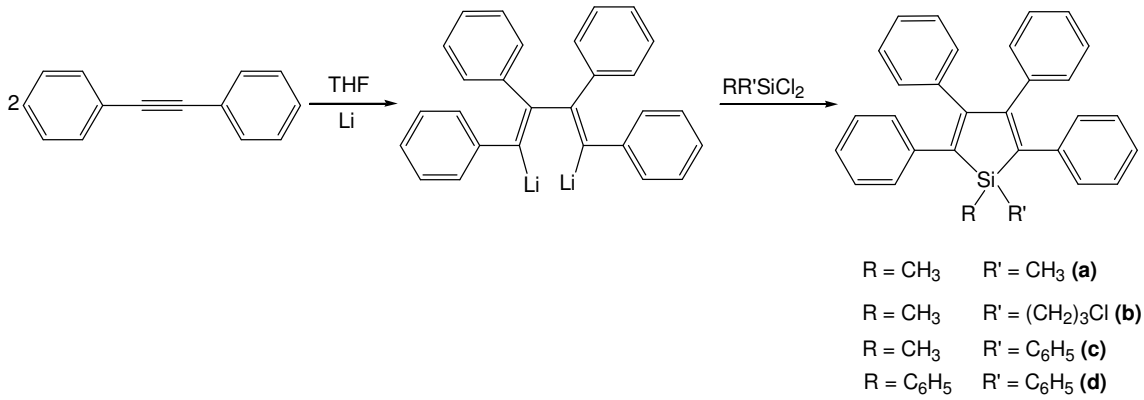

Figure 1.30: Synthetic route to blue emissive siloles.[90]

The siloles in **Figure 1.30** show only one peak in their emission spectra. Similar to the absorption, a red-shift is observed in the emission if methyl is changed to phenyl at the R and R' substituents. The methyl-substituted compound (**Figure 1.30.a**) emits at about 470 nm, whereas the phenyl one (**Figure1.30.d**) shows a 35 nm red-shift and emits at about 505 nm.[90]

In 2004, Pagenkopf et al.[92] reported a series of donor-acceptor π-conjugated siloles (**Figure 1.31**) by adapting the synthetic methodology from Tamao and co-workers.[88, 89, 93] Pagenkopf et al. found that by increasing the degree of electron delocalisation between the donor (D) and acceptor (A), the absorption λ_{max} can shift from 429 nm for the parent silole (D & A = H) to 496 nm for the most polar silole (D = -NMe_2; A = -NO_2). In fact, they also found that the consequences of varying the D and A groups are also observed in the photoluminescence spectra. Interestingly, the silole with D = OMe and A = NO_2 was the one to display the lowest energy emission wavelength at 649 nm rather than the most polar one.[92]

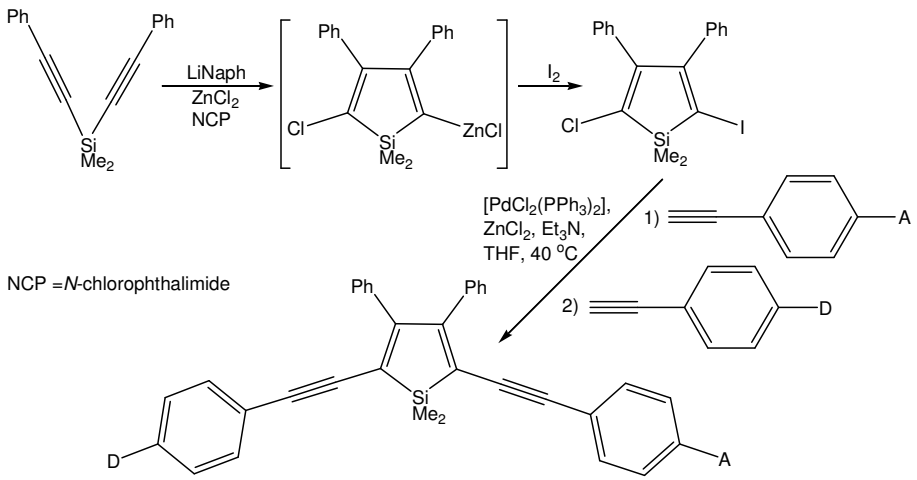

Figure 1.31: Synthesis of donor-acceptor π-conjugated siloles.[92]

1.4.2 Phospholes

The synthetic methodology for preparing phospholes was also reported in the same year as siloles.[94] Due to the fact that phospholes are not aromatic,[87] they promote delocalisation of the endocyclic π-system along the conjugated chain. At the same time, the phosphorus atom becomes versatile in terms of its reactivity. Calculations at the HF/6-31 + G*//B3LYP/6-31 + G* level show that the LUMO energy level of the parent phosphole is very close to that of the silole (LUMO: silole, 1.39 eV; phosphole, 1.50 eV), which is known as a highly electron-deficient heterocycle.[95] In other words, the interaction between the π* orbitals from the butadiene moiety and the low-lying σ* orbital from the P-R moiety in the phosphole are very similar to those of the silole as shown in **Figure 1.29**.

The absorption λ_{max} of a phosphole is dependent on the hydrogen bond donor ability (HBDA) of the solvent to the lone pair of electrons on the phosphorus atom.[95] The absorption and emission λ_{max} values of a phosphole recorded in different solvents are shown in **Table 1.3**. The HBDA influence on the emission λ_{max} is negligible. In the

absorption spectra, there is a bathochromic shift upon increasing the HBDA of the solvent.[95] For this reason, absorption and emission spectra of the phospholes should be recorded in the non-hydrogen-bonding solvent, THF.

Table 1.3: Influence of the solvent on the absorption and emission λ_{max} of phosphole.[95]

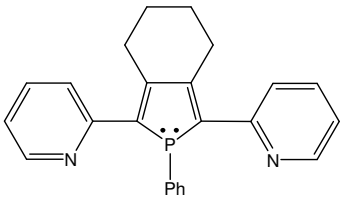

Solvents	λ_{max} ABS	λ_{max} EM
Tetrahydrofuran (THF)	390	463
Dichloromethane (DCM)	374	463
Chloroform ($CHCl_3$)	372	463
Ethanol (EtOH)	364	466

Similarly to siloles, the band in the phosphole's absorption spectrum is attributed to the $\pi \rightarrow \pi^*$ transition, which is due to the extended π-conjugated system of the phosphole. The λ_{max} value of the absorption and emission are greatly influenced by the 2,5-substituents of the phosphole ring. For example, replacing the phenyl groups (**Figure 1.32.a**) with either 2-pyridyl (**Figure 1.32.b**) or 2-thienyl (**Figure 1.32.c**) rings shifts the absorption λ_{max} from 354 nm to 390 and 412 nm, respectively.[87] This is due to the charge transfer from the 2-thienyl or 2-pyridyl substituents to the highly electron-deficient heterocycle ring of the phosphole. Calculations (**Table 1.4**) indicate that the 2-thienyl substituent stabilises the LUMO but also destabilises the HOMO; as a result, the HOMO-

LUMO gap decreases causing a red-shift in its absorption spectrum compared to the 2,5-diphenyl analogue.[95]

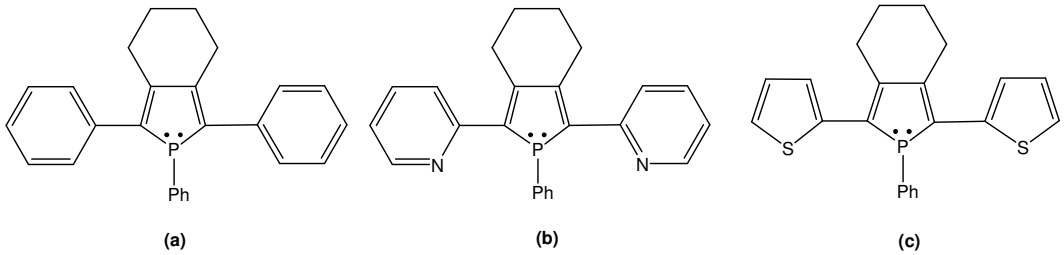

Figure 1.32: The structures of (**a**) 2,5-diphenylphosphole, (**b**) 2,5-di-2-pyridylphosphole, and (**c**) 2,5-di-2-thienylphosphole.

Table 1.4: Calculated energy levels (eV) of the HOMO and LUMO of phospholes at the HF/6-31 + G*//B3LYP/6-31 + G* level.[95]

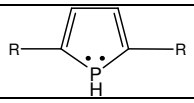	R = phenyl	R = 2-pyridyl	R = 2-thienyl
LUMO	1.24	0.97	0.96
HOMO	-7.36	-7.49	-7.17
HOMO-LUMO gap	8.60	8.46	8.13

Réau and co-workers also studied the effect of a combination of thienyl and pyridyl substituents on the absorption and emission spectra of a phosphole (**Figure 1.33**). It was found that both the absorption and emission shifted to lower energy (λ_{max}: ABS, 427 nm; EM, 570 nm) compared to either thienyl (λ_{max}: ABS, 412 nm; EM, 501 nm) or pyridyl (λ_{max}: ABS, 390 nm; EM, 463 nm) individual substituents.[96]

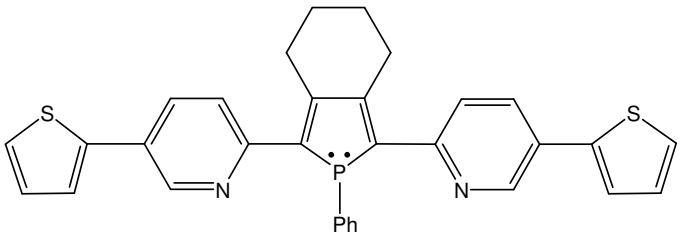

Figure 1.33: 2,5-bis(2-pyridyl-2-thienyl)phosphole.[96]

The Réau group prepared a series of polarised $P^{\delta+}=Y^{\delta-}$ phospholes (Y = Se, S, and O) in order to observe the effect on the photophysical properties of phospholes (**Figure 1.34**). Synthetically, 2,5-bis(2-thienyl)phosphole was treated with selenium, sulfur and bis(trimethylsilyl)peroxide, respectively, to give polarised $P^{\delta+}=Y^{\delta-}$ phospholes in very high yields (> 90%). For the Y = Se, S and O derivatives, a bathochromic shift of λ_{max} ABS = 11 – 22 nm, and λ_{max} EM = 46 – 55 nm was observed with respect to the 2,5-bis(2-thienyl)phosphole.[96] Increasing the electronegativity of Y leads to an increase in the bathochromic shift.

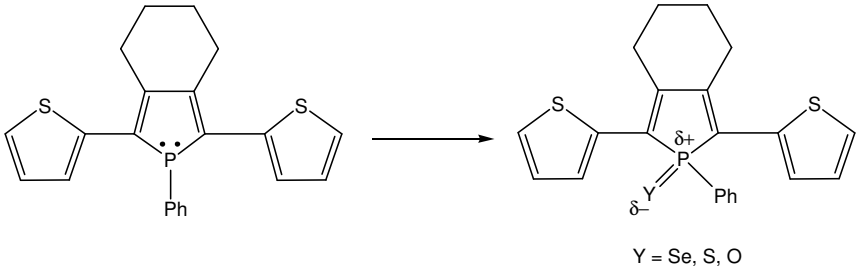

Figure 1.34: Preparation of the phospholes with polarised $P^{\delta+}=Y^{\delta-}$ (Y = Se, S, and O).[96]

Very recently, the synthesis and photophysical properties of a series of 2,5-bis(*p*-X-arylethynyl)phospholes, where X = H (**a**), NO_2 (**b**) and NMe_2 (**c**) in **Figure 1.35**, have been reported by Matano et al.[97] The λ_{max} value of both absorption and emission were bathochromically shifted to lower energy from X = NO_2 to NMe_2, because the NMe_2

substituent has a greater effect on the π-conjugative push-pull interaction when compared to the NO_2 substituent. The absorption maxima are assigned to the π → π* transition of the π-conjugated system of the 2,5-bis(*p*-X-arylethynyl)phospholes. The λ_{max} values for fluorescence were found at 449 nm for X = H, 499 nm for X = NO_2 and 518 nm for X = NMe_2, with Φ_f of 0.10, 0.09 and 0.13, respectively.

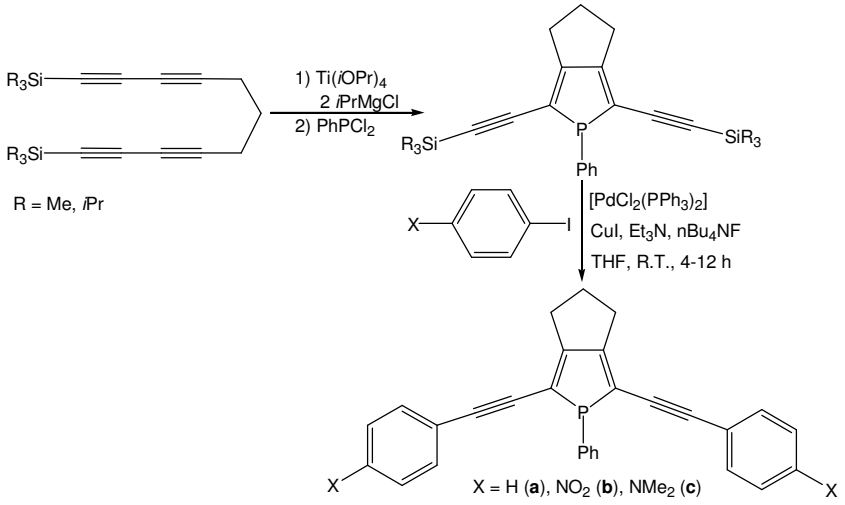

Figure 1.35: Synthetic route to 2,5-bis(*p*-X-arylethynyl)phospholes.[97]

1.4.3 Thiophenes

As a π-conjugated system, thiophenes show interesting electronic and luminescent properties.[98-101] In 2007, Marder et al.[101] reported the photophysical properties of a series of 2,5-bis(phenylethynyl)thiophenes (BPETs) (**Figure 1.36**). Compounds with substituents at the *para*-position of the phenyl ring ranging from the strong electron withdrawing group, NO_2, to the strong electron donating group, NMe_2, were prepared in good yields using standard Sonogashira coupling reactions.

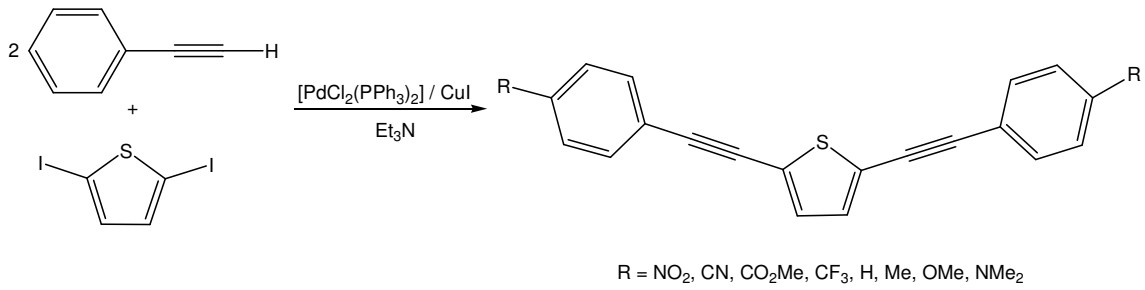

Figure 1.36: Synthesis of BPETs.[101]

Both electron withdrawing and electron donating substituents at the *para*-position of the phenyl ring cause a bathochromic shift compared to the parent (R = H) compound. The greatest red-shift was observed with the strongest electron withdrawing and electron donating substituents in the series, from 350 nm for the parent to 386 nm (R = NMe_2) and 387 nm (R = NO_2) in the absorption spectra, and from 382 nm for the parent to 434 nm (R = NMe_2) and 435 nm (R = NO_2) in the emission spectra.[101] The reason for this is due to the fact that electron donating groups raise the HOMO more than the LUMO, while electron withdrawing groups stabilise the LUMO more than the HOMO and, as a result, both significantly reduce the HOMO-LUMO gap. Lower emission quantum yields of BPETs were observed compared to the 1,4-bis(arylethynyl)benzene (BPEB) and 9,10-bis(arylethynyl)anthracene (BPEA) analogues, because the excited singlet state in BPETs undergoes relatively rapid ISC to the non-emissive (at room temperature) triplet excited state, T_1. The presence of sulfur as the heteroatom in the BPETs is believed to facilitate the ISC.[101]

1.5 Rhodacyclopentadienes: the chemistry and photophysical properties

The main group heterocycles (EC_4) are able to exhibit interesting luminescent properties with the $\pi \rightarrow \pi^*$ transitions. Similar to those transition metal analogues such as $[Ir(ppy)_3]$, their emission colours can also be tuned either by attaching a different ligand at the centre atom (E) or using different electron withdrawing and electron donating substituents at the *para*-position of the phenyl rings. However, unlike the transition metal analogues, the EC_4 analogues could not phosphorescence because the E atom does not offer a highly efficiency SOC like the 2nd and 3rd row transition metals do. Therefore, it is very interesting to investigate the photophysical properties of the **e-**type metallacyclopentadiene in **Figure 1.27**, which is structurally-related to the EC_4 analogues. So far until now, only one publication was found to report briefly about the luminescent properties of the **e-**type metallacyclopentadiene called rhodacyclopentadiene from Marder and Rourke et al.[102]

The first rhodacyclopentadiene was reported by Mague and Wilkinson in 1968 when they synthesised $[RhCl(SbPh_3)_2C_4(CF_3)_4]$ by reaction of $[RhCl(SbPh_3)_3]$ with two equivalents of CF_3-C≡C-CF_3 (**Figure 1.37**). The rhodacyclopentadiene's identity was then confirmed by X-ray crystallography a year later.[103, 104]

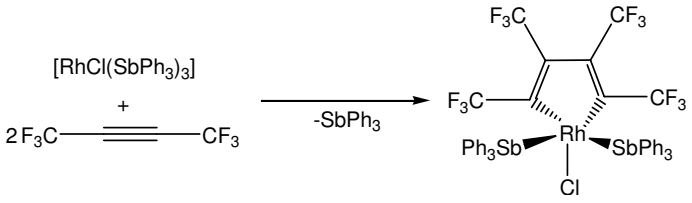

Figure 1.37: Synthesis of the five coordinate rhodacyclopentadiene complex, $[RhCl(SbPh_3)_2C_4(CF_3)_4]$.[103, 104]

Two years later, Mague reported a rhodacyclopentadiene complex (**Figure 1.38**).[105] $[RhCl(CO)(AsMe_3)_2]$ reacted CF_3-C≡C-CF_3 to give an initial complex, $[RhCl(CO)(AsMe_3)_2C_4(CF_3)_4]$, then, the CO group was removed in refluxing wet benzene to form $[RhCl(H_2O)(AsMe_3)_2C_4(CF_3)_4]$. The structure of the product was confirmed by X-ray crystallography in 1973.[106] Mague noted that the C_2-C_3 bond length is significantly longer than C_1-C_2 and C_3-C_4 bond lengths in the heterocycle ring, resembling a *cis*-1,3-butadienylene moiety.[105, 106]

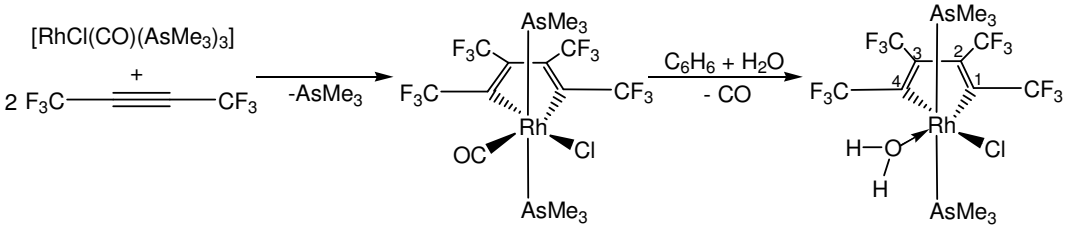

Figure 1.38: Preparation of an octahedral rhodacyclopentadiene with a coordinated water molecule.[105]

In 1972, Müller and co-workers reacted $[RhCl(PPh_3)_3]$ with 2,2'-bis(arylethynyl)biphenyl to form a rhodacyclopentadiene complex (**Figure 1.39.a**) and a valence isomeric cyclobutadienylrhodium complex (**Figure 1.39.b**).[107] Then, adding one equivalent of alkyne to the rhodacyclopentadiene complex led to the formation of a triphenylene derivative (**Figure 1.39.c**).[107]

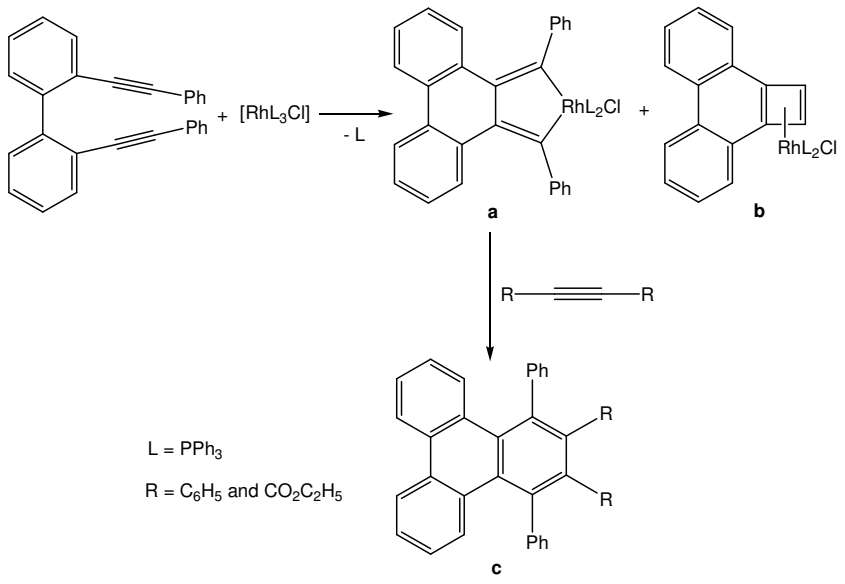

Figure 1.39: Reaction of $[RhClL_3]$ with a di-alkyne compound to form rhodacyclopentadiene and cyclobutadienylrhodium complexes.[107]

In 2001, Marder and Rourke et al.[102] developed a high yield, one-pot, regiospecific synthesis of a luminescent rhodacyclopentadiene from two equivalents of 1,4-bis(*p*-tolyl)buta-1,3-diyne with $[Rh(C{\equiv}C\text{-}SiMe_3)(PMe_3)_4]$. The chemistry of rhodacyclopentadienes in the Marder group was developed further when Ward[108] synthesised a series of six-coordinate rhodacyclopentadienes with different σ-donor ligands attached to the rhodium centre; the synthesis with $Me_3SiC{\equiv}C$- (TMSE) as the σ-donor ligand is shown in **Figure 1.40**.

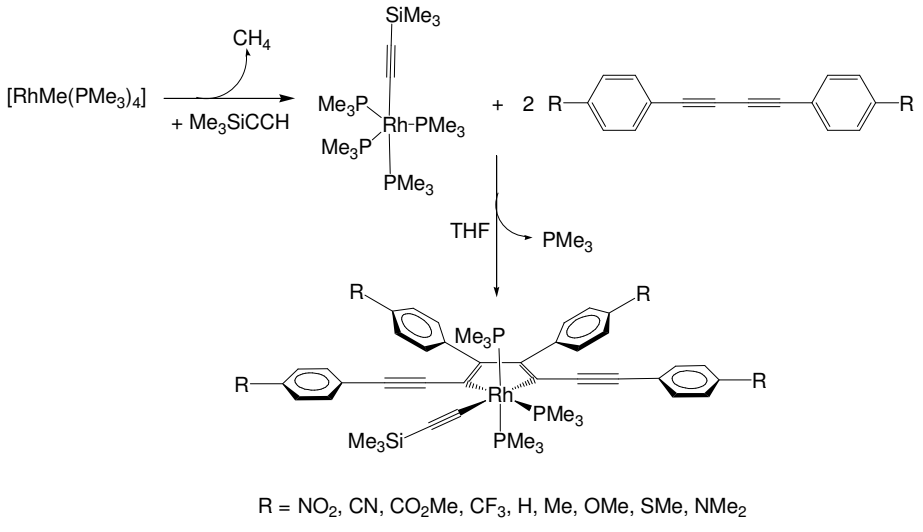

Figure 1.40: The synthesis of rhodacyclopentadiene complexes with TMSE- as the σ-donor ligand.[108]

All of the rhodacyclopentadienes in **Figure 1.40** have been characterised using spectroscopic techniques and several structures have been confirmed by X-ray crystallography. Besides Ward, van Leeuwen[109] in the Marder group also synthesised a series of rhodacyclopentadienes with 4-[4-(*N*,*N*-di-*n*-hexylamino)phenylethynyl]phenyl ethynyl- (-C≡C-C_6H_4-C≡C-C_6H_4-*p*-$NHex_2$) as the alkynyl ligand in order to investigate the effect of a long conjugated carbon chain on the photophysical properties of rhodacyclopentadienes.

The mechanism of rhodacyclopentadiene formation was also studied by Ward.[108] He found that the intermediate π-complexes formed very quickly when one equivalent of diarylbutadiyne was added to the [$RhMe(PMe_3)_4$] in THF. The formation of the intermediate π-complex is represented in **Step 1 – 3** in **Figure 1.41**.

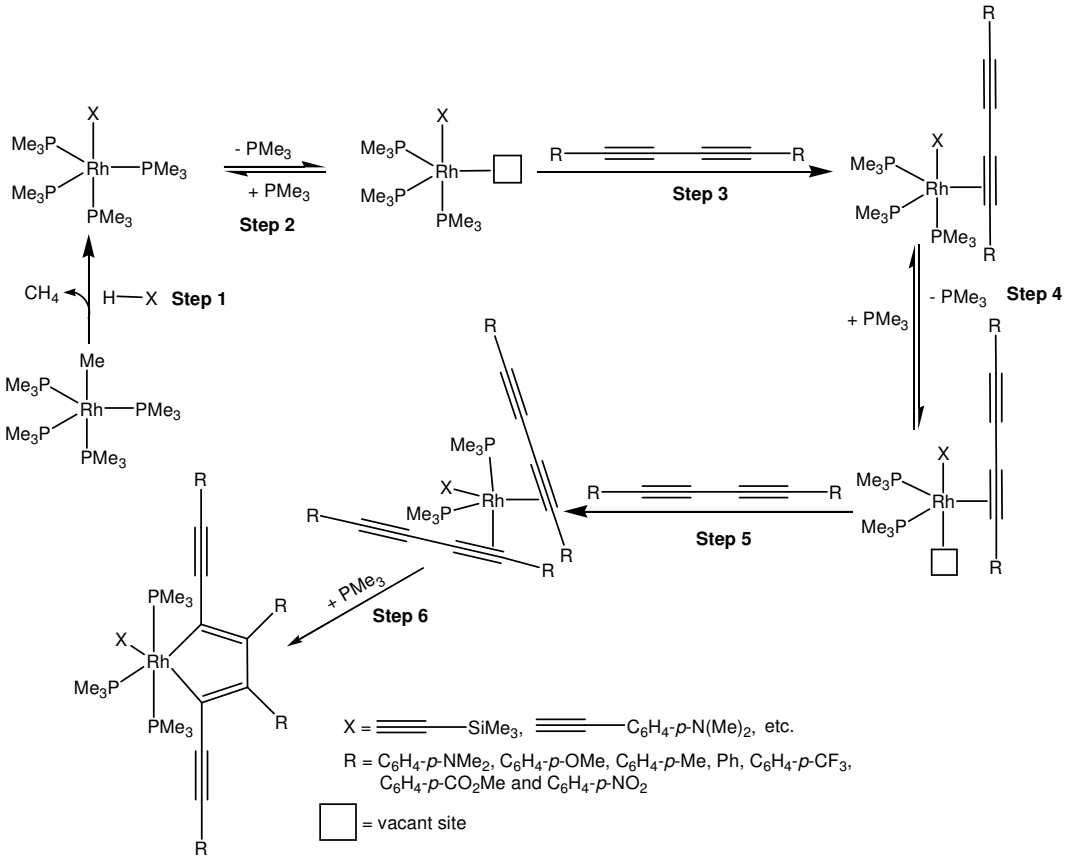

Figure 1.41: Proposed rhodacyclopentadiene formation mechanism.[108]

In order to form the metallacycle ring, one equivalent of PMe_3 must dissociate from the intermediate π-complex before it can bind the second butadiyne (**Step 4**) and form a bis(π-complex) (**Step 5**). The bis(π-complex) then undergoes a reductive coupling (**Step 6**) to form a five-membered metallacycle ring. The remaining vacant site at the rhodium centre is then filled by the PMe_3 which dissociated in **Step 4**, giving the six-coordinate rhodacyclopentadiene. **Step 2** and **4** are reversible processes, where the concentration of PMe_3 is the key to facilitate the reaction to move forward. Therefore, removal of PMe_3 during the reaction is necessary.

1.5.1 The photophysical properties

The photophysical properties of the rhodacyclopentadienes have also been studied by Ward[108] and van Leeuvan.[109] Photophysical data of the TMSE-rhodacyclopentadienes are listed in **Table 1.5**, and their absorption and emission spectra are shown in **Figure 1.42**.

Table 1.5: Summary of photophysical data for the TMSE-2,5-bis(*p*-R-arylethynyl)-rhodacyclopentadienes (see **Figure 1.40**) in toluene solution at room temperature.[108]

R group	λ_{max} ABS (nm)	ε (mol^{-1} cm^{-1} dm^3)	λ_{max} EM (nm)	Stokes shift (cm^{-1})	Φ	τ (ns)
H	453	26000	496	1910	0.15	0.87
SMe	468	35000	515	1950	0.10	0.71
CO_2Me	485	21000	536	1960	0.16	0.98
NO_2	517	22000	590	2390	0.18	1.21

The bathochromic shift of λ_{max} for both absorption and emission are dependent on the electron withdrawing and electron donating substituents at the *para*-position of the phenyl ring. However, electron withdrawing substituents have a greater effect on the bathochromic shift than electron donating substituents. The stronger the electron-withdrawing group, the greater the bathochromic shift.[108]

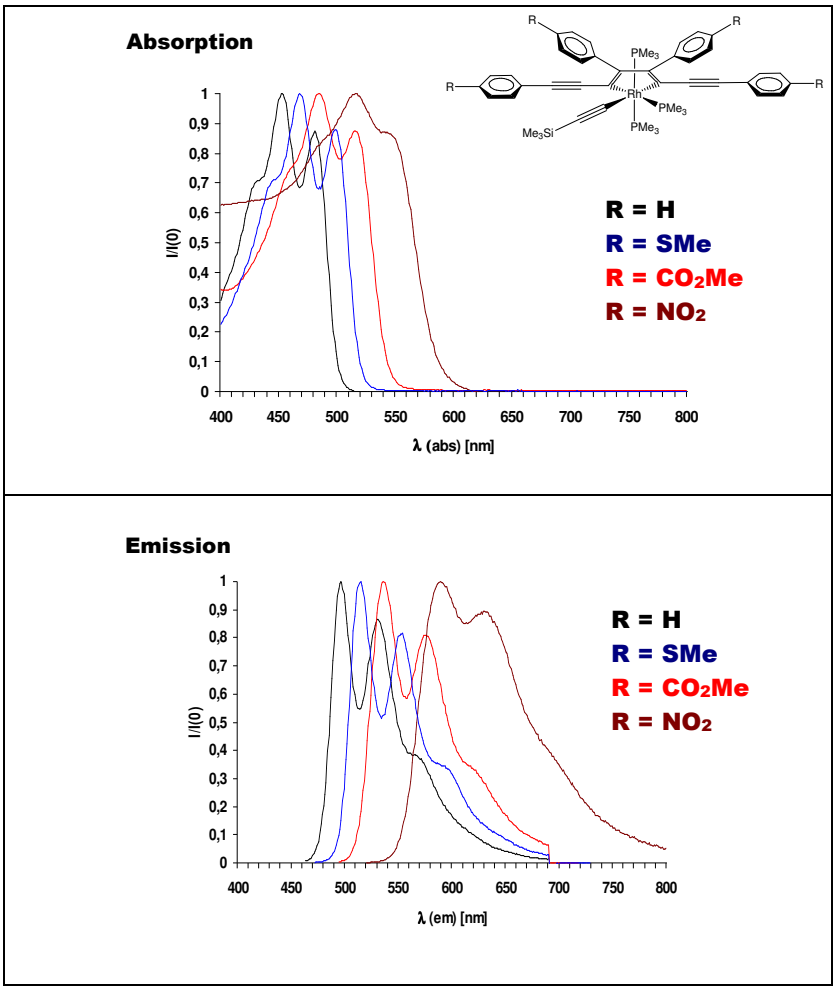

Figure 1.42: Absorption (top) and emission (bottom) spectra of the TMSE-rhodacyclopentadienes.[108]

Comparing the emission lifetimes of the rhodacyclopentadienes to the lifetimes of $[Ru(bpy)_3]^{2+}$, $[Ir(ppy)_3]$ and $[Rh(bpy)_3]^{3+}$ analogues, we note that the rhodacyclopentadienes have the shortest lifetimes. The single decay component lifetimes in the nanosecond range indicate that the emissions occur purely from the singlet excited state. Fluorescence is rarely observed in organometallics with 4d/5d transition metal centres, because the singlet excited states are too short-lived, due to the strong SOC of the metal that can facilitate ISC to form the triplet excited states. As mentioned in **section**

1.3.1, the singlet lifetime of $[Ru(bpy)_3]^{2+}$ is only $\leq$ 10 ps,[51] but the singlet lifetimes of rhodacyclopentadienes are on the nanosecond timescale, which is a long-lived singlet emission lifetime and absolutely unexpected for organometallic complexes. Indeed, these unusual results for the rhodacyclopentadienes have become a driving force for this project to investigate further their photophysical behaviour.

1.6 Objectives

The main objective of this project was to explore as well as to understand the photophysical behaviour of the rhodacyclopentadienes. Many photophysical experiments such as time-resolved infrared (TRIR) measurements were carried out in order to understand the structure-properties relationship of the rhodacyclopentadienes.

This project also aimed to develop synthetic methodology for the preparation of novel rhodacyclopentadienes. For example, we have developed new synthetic methodology for the preparation of η^2-benzoato- (**Figure 1.43.a**) and acetylacetonato- (acac-) (**Figure 1.43.b**) rhodacyclopentadienes. The reason for using η^2-benzoato- and acac- ligands is to increase the Rh participation in the excited state by destabilising the Rh d-orbitals since the η^2-benzoato- and acac- ligands are strong σ- and π- donors. These two series of rhodacyclopentadienes have been spectroscopically characterised and their photophysical data were collected and discussed in detail in **Chapter 3**.

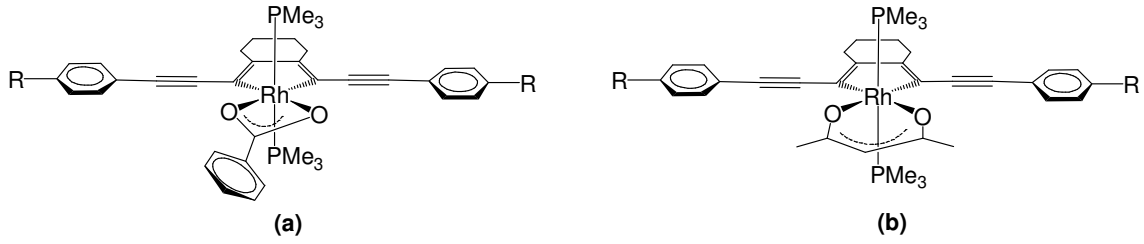

Figure 1.43: Rhodacyclopentadienes with (**a**) η^2-benzoato-, and (**b**) acac- ligands.

References:

1. A. Gilbert and J. Baggott, *Essentials of Molecular Photochemistry*, 1st edn., Blackwell Science, Oxford, 1991.
2. J. R. Lakowicz, *Principles of Fluorescence Spectroscopy*, 2nd edn., Kluwer Academic / Plenum Publishers, New York, 1999.
3. M. Kasha, *Disc. Faraday Soc.*, 1950, **9**, 14.
4. N. J. Turro, *Modern Molecular Photochemistry*, 1st edn., University Science Books, Sausalito, 1991.
5. W. Siebrand, *J. Chem. Phys.*, 1967, **47**, 2411.
6. J. S. Wilson, N. Chawdhury, M. R. A. Al-Mandhary, M. Younus, M. S. Khan, P. R. Raithby, A. Köhler and R. H. Friend, *J. Am. Chem. Soc.*, 2001, **123**, 9412.
7. G. W. Robinson and R. P. Frosch, *J. Chem. Phys.*, 1963, **38**, 1187.
8. S. K. Lower and M. A. El-Sayed, *Chem. Rev.*, 1966, **66**, 199.
9. M. Montalti, A. Credi, L. Prodi and M. T. Gandolfi, *Handbook of Photochemistry*, 3rd edn., CRC Taylor & Francis, Boca Raton, 2006.
10. K. A. King, P. J. Spellane and R. J. Watts, *J. Am. Chem. Soc.*, 1985, **107**, 1431.
11. M. A. Baldo, M. E. Thompson and S. R. Forest, *Nature*, 2000, **403**, 750.
12. A. Juris, V. Balzani, F. Barigelletti, S. Campagna, P. Belser and A. von Zelewsky, *Coord. Chem. Rev.*, 1988, **84**, 85.
13. J. Slinker, D. Bernards, P. L. Houston, H. D. Abruna, S. Bernhard and G. G. Malliaras, *Chem. Commun.*, 2003, 2392.
14. M. A. Baldo, D. F. O'Brien, Y. You, A. Shoustikov, S. Sibley, M. E. Thompson and S. R. Forrest, *Nature*, 1998, **395**, 151.
15. E. Holder, B. M. W. Langeveld and U. S. Schubert, *Adv. Mater.*, 2005, **17**, 1109.
16. D. Beljonne, Z. Shuai, G. Pourtois and J. L. Bredas, *J. Phys. Chem. A*, 2001, **105**, 3899.
17. J. B. Birks, *Photochemistry of Aromatic Molecules*, John Wiley, New York, 1970.
18. C. Schweitzer and R. Schmidt, *Chem. Rev.*, 2003, **103**, 1685.
19. C. G. Hübner, A. Renn, I. Renge and U. P. Wild, *J. Chem. Phys.*, 2001, **115**, 9619.
20. T. Förster, *Ann. Physik*, 1948, **2**, 55.
21. T. Förster, *Disc. Faraday Soc.*, 1959, **27**, 7.
22. R. C. Evans, P. Douglas and C. J. Winscom, *Coord. Chem. Rev.*, 2006, **250**, 2093.
23. B. W. D'Andrade and S. R. Forrest, *Adv. Mater.*, 2004, **16**, 1585.
24. E. Polikarpov and M. E. Thompson, *Mater. Matters*, 2007, **2**, 21.
25. K. K.-W. Lo, C.-K. Chung, T. K.-M. Lee, L.-K. Lui, K. H.-K. Tsang and N. Zhu, *Inorg. Chem.*, 2003, **42**, 6886.
26. K. K.-W. Lo, W.-K. Hui, C.-K. Chung, K. H.-K. Tsang, D. C.-M. Ng, N. Zhu and K.-K. Cheung, *Coord. Chem. Rev.*, 2005, **249**, 1434.
27. B. S. Murray, E. J. New, R. Pal and D. Parker, *Org. Biomol. Chem.*, 2008, **6**, 2085.
28. J. K. Borchardt, *Mater. Today*, 2004, **7**, 42.
29. S. Sibley, M. E. Thompson, P. E. Burrows and S. R. Forrest, *Electroluminescence in Molecular Materials* in *Optoelectronic Properties of Inorganic Compounds*,

eds. D. M. Roundhill and J. P. Fackler Jr., Plenum Press, New York, 1st edn., 1999, pp. 29
30. A. P. Kulkarni, C. J. Tonzola, A. Babel and S. A. Jenekhe, *Chem. Mater.*, 2004, **16**, 4556.
31. C. W. Tang and S. A. Van Slyke, *Appl. Phys. Lett.*, 1987, **51**, 913.
32. H. Yersin, *Top. Curr. Chem.*, 2004, **24**, 1.
33. R. Pal and D. Parker, *Chem. Commun.*, 2007, 474.
34. D. Lancet and I. Pecht, *Biochem.*, 1977, **16**, 5150.
35. R. Sjöback, J. Nygren and M. Kubista, *Spectrochim. Acta A*, 1995, **51**, L7.
36. P. G. Sammes and G. Yahioglu, *Nat. Prod. Rep.*, 1996, **13**, 1.
37. K. K.-W. Lo, W.-K. Hui, C.-K. Chung, K. H.-K. Tsang, T. K.-M. Lee, C.-K. Li, J. S.-Y. Lau and D. C.-M. Ng, *Coord. Chem. Rev.*, 2006, **250**, 1724.
38. K. K.-W. Lo, D. C.-M. Ng and C.-K. Chung, *Organometallics*, 2001, **20**, 4999.
39. K. K.-W. Lo, D. C.-M. Ng, W.-K. Hui and K.-K. Cheung, *J. Chem. Soc., Dalton Trans.*, 2001, 2634.
40. C. P. Montgomery, E. J. New, D. Parker and R. D. Peacock, *Chem. Commun.*, 2008, 4261.
41. F. Kielar, A. Congreve, G.-L. Law, E. J. New, D. Parker, K.-L. Wong, P. Castreňo and J. de Mendoza, *Chem. Commun.*, 2008, 2435.
42. K. A. Belmore, R. A. Vanderpool, J. C. Tsai, M. A. Khan and K. M. Nicholas, *J. Am. Chem. Soc.*, 1988, **110**, 2004.
43. N. D. Silavwe, A. S. Goldman, R. Ritter and D. R. Tyler, *Inorg. Chem.*, 1989, **28**, 1231.
44. R. Gao, D. G. Ho, B. Hernandez, M. Selke, D. Murphy, P. I. Djurovich and M. E. Thompson, *J. Am. Chem. Soc.*, 2002, **124**, 14828.
45. G. Di Marco, M. Lanza, A. Mamo, I. Stefio, C. Di Pietro, G. Romeo and S. Campagna, *Anal. Chem.*, 1998, **70**, 5019.
46. M. H. Keefe, K. D. Benkstein and J. T. Hupp, *Coord. Chem. Rev.*, 2000, **205**, 201.
47. M. C. DeRosa, D. J. Hodgson, G. D. Enright, B. Dawson, C. E. B. Evans and R. J. Crutchley, *J. Am. Chem. Soc.*, 2004, **126**, 7619.
48. H. Yersin, *Highly Efficient OLEDs with Phosphorescent Materials*, Wiley-VCH Verlag Gmbh & Co. Kgaa, Weinheim, 2008.
49. D. F. Shriver and P. W. Atkins, *Inorganic Chemistry*, 3rd edn., Oxford University Press, Oxford, 2001.
50. H. Gaffney and A. W. Adamson, *J. Am. Chem. Soc.*, 1972, **94**, 8238.
51. F. E. Lytle and D. M. Hercules, *J. Am. Chem. Soc.*, 1969, **91**, 253.
52. D. M. Klassen and G. A. Crosby, *J. Chem. Phys.*, 1968, **48**, 1853.
53. R. Bensasson, C. Salet and V. Balzani, *J. Am. Chem. Soc.*, 1976, **98**, 3722.
54. J. N. Demas and G. A. Crosby, *J. Am. Chem. Soc.*, 1971, **93**, 2841.
55. A. Cannizzo, F. van Mourik, W. Gawelda, G. Zgrablic, C. Bressler and M. Chergui, *Angew. Chem. Int. Ed.*, 2006, **45**, 3174.
56. S. D. Bergman, I. Goldberg, A. Barbieri, F. Barigelletti and M. Kol, *Inorg. Chem.*, 2004, **43**, 2355.
57. S. Campagna, F. Puntoriero, F. Nastasi, G. Bergamini and V. Balzani, *Top. Curr. Chem.*, 2007, **280**, 117.

58. A. Bouskila, B. Drahi, E. Amouyal, I. Sasaki and A. Gaudemer, *J. Photochem. Photobiol. A*, 2004, **163**, 381.
59. Y. You and S. Y. Park, *Dalton Trans.*, 2009, 1267.
60. P. J. Hay, *J. Phys. Chem. A*, 2002, **106**, 1634.
61. K. C. Tang, K. L. Liu and I. C. Chen, *Chem. Phys. Lett.*, 2004, **386**, 437.
62. G. J. Hedley, A. Ruseckas and I. D. W. Samuel, *Chem. Phys. Lett.*, 2008, **450**, 292.
63. K. Dedeian, J. Shi, N. Shepherd, E. Forsythe and D. C. Morton, *Inorg. Chem.*, 2005, **44**, 4445.
64. W. Holzer, A. Penzkofer and T. Tsuboi, *Chem. Phys.*, 2005, **308**, 93.
65. G. Zhou, C.-L. Ho, W.-Y. Wong, Q. Wang, D. Ma, L. Wang, Z. Lin, T. B. Marder and A. Beeby, *Adv. Funct. Mater.*, 2008, **18**, 499.
66. M. Tavasli, S. Bettington, M. R. Bryce, H. A. A. Attar, F. B. Dias, S. King and A. P. Monkman, *J. Mater. Chem.*, 2005, **15**, 4963.
67. S. Lamansky, P. Djurovich, D. Murphy, F. Abdel-Razzaq, H.-E. Lee, C. Adachi, P. E. Burrows, S. R. Forrest and M. E. Thompson, *J. Am. Chem. Soc.*, 2001, **123**, 4304.
68. S.-C. Lo, C. P. Shipley, R. N. Bera, R. E. Harding, A. R. Cowley, P. L. Burn and I. D. W. Samuel, *Chem. Mater.*, 2006, **18**, 5119.
69. T. Sajoto, P. I. Djurovich, A.Tamayo, M. Yousufuddin, R. Bau, M. E. Thompson, R. J. Holmes and S. R. Forrest, *Inorg. Chem.*, 2005, **44**, 7992.
70. C. S. K. Mak, A. Hayer, S. I. Pascu, S. E. Watkins, A. B. Holmes, A. Köhler and R. H. Friend, *Chem. Commun.*, 2005, 4708.
71. K. Ono, M. Joho, K. Saito, M. Tomura, Y. Matsushita, S. Naka, H. Okada and H. Onnagawa, *Eur. J. Inorg. Chem.*, 2006, 3676.
72. K. Dedeian, J. Shi, E. Forsythe, D. C. Morton and P. Y. Zavalij, *Inorg. Chem.*, 2006, **46**, 1603.
73. M. K. Nazeeruddin, R. Humphry-Baker, D. Berner, S. Rivier, L. Zuppiroli and M. Graetzel, *J. Am. Chem. Soc.*, 2003, **125**, 8790.
74. M. T. Indelli, C. Chiorboli and F. Scandola, *Top. Curr. Chem.*, 2007, **280**, 215.
75. H. Yersin, W. Humbs and J. Strasser, *Coord. Chem. Rev.*, 1997, **159**, 325.
76. M. Nishizawa, T. M. Suzuki, S. Sprouse, R. J. Watts and P. C. Ford, *Inorg. Chem.*, 1984, **23**, 1837.
77. K. Nozaki, K. Takamori, Y. Nakatsugawa and T. Ohno, *Inorg. Chem.*, 2006, **45**, 6161.
78. D. H. W. Carstens and G. A. Crosby, *J. Mol. Spectrosc.*, 1970, **34**, 113.
79. M. T. Indelli, A. Carioli and F. Scandola, *J. Phys. Chem.*, 1984, **88**, 2685.
80. M. Maestri, D. Sandrini, V. Balzani, U. Maeder and A. von Zelewsky, *Inorg. Chem.*, 1987, **26**, 1323.
81. M. G. Colombo, T. C. Brunold, T. Riedener, H. U. Güdel, M. Förtsch and H.-B. Bürgi, *Inorg. Chem.*, 1994, **33**, 545.
82. A. Morneau, B. T. Donovan-Merkert and W. E. Geiger, *Inorg. Chim. Acta*, 2000, **300-302**, 96.
83. F. Hartl, P. Rosa, L. Ricard, P. Le Floch and S. Záliš, *Coord. Chem. Rev.*, 2007, **251**, 557.
84. S. D. Ittel, L. K. Johnson and M. Brookhart, *Chem. Rev.*, 2000, **100**, 1169.

85. E. H. Braye, W. Hübel and I. Caplier, *J. Am. Chem. Soc.*, 1961, **83**, 4406.
86. J. Lee, Q.-D. Liu, D.-R. Bai, Y. Kang, Y. Tao and S. Wang, *Organometallics*, 2004, **23**, 6205.
87. M. Hissler, P. W. Dyer and R. Réau, *Coord. Chem. Rev.*, 2003, **244**, 1.
88. K. Tamao and S. Yamaguchi, *J. Organometal. Chem.*, 2000, **611**, 5.
89. S. Yamaguchi and K. Tamao, *J. Chem. Soc., Dalton Trans.*, 1998, 3693.
90. B. Z. Tang, X. Zhan, G. Yu, P. P. S. Lee, Y. Liu and D. Zhu, *J. Mater. Chem.*, 2001, **11**, 2974.
91. S. Yamaguchi, R.-Z. Jin and K. Tamao, *J. Organometal. Chem.*, 1998, **559**, 73.
92. A. J. Boydston, Y. Yin and B. L. Pagenkopf, *J. Am. Chem. Soc.*, 2004, **126**, 3724.
93. S. Yamaguchi, R.-Z. Jin, K. Tamao and M. Shiro, *Organometallics*, 1997, **16**, 2230.
94. F. C. Leavitt, T. A. Manuel and F. Johnson, *J. Am. Chem. Soc.*, 1959, **81**, 3163.
95. C. Hay, M. Hissler, C. Fischmeister, J. Rault-Berthelot, L. Toupet, L. Nyulászi and R. Réau, *Chem. Eur. J.*, 2001, **7**, 4222.
96. C. Hay, C. Fischmeister, M. Hissler, L. Toupet and R. Réau, *Angew. Chem. Int. Ed.*, 2000, **39**, 1812.
97. Y. Matano, M. Nakashima and H. Imahori, *Angew. Chem. Int. Ed.*, 2009, **48**, 4002.
98. J. G. Rodriguez, J. Esquivias, A. Lafuente and L. Rubio, *Tetrahedron*, 2006, **62**, 3112.
99. T. Yasuda, T. Imase, Y. Nakamura and T. Yamamoto, *Macromolecules*, 2005, **38**, 4687.
100. S.-S. Sun and A. J. Lees, *J. Am. Chem. Soc.*, 2000, **122**, 8956.
101. J. S. Siddle, R. M. Ward, J. C. Collings, S. R. Rutter, L. Porrés, L. Applegarth, A. Beeby, A. S. Batsanov, A. L. Thompson, J. A. K. Howard, A. Boucekkine, K. Costuas, J.-F. Halet and T. B. Marder, *New J. Chem.*, 2007, **31**, 841.
102. J. P. Rourke, A. S. Batsanov, J. A. K. Howard and T. B. Marder, *Chem. Commun.*, 2001, 2626.
103. J. T. Mague, *J. Am. Chem. Soc.*, 1969, **91**, 3983.
104. J. T. Mague and G. Wilkinson, *Inorg. Chem.*, 1968, **7**, 542.
105. J. T. Mague, *J. Am. Chem. Soc.*, 1971, **93**, 3550.
106. J. T. Mague, *Inorg. Chem.*, 1973, **12**, 2649.
107. E. Müller, R. Thomas and G. Zountsas, *Liebigs Ann. Chem.*, 1972, **758**, 16.
108. R. M. Ward, *Diethynylrhodacyclopentadienes: A New Class of Luminescent Organometallics*, Ph.D. Thesis, Durham University, 2007.
109. M. van Leeuwen, *The Synthesis and Properties of Rhodacyclopentadienes*, M. Chem. Fourth-Year Project Report, Durham University, 2006.

Chapter 2

The synthesis and characterisation of butadiynes and 1,3,9,11-dodecatetraynes

2.1 Introduction

2.1.1 Introduction to butadiynes

Butadiynes and 1,3,9,11-dodecatetraynes served as the important starting materials for the synthesis of the rhodacyclopentadienes (**Figure 1.40** and **1.41**). Therefore, this chapter will discuss the chemistry, syntheses and characterisations of the butadiynes and novel 1,3,9,11-dodecatetraynes.

Butadiynes contain the -C≡C-C≡C- moiety and they are present in a variety of natural products. Many of these have been studied with regard to their biological activities.[1, 2] For example, the butadiyne-containing natural products shown in **Figure 2.1** have been examined with regard to their anti-bacterial activities (**Figure 2.1.a** and **Figure 2.1.b**) by Gibbons et al. in 2004,[3, 4] and their anti-cancer properties (**Figure 2.1.c**) by Kim and co-workers in 1989.[2]

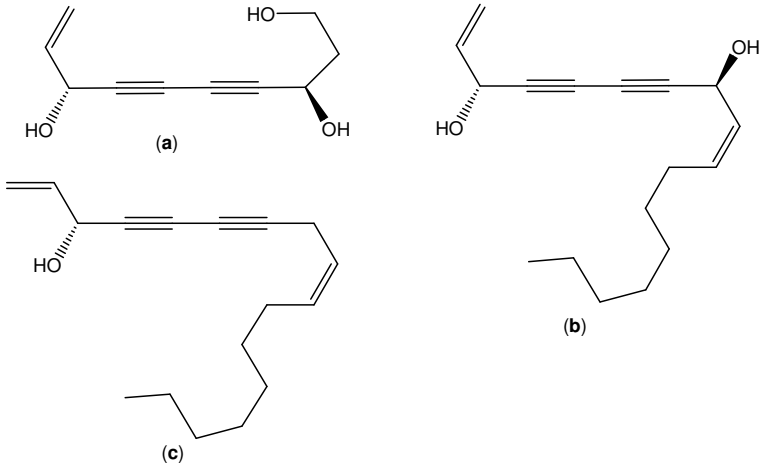

Figure 2.1: Butadiyne containing natural products.[2-4]

In addition, butadiyne derivatives can be highly toxic. For example, cicutoxin, which is shown in **Figure 2.2**, is a highly poisonous butadiyne that can be found in water hemlock

(*Cicuta virosa*). Cicutoxin can cause nausea, emesis and abdominal pain in humans and subsequently lead to death.[5]

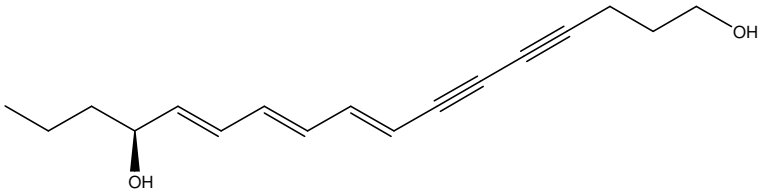

Figure 2.2: Cicutoxin.[5]

Several researchers are also interested in the electronic properties, liquid crystal phase behaviour[6-8] and non-linear optical properties[9-11] of rigid-rod conjugated butadiynes. However, information in the literature regarding the photophysical properties of butadiynes remains rare. In 2003, Kang and co-workers reported the luminescent properties of a butadiyne, which is shown in **Figure 2.3.a**.[12] Its absorption λ_{max} value is 356 nm, which is attributed to the $\pi \rightarrow \pi^*$ transition, whereas its emission λ_{max} value is 405 nm, with a fluorescence quantum yield of 0.31 at room temperature. Interestingly, a weak phosphorescent emission (λ_{max} = 561 nm) was also observed at 77 K with a lifetime of 550 μs. On the other hand, the authors also reported the luminescence properties of the tolan-based compound for comparison purposes (**Figure 2.3.b**). They found that increasing the number of C≡C bonds in the structure causes a red-shift of the λ_{max} values in both absorption and emission.[12]

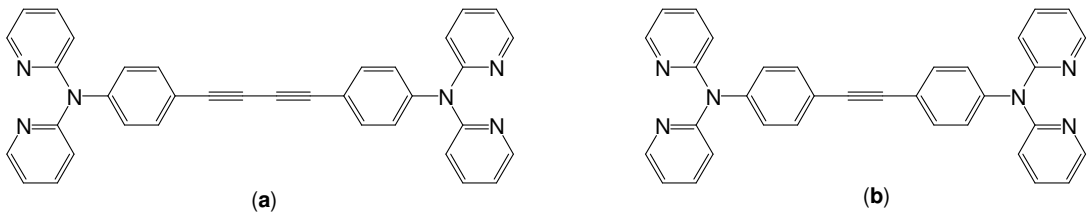

Figure 2.3: Luminescent π-conjugated organic compounds.[12]

Ward investigated the photophysical properties of some 1,4-bis(*p*-R-phenyl)-1,3-butadiynes (**Figure 2.4**) in his Ph.D. studies.[13] His findings were consistent with Kang et al., in which both absorption and emission λ_{max} values of extended, conjugated butadiynes where R = 3,5-$(CF_3)_2$-C_6H_3-C≡C (**Figure 2.4.a**) and 4-(*n*-Hex)$_2$N-C_6H_4-C≡C (**Figure 2.4.b**) are shifted to lower energy compared to their shorter analogues. In addition, Ward also found that the extended conjugated butadiynes have higher quantum yields than their shorter analogues.[12, 13]

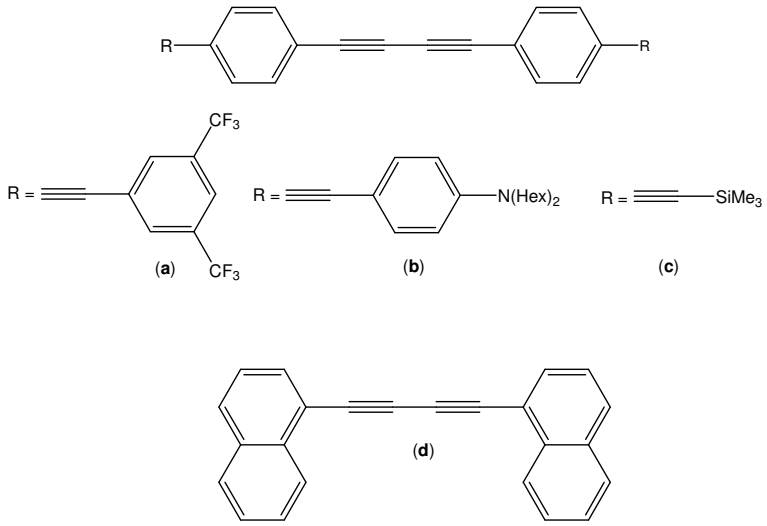

Figure 2.4: π-conjugated butadiynes synthesised by Ward.[13]

2.1.2 Coupling chemistry in butadiyne synthesis

Oxidative homo-couplings of terminal alkynes have been known since 1869, when Glaser homo-coupled two equivalents of phenylacetylene to produce a butadiyne in the presence of EtOH, NH_4OH, CuCl and oxygen (**Figure 2.5**).[14, 15]

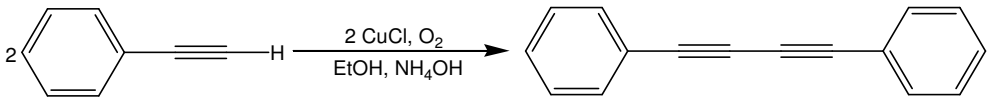

Figure 2.5: The first acetylenic coupling reported by Glaser.[14, 15]

Since that time, this coupling chemistry has been extensively developed due to its ability to form a new carbon-carbon bond by the coupling of two sp-hybridised carbons. In 1959, Eglinton and Galbraith reported an oxidative homo-coupling reaction using $Cu^{(II)}$ as the oxidising agent to produce butadiynes in the presence of water and oxygen. The reaction worked well with water-soluble ethynyl compounds such as $HC{\equiv}CMe_2OH$, but for water-insoluble compounds, the reactions were very slow and required excess $Cu^{(II)}$.[16] Then, in 1962, Hay[17] found that most $Cu^{(II)}$ salts (except $Cu^{(II)}$ carboxylates) are ineffective in the coupling reactions. Indeed, Hay noticed that $Cu^{(I)}$ salts can perform much better than $Cu^{(II)}$ salts, and he suggested that the use of CuCl and the bidentate amine ligand, *N*,*N*,*N*',*N*'-tetramethylethylenediamine, is best for homo-coupling compared to the other two conditions [(i) $Cu(OAc)_2$ + pyridine and (ii) CuCl + pyridine] in his study.[17]

Catalytic systems based on palladium and copper have been developed, which can help to complete the reaction in a shorter time. For example, Liu and Burton[18] reported the synthesis of symmetrical butadiynes via oxidative homo-coupling of two alkynes with iodine as the oxidising agent in the presence of $[PdCl_2(PPh_3)_2]$ (1.3 mol%) and CuI (5 mol%) in diisopropyl amine, obtaining good to excellent yields of the products.

Haley and co-workers studied[19] the catalytic function of $Cu^{(II)}$, $Cu^{(I)}$ and Pd complexes with mono- and bidentate phosphine ligands in the ring closure of 14- and 15-membered ring containing dehydrobenzoannulenes (DBAs) (**Figure 2.6**). The authors found that the

yield of 14-membered ring DBA was better using Pd and CuI co-catalysts rather than Cu catalysts, whereas 15-membered gave the opposite result. This is because the smaller ring compound is formed via the cis-Pd-bis(acetylide) intermediate (**Pathway I**, **Figure 2.6**), whereas the larger ring is formed via a dimeric $Cu^{(I)}$ acetylide intermediate (**Pathway II**, **Figure 2.6**).

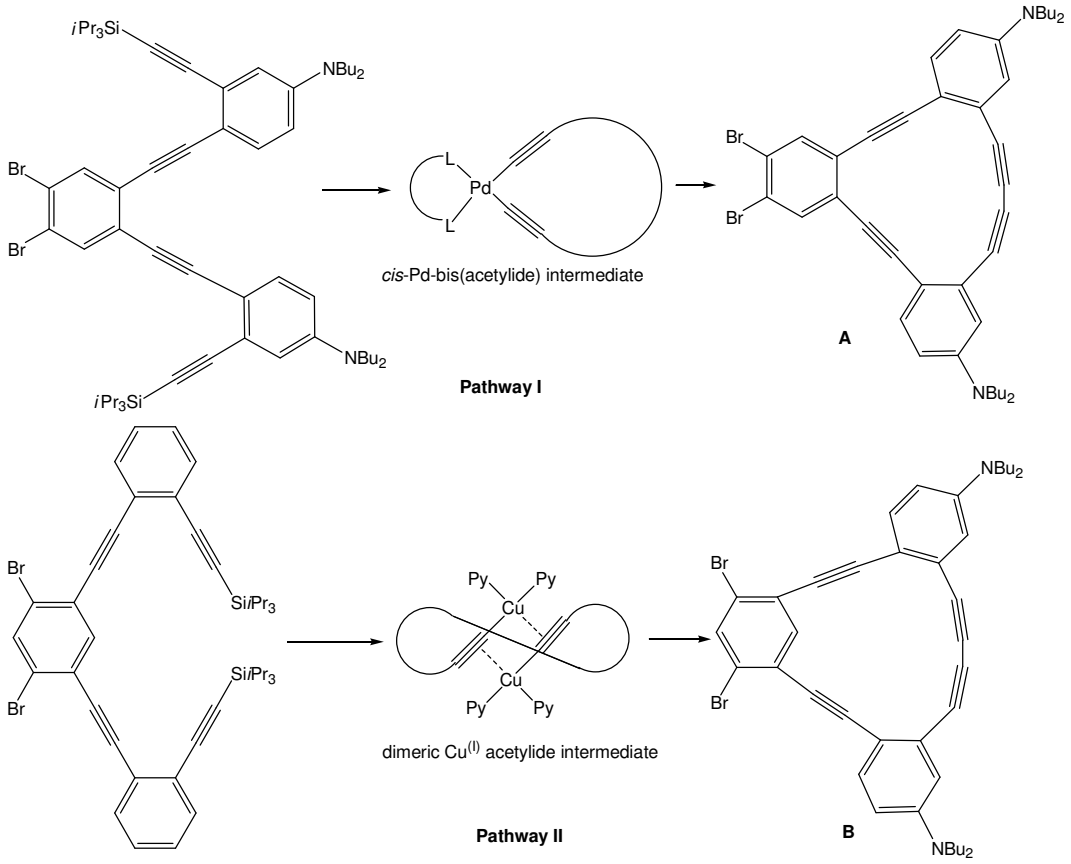

A yield %	Catalyst	B yield %
24	$Cu(OAc)_2$	80
35	CuCl	76
67	$[(PPh_3)_2PdCl_2]$, CuI	24
76	$[(dppe)PdCl_2]$, CuI	12

Figure 2.6: Comparison of Cu and Pd catalysts in the ring closure of DBAs.[19]

In the development of cross-coupling reactions, Cadiot and Chodkiewicz cross-coupled a haloalkyne with terminal alkyne to produce an unsymmetrical butadiyne in the presence of $Cu^{(I)}$ in a basic solution (e.g. aqueous *n*-butylamine).[15, 20, 21] Reducing agents such as hydroxylamine hydrochloride were added to the reaction to prevent the $Cu^{(I)}$ being oxidised to $Cu^{(II)}$. The chemistry of the Cadiot-Chodkiewicz coupling can be represented by the two equations below:

$$RC{\equiv}CH + Cu^{+} \rightarrow RC{\equiv}C\text{-}Cu + H^{+} \text{ (fast)} \qquad (\mathbf{1})$$

$$RC{\equiv}C\text{-}Cu + XC{\equiv}CR' \rightarrow RC{\equiv}C\text{-}C{\equiv}CR' + CuX \qquad (\mathbf{2})$$

where X = Br; R, R' = aryl, allyl

The nature of the R group in the ethynyl compounds can directly affect the product yields from the reaction. For example, terminal alkynes that bear electron withdrawing groups give higher yields than those with electron donating groups, because the ethynyl hydrogen is more acidic for electron withdrawing groups than electron donating groups. As a result, the reaction in **Eq. 1** is faster in the electron withdrawing group case.[21]

Unlike the R group in the terminal alkynes, the R' group in the haloalkyne only has a small effect on the reaction. This is due to the fact that the halogen (normally Br) in the haloalkyne is highly reactive towards the $Cu^{(I)}$ acetylide (**Eq. 2**).[21] In addition, Eglinton and McCrae also recommended that bromoalkynes are the best choice compared to the other haloalkynes. They stated that chloroalkynes are not reactive, while, iodoalkynes are excessively reactive.[21]

In order to reduce the possibility of homo-coupling occurring in the reaction, it is important to maintain the reaction under the following conditions: (i) Cu^+ must be kept in low concentration (ca. 1 - 2 mol%), because Cu^+ can also homo-couple haloalkynes to produce a symmetrical butadiyne as shown in **Eq. 3**; (ii) the bromoalkyne needs to be added to the reaction slowly; (iii) a reducing agent must be used; and (iv) the reaction must be kept free of oxidants such as oxygen.

$$2R'C{\equiv}CBr + 2Cu^+ \rightarrow R'C{\equiv}C\text{-}C{\equiv}CR' + 2Br^- + 2Cu^{2+} \qquad (\mathbf{3})$$

2.1.3 Palladium (Pd) catalysed cross-coupling reactions

The use of Pd as a catalyst is one of the most remarkable developments in C-C coupling chemistry. In general, most of the Pd-catalysed cross-coupling reactions can be represented by the equation shown in **Figure 2.7**:[22]

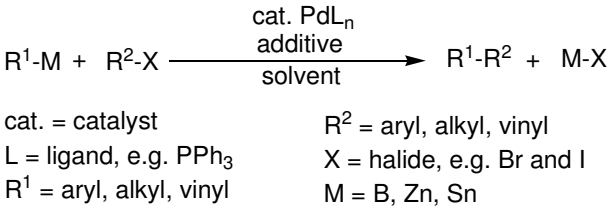

Figure 2.7: General equation for Pd-catalysed cross-coupling reactions.[22]

The 'M' in **Figure 2.7** can be various elements, the most well known being B, Zn and Sn, as reported by Suzuki-Miyaura,[23-26] Negishi,[25, 27, 28] and Stille,[29, 30] respectively.

The general catalytic cycle for Pd-catalysed cross-coupling is shown in **Figure 2.8**. It involves three major steps, namely oxidative addition, transmetallation and reductive

elimination. Oxidative addition involves the reaction of R^2-X with the Pd metal centre to form an R^2-Pd-X species, in which the oxidation state of Pd increases from 0 to +2. Transmetallation is a step in which two metals exchange their ligands. In a cross-coupling reaction, R^1-M exchanges its R^1 group with the X ligand from R^2-Pd-X to form R^2-Pd-R^1 and CuX. Lastly, in the reductive elimination step, R^2-Pd-R^1 eliminates R^1-R^2 as the cross-coupling product, with the Pd returning to the 0 oxidation state and then being available to repeat the catalytic cycle.

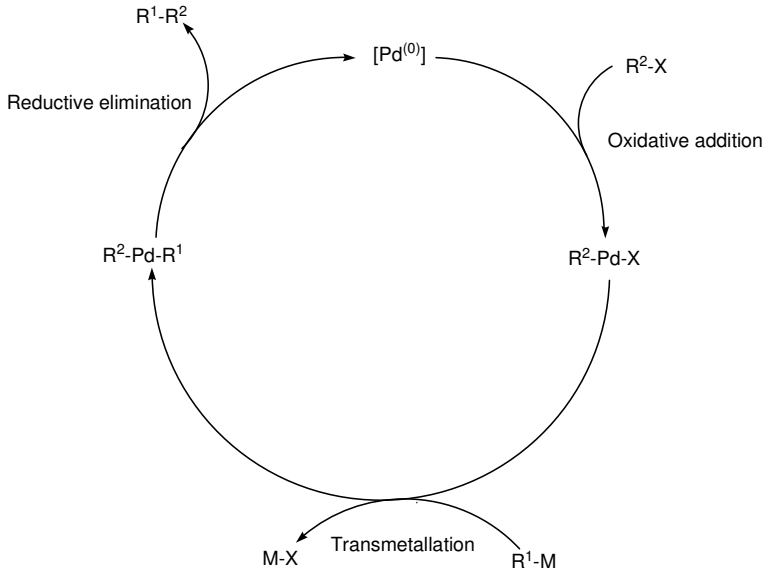

Figure 2.8: General catalytic cycle for Pd-catalysed reaction.

2.1.3.1 Sonogashira cross-coupling reaction

The Pd/Cu based catalytic system in cross-coupling chemistry was initiated by Sonogashira and co-workers,[31] who used $[PdCl_2(PPh_3)_2]$, CuI and Et_3N to synthesise alkynyl-arenes. The main difference between Sonogashira cross-coupling and other cross-coupling reactions (e.g. Suzuki-Miyaura coupling and Stille coupling) is that the

R^1-M species in the Sonogashira reaction is formed *in-situ*, whereas in the other cross-coupling reactions, it has to be pre-formed. As illustrated in the catalytic cycle proposed by Sonogashira et al.[31] (**Figure 2.9**), two important components are involved in the cross-coupling reaction, namely (i) the reductive initiation step in which $Pd^{(II)}$ is reduced to $Pd^{(0)}$, and (ii) the main catalytic cycle involving oxidative addition, transmetallation and reductive elimination to give the cross-coupled product.

$Cu^{(I)}$ plays an important role in the initiation reductive step and the transmetallation step. In the reductive initiation step, $Cu^{(I)}$ exchanges its acetylide (C≡C-R) ligand with $[PdCl_2(PPh_3)_2]$ to give the $[Pd(C{\equiv}C\text{-}R)_2(PPh_3)_2]$ species. Then, $[Pd(C{\equiv}C\text{-}R)_2(PPh_3)_2]$ undergoes reductive elimination to give a $[Pd^{(0)}(PPh_3)_2]$ species as the active catalyst in the catalytic cycle and a butadiyne as the by-product from the reaction. Indeed, Marder and co-workers found that under conditions where an oxidant (e.g. air or oxygen) is present, this reductive initiation step can be repeated in a catalytic cycle to produce significant amounts of butadiyne and that the re-oxidation of $Pd^{(0)}$ to $Pd^{(II)}$ is faster than oxidative addition of aryl halide under standard Sonogashira conditions.[32, 33] This finding is also consistent to the result from Liu and Burton, who used I_2 as the oxidising agent to homo-couple two terminal alkynes with catalytic amounts of $[PdCl_2(PPh_3)_2]$ and CuI.[18]

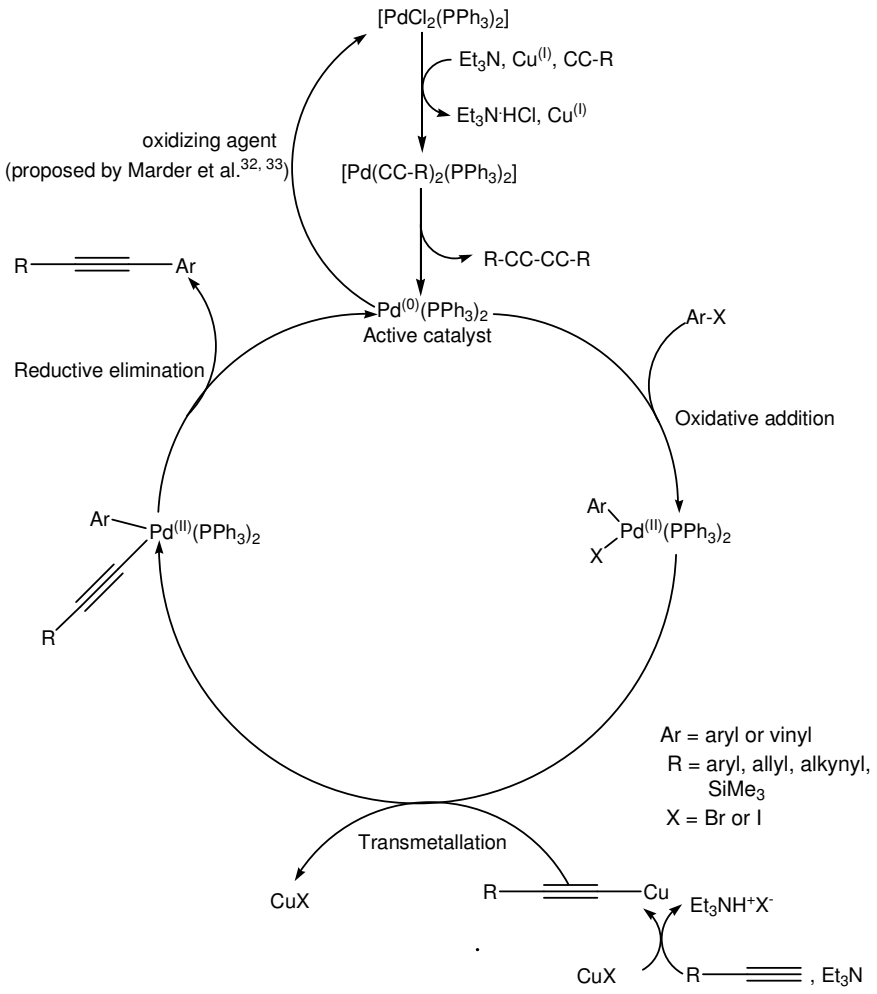

Figure 2.9: Catalytic of the Sonogashira cross-coupling reaction.[31-33]

Lin, Marder and Fairlamb et al.[33] have performed DFT (B3LYP) and CCSD(T) calculations to explain the alkyne homo-coupling reactions (**Eq**. **4** – **6**) from the view of reaction energy (ΔE) and free energy (ΔG) (**Table 2.1**). They concluded that **Eq**. **(4)** is slightly endothermic, i.e., thermodynamically unfavourable. **Eq**. **(5)** shows that, in the presence of oxidant (e.g. O_2), the homo-coupling reactions are favourable due to the energetically favourable formation of water.

$$2\ RC{\equiv}CH \rightarrow RC{\equiv}C\text{-}C{\equiv}CR + H_2 \quad \textbf{(4)}$$

$$2\ RC{\equiv}CH + \tfrac{1}{2}O_2 \rightarrow RC{\equiv}C\text{-}C{\equiv}CR + H_2O \quad \textbf{(5)}$$

$$H_2 + \tfrac{1}{2}O_2 \rightarrow H_2O \quad \textbf{(6)}$$

Table 2.1: Reaction energies and free energies (kcal mol^{-1}) for **Eq**. **(4)** – **(6)**, calculated using two different theoretical methods.[33]

		ΔE_1**(4)**	ΔG_1**(4)**	ΔE_2**(5)**	ΔG_2**(5)**	ΔE_3**(6)**	ΔG_3**(6)**
B3LYP	R = Me	0.9	-0.8	-57.9	-51.3	-58.3	-50.6
	R = Ph	-1.2	-1.3	-60.0	-51.8		
CCSD(T)	R = Me	3.7		-56.4		-60.1	

As illustrated in **Figure 2.9**, the $[Pd^{(0)}(PPh_3)_2]$ species acts as a reagent in the oxidative addition step with aryl halide, forming an Ar-Pd-X intermediate. The halide can significantly influence the rate of reaction. In fact, Fitton and Rick[34] found that the reaction rates are ArI > ArBr >> ArCl.

Marder and Lin et al.[35] used DFT calculations to study the effect of the halide group on the oxidative addition step, and found that the choice of monophosphine vs. bisphosphine Pd pathways changes as a function of the nature of ArX (**Figure 2.10**).

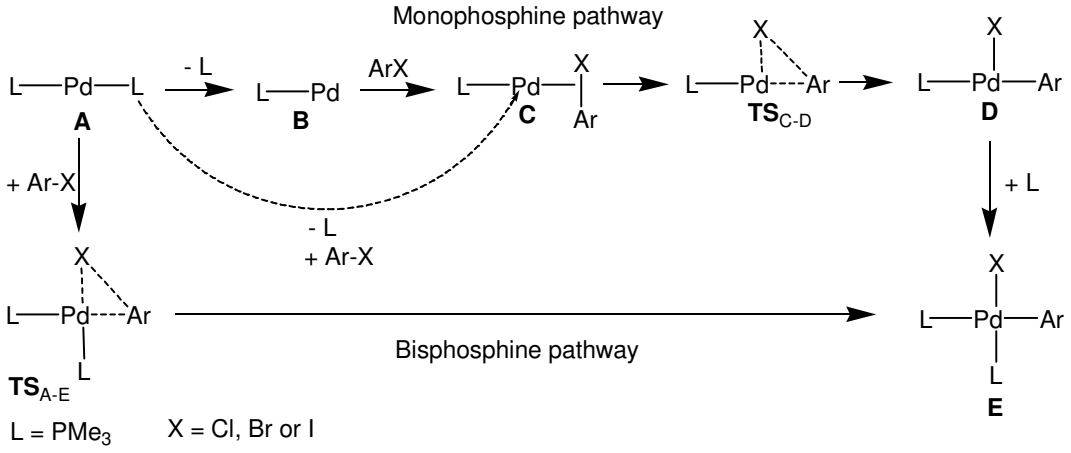

Figure 2.10: Two pathways of oxidative addition proposed by Marder and Lin et al.[35]

The authors found that ArCl prefers the monophosphine pathway, and that **TS**$_{C-D}$ is calculated to have a significantly higher energy than intermediate **B**, meaning that the oxidative addition of ArCl is generally very slow. For ArBr, the reaction also prefers the monophosphine pathway, but the calculations show that **TS**$_{C-D}$ has a similar stability to that of **B**. In the ArI case, the calculations still indicate that the monophosphine one is the preferable pathway, but the energy profile shows that the barrier for the bisphosphine pathway is very close to that of the monophosphine pathway. Therefore, it is believed that the two pathways may exist simultaneously in the ArI case.

In the transmetallation step, the amine, which is often the solvent used in the reaction, deprotonates the acetylene to generate a $Cu^{(I)}$ acetylide and an ammonium salt. Then, the $Cu^{(I)}$-acetylide undergoes transmetallation with Ar-Pd-X to yield CuX and Ar-Pd-(C≡CR). Ar-Pd-(C≡CR) undergoes reductive elimination to give Ar-C≡CR as the product, and regenerates $Pd^{(0)}$. Different substituents in the *para*-position of the phenyl ring can strongly affect the rate of the reaction. Generally, electron withdrawing groups such as C≡N, NO_2, CO_2Me lead to much faster reactions than electron donating groups

such as Me, OMe and SMe. Fitton[34] explained that this is due to the fact that electron withdrawing substituents lower the energies of the Ar-X antibonding orbitals, consequently causing a more facile oxidative addition.

2.1.3.2 C(sp)-C(sp) Pd-catalysed cross-coupling in unsymmetrical butadiynes synthesis

The main problem of synthesising unsymmetrical butadiynes by Pd-catalysed cross-coupling is the formation of homo-coupling products,[36] which can potentially reduce the isolated yield of unsymmetrical butadiyne. **Figure 2.11** shows a schematic diagram to explain how the homo-coupling products can be formed in an unsymmetrical butadiyne synthesis reaction.[37] The key step, namely reductive elimination, is very important, as it leads to the desired cross-coupling product R^1-C≡C-Pd-C≡C-R^2, through **Path A**. However, the R^1-C≡C-Pd-C≡C-R^2 species also can undergo a transmetallation process with $Cu^{(I)}$-acetylides present in the reaction system to form the homo-coupling products via **Paths B** and **C**. In this case, if transmetallations are faster than reductive elimination, there will be more homo-coupling products are formed.

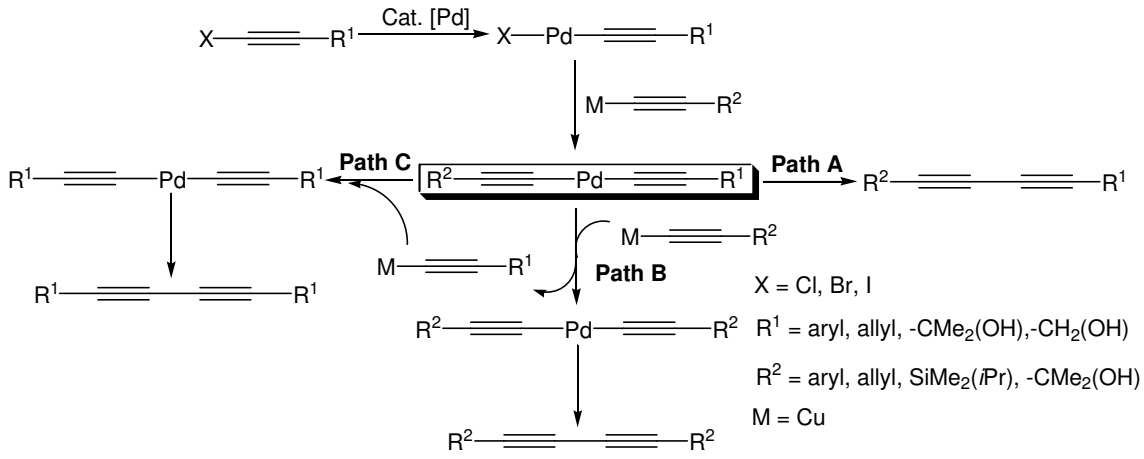

Figure 2.11: Proposed pathways for Pd-catalysed C(sp)-C(sp) coupling.[37]

In order to eliminate homo-coupling product formation in the unsymmetrical butadiyne synthesis, many alternative ligands such as bulky ligands[25] and π-acid ligands,[38-40] which can facilitate the reductive elimination process, have been developed and investigated. In 2008, Lei et al. reported a new phosphine containing an electron-deficient olefin, hence forth refined to as the "P-olefin ligand" (**Figure 2.12**), which gave promising results in promoting reductive elimination process and produced high yields of cross-coupling products in most cases.[37]

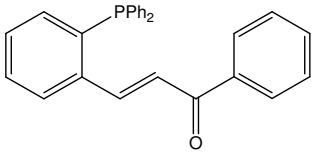

Figure 2.12: "P-olefin ligand".[37]

The group also compared their method to other palladium catalysts and ligands (**Table 2.2**) by using the reaction of bromoethynylbenzene and 2-methylbut-3-yn-2ol as the model reaction.

Table 2.2: Comparing Lei's method to other Pd-catalysed methods for the cross-coupling of BrC≡CPh with HC≡C-$(CH_3)_2$OH.[37]

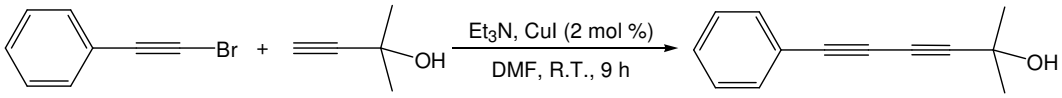

entry	Pd (2 mol %)	ligand	yield (%)	Selectivity (cross-/homo-)
1	None	none	8	-
2	$[PdCl_2(PPh_3)_2]$	none	42	69:31
3	$[Pd(dba)_2]$	none	69	83:17
4	$[Pd(dba)_2]$	P-olefin	90	91:9

Based on the results in **Table 2.2**, it is noticeable that $[Pd(dba)_2]$ worked better than $[PhCl_2(PPh_3)_2]$ in the cross-coupling reaction. Addition of the P-olefin ligand, increased both the selectivity by 8% (entries 3 and 4), and the isolated yield of the desired product by 21%.

Alami and Ferri pointed out that the use of amines can affect the cross-coupling reaction to synthesise unsymmetrical butadiynes.[41] In the cross-coupling conditions shown in **Table 2.3**, Et_2NH, Et_3N, *i*Pr_2NH and *i*Pr_2NH-THF gave very poor yields of the cross-coupling product. However, in the case where pyrrolidine was used, the reaction was completed in shorter time, and produced higher yield of cross-coupling product (yield = 95%) compared to the other amines.[41]

Table 2.3: Comparing cross-coupling product yields in different amines.

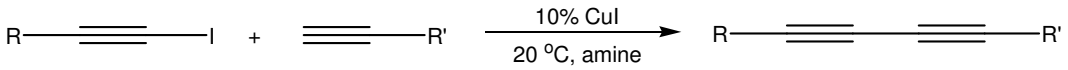

R = C_5H_{11}
R' = $(CH_2)_2OH$

entry	amine	Time	Cross-coupling product yield
1.	Et_3N	24 h	20
2.	Et_2NH	7 h	35
3.	$BuNH_2$	6 h	54
4.	iPr_2NH	3 h	25
5.	piperidine	2 h	79
6.	pyrrolidine	15 min	95

2.1.4 Miscellaneous methods to synthesise unsymmetrical butadiynes

Alternatively, rather than using cross-coupling based synthetic routes, unsymmetrical butadiynes can also be synthesised by converting a carbonyl moiety to an alkyne. For example, Tykwinski et al.[42] reported this method using starting materials such as aryl- or vinyl-aldehydes, carboxylic acids or acid chlorides to form alkynyl alcohols which were oxidised to ketones and then converted to 1,1-dibromo-olefins (**Figure 2.13.c**). The 1,1-dibromo-olefin was then reacted with butyllithium to produce a carbene/carbenoid intermediate, followed by rearrangement to afford a unsymmetrical butadiyne in good yield (**Figure 2.13**).

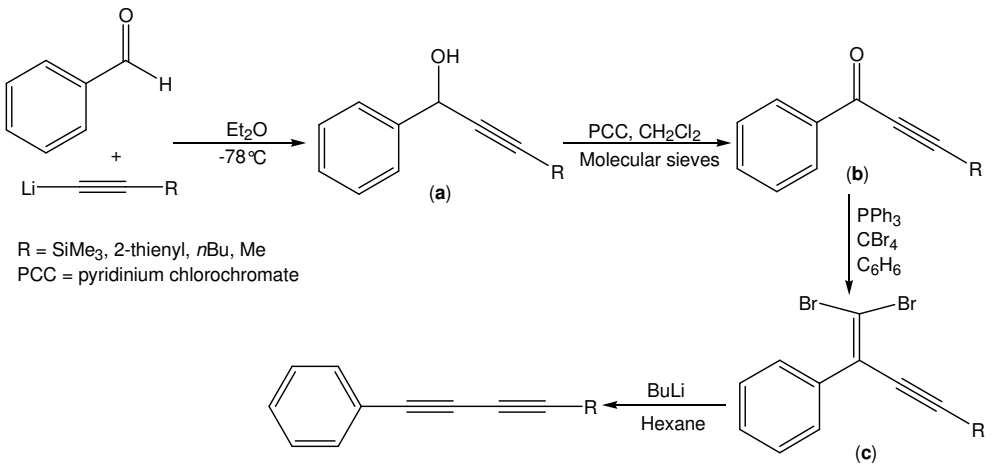

Figure 2.13: Alternative synthetic route to unsymmetrical butadiynes.[42]

On the other hand, Wong et al. prepared terminal butadiynes (**Figure 2.14**) via the cross-coupling of alkynes with *cis*-1,2-dichloroethylene, and HCl elimination from the resulting compound with lithium diisopropylamide (LDA) gave the terminal butadiyne.[43] This method is the same as that used by Marder et al.[44] for the syntheses of ferrocenyl butadiynes, which was based on the earlier report of Kende and Smith.[45]

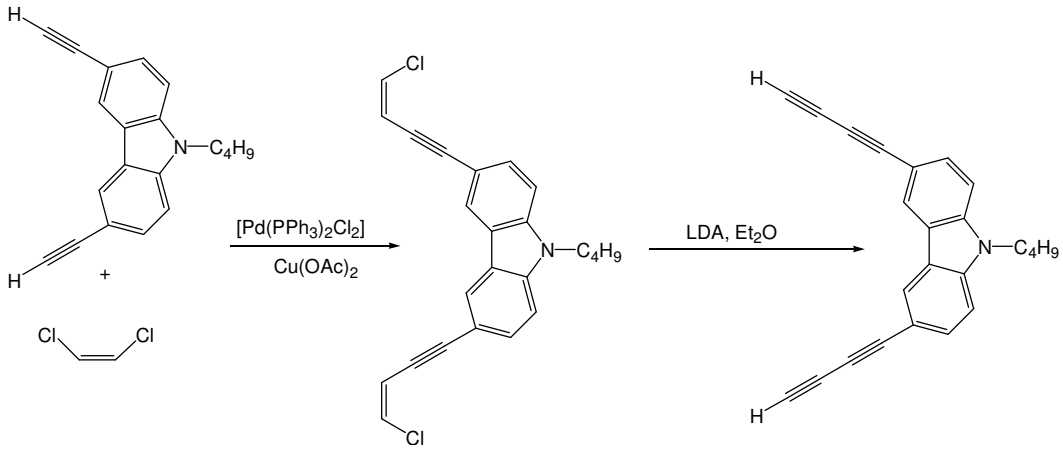

Figure 2.14: Synthesis of a terminal butadiyne.[43]

Compared to internal butadiynes, the terminal butadiynes were often reported to be unstable; however, the ferrocenyl terminal butadiyne, which was reported by Marder et al.,[44] was shown to be stable. Bryce and co-workers[46] have also reported an alternative synthesis of terminal arylbutadiynes and have shown these to be stable; several have been characterised by crystallography.

2.1.5 Outline of the synthetic routes to butadiynes and 1,3,9,11-dodecatetraynes

In this project, cross-coupling and oxidative homo-coupling reactions were used to synthesise all of the required butadiynes and 1,3,9,11-dodecatetraynes. Two types of diarylbutadiynes were synthesised, namely the simple 1,4-bis(*p*-R-phenyl)buta-1,3-diynes and extended phenyl ethynylene butadiynes.

The synthetic route to the simple diarylbutadiynes is shown in **Figure 2.15**. In general, the synthesis of the butadiynes involves three steps namely: i) the cross-coupling of an aryl halide with trimethylsilylacetylene (TMSA) to give a (trimethylsilylethynyl)arene using a Sonogashira reaction; ii) its deprotection by removal of the trimethylsilyl ($SiMe_3$) group to form an ethynyl-arene; and iii) the oxidative homo-coupling of the ethynyl-arene to produce the corresponding butadiyne.

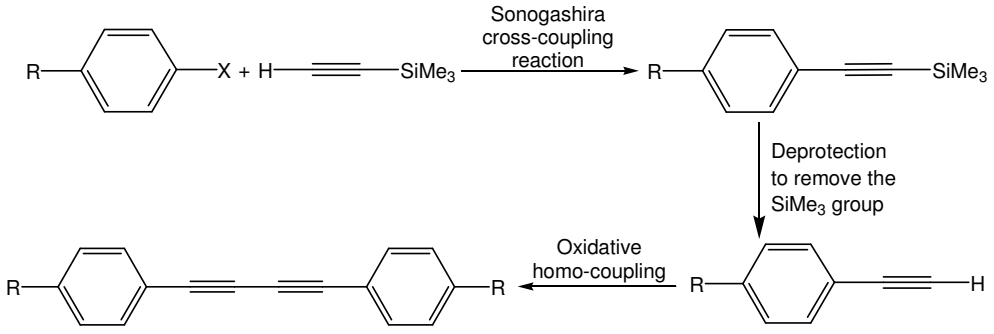

Figure 2.15: Synthetic route to simple diarylbutadiyne.

Similar to that of the simple butadiynes, the synthesis of the extended bis(arylethynyl)diarylbutadiynes (**Figure 2.16**) begins with a Sonogashira cross-coupling reaction of 1-bromo-4-iodobenzene with 2-methylbut-3-yn-2-ol to give 4-(4-bromophenyl)-2-methylbut-3-yn-2-ol. Then, the resulting product was cross-coupled with TMSA using the Sonogashira reaction to produce 4-(4-trimethylsilylethynylphenyl)-2-metylbut-3-yn-2-ol. The protecting group, 2-methyl-2-ol [-$C(CH_3)_2OH$], was then removed to produce 4-(ethynylphenylethynyl)trimethylsilane. This compound was cross-coupled with the appropriate aryl halide to form (trimethylsilylethynylphenylethynyl)-arenes, followed by removal the trimethylsilyl protecting group to give (ethynylphenylethynyl)arenes, which were homo-coupled to form the extended bis(arylethynyl)diarylbutadiynes.

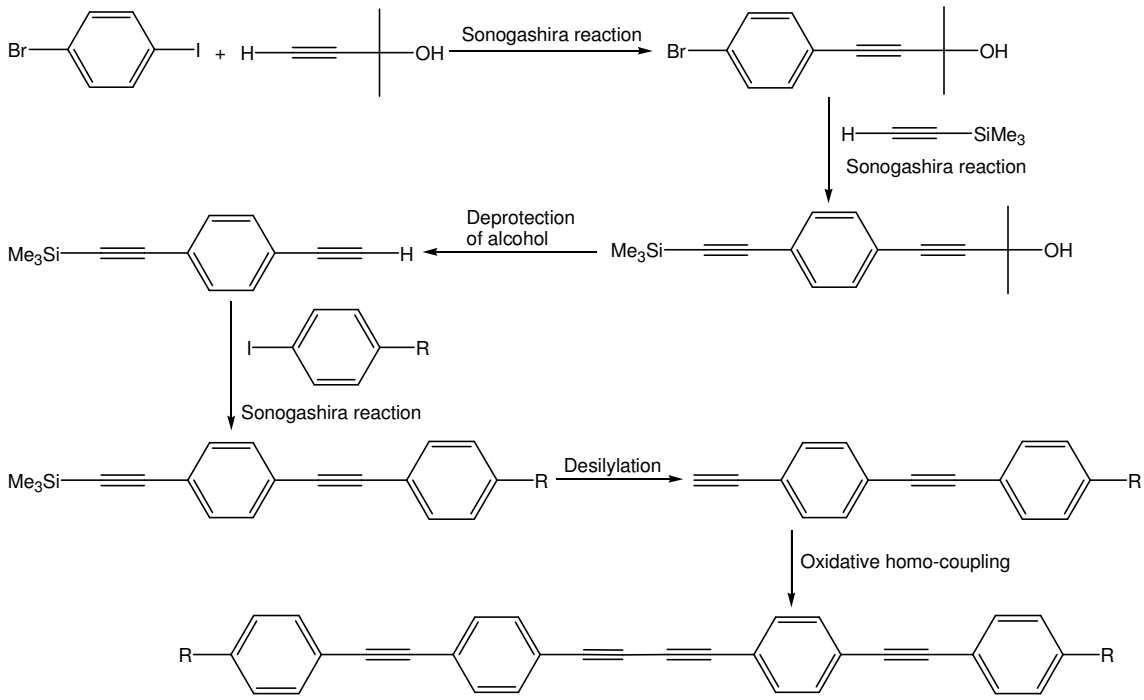

Figure 2.16: Synthetic route to the extended bis(arylethynyl)diarylbutadiynes.

For the synthesis of the 1,3,9,11-dodecatetraynes (**Figure 2.17**), ethynyl arenes were cross-coupled with 1,8-dibromoocta-1,7-diyne to produce the desired product.

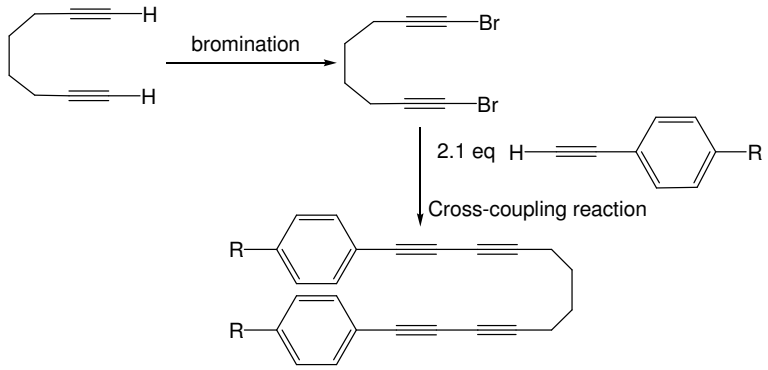

Figure 2.17: Synthetic route to 1,3,9,11-dodecatetraynes.

Very recently, two structurally-related 1,3,8,10-undecatetraynes (**Figure 2.18**) have been reported by Manato and co-workers[47] in the course of their study on the luminescent properties of 2,5-bis(arylethynyl)phospholes. The starting material, hepta-1,6-diyne, was iodinated using *n*BuLi and I_2 in THF to produce the 1,7-diiodohepta-1,6-diyne in 87% yield. Then, the resulting compound was further cross-coupled with H-C≡C-SiR_3 (where, R = Me and *i*Pr) using CuI in piperidine, give 1,11-bis(trialkylsilyl)undeca-1,3,8,10-tetraynes in yields of 86% for R = Me and 76% for R = *i*Pr.[47]

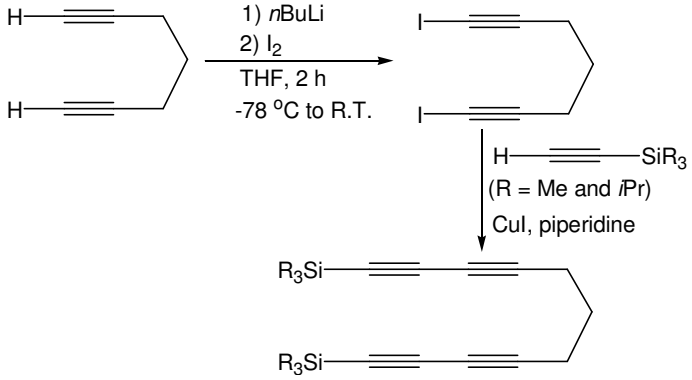

Figure 2.18: Synthetic route to 1,11-bis(trialkylsilyl)undeca-1,3,8,10-tetraynes.[47]

2.2 Results and discussion

2.2.1 Synthesis of 1,4-bis(*p*-R-phenyl)buta-1,3-diynes

The first step of the butadiyne synthesis is shown in **Figure 2.19**; (trimethylsilylethynyl) arenes were prepared from the reaction of aryl halides with TMSA using standard Sonogashira cross-coupling conditions, and the yields of (trimethylsilylethynyl) arenes are shown in **Table 2.4**.

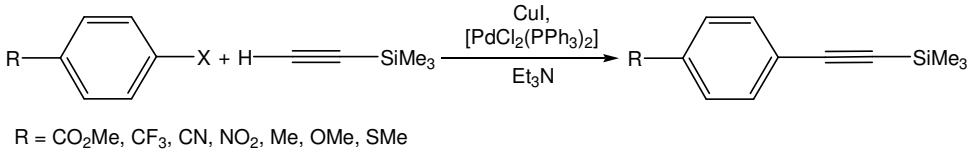

Figure 2.19: The synthesis of (trimethylsilylethynyl)arenes.

Table 2.4: Yields of (trimethylsilylethynyl)arenes.

Compound	R Group	X	Yield (%)
1	-CO_2Me	I	99
2	-CF_3	Br	29
3	-C≡N	Br	62
4	-NO_2	Br	87
5	-Me	Br	83
6	-OMe	I	85
7	-SMe	Br	74

For the electron donating substituted aryl halides in which X = Br, such as compounds **5** and **7**, the reactions were heated at 60 °C and monitored by GC-MS. The reaction to produce **5** was complete in 15 h, but the reaction for **7** took about 72 h to finish. The yield

obtained for **2** was relatively low (29%) compared to the others. This is due to the high volatility of **2**, causing yield losses during the work-up process. The ^{1}H NMR spectrum of **1** (**Figure 2.20**) displays a singlet at 0.24 ppm, which is assigned to the trimethylsilyl group, while two symmetric doublets in the region 7.48 – 7.97 ppm indicate that the CO_2Me group is in the *para*-position relative to trimethylsilylethynyl group.

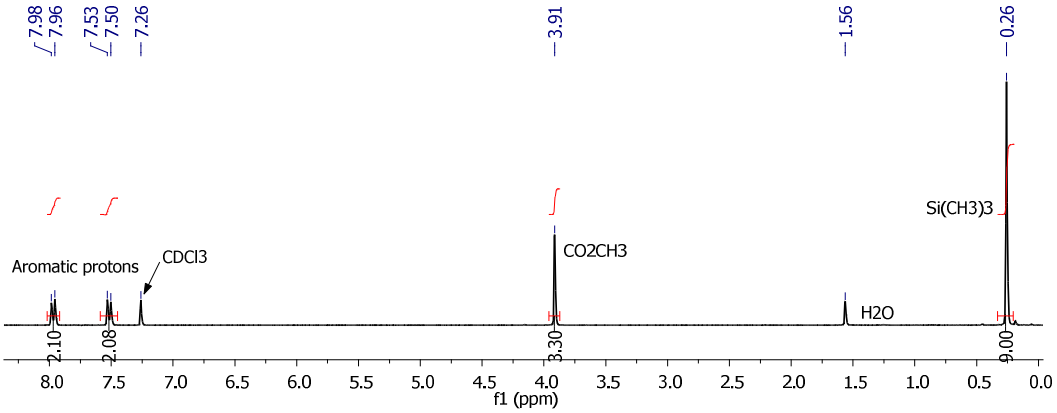

Figure 2.20: ^{1}H NMR spectrum (300 MHz, $CDCl_3$) of **1**.

Comparing compounds **1**, **5**, **6** and **7**, the singlet, associated with the CH_3 protons, occurs at 3.91 (CH_3O-C=O), 2.30 (CH_3), 3.58 (CH_3O) and 2.44 ppm (CH_3S), respectively.

The second step of the butadiyne preparation is shown in **Figure 2.21**, wherein the $SiMe_3$ protecting group was removed using a basic solution containing sodium carbonate (Na_2CO_3) in a mixture of methanol (MeOH) and water.[48]

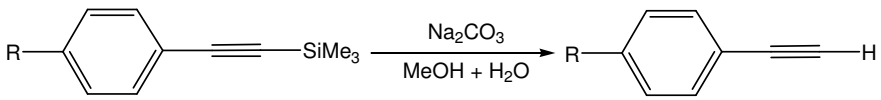

R = CO_2Me, CF_3, CN, NO_2, Me, OMe, SMe

Fgure 2.21: Deprotection of the TMS group to produce ethynyl arenes.

The deprotection reactions were complete in 4 to 5 h, and the products were extracted using dichloromethane (CH_2Cl_2). Large amounts of water were needed in order to remove residual MeOH and carbonate during the extraction. The CH_2Cl_2 layer was separated, dried over $MgSO_4$ and removed *in vacuo* to give the ethynyl arenes.

The fact that the $SiMe_3$ peak at 0.24 ppm has disappeared in the ^1H NMR spectrum proves that the protecting group has been removed (**Figure 2.22** for compound **8**). An additional singlet was observed at 3.23 ppm which is assigned to the alkyne proton, C≡C-H. The yields obtained from this method are shown in **Table 2.5**. Again, the low yield obtained for **9**, the compound with a CF_3 substituent, is due to the high volatility of this compound.

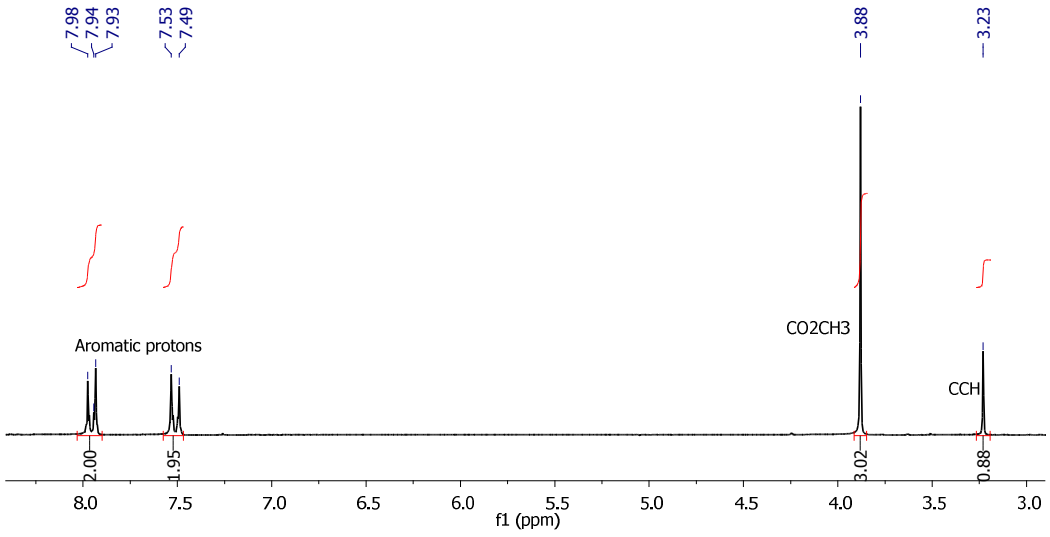

Figure 2.22: ^1H NMR spectrum (200 MHz, $CDCl_3$) of **8**.

Table 2.5: Yields of ethynyl arenes following deprotection.

Compound	R Group	Yield (%)
8	-CO_2Me	97
9	-CF_3	29
10	-C≡N	74
11	-NO_2	89
12	-Me	70
13	-OMe	74
14	-SMe	50

The six terminal alkynes (i.e., all except R = OMe) above were homo-coupled under Pd-catalysed oxidative homo-coupling conditions, utilising either O_2 or I_2 as oxidants, and the yields obtained are shown in **Table 2.6**.

Table 2.6: Yields of buta-1,3-diynes **15** - **20**.

Compound	R Group	Oxidant	Yield (%)
15	-CO_2Me	I_2	80
16	-CF_3	O_2	26
17	-C≡N	I_2	56
18	-NO_2	I_2	69
19	-Me	O_2	61
20	-SMe	O_2	63

According to the ^{1}H NMR spectrum of **15** in **Figure 2.23**, the disappearance of the C≡C-H singlet at 3.23 ppm shows that the homo-coupling of the two ethynyl arenes to form a butadiyne was successful.

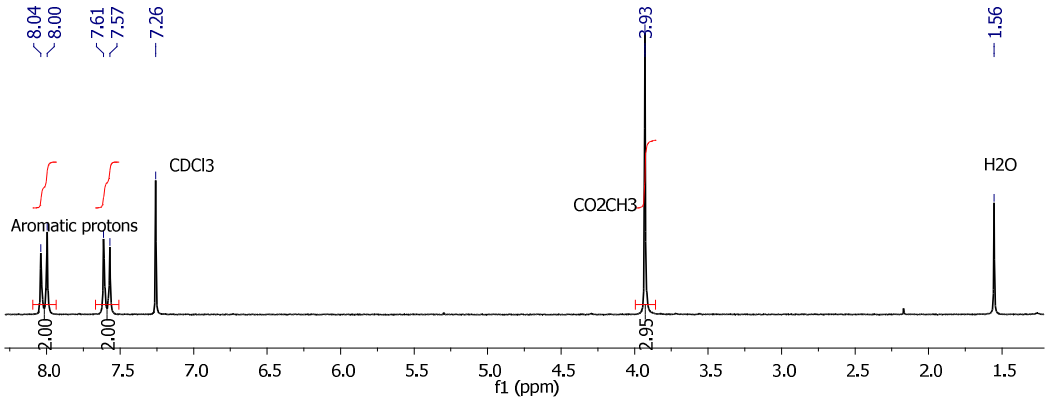

Figure 2.23: ^{1}H NMR spectrum (300 MHz, $CDCl_3$) of **15**.

It is worth noting that the solubility of compounds **17** and **18** in CH_2Cl_2 is very poor. High purity samples of these two compounds can be obtained by recrystallisation from boiling toluene and washing with CH_2Cl_2 at room temperature.

1,4-bis(*p*-methoxyphenyl)buta-1,3-diyne (**21**, R = OMe) was synthesised by Eglinton-Galbraith coupling using 3 equivalent of $Cu(OAc)_2$ in a mixture of MeOH and pyridine, and the reaction was heated at 70 °C for 15 min. 1.0 M hydrochloric acid (HCl) was added to the reaction mixture and the product was extracted with Et_2O. The solvent was removed *in vacuo* to give **21** as a yellow solid in 81% yield.

2.2.2 Synthesis of extended bis(arylethynyl)diarylbuta-1,3-diynes

In this project, two extended bis(arylethynyl)diarylbutadiynes were also synthesised as the starting materials for the preparation of rhodacyclopentadienes. The first two steps of

the extended bis(arylethynyl)diarylbutadiyne synthesis (preparation of **22** and **23**) is shown in **Figure 2.24**.

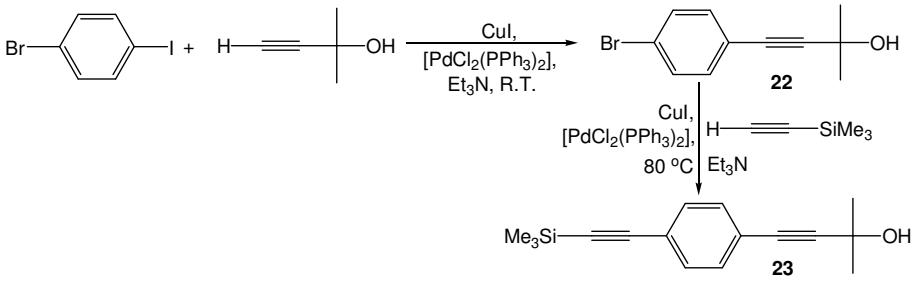

Figure 2.24: Synthetic route to **23**.

In the first step, 1-bromo-4-iodobenzene was cross-coupled with 2-methyl-but-3-yn-2-ol under standard Sonogashira conditions at room temperature to give **22** in 85% yield. The appearance of singlets at 2.55 ppm for OH and 1.60 ppm for CH_3 in the ^1H NMR spectrum indicates that the $–C(CH_3)_2OH$ moiety is present in **22**.

Compound **22** was further cross-coupled with TMSA under Sonogashira conditions at 80 °C and monitored by GC-MS until all of the starting materials had reacted to produce **23** as a beige solid. The isolated yield of **23** was 80% after purification by recrystallisation from hot hexane.

Removal of the $–C(CH_3)_2OH$ protecting group in **23** required reaction with 0.1 equivalent of freshly powdered NaOH in a refluxing toluene solution at 110 °C for 2 h. The reaction is an equilibrium (**Figure 2.25**) which requires the acetone generated to be removed by heating up to 110 °C under a stream of nitrogen gas.

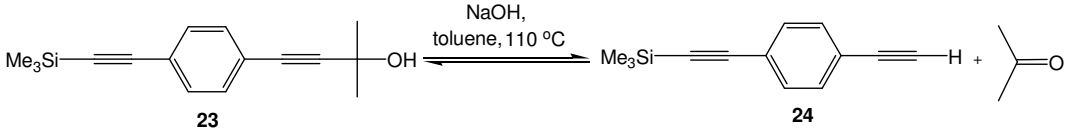

Figure 2.25: Removal of the alcohol protecting group in basic toluene solution.

Once the reaction was complete, the black toluene solution was filtered using a sinter funnel and the toluene was removed *in vacuo* to give a black-brown solid. Filtration of a hexane solution of the black-brown solid through a short silica gel pad was needed to obtain the high-purity product **24** in 78% yield.

Iodooctylbenzoate **25** in **Figure 2.26** was prepared via esterification of 4-iodobenzoic acid with octan-1-ol in the presence of 4-(dimethylamino)pyridine (DMAP), *N*,*N*'-dicyclohexylcarbodiimede (DCCI) and CH_2Cl_2. The mixture was stirred overnight at room temperature and the solvent was removed *in vacuo*.

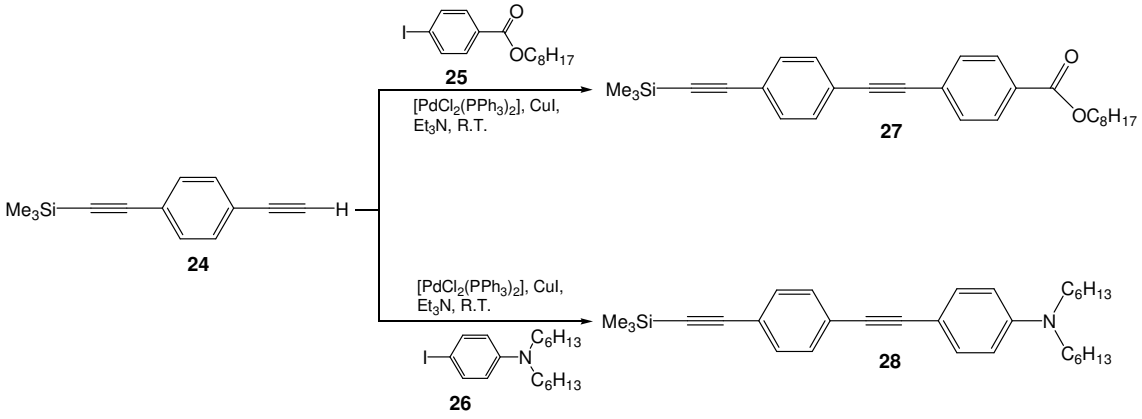

Figure 2.26: Cross-coupling reactions of **24** to give **27** and **28**.

The crude product was passed through a 5 cm silica gel column, eluting with hexane. However, the hexane eluent contained the mixture of **25** and DCCI. Separation of the mixtures was carried out using Kugelrohr distillation at 120 – 130 °C, 3.1 x 10^{-3} Torr, with the impurities being distilled into the second flask leaving a yellow-brown oil in the first flask. The oil was examined by GC-MS to confirm that **25** was pure (**Figure 2.27**). However, there was some yield loss during the distillation process, as some of the product also distilled into the second flask, and the isolated yield of **25** was 49%.

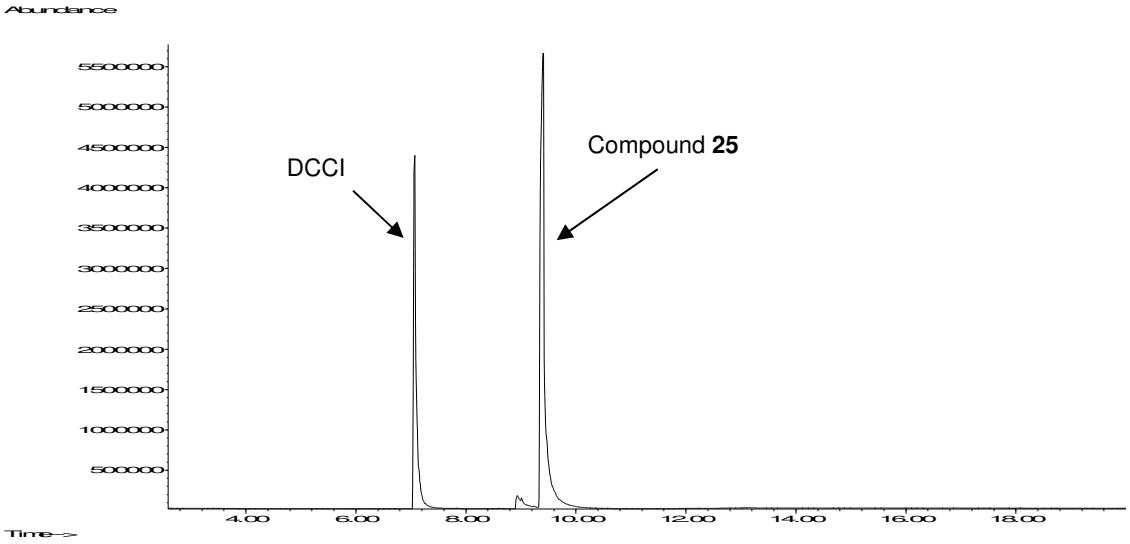

Figure 2.27 (a): The GC-MS TIC of **25** and DCCI.

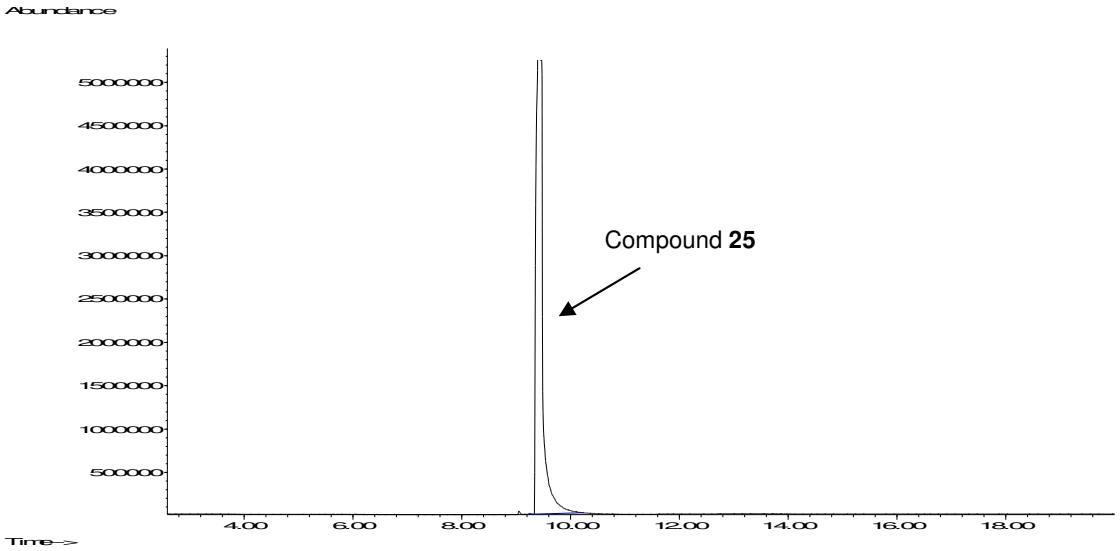

Figure 2.27 (b): The GC-MS TIC of pure **25** after removal of DCCI by Kugelrohr distillation.

Iododihexylaniline **26** was synthesised by reacting *p*-iodoaniline with excess 1-iodohexane in a weakly basic (excess Na_2CO_3) DMF solution at reflux for 40 h. One problem that occurred in the synthetic process was the formation of the monohexyl by-product, which can be seen from the ^1H NMR and GC-MS spectra (**Figure 2.28**).

Compound **26** was purified further by passage through a silica gel column with hexane : CH_2Cl_2 (10 : 1 v/v).

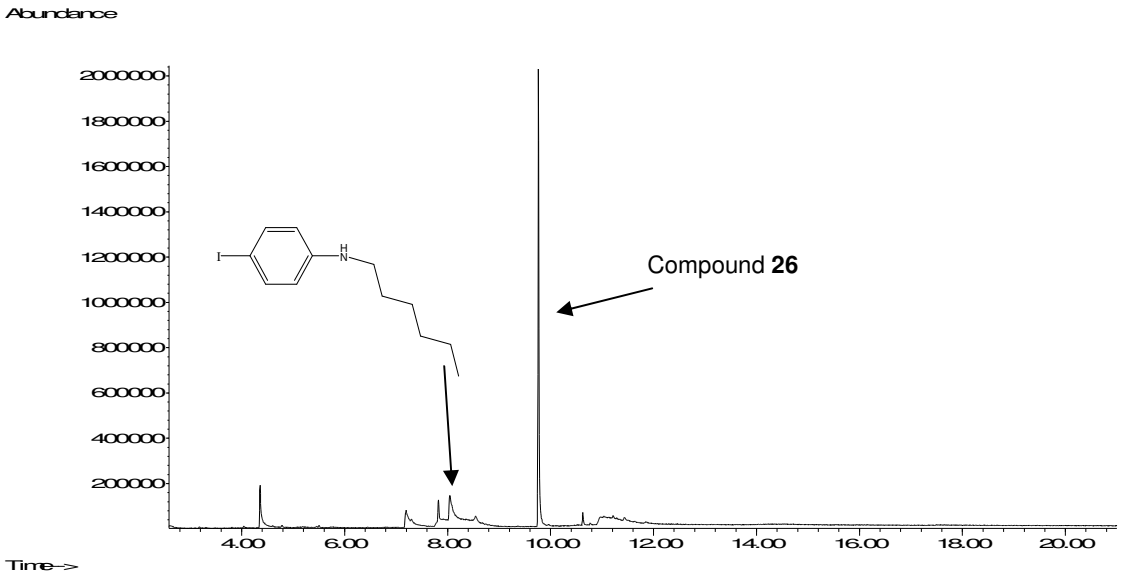

Figure 2.28: GC-MS TIC data for **26** before further purification.

Compound **24** was then cross-coupled, using standard Sonogashira conditions, with two different 1-iodo-4-R-benzenes [R = CO_2(*n*-C_8H_{17}), **25**; R = N(*n*-$C_6H_{13})_2$, **26**] to produce **27** and **28** as shown in **Figure 2.26**. The yields obtained were 94 and 88%, respectively.

The TMS protecting group in **27** was removed using [*n*-Bu_4N]F (TBAF) (1.0 M solution in THF) to give **29** in 67% yield after purification. This deprotection method is different from that described in **Section 2.2.1**, because the *n*-octyl ester in **27** is converted to the methyl ester if it is stirred in a basic solution of MeOH and water.[49]

The removal of TMS group in **28** was carried out using the typical method described in **Section 2.2.1**; however, Et_2O was added in order to dissolve **28**, which is insoluble in MeOH. The yield obtained for the terminal alkyne product **30** was 79%.

The two terminal alkyne products were each homo-coupled in the presence of oxidants, namely I_2 for R = $CO_2(n\text{-}C_8H_{17})$ and O_2 for R = $N(n\text{-}C_6H_{13})$, to produce **31** and **32**, as shown in **Figure 2.29**.

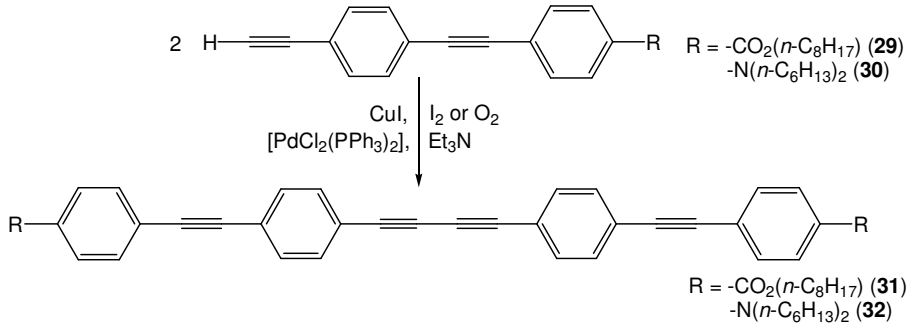

Figure 2.29: Synthesis of extended bis(arylethynyl)diarylbutadiynes, **31** and **32**.

2.2.3 Synthesis of 1,12-bis(*p*-R-phenyl)dodeca-1,3,9,11-tetraynes

The synthesis was initiated by the bromination of 1,7-octadiyne to form 1,8-dibromo-1,7-octadiyne (**33**, **Figure 2.30**) using excess *N*-bromosuccinimide (NBS) and $AgNO_3$ as the catalyst in acetone.

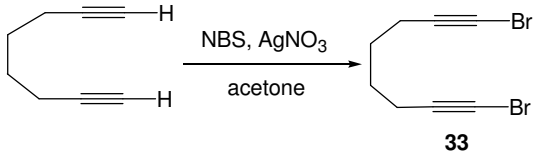

Figure 2.30: Bromination of 1,7-octadiyne to produce **33**.

A CH_2Cl_2/H_2O extraction was used to remove the NBS and $AgNO_3$ residues. The presence of trace NBS can be detected in the ^1H NMR spectrum by the peak at 2.76 ppm (**Figure 2.31**). The golden-yellow, oily product was stored in a refrigerator to avoid decomposition.

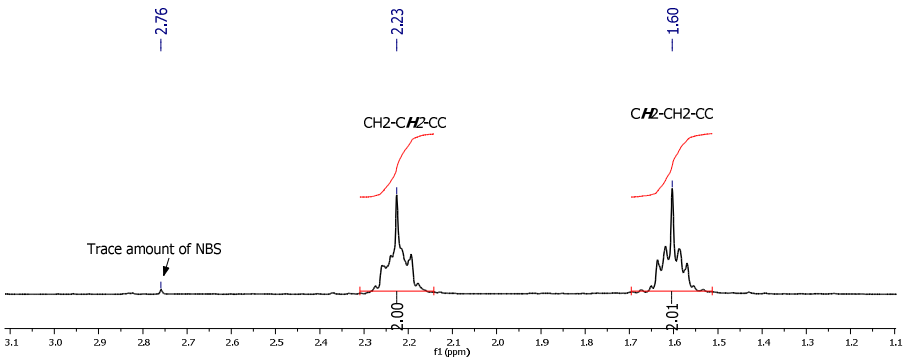

Figure 2.31: ^{1}H NMR spectrum (400 MHz, $CDCl_3$) of **33** with trace amount of NBS.

With the exception of the parent compound (R = H), all of the 1,12-bis(*p*-R-phenyl)dodeca-1,3,9,11-tetraynes were prepared by cross-coupling of 1,8-dibromo-1,7-octadiyne with 2.1 equivalent of the respective ethynyl arenes using the method and conditions described by Lei et al. (**Figure 2.32**).[37]

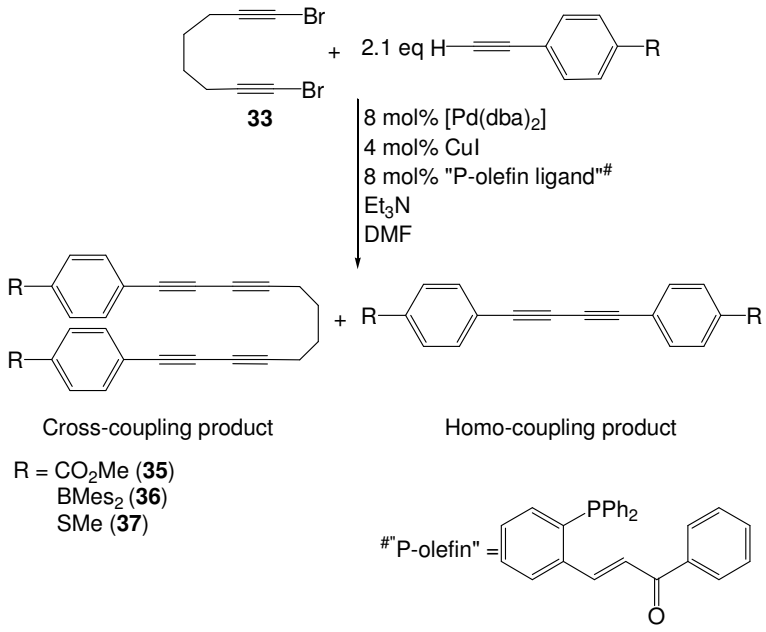

Figure 2.32: Synthetic route to **35**, **36** and **37** using Lei's method.[37]

To synthesise the parent compound [R = H, **34(a)**, **Figure 2.33**], Cadiot-Chodkiewicz coupling was used. About two equivalents of phenyl acetylene and 1,8-dibromo-1,7-octadiyne were stirred in an aqueous *n*-butylamine solution in the presence of CuCl and hydroxyamine hydrochloride. The crude material contained the desired **34(a)**, the homo-coupling product [**34(b)**], and a small amount of the mono-cross-coupling product [**34(c)**]. The crude material was further purified by recrystallisation from hot hexane to give a white solid at room temperature, which was separated by filtration, and washed with hexane again in order to remove the unwanted **34(b)**, and afford the pure product **34(a)** in 42% yield.

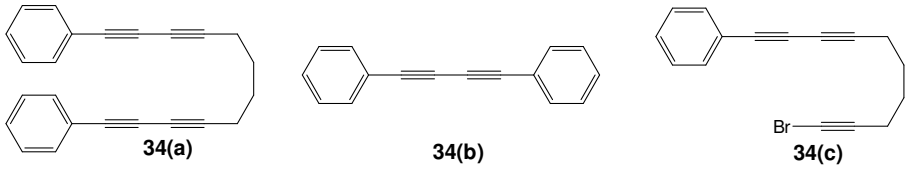

Figure 2.33: Three products obtained from Cadiot-Chodkiewicz coupling.

The synthesis of 1,12-bis(*p*-carbomethoxyphenyl)dodeca-1,3,9,11-tetrayne (**35**) was initially attempted by using the Sonogashira cross-coupling method. Thus, 1.2 equivalents of 1,7-octadiyne was stirred with two equivalents of 4-(bromoethynyl)benzoic acid methyl ester under standard Sonogashira conditions for 40 h. The ^{1}H NMR spectrum of the crude material (**Figure 2.34**) shows that the reaction was not complete although it had been stirred for 40 h.

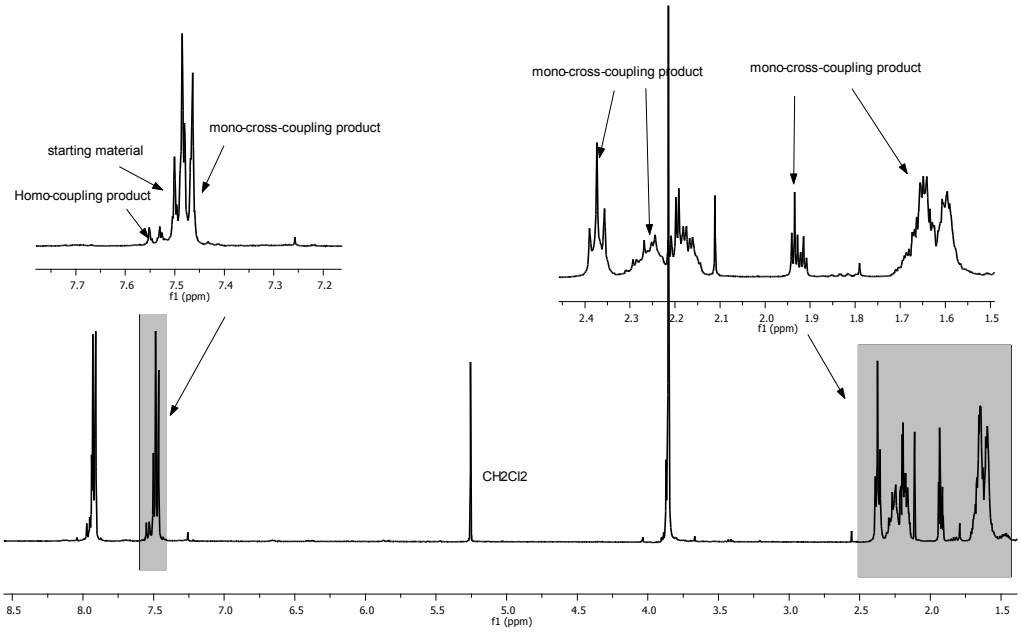

Figure 2.34: ^{1}H NMR spectrum (400 MHz, $CDCl_3$) of crude material of **35** using the standard Sonogashira cross-coupling method.

There are number of compounds present in the crude material and three of them are the homo-coupling by-product, the mono-cross-coupling product and the starting material, 4-(bromoethynyl)benzoic acid methyl ester. No desired product was observed in the ^{1}H NMR spectrum. The result from **Figure 2.34** implies that the Sonogashira method is not appropriate for the synthesis of **35** because the reaction was very slow. At the same time, the homo-coupling product was forming in the reaction, which will eventually reduce the yields of the desired product. In view of this, a method which can produce the cross-coupling product faster than the homo-coupling product is essential for these syntheses. By using the same conditions reported by Lei et al.,[37] the ratio of the cross-coupled product to the homo-coupled product is about 2:1 based on the ^{1}H NMR spectrum

(**Figure 2.35**) of the crude material. After passage through two silica gel columns, the pure product was obtained in ca. 30% yield.

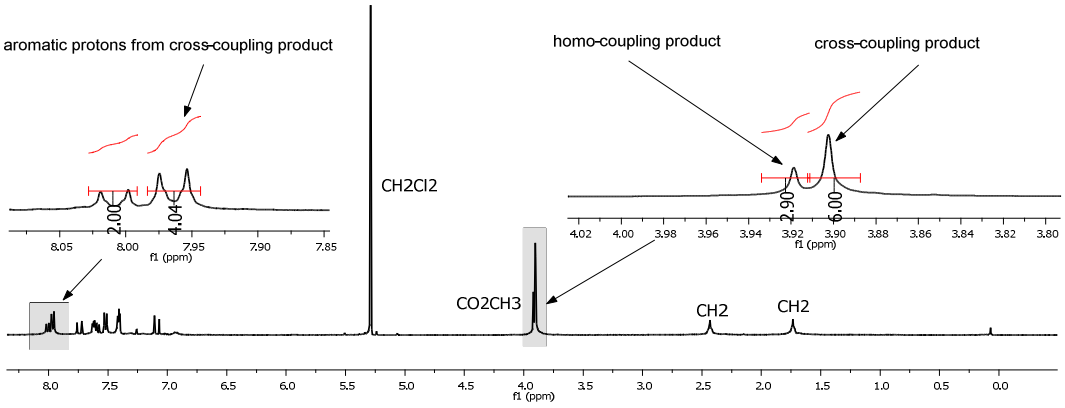

Figure 2.35: ^{1}H NMR spectrum (400 MHz, $CDCl_3$) of the crude material of **35** using Lei's method.

Cadiot-Chodkiewicz coupling was not attempted for the synthesis of **35** because it had failed for the preparation 1,12-bis(*p*-nitrophenyl)dodeca-1,3,9,11-tetrayne; after 48 h of stirring under an inert atmosphere, the starting materials still remained as the major components observed by GC-MS, which indicated that the Cadiot-Chodkiewicz coupling method was not successful.

Since **35** was obtained in reasonable yield by Lei's method, **36** (R = $BMes_2$, where Mes = mesityl) and **37** (R = SMe) were also synthesised using similar conditions. The ratios of cross-coupled products to homo-coupled products in crude **36** and **37** were also 2:1 based on ^{1}H NMR spectroscopy. By following work-up processes similar to that used for **35**, tetrayne **36** was obtained in 41% yield, whereas **37** was obtained in 33% yield.

The elemental analysis result of **36** shows only 86.88% for the C% value, which is 2.89% lower than the calculated one. This is a common problem that often occurs in the

compounds containing $BMes_2$, which has been postulated to be due to boron carbide formation during the elemental analysis; that causes the C% to be lower than the calculated value. In order to confirm the composition of **36**, the sample was submitted for accurate mass MS measurement, and the result shows that the accurate mass of **36** is 801.5075, which is 4.3 ppm different from the calculated mass of 801.5032.

For the barely soluble 1,3,9,11-dodecatetraynes with R = NO_2 and CN, the separation of the cross-coupling products from the homo-coupling products was even more difficult. Unfortunately, due to the poorly solubility of the homo- and cross-coupling products, these always eluted together product in all attempts at chromatographic separation.

2.2.4 Crystallographic data for 34(a) and 35

Tetrayne **34(a)** was recrystallised by dissolution in hot hexane and cooling to 5 °C to produce single crystals, which were characterised by X-ray diffraction. The molecular structure of **34(a)** is shown in **Figure 2.36**, and the crystallographic data are listed in **Table 2.7**. Compound **34(a)** crystallises in the monoclinic space group, $P2_1/n$. The centres of the molecules are co-incident with crystallographic inversion centres. The C≡C bond lengths for C8-C7 and C9-C10 are 1.1994(12) and 1.2026(12) Å, respectively, which are typical for C≡C triple bonds. However, the C8-C9 bond length of 1.3771(12) Å is much shorter than a typical single C-C bond length (1.54 Å), due to the sp hybridisation at these atoms. The C11-C12 and C12-C12' single C-C bond lengths are about 1.5361(12) and 1.5206(17) Å, respectively.

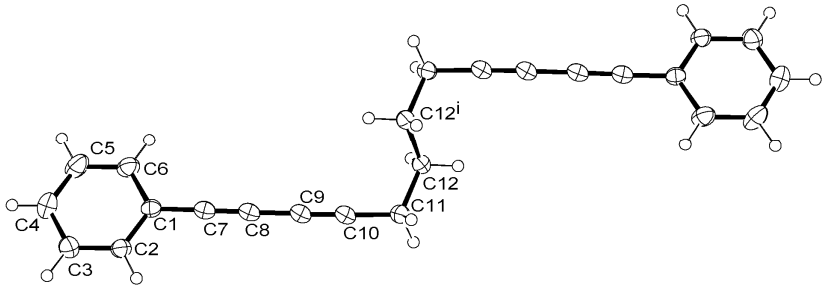

Figure 2.36: Molecular structure of **34(a)**. Thermal ellipsoids are shown at 50% probability.

A single crystal of **35** was grown at -20 °C from a concentrated CH_2Cl_2 solution. The crystal was characterised by single-crystal X-ray diffraction and the structure is shown in **Figure 2.37**, and the crystallographic data are listed in **Table 2.7**. Compound **35** crystallised in the triclinic space group, $P\bar{1}$. Similar to **34(a)**, the centres of the molecules are also co-incident with crystallographic inversion centres. The C13-C14 and C14-C14'single C-C bond lengths are 1.535(3) and 1.509(4) Å, respectively, and the C10-C11 bond length of 1.379(2) Å is indicative of sp hybridisation. The sp^2-sp^2 C1-C7 single bond length is 1.490(2) Å. Similarly to **34(a)**, the C≡C bond lengths for C9-C10 and C11-C12 are 1.200(2) and 1.199(2) Å, respectively.

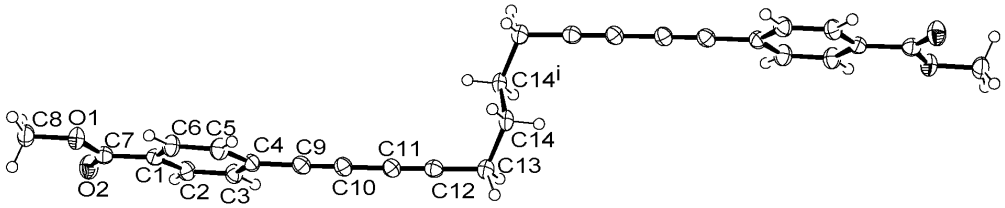

Figure 2.37: Molecular structure of **35**. Thermal ellipsoids are shown at 50% probability.

Tale 2.7: Crystallographic data for **34(a)** and **35**

Compound	**34(a)**	**35**
Empirical formula	$C_{24}H_{18}$	$C_{28}H_{22}O_4$
Formula weight	306.38	422.46
Temperature (K)	120(2)	120(2)
Crystal system	Monoclinic	Triclinic
Space group	$P2_1/n$	$P\bar{1}$
a(Å)	6.3896(3)	5.2122(3)
b (Å)	8.3988(3)	9.6467(5)
c (Å)	16.6290(6)	11.5659(5)
α (º)	90.00	72.603(18)
β (º)	99.937(6)	77.652(18)
γ (º)	90.00	75.178(18)
Volume ($Å^3$)	879.01(6)	530.49(5)
Z	2	1
Density (calculated) (Mg/m^3)	1.158	1.322
Absorption coefficient (mm^{-1})	0.065	0.088
Crystal size (mm^3)	0.40 x 0.35 x 0.25	0.40 x 0.11 x 0.02
Θ range for data collection (º)	2.49 to 29.98	2.26 to 29.92
Reflections collected	15809	5009
Independent reflections	2550	1877
Data / Restraints / Parameters	2550 / 0 / 145	1877 / 0 / 189
Final *R* indices [I > 2σ(I)]	*R*1 = 0.0437 *wR*2 = 0.1220	*R*1 = 0.0471 *wR*2 = 0.1113
R indices (all data)	*R*1 = 0.0491 *wR*2 = 0.1269	*R*1 = 0.0678 *wR*2 = 0.1227

2.3 Conclusions

Seven known 1,4-bis(*p*-R-phenyl)buta-1,3-diynes and two known extended phenyl ethynylene butadiynes have been synthesised using standard oxidative homo-coupling methods in the presence of the oxidants I_2 and O_2. All of them have been purified and characterised by NMR, MS and elemental analysis.

Four novel 1,12-bis(*p*-R-phenyl)dodeca-1,3,9,11-tetraynes have been synthesised and characterised by NMR, IR, MS and elemental analysis. The phenyl-based compound (R = H) was synthesised via Cadiot-Chodkiewicz coupling and the yield obtained was 42%. The other three compounds, with R = CO_2Me, $BMes_2$ and SMe, were synthesised using the procedures described by Lei et al.[37] The ratios of cross-coupled product to homo-coupled product for these three compounds in the crude material were 2:1. The yields of pure compounds obtained varied from 30% to 46%. The solubility of the homo- and cross-coupling products plays an important role in determining the yield of the isolated cross-coupling products. For highly soluble compounds such as **36** (R = $BMes_2$), the cross-coupling product can be separated from homo-coupling product much more easily than for insoluble compounds with R = CN and NO_2.

2.4 Experimental

2.4.1 General

All of the homo- and cross-coupling reactions namely Sonogashira, Cadiot-Chodkiewicz and Lei reactions were carried out in a fume cupboard equipped with a Schlenk vacuum line. Triethylamine, which was used for the Sonogashira and Lei reactions, was distilled from CaH_2 under nitrogen. The "P-olefin ligand" was supplied by Prof. Lei's group from the Green Catalyst Institute, Wuhan University, China. The compound 4-ethynylphenyldimesitylborane was supplied by Dr. Jonathan Collings from our group.

NMR spectra were recorded using Varian Mercury 200, Varian Unity 300, Bruker Avance 400 and Varian Inova 500 spectrometers at the following frequencies: ^{1}H – 200, 300 and 400 MHz, $^{13}C\{^{1}H\}$ NMR – 50.3, 100.6 MHz, $^{19}F\{^{1}H\}$NMR – 188, 376 MHz in $CDCl_3$ solvent. ^{13}C assignments for **33**, **34(a)**, **35** and **37** were based on the ChemNMR C-13 Estimation from *ChemDraw Ultra*® software version 7.0.1. Proton and carbon spectra were referenced to external $SiMe_4$ via residual protons in the deuterated solvents or the solvent resonance, respectively.

Elemental analyses were performed using an Exeter Analytical CE-440 Elemental Analyser in the Department of Chemistry at Durham University. GC-MS spectra were obtained from Hewlett-Packard 6890 Series II gas chromatograph equipped with a 5973 inert mass selective detector in EI mode and a 10 m fused silica capillary column (5% cross linked phenylmethylsilicone), under the following operating conditions: injector temperature at 250 °C, detector temperature 300 °C, the oven temperature was increased

at a rate of 20 °C/min from 50 - 280 °C. Ultra high purity grade helium gas was used as the carrier.

The mass spectra of **17**, **18**, **20**, **29**, **31**, **34(a)**, **35**, **36** and **37** were obtained using an Applied Biosystem Voyager-DE STR MALDI ToF mass spectrometer. The mass spectrum of **32** was obtained by electrospray (ES) using a Thermo-Finnigan LTQ FT spectrometer operating in positive ion mode.

IR spectra for **34(a)**, **35**, **36** and **37** were recorded as KBr discs using a Perkin Elmer Spectrum 100 series FT-IR spectrometer.

The crystallographic data collections and structure solutions were carried out by Dr. Andrei S. Batsanov, Department of Chemistry, Durham University, using a Bruker three-circle diffractometer with a CCD area detector. The structures were solved by direct methods and refined by full-matrix least squares against F^2 of all data, using SHELXTL software.

2.4.2 Preparation of trimethylsilyl (TMS) protected ethynylbenzenes

1 – Preparation of 4-[(trimethylsilyl)ethynyl]benzoic acid methyl ester[50-53]

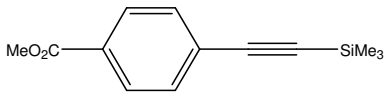

The compounds 4-iodobenzoic acid methyl ester (9.17 g, 35.0 mmol), CuI (0.13 g, 0.70 mmol) and $[PdCl_2(PPh_3)_2]$ (0.25 g, 0.35 mmol) were added to a flask which had been evacuated and refilled 3 times with N_2. Dry, degassed Et_3N (200 mL) was added via cannula. Trimethylsilylacetylene (TMSA) (3.78 g, 38.5 mmol) was added to the rapidly stirred mixture under N_2. The reaction was monitored *in situ* by GC-MS and the solvent was removed *in vacuo* once the reaction was complete (ca. 3 h). The grey solid residue

was transferred to the top of a 5 cm silica gel column and eluted with hexane. The hexane eluant was evaporated *in vacuo* to give **1** as a beige solid. Yield: 8.03 g, 99%. ^{1}H NMR (300 MHz, $CDCl_3$) δ: 7.97 (d, J = 8 Hz, 2H, CH_{arom}), 7.52 (d, J = 8 Hz, 2H, CH_{arom}), 3.91 (s, 3H, CO_2CH_3), 0.26 (s, 9H, $Si(CH_3)_3$). MS(EI) *m*/*z*: 232 [M^+].

2 – Preparation of 4-[(trimethylsilyl)ethynyl]benzotrifluoride[50, 54]

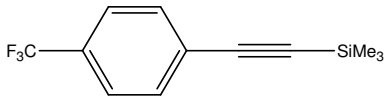

The compounds 4-bromobenzotrifluoride (22.50 g, 100.0 mmol), CuI (0.38 g, 2.00 mmol) and $[PdCl_2(PPh_3)_2]$ (0.70 g, 1.00 mmol) were added to a flask, which had been evacuated and refilled 3 times with N_2. Dry, degassed Et_3N (450 mL) was added to the flask via cannula. TMSA (10.80 g, 110.0 mmol) was added into the rapidly stirred mixture under N_2. The reaction was heated at 60 °C for 15 h and examined by GC-MS. Once complete, the solvent was removed *in vacuo*. The residue was transferred to the top of a 5 cm silica gel column and eluted with hexane. The hexane eluant was evaporated *in vacuo* to give **2** as a brown-yellow oil. Yield: 7.09 g, 29%. ^{1}H NMR (400 MHz, $CDCl_3$) δ: 7.55 (m, 4H, CH_{arom}), 0.26 (s, 9H, $Si(CH_3)_3$). $^{19}F\{^{1}H\}$ NMR (188 MHz, $CDCl_3$) δ: -63.30 (s, 3F, CF_3). MS (EI) *m*/*z*: 242 [M^+].

3 – Preparation of 4-[(trimethylsilyl)ethynyl]benzonitrile[51, 55]

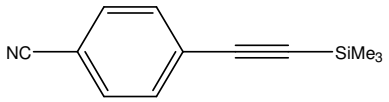

The compounds 4-bromobenzonitrile (10.19 g, 56.0 mmol), CuI (0.21 g, 1.12 mmol) and $[PdCl_2(PPh_3)_2]$ (0.39 g, 0.56 mmol) were added to a flask, which had been evacuated

and refilled 3 times with N_2. Dry, degassed Et_3N (250 mL) was added via cannula. TMSA (6.05 g, 61.6 mmol) was added to the rapidly stirred mixture under N_2. The reaction was stirred at room temperature for 4 h and monitored *in situ* by GC-MS and the solvent was removed *in vacuo* once the reaction was complete. The residue was transferred to the top of a 5 cm silica gel column and eluted with hexane. The hexane eluant was evaporated *in vacuo* to give **3** as a yellow solid. Yield: 6.91 g, 62%. ^{1}H NMR (200 MHz, $CDCl_3$) δ: 7.54 (m, 4H, CH_{arom}), 0.25 (s, 9H, $Si(CH_3)_3$). MS (EI) *m*/*z*: 199 [M^+].

4 – Preparation of 4-[(trimethylsilyl)ethynyl]nitrobenzene[55, 56]

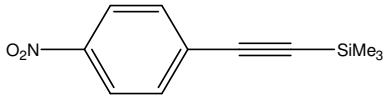

The compounds 1-iodo-4-nitrobenzene (18.68 g, 75.00 mmol), CuI (0.29 g, 1.50 mmol) and $[PdCl_2(PPh_3)_2]$ (0.53 g, 0.75 mmol) were added to a flask, which had been evacuated and refilled 3 times with N_2. Dry, degassed Et_3N (350 mL) was added via cannula. TMSA (8.10 g, 82.50 mmol) was added to the rapidly stirred mixture under N_2. The reaction was stirred at room temperature for 4 h and monitored *in situ* by GC-MS and the solvent was removed *in vacuo* once the reaction was complete. The residue was transferred to the top of a 5 cm silica gel column and eluted with hexane. The hexane eluant was evaporated *in vacuo* to give **4** as a yellow solid. Yield: 14.39 g, 87%. ^{1}H NMR (200 MHz, $CDCl_3$) δ: 8.17 (d, J = 8 Hz, 2H, CH_{arom}), 7.59 (d, J = 8 Hz, 2H, CH_{arom}), 0.27 (s, 9H, $Si(CH_3)_3$). MS (EI) *m*/*z*: 219 [M^+].

5 – Preparation of 4-[(trimethylsilyl)ethynyl]toluene[55-57]

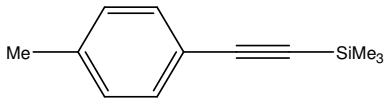

The compounds 4-bromotoluene (15.40 g, 90.02 mmol), CuI (0.34 g, 1.80 mmol) and $[PdCl_2(PPh_3)_2]$ (0.63 g, 0.90 mmol) were added to a flask, which had been evacuated and refilled with N_2 3 times. Dry, degassed Et_3N (350 mL) was added via cannula. TMSA (9.73 g, 99.02 mmol) was added to the rapidly stirred mixture under N_2. The reaction was heated to 65 - 68 °C for 15 h and then examined by GC-MS. Once complete, the solvent was removed *in vacuo*. The dark grey solid residue was transferred to the top of a 5 cm silica gel column and eluted with hexane. The hexane eluant was evaporated *in vacuo*, which gave **5** as a dark brown oil. Yield: 14.08 g, 83%. ^{1}H NMR (200 MHz, $CDCl_3$) δ: 7.35 (d, J = 8 Hz, 2H, CH_{arom}), 7.07 (d, J = 8 Hz, 2H, CH_{arom}), 2.29 (s, 3H, CH_3), 0.26 (s, 9H, $Si(CH_3)_3$). MS (EI) m/z: 188 [M^+].

6 – Preparation of 4-[(trimethylsilyl)ethynyl]anisole[50, 55-57]

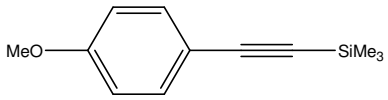

The compounds 4-iodoanisole (4.91 g, 20.99 mmol), CuI (0.08 g, 0.42 mmol) and $[PdCl_2(PPh_3)_2]$ (0.15 g, 0.21 mmol) were added to a flask, which had been evacuated and refilled 3 times N_2. Dry, degassed Et_3N (150 mL) was added to the flask via cannula. TMSA (2.27 g, 23.10 mmol) was added to the rapidly stirred mixture under N_2. The reaction was heated to 60 – 65 °C for 15 h and monitored *in situ* by GC-MS. Once completed, the solvent was removed *in vacuo*. The residue was transferred to the top of a 5 cm silica gel column and eluted with hexane. The hexane eluant was evaporated *in*

vacuo giving **6** as a yellowish-brown oil. Yield: 3.65 g, 85%. ^{1}H NMR (400 MHz, $CDCl_3$) δ: 7.42 (d, *J* = 8 Hz, 2H, CH_{arom}), 6.81 (d, *J* = 8 Hz, 2H, CH_{arom}), 3.75 (s, 3H, OCH_3), 0.28 (s, 9H, $Si(CH_3)_3$). MS (EI) *m*/*z*: 204 [M^+].

7 – Preparation of 4-[(trimethylsilyl)ethynyl]thioanisole[58, 59]

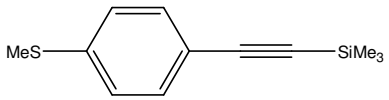

The compounds 4-bromothioanisole (15.01 g, 73.90 mmol), CuI (0.28 g, 1.48 mmol) and $[PdCl_2(PPh_3)_2]$ (0.52 g, 0.74 mmol) were added to a flask, which had been evacuated and refilled 3 times N_2. Dry, degassed Et_3N (350 mL) was added to the flask via cannula. TMSA (7.98 g, 81.29 mmol) was added to the rapidly stirred mixture under N_2. The reaction was heated at 60 °C for 72 h and the solvent was removed *in vacuo* when the reaction completed. The residue was transferred to the top of a 5 cm silica gel column and eluted with hexane. The hexane eluant was evaporated *in vacuo* giving **7** as a yellowish oil. Yield: 12.06 g, 74%. ^{1}H NMR (400 MHz, $CDCl_3$) δ: 7.40 (d, *J* = 8 Hz, 2H, CH_{arom}), 7.15 (d, *J* = 8 Hz, 2H, CH_{arom}), 2.44 (s, 3H, SCH_3), 0.25 (s, 9H, $Si(CH_3)_3$). MS (EI) *m*/*z*: 220 [M^+].

2.4.3 Preparation of ethynylbenzenes

8 – 4-ethynylbenzoic acid methyl ester[32, 51, 52]

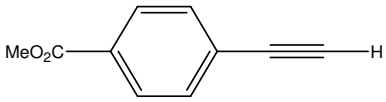

Compound **1** (1.63 g, 7.00 mmol) was added to a suspension of Na_2CO_3 (2.97 g, 28.00 mmol) in MeOH (175 mL) and water (50 mL) and the mixture was stirred for 4 h. Then,

water (ca. 450 mL) was added to into the reaction. The suspension was transferred to a separatory funnel and Et_2O (3 x 50 mL) was added. The organic layer was separated and dried over $MgSO_4$. The solvent was removed *in vacuo* to give **8** as a white solid. Yield: 1.09 g, 97%. ^{1}H NMR (200 MHz, $CDCl_3$) δ: 7.95 (d, J = 8 Hz, 2H, CH_{arom}), 7.50 (d, J = 8 Hz, 2H, CH_{arom}), 3.87 (s, 3H, CO_2CH_3), 3.23 (s, 1H, C≡C-H). MS (EI) *m*/*z*: 160 [M^+].

9 – 4-ethynylbenzotrifluoride[32, 54]

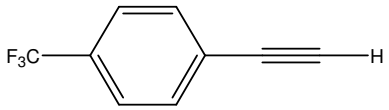

Compound **2** (7.01 g, 28.92 mmol) was added to a suspension of Na_2CO_3 (12.26 g, 115.68 mmol) in MeOH (400 mL) and H_2O (100 mL) and the mixture was stirred for 24 h. Water (ca. 700 mL) was added into the reaction and the suspension was transferred to a separatory funnel, then, Et_2O (3 x 100 mL) was added. The organic layer was separated and dried over $MgSO_4$. The Et_2O solvent was removed by distillation at ambient pressure. (**CAUTION:** Terminal alkynes should not be distilled at elevated temperatures as explosions have been reported.) The remaining liquid was dissolved in CH_2Cl_2 (150 mL) and filtered through a sinter. Then, most of the solvent was removed by distillation using a Vigreux column and the remainder was removed via evaporation at ambient temperature to give **9** as a light yellow oil. Yield: 1.43 g, 29%. ^{1}H NMR (400 MHz, $CDCl_3$) δ: 7.60 (m, 4H, CH_{arom}), 3.20 (s, 1H, C≡C-H). ^{19}F{^{1}H} NMR (376 MHz, $CDCl_3$) δ: -63.32 (s, 3F, CF_3). MS (EI) *m*/*z*: 170 [M^+].

10 – 4-ethynylbenzonitrile[32, 51, 60]

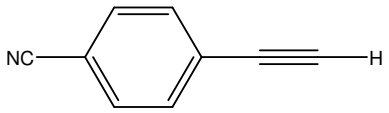

Compound **3** (5.01 g, 25.12 mmol) was added to a suspension of Na_2CO_3 (10.65 g, 100.48 mmol) in MeOH (350 mL) and H_2O (80 mL) and the mixture was stirred for 15 h. Then, water (ca. 500 mL) was added into the reaction. The suspension was transferred to separatory funnel and Et_2O (3 x 100 mL) was added. The organic layer was separated and dried over $MgSO_4$. The solvent was removed *in vacuo* to give **10** as a yellow-orange solid. Yield: 2.37 g, 74%. ^{1}H NMR (200 MHz, $CDCl_3$) δ: 7.59 (m, 4H, CH_{arom}), 3.30 (s, 1H, C≡C-H). MS (EI) *m*/*z*: 127 [M^+].

11 – 4-ethynylnitrobenzene[32, 55]

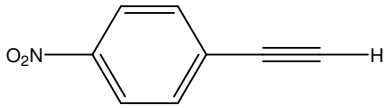

Compound **4** (10.01 g, 45.65 mmol) was added to a suspension of Na_2CO_3 (19.35 g, 182.60 mmol) in MeOH (400 mL) and H_2O (100 mL) and the mixture was stirred for 15 h. Then, water (ca. 700 mL) was added into the reaction. The suspension was transferred to separatory funnel and CH_2Cl_2 (3 x 100 mL) was added. The organic layer was separated and dried over $MgSO_4$. The solvent was removed *in vacuo* to give **11** as a yellow solid. Yield: 5.95 g, 89%. ^{1}H NMR (200 MHz, $CDCl_3$) δ: 8.20 (d, J = 8 Hz, 2H, CH_{arom}), 7.64 (d, J = 8 Hz, 2H, CH_{arom}), 3.35 (s, 1H, C≡C-H). MS (EI) *m*/*z*: 147 [M^+].

12 – 4-ethynyltoluene[32, 57, 61]

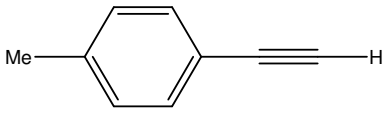

Compound **5** (10.01 g, 53.16 mmol) was added to a suspension of Na_2CO_3 (22.54 g, 212.64 mmol) in MeOH (400 mL) and H_2O (100 mL) and the mixture was stirred 15 h. Then, water (ca. 700 mL) was added into the reaction. The suspension was transferred to a separatory funnel and Et_2O (3 x 100 mL) was added. The organic layer was separated and dried over $MgSO_4$. The solvent was removed *in vacuo* to give **12** as a brown oil. Yield: 4.35 g, 70%. ^{1}H NMR (400 MHz, $CDCl_3$) δ: 7.41 (d, J = 8 Hz, 2H, CH_{arom}), 7.14 (d, J = 8 Hz, 2H, CH_{arom}), 3.05 (s, 1H, C≡C-H), 2.37 (s, 3H, CH_3). MS (EI) *m*/*z*: 116 [M^+].

13 – 4-ethynylanisole[32, 57]

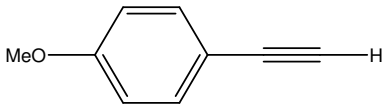

Compound **6** (1.00 g, 4.90 mmol) was added to a suspension of Na_2CO_3 (2.08 g, 19.6 mmol) in MeOH (150 mL) and H_2O (50 mL) and the mixture was stirred for 15 h. Then, water (ca. 450 mL) was added into the reaction. The suspension was transferred to a separatory funnel and CH_2Cl_2 (3 x 50 mL) was added. The organic layer was separated and dried over $MgSO_4$. The solvent was removed *in vacuo* to give **13** as a light yellow-green solid. Yield: 0.48 g, 74%. ^{1}H NMR (400 MHz, $CDCl_3$) δ: 7.44 (d, J = 8 Hz, 2H, CH_{arom}), 6.84 (d, J = 8 Hz, 2H, CH_{arom}), 3.80 (s, 3H, OCH_3), 3.02 (s, 1H, C≡C-H). MS (EI) *m*/*z*: 132 [M^+].

14 – 4-ethynylthioanisole[32, 62, 63]

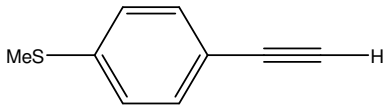

Compound **7** (12.02 g, 54.53 mmol) was added to a suspension of Na_2CO_3 (23.12 g, 218.12 mmol) in MeOH (450 mL) and H_2O (100 mL) and the mixture was stirred for 15 h. Then water (ca. 1.0 L) was added into the reaction. The suspension was transferred to a separatory funnel and CH_2Cl_2 (3 x 100 mL) was added. The organic layer was separated and dried over $MgSO_4$. The solvent was removed *in vacuo* to give **14** as a light yellow-green solid. Yield: 4.02 g, 50%. ^{1}H NMR (400 MHz, $CDCl_3$) δ: 7.40 (d, J = 8 Hz, 2H, CH_{arom}), 7.16 (d, J = 8 Hz, 2H, CH_{arom}), 3.15 (s, 1H, C≡C-H), 2.42 (s, 3H, SCH_3). MS (EI) m/z: 148 [M^+].

2.4.4 Preparation of 1,4-bis(*p*-R-phenyl)buta-1,3-diynes

15 – 1,4-bis(*p*-carbomethoxyphenyl)buta-1,3-diyne[33, 64]

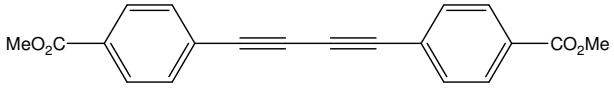

Compound **8** (1.00 g, 6.25 mmol), CuI (0.011 g, 0.06 mmol), [$PdCl_2(PPh_3)_2$] (0.021 g, 0.03 mmol), I_2 (0.76 g, 3.00 mmol) and Et_3N (100 mL) were added to a round bottom flask and the reaction was stirred in air for 15 h. The reaction was monitored *in situ* by GC-MS, and the Et_3N was removed *in vacuo* once the reaction was complete. The residue was dissolved in CH_2Cl_2 (150 mL). The organic fraction was washed thoroughly with a saturated $Na_2S_2O_3$ solution, dried over $MgSO_4$ and then the solvent was removed *in vacuo* to give a brown solid. The solid was placed on the top of a 5 cm silica gel column and eluted with hot toluene. The toluene eluant was evaporated *in vacuo* to give **15** as a

white solid. Yield: 0.80 g, 80%. ^{1}H NMR (300 MHz, $CDCl_3$) δ: 8.02 (d, *J* = 8 Hz, 4H, CH_{arom}), 7.59 (d, 4H, *J* = 8 Hz, CH_{arom}), 3.93 (s, 6H, CO_2CH_3). Anal. Calcd. For $C_{20}H_{14}O_4$: C, 75.46; H, 4.43. Found: C, 75.42, H, 4.38%. MS (EI) *m*/*z*: 318 [M^+].

16 – 1,4-bis(*p*-trifluoromethylphenyl)buta-1,3-diyne[33, 65, 66]

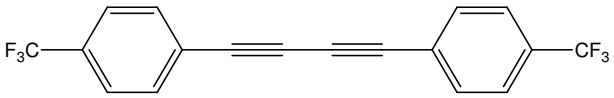

Compound **9** (3.40 g, 20.00 mmol), CuI (0.038 g, 0.20 mmol), [$PdCl_2(PPh_3)_2$] (0.07 g, 0.10 mmol) and Et_3N (150 mL) were added to a round bottom flask and the reaction was stirred in air for 15 h. The reaction was monitored *in situ* by GC-MS, and the Et_3N was removed *in vacuo* once the reaction was complete. The residue was placed on the top of a 5 cm silica gel column, which was eluted with hexane. The hexane eluant was evaporated *in vacuo* and gave **16** as a yellow solid. Yield: 0.87 g, 26%. ^{1}H NMR (300 MHz, $CDCl_3$) δ: 7.65 (s, 8H, CH_{arom}). ^{19}F{^{1}H} NMR (376 MHz, $CDCl_3$) δ: -63.42 (s, 6F, CF_3). Anal. Calcd. for $C_{18}H_8F_6$: C, 63.92; H, 2.38. Found: C, 63.93; H, 2.47%. MS (EI) *m*/*z*: 338 [M^+].

17 – 1,4-bis(*p*-cyanophenyl)buta-1,3-diyne[8, 33, 67]

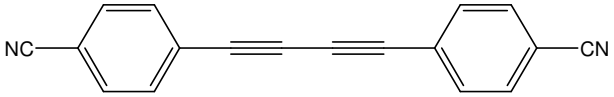

Compound **10** (1.00 g, 7.87 mmol), CuI (0.015 g, 0.079 mmol), [$PdCl_2(PPh_3)_2$] (0.027 g, 0.039 mmol), I_2 (1.14 g, 4.50 mmol) and Et_3N (100 mL) were added to a round bottom flask and the reaction was stirred in air for 48 h. The Et_3N was removed *in vacuo*. The resulting dark grey brown solid was transferred to the top of a 5 cm silica gel column and

eluted with boiling toluene. The toluene was removed *in vacuo* to give a brown-yellow solid. The brown-yellow solid was washed with CH_2Cl_2 (150 mL) and the remaining white solid was recrystallised from hot toluene to yield pure **17**. Yield: 0.56 g, 56%. ^{1}H NMR (400 MHz, $CDCl_3$) δ: 7.64 (d, *J* = 9 Hz, 4H, CH_{arom}), 7.61 (d, *J* = 9 Hz, 4H, CH_{arom}). Anal. Calcd. for $C_{18}H_8N_2$: C, 85.70; H, 3.20; N, 11.10. Found: C, 85.44; H, 3.24; N, 11.14%. MS (MALDI$^+$) *m*/*z*: 252 [M^+].

18 – 1,4-bis(*p*-nitrophenyl)buta-1,3-diyne[8, 68-70]

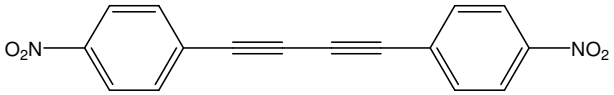

Compound **11** (2.00 g, 13.60 mmol), CuI (0.026 g, 0.136 mmol), $[PdCl_2(PPh_3)_2]$ (0.048 g, 0.068 mmol), I_2 (1.78 g, 7.00 mmol) and Et_3N (150 mL) were added to a round bottom flask and the reaction was stirred in air for 48 h. The Et_3N was removed *in vacuo*. The resulting dark grey-brown solid was transferred to the top of a 5 cm silica gel column and eluted with boiling toluene. The toluene was removed *in vacuo* and gave a brown-yellow solid in the round bottom flask. The brown-yellow solid was washed with CH_2Cl_2 (150 mL) and the remaining yellow solid was recrystallised from hot toluene. Yield: 1.38 g, 69%. ^{1}H NMR (400 MHz, $CDCl_3$) δ: 8.24 (d, *J* = 8 Hz, 4H, CH_{arom}), 7.70 (d, *J* = 8 Hz, 4H, CH_{arom}). Anal. Calcd. for $C_{16}H_8N_2O_4$: C, 65.76; H, 2.76; N, 9.59. Found: C, 65.89; H, 2.78; N, 9.25%. MS (MALDI$^+$) *m*/*z*: 292 [M^+].

19 – 1,4-bis(*p*-tolyl)buta-1,3-diyne[33, 65, 66]

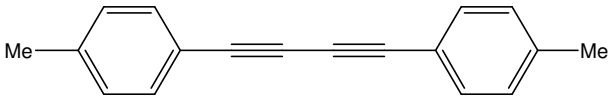

Compound **12** (1.00 g, 8.62 mmol), CuI (0.016 g, 0.086 mmol), $[PdCl_2(PPh_3)_2]$ (0.030 g, 0.043 mmol) and Et_3N (100 mL) were added to a round bottom flask and the solution was stirred for 15 h in the open air. The reaction was monitored *in situ* by GC-MS and the Et_3N was removed *in vacuo* once the reaction was complete. The residue brown-grey solid was applied to the top of a silica pad and eluted by Et_2O. The Et_2O was removed *in vacuo* and giving a brown solid, which was sublimed at 2.0 x 10^{-3} Torr and 240 °C to give **19** as white solid. Yield: 0.61 g, 61%. ^{1}H NMR (400 MHz, $CDCl_3$) δ: 7.35 (d, J = 9 Hz, 4H, CH_{arom}), 7.07 (d, J = 9 Hz, 4H, CH_{arom}), 2.30 (s, 6H, CH_3). Anal. Calcd. for $C_{18}H_{14}$: C, 93.87; H, 6.13. Found: C, 93.42; H, 6.11%. MS (EI) *m*/*z*: 230 [M^+].

20 – 1,4-bis(*p*-methylthiophenyl)buta-1,3-diyne[33]

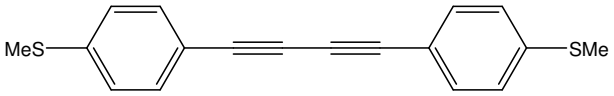

Compound **14** (2.00 g, 13.51 mmol), CuI (0.026 g, 0.135 mmol), $[PdCl_2(PPh_3)_2]$ (0.048 g, 0.068 mmol) and Et_3N (100 mL) were added to a round bottom flask and the mixture was stirred open air for 15 h. The reaction was monitored *in situ* by GC-MS and the Et_3N was removed *in vacuo* once the reaction was complete. The residual brown-grey solid was applied to the top of a silica gel pad and eluted with Et_2O. The Et_2O was removed *in vacuo* giving a dark brown solid. The pure product was obtained via recrystallisation from hot $CHCl_3$ at 5 °C for 15 h. White solid was formed, separated, and dried *in vacuo*. Yield: 1.26 g, 63%. ^{1}H NMR (400 MHz, $CDCl_3$) δ: 7.42 (d, J = 8 Hz, 4H, CH_{arom}), 7.17

(d, J = 8 Hz, 4H, CH_{arom}), 2.49 (s, 6H, SCH_3). Anal. Calcd. for $C_{18}H_{14}S_2$: C, 73.43; H, 4.79. Found: C, 72.95; H, 4.77%. MS (MALDI$^+$) *m*/*z*: 294 [M^+].

21 – 1,4-bis(*p*-methoxyphenyl)buta-1,3-diyne[33, 65, 66, 71]

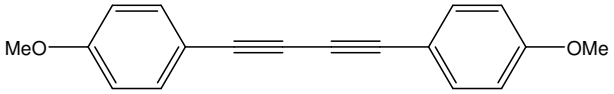

The compound $Cu(OAc)_2$ (1.13 g, 6.24 mmol), slurried in MeOH (20 mL) and pyridine (20 mL) was added dropwise to a solution of **13** (0.50 g, 3.78 mmol) in MeOH (50 mL). The mixture was refluxed at 70 °C for 15 min and allowed to cool to room temperature. Aqueous HCl (1.0 M, 20 mL) was added to the mixture and the product was extracted by Et_2O (3 x 30 mL). The organic fraction was washed with water (3 x 30 mL), separated and dried over $MgSO_4$. The organic solvent was removed *in vacuo* giving **20** as a yellow solid. Yield: 0.40 g, 81%. ^{1}H NMR (400 MHz, $CDCl_3$) δ: 7.39 (d, J = 9 Hz, 4H, CH_{arom}), 6.79 (d, J = 9 Hz, 4H, CH_{arom}), 3.76 (s, 6H, OCH_3). Anal. Calcd. for $C_{18}H_{14}O_2$: C, 82.42; H, 5.38. Found: C, 81.79; H, 5.35%. MS (EI) *m*/*z*: 262 [M^+].

2.4.5 Preparation of extended bis(arylethynyl)diarylbuta-1,3-diynes and related compounds

22 – 4-(4-bromophenyl)-2-methylbut-3-yn-2-ol[72]

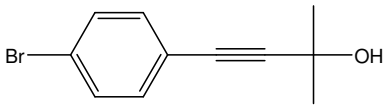

The compounds 1-bromo-4-iodobenzene (28.30 g, 100.04 mmol), CuI (0.38 g, 2.00 mmol) and $[PdCl_2(PPh_3)_2]$ (0.70 g, 1.00 mmol) were added to dry and degassed Et_3N (ca. 450 mL) in a round bottom flask, which had been evacuated and refilled with N_2 3 times.

2-Methylbut-3-yn-2-ol (9.26 g, 110.04 mmol) was added to the rapidly stirred mixture under N_2. The reaction was stirred at room temperature for 15 h and then examined by GC-MS. Once complete, the solvent was removed *in vacuo*. The dark brown solid residue was transferred to the top of a 5 cm silica gel column and eluted with hexane : CH_2Cl_2 (4 : 1 v/v) (ca. 1.5 L). The solvent was removed *in vacuo* to give a bright yellow solid. The product was further purified by recrystallisation from hot hexane at -20 °C for 15 h. The resulting white solid was collected by filtration and dried *in vacuo*. Yield: 20.4 g, 85%. ^{1}H NMR (400 MHz, $CDCl_3$) δ: 7.35 (d, J = 9 Hz, 2H, CH_{arom}), 7.20 (d, J = 9 Hz, 2H, CH_{arom}), 3.33 (s, 1H, OH), 1.58 (s, 6H, $C(CH_3)_2$). MS (EI) m/z: 238 [M^+].

23 – 4-(4-trimethylsilylethynylphenyl)-2-methylbut-3-yn-2-ol[73, 74]

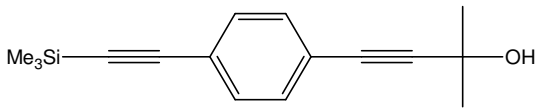

Compound **22** (10.20 g, 42.65 mmol), CuI (0.16 g, 0.85 mmol) and [$PdCl_2(PPh_3)_2$] (0.30 g, 0.43 mmol) were added to a flask, which had been evacuated and refilled with N_2 3 times. Dry, degassed Et_3N (250 mL) was added via cannula. TMSA (4.61 g, 46.92 mmol) was added to the rapidly stirred mixture under N_2. The reaction was heated at 80 °C for 15 h and then examined by GC-MS. Once complete, the solvent was removed *in vacuo*. The dark grey solid residue was transferred to the top of a 5 cm silica gel column and eluted with hexane : CH_2Cl_2 (4 : 1 v/v) (ca. 1.0 L). The solvent was removed *in vacuo* to give **23** as a light brown solid. The product was further purified by passage through a silica gel column eluting with hexane : CH_2Cl_2 (9 : 1 v/v). The solvent was removed *in vacuo* to give the pure product as a white solid. Yield: 8.50 g, 78%. ^{1}H NMR

(400 MHz, $CDCl_3$) δ: 7.37 (d, J = 8 Hz, 2H, CH_{arom}), 7.31 (d, J = 8 Hz, 2H, CH_{arom}), 2.52 (s, 1H, OH), 1.59 (s, 6H, $C(CH_3)_2$), 0.24 (s, 9H, $Si(CH_3)_3$). MS (EI) m/z: 256 [M^+].

24 – 4-ethynylphenylethynyltrimethylsilane[73, 74]

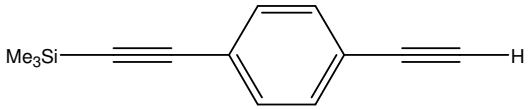

Compound **23** (8.00 g, 31.25 mmol), freshly powdered NaOH (0.13 g, 3.13 mmol) and toluene (100 mL) were added to a two neck round bottom flask and the reaction mixture was refluxed at 110 °C for 2 h. The system was purged with nitrogen gas to assist the removal of acetone, which formed in the reaction, through the condenser. Once the reaction was complete, the black-brown toluene solution was filtered and the solvent was removed *in vacuo* to give a dark brown solid. The solid was transferred to the top of a silica gel column and eluted with hexane. The solvent was removed *in vacuo* to give **24** as a light yellow solid. Yield: 4.83 g, 78%. ^{1}H NMR (400 MHz, $CDCl_3$) δ: 7.41 (s, 4H, CH_{arom}), 3.16 (s, 1H, C≡CH), 0.25 (s, 9H, $Si(CH_3)_3$). MS (EI) m/z: 198 [M^+].

25 – 4-iodobenzoic acid *n*-octyl ester[75]

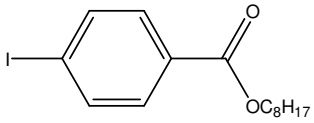

To an ice cooled and stirred solution of 4-iodobenzoic acid (7.40 g, 29.84 mmol), *n*-octan-1-ol (4.55 g, 34.94 mmol) and 4-*N*,*N*-dimethylaminopyridine (DMAP) (0.378 g, 3.09 mmol) in 150 mL of CH_2Cl_2, was added dropwise a solution of *N*,*N*'-dicyclohexylcarbodiimide (DCCI) (12.70 g, 61.50 mmol) in 30 mL of CH_2Cl_2. The mixture was stirred for 15 h. The solution was filtered and the solvent was removed *in*

vacuo. The crude product was transferred to the top of a 5 cm silica gel pad and eluted with hexane. Hexane was removed *in vacuo* and followed by Kugelrohr distillation (120 – 130 °C, 3.1 x 10^{-3} Torr) gave a brown-yellow oil. Yield: 5.34 g, 50%, ^{1}H NMR (400 MHz, $CDCl_3$) δ: 7.76 (d, *J* = 9 Hz, 2H, CH_{arom}), 7.71 (d, *J* = 9 Hz, 2H, CH_{arom}), 4.28 (t, *J* = 7 Hz, 2H, OCH_2), 1.73 (quint, *J* = 7 Hz, 2H, OCH_2CH_2), 1.34 (m, 2H, CH_2CH_3), 1.27 (m, 8H, CH_2), 0.86 (t, *J* = 7 Hz, 3H, CH_2CH_3). Anal. Calcd. for $C_{15}H_{21}O_2I$: C, 50.01; H, 5.88. Found: C, 49.91; H, 5.90%. MS (EI) *m*/*z*: 360 [M^+].

26 – di-*n*-hexyl-(4-iodophenyl)-amine[76-78]

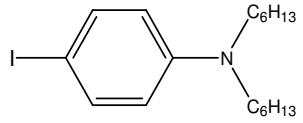

To a solution of *p*-iodoaniline (10.95 g, 50.00 mmol) in DMF (ca. 160 mL) was added 1-iodohexane (34.0 g, 160.32 mmol) and Na_2CO_3 (9.20 g, 86.80 mmol). The reaction was heated at 120 °C for 40 h. Then the solvent was removed *in vacuo*, and the residue was dissolved in CH_2Cl_2 and passed through a 5 cm celite column. The solvent was removed *in vacuo* to give a dark brown oil which was purified by passing through a silica gel column eluting with CH_2Cl_2 : hexane, (1 : 10 v/v) (ca. 750 mL). The solvent was removed *in vacuo* to give the pure product as light brown oil. Yield: 10.73 g, 55%. ^{1}H NMR (400 MHz, $CDCl_3$) δ: 7.47 (d, *J* = 9 Hz, 2H, CH_{arom}), 6.48 (d, *J* = 9 Hz, 2H, CH_{arom}), 3.23 (t, 4H, $N(CH_2)_2$), 1.56 (quint, *J* = 6 Hz, 4H, $N(CH_2CH_2)_2$), 1.32 (m, 12H, CH_2), 0.92 (t, *J* = 6 Hz, 6H, 2 x CH_3). MS (EI) *m*/*z*: 387 [M^+].

27 – 4-(4-trimethylsilylethynylphenylethynyl)-benzoic acid *n*-octylester[49]

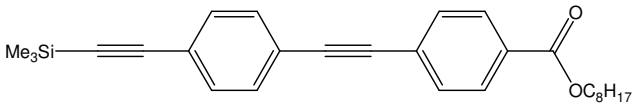

Compound **25** (1.80 g, 5.00 mmol), CuI (0.019 g, 0.10 mmol) and $[PdCl_2(PPh_3)_2]$ (0.035 g, 0.05 mmol) were added to a round bottom flask, which had been evacuated and refilled with N_2 3 times. Dry, degassed Et_3N (100 mL) was added via cannula. Compound **24** (1.09 g, 5.50 mmol) was added to the rapidly stirred mixture under N_2. The reaction was stirred at room temperature for 15 h and then examined by GC-MS. Once complete, the solvent was removed *in vacuo*. The crude solid was transferred to the top of a 5 cm silica gel pad and eluted with hexane : CH_2Cl_2, (4 : 1 v/v) (ca. 500 mL). The solvent was removed *in vacuo* to give a yellow solid. The product was further purified by recrystallisation by dissolution in hot hexane and then cooling to -20 °C. The pure product was isolated as a yellowish solid. Yield: 2.02 g, 94%. ^{1}H NMR (200 MHz, $CDCl_3$) δ: 8.02 (d, J = 9 Hz, 2H, CH_{arom}), 7.58 (d, J = 9 Hz, 2H, CH_{arom}), 7.46 (s, 4H, CH_{arom}), 4.32 (t, J = 7 Hz, 2H, OCH_2), 1.75 (quint, J = 7 Hz, 2H, OCH_2CH_2), 1.30 (m, 10H, CH_2), 0.88 (t, J = 7 Hz, 3H, CH_3). Anal. Calcd. for $C_{28}H_{34}O_2Si$: C, 78.09; H, 7.96. Found: C, 77.98; H, 7.90%. MS (EI) m/z: 430 [M^+].

28 – di-*n*-hexyl-[4-(4-trimethylsilylethynylphenylethynyl)phenyl]-amine

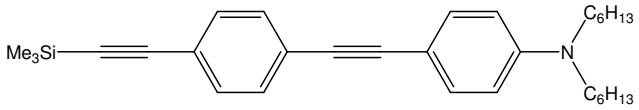

Compound **26** (3.87 g, 9.99 mmol), CuI (0.038 g, 0.20 mmol) and $[PdCl_2(PPh_3)_2]$ (0.070 g, 0.10 mmol) were added to a round bottom flask, which had been evacuated and refilled with N_2 3 times. Dry, degassed Et_3N (150 mL) was added via cannula. Compound

24 (2.18 g, 11.00 mmol) was added to the rapidly stirred mixture under N_2. The reaction was stirred at room temperature for 15 h and then examined by GC-MS. Once complete, the solvent was removed *in vacuo*. The dark brown solid residue was transferred to the top of a 5 cm silica gel pad and eluted with hexane. The solvent was removed *in vacuo* to give a yellow solid. Yield: 4.02 g, 88%. ^{1}H NMR (400 MHz, $CDCl_3$) δ: 7.41 (s, 4H, CH_{arom}), 7.34 (d, J = 9 Hz, 2H, CH_{arom}), 6.56 (d, J = 9 Hz, 2H, CH_{arom}), 3.27 (t, J = 7 Hz, 4H, $N(CH_2)_2$), 1.58 (m, 4H, $N(CH_2C\mathit{H}_2)_2$), 1.32 (m, 12H, CH_2), 0.90 (t, J = 6 Hz, 6H, 2 x CH_3), 0.25 (s, 9H, $Si(CH_3)_3$). Anal. Calcd. for $C_{31}H_{43}NSi$: C, 81.34; H, 9.47; N, 3.06. Found: C, 81.46; H, 9.46; N, 2.81%. MS (EI) *m*/*z*: 457 [M^+].

29 – 4-(4-ethynylphenylethynyl)-benzoic acid *n*-octyl ester[49]

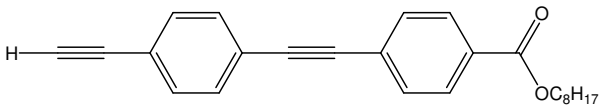

Compound **27** (1.40 g, 3.25 mmol), [n-Bu_4N]F (1.0 M in THF) (3.25 mL, 3.25 mmol) and Et_2O (50.0 mL) were added to a round bottom flask and the reaction mixture was stirred for 2 h. The solvent was removed *in vacuo* and the residue was transferred to a sinter funnel and washed with hot water. The product was extracted with Et_2O (ca. 3 x 50 mL) in a separatory funnel. The organic layer was separated and dried over $MgSO_4$. The solvent was removed *in vacuo* to give a pale yellow-white solid. Yield: 0.78 g, 67%. ^{1}H NMR (200 MHz, $CDCl_3$) δ: 8.02 (d, J = 9 Hz, 2H, CH_{arom}), 7.58 (d, J = 9 Hz, 2H, CH_{arom}), 7.49 (s, 4H, CH_{arom}), 4.32 (t, J = 7 Hz, 2H, OCH_2), 3.19 (s, 1H, C≡CH), 1.75 (quint, J = 7 Hz, 2H, $OCH_2C\mathit{H}_2$), 1.30 (m, 10H, CH_2), 0.88 (t, J = 6 Hz, 3H, CH_3). Anal. Calcd. for $C_{25}H_{26}O_2$: C, 83.76; H, 7.31. Found: C, 82.87; H, 7.32%. MS (MALDI$^+$) *m*/*z*: 358 [M^+].

30 – [4-(4-ethynylphenylethynyl)phenyl]-di-*n*-hexylamine

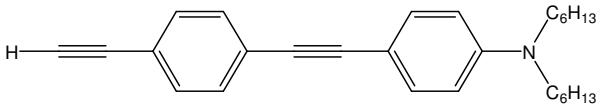

To a solution of compound **28** (2.29 g, 5.00 mmol) in Et_2O (100 mL), MeOH (100 mL) and water (30 mL) was added K_2CO_3 (2.76 g, 20.0 mmol), and the reaction mixture was stirred at room temperature for 15 h. Then, water (ca. 600 mL) was added into the reaction. The suspension was transferred to a separatory funnel and CH_2Cl_2 (3 x 75 mL) was added. The organic layer was separated and dried over $MgSO_4$. The solvent was removed *in vacuo* to give **30** as a yellow solid. Yield: 1.62 g, 84%. ^{1}H NMR (400 MHz, $CDCl_3$) δ: 7.45 (s, 4H, CH_{arom}), 7.37 (d, J = 9 Hz, 2H, CH_{arom}), 6.57 (d, J = 9 Hz, 2H, CH_{arom}), 3.28 (t, J = 8 Hz, 4H, $N(CH_2)_2$), 3.16 (s, 1H, C≡CH), 1.59 (m, 4H, $N(CH_2CH_2)_2$), 1.33 (m, 12H, CH_2), 0.92 (t, J = 6 Hz, 6H, 2 x CH_3). Anal. Calcd. for $C_{28}H_{35}N$: C, 87.22; H, 9.15; N, 3.63. Found: C, 87.20; H, 9.01; N, 3.34%. MS (EI) *m*/*z*: 385 [M^+].

31 – 4,4'-bis-(4''-carbo-*n*-octyloxylphenylethynyl)diphenyl-buta-1,3-diyne[49]

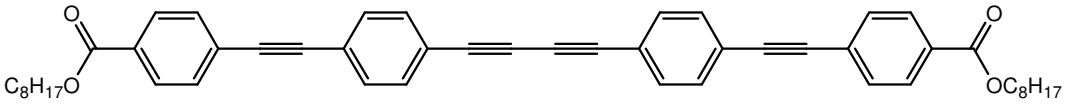

Compound **29** (0.50 g, 1.39 mmol), CuI (0.003 g, 0.014 mmol) and $[PdCl_2(PPh_3)_2]$ (0.005 g, 0.007 mmol) were added to a round bottom flask. Et_3N (100 mL) was added to the mixture followed by I_2 (0.36 g, 1.40 mmole). The reaction was stirred open to the air at room temperature for 24 h and then examined by GC-MS. Once complete, the solvent was removed *in vacuo*. The residue was transferred to the top of a 5 cm silica gel column and eluted with hexane : CH_2Cl_2 (4 : 1 v/v) (ca. 500 mL). The solvent was removed *in*

vacuo to give **31** as a white solid. Yield: 0.38 g, 76%. ^{1}H NMR (400 MHz, $CDCl_3$) δ: 8.03 (d, *J* = 8 Hz, 4H, CH_{arom}), 7.58 (d, *J* = 8 Hz, 4H, CH_{arom}), 7.52 (s, 8H, CH_{arom}), 4.32 (t, *J* = 7 Hz, 4H, OCH_2), 1.77 (quint, *J* = 7 Hz, 4H, OCH_2CH_2), 1.30 (m, 20H, CH_2), 0.89 (t, *J* = 7 Hz, 6H, CH_3). Anal. Calcd. for $C_{50}H_{50}O_4$: C, 84.00; H, 7.05. Found: C, 83.95; H, 6.99%. MS (MALDI$^+$) *m/z*: 714 [M^+].

32 – 4,4'-bis-(4''-di-*n*-hexylaminophenylethynyl)diphenyl-buta-1,3-diyne[13]

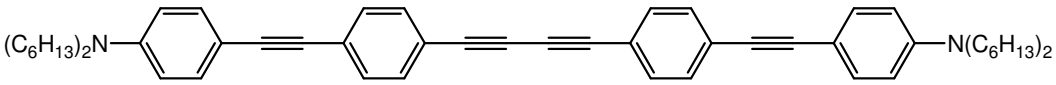

Compound **30** (1.00 g, 2.59 mmol), CuI (0.005 g, 0.026 mmol) and [$PdCl_2(PPh_3)_2$] (0.009 g, 0.001 mmol) were added to round bottom flask. Et_3N (100 mL) was added to the mixture, which was then stirred at room temperature for 24 h and monitored by GC-MS. Once completed, the solvent was removed *in vacuo*. The residue was transferred to the top of a 5 cm silica gel pad and eluted with hexane : CH_2Cl_2 (4 : 1 v/v) (ca. 1000 mL). The solvent was removed *in vacuo* to give an orange-brown solid. The solid was further purified by recrystallisation by dissolution in hot hexane (ca. 15 mL) and cooling to ca. -20 °C, giving a yellow solid. Yield: 0.79 g, 79%. ^{1}H NMR (400 MHz, $CDCl_3$) δ: 7.45 (s, 8H, CH_{arom}), 7.36 (d, *J* = 8 Hz, 4H, CH_{arom}), 6.57 (d, *J* = 8 Hz, 4H, CH_{arom}), 3.28 (t, *J* = 8 Hz, 8H, $N(CH_2)_2$), 1.58 (m, 8H, $N(CH_2CH_2)_2$), 1.33 (m, 24H, CH_2), 0.91 (t, *J* = 6 Hz, 12H, CH_3). Anal. Calcd. for $C_{56}H_{68}N_2$: C, 87.45; H, 8.91; N, 3.64. Found: C, 86.83; H, 8.85; N, 3.45%. MS (ES$^+$) *m/z*: 768 [M^+], 769 [M + H^+].

2.4.6 Preparation of 1,12-bis(*p*-R-phenyl)dodeca-1,3,9,11-tetraynes and related compounds

33 – 1,8-dibromo-1,7-octadiyne[79, 80]

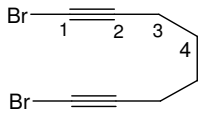

To a solution of 1,7-octadiyne (9.98 g, 94.00 mmol) in acetone (200 mL) was added recrystallised NBS (66.92 g, 376 mmol) and $AgNO_3$ (1.60 g, 9.40 mmol), and the reaction was stirred for 15 h at room temperature. Acetone was removed *in vacuo* and the residue was treated with hexane (200 mL). Water (5 x 200 mL) was added to the hexane suspended solution. The organic layer was separated, dried over $MgSO_4$ and removed *in vacuo* to give **33** as a yellow oil. Yield: 21.06 g, 85%. ^{1}H NMR (400 MHz, $CDCl_3$) δ: 2.25 (m, 4H, C≡C-CH_2), 1.62 (m, 4H, CH_2). $^{13}C\{^1H\}$ NMR (100.4 MHz, $CDCl_3$) δ: 79.7 (C2), 38.1 (C1), 27.2 (C4), 19.2 (C3).

34(a) – 1,12-diphenyldodeca-1,3,9,11-tetrayne

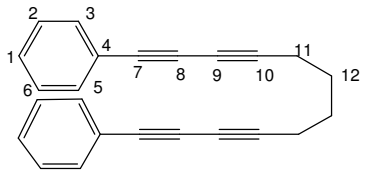

CuCl (0.025 g, 0.25 mmol) followed by hydroxylamine hydrochloride, $NH_2OH{\cdot}HCl$, (ca. 0.50 g) was added into a degassed mixture of *n*-$BuNH_2$ (20 mL) and water (45 mL) and the mixture was stirred for 1 h under N_2. Phenylacetylene (1.30 g, 12.75 mmol) was added to the solution which was then cooled to 0 °C. Compound **33** (1.60 g, 6.07 mmoles) was added to the cold solution and the mixture was stirred for 5 min. The

reaction was allowed to warm to room temperature, then a large amount of $NH_2OH{\cdot}HCl$ (ca. 10 g) was added to the mixture. The mixture was stirred for 15 h, then ethyl acetate (EA) (3 x 20 mL) was added to the reaction. The organic layer was separated and dried over $MgSO_4$. The solvent was removed *in vacuo* to give a yellow-brown crude material and further purified via recrystallisation via dissolution in hot hexane and cooling to ca. -20 °C. A white solid was formed, which was separated and washed with hexane (ca. 5 mL). Yield: 0.79 g, 42%. ^{1}H NMR (200 MHz, $CDCl_3$) δ: 7.50 (m, 4H, CH_{arom}), 7.33 (m, 6H, CH_{arom}), 2.43 (m, 4H, C≡C-CH_2), 1.74 (m, 4H, CH_2). $^{13}C\{^1H\}$ NMR (50.3 MHz, $CDCl_3$) δ: 132.7 (C3 & C5), 129.1 (C2 & C6), 128.6 (C1), 122.2 (C4), 84.1 (C10), 75.2 (C7), 74.5 (C8), 65.9 (C9), 27.5 (C12), 19.4 (C11). Anal. Calcd. for $C_{24}H_{18}$: C, 94.08; H, 5.92. Found: C, 93.26; H, 6.04%. MS (MALDI$^+$) *m/z*: 306. IR (KBr) $\upsilon_{C\text{-}H}$ = 2937; $\upsilon_{C\equiv C}$ = 2239; υ_{Ar} = 1591 cm^{-1}.

35 – 1,12-bis(*p*-carbomethoxyphenyl)dodeca-1,3,9,11-tetrayne

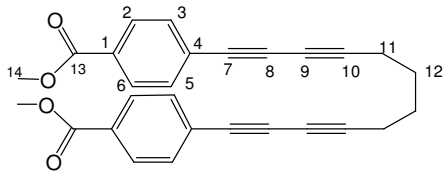

[$Pd(dba)_2$] (0.30 g, 0.52 mmol), CuI (0.50 g, 0.26 mmol), and the "P-olefin ligand" (0.20 g, 0.52 mmol) were added to a two neck round bottom flask in a N_2 filled glove box. Dried, degassed DMF (80 mL), Et_3N (10 mL) and **33** (1.71 g, 6.49 mmol) were added to the round bottom flask and the mixture was stirred for 5 min. The compound 4-ethynylbenzoic acid methyl ester (**8**, 2.18 g, 13.63 mmol) was added to the mixture and the reaction was stirred for 15 h outside of the glove box. Upon completion, the Et_3N was removed *in vacuo*, then CH_2Cl_2 (50 mL) was added to the flask. The dark brown solution

was transferred to a 500 mL separatory funnel and brine (5 x 200 mL) was added. The organic layer was separated, dried over $MgSO_4$ and then the solvent was removed *in vacuo*. The product was purified via silica gel column chromatography slowly increasing the solvent polarity until the ratio of hexane : CH_2Cl_2 reached 2 : 3 (v/v). Compound **35** was isolated appears as an off-white solid. Single crystals of **35** were obtained by dissolution in hot CH_2Cl_2 and cooling to ca. 5 °C. Yield: 0.81 g, 30%. ^{1}H NMR (200 MHz, $CDCl_3$) δ: 7.95 (d, *J* = 8 Hz, 4H, CH_{arom}), 7.52 (d, *J* = 8 Hz, 4H, CH_{arom}), 3.91 (s, 6H, CO_2CH_3), 2.44 (m, 4H, C≡C-CH_2), 1.74 (m, 4H, CH_2). ^{13}C{^{1}H} NMR (50.3 MHz, $CDCl_3$) δ: 166.6 (C13), 132.6 (C3 & C5), 130.2 (C1), 129.7 (C2 & C6), 126.9 (C4), 85.7 (C10), 77.3 (C7), 74.3 (C8), 65.6 (C9), 52.5 (C14), 27.3 (C12), 19.4 (C11). Anal. Calcd. for $C_{28}H_{22}O_4$: C, 79.60; H, 5.25. Found: C, 78.86; H, 5.20%. MS (MALDI$^+$) *m/z*: 422. IR (KBr) υ_{C-H} = 2935; $\upsilon_{C\equiv C}$ = 2235; $\upsilon_{C=O}$ = 1719; υ_{Ar} = 1602 cm^{-1}.

36 – 1,12-bis(*p*-dimesitylborylphenyl)dodeca-1,3,9,11-tetrayne

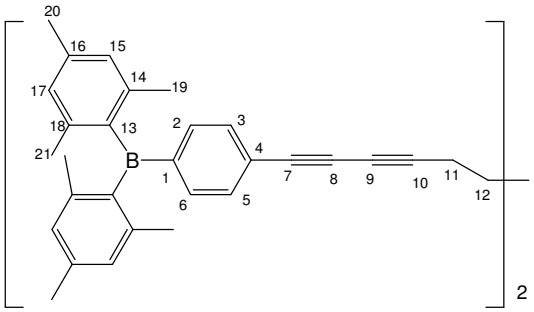

In a N_2 filled glove, the compounds [$Pd(dba)_2$] (0.014 g, 0.024 mmol), CuI (0.002 g, 0.012 mmol), and the "P-olefin ligand" (0.009 g, 0.024 mmol) were added to a 25 mL vial. Dried and degassed DMF (10.0 mL), Et_3N (3.0 mL) and **33** (0.079 g, 0.30 mmol) were added to the vial and the mixture was stirred for 5 min. The compound 4-ethynylphenyldimesitylborane (0.22 g, 0.63 mmol) was added to the mixture and the

reaction was stirred for 15 h in the glove box. The vial was removed from the glove box and the contents were transferred into a 100 mL round bottom flask. The Et_3N was removed *in vacuo*, then CH_2Cl_2 (50 mL) was added to the flask. The dark brown solution was transferred into a separatory funnel and brine (5 x 50 mL) was added. The organic layer was separated, dried over $MgSO_4$ and then the solvent was removed *in vacuo*. The product was separated via silica gel column chromatography slowly increasing solvent polarity until the ratio of hexane : CH_2Cl_2 reached 4 : 1 (v/v). Compound **36** was isolated as a light yellow solid. Yield: 0.10 g, 42%, ^{1}H NMR (400 MHz, $CDCl_3$) δ: 7.46 (s, 8H, CH_{arom}), 6.82 (s, 8H, CH_{arom}), 2.42 (m, 4H, C≡C-CH_2), 2.32 (s, 12H, Ar-C20H_3), 2.00 (s, 24H, Ar-C19H_3 & Ar-C21H_3), 1.75 (m, 4H, CH_2). ^{13}C{^{1}H} NMR (100.6 MHz, $CDCl_3$) δ: 146.7, 141.7, 141.0, 139.2, 136.2, 132.2, 128.5, 125.5, 85.7, 76.5, 75.5, 66.0, 29.4, 23.7, 21.5, 19.5. Anal. Calcd. for $C_{60}H_{60}B_2$: C, 89.77; H, 7.53. Found: C, 86.88; H, 7.61%. MS (MALDI$^+$) *m/z*: 802, Accurate Mass MS (ASAP) *m/z*: 801.5075. IR (KBr) υ_{C-H} = 2135; $\upsilon_{C\equiv C}$ = 2240; υ_{Ar} = 1606 cm^{-1}.

37 – 1,12-bis(*p*-methylthiophenyl)dodeca-1,3,9,11-tetrayne

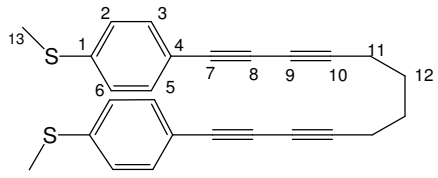

In a N_2 filled glove box, the compounds [Pd(dba)$_2$] (0.349 g, 0.606 mmol), CuI (0.058 g, 0.303 mmol), and the "P-olefin ligand" (0.238 g, 0.606 mmol) were added to a 100 mL two neck round bottom flask. Dried, degassed DMF (25.0 mL), Et_3N (10.0 mL) and **33** (2.00 g, 7.58 mmol) were added to the flask and the mixture was stirred for 5 min. The compound 4-ethynylthioanisole (**14**, 2.36 g, 15.92 mmol) was added to the mixture and

the reaction was stirred for 15 h at room temperature outside of the glove box. Upon completion, the Et_3N was removed *in vacuo* then CH_2Cl_2 (50 mL) was added to the flask. The dark brown solution was transferred to a 500 mL separatory funnel and brine (5 x 200 mL) was added. The organic layer was separated, dried over $MgSO_4$ and then the solvent was removed *in vacuo*. The product was separated via silica gel column chromatography, slowly increasing solvent polarity until the ratio of hexane : CH_2Cl_2 reached 3 : 2 (v/v). Pure compound **37** was isolated as an off-white solid. Crystals of **37** were obtained by dissolution in a mixture of hot hexane/CH_2Cl_2 and cooling to ca. 5 °C. Yield: 1.0 g, 33%. ^{1}H NMR (400 MHz, $CDCl_3$) δ: 7.37 (d, J = 8 Hz, 4H, CH_{arom}), 7.14 (d, J = 8 Hz, 4H, CH_{arom}), 2.47 (s, 6H, SCH_3), 2.42 (m, 4H, C≡C-CH_2), 1.72 (m, 4H, CH_2). $^{13}C\{^1H\}$ NMR (50.3 MHz, $CDCl_3$) δ: 140.1 (C1), 133.0 (C3 & C5), 125.8 (C2 & C6), 118.3 (C4), 85.7 (C10), 75.1 (C7), 74.5 (C8), 66.0 (C9), 27.5 (C12), 19.4 (C13), 15.4 (C11). Anal. Calcd. for $C_{26}H_{22}S_2$: C, 78.35; H, 5.56. Found: C, 78.50; H, 5.52%. MS (MALDI$^+$) *m/z*: 398. IR (KBr) υ_{C-H} = 2935; $\upsilon_{C\equiv C}$ = 2236; υ_{Ar} = 1582 cm^{-1}.

Reference:

1. M. L. Lerch, M. K. Harper and D. J. Faulkner, *J. Nat. Prod.*, 2003, **66**, 667.
2. Y. S. Kim, S. H. Jin, S. I. Kim and D. R. Hahn, *Arch. Pharmacol. Res.*, 1989, **12**, 207.
3. D. Lechner, M. Stavri, M. Oluwatuyi, R. Pereda-Miranda and S. Gibbons, *Phytochemistry*, 2004, **65**, 331.
4. M. Stavri, K. T. Mathew, T. Gibson, R. T. Williamson and S. Gibbons, *J. Nat. Prod.*, 2004, **67**, 892.
5. K. Uwai, K. Ohashi, Y. Takaya, T. Ohta, T. Tadano, K. Kisara, K. Shibusawa, R. Sakakibara and Y. Oshima, *J. Med. Chem.*, 2000, **43**, 4508.
6. C. Fouquey, J.-M. Lehn and J. Malthête, *J. Chem. Soc., Chem. Commun.*, 1987, 1424.
7. J. Y. Chang, J. H. Baik, C. B. Lee, M. J. Han and S.-K. Hong, *J. Am. Chem. Soc.*, 1997, **119**, 3197.
8. T. Kitamura, C. H. Lee, Y. Taniguchi, Y. Fujiwara, M. Matsumoto and Y. Sano, *J. Am. Chem. Soc.*, 1997, **119**, 619.
9. D. R. Kanis, M. A. Ratner and T. J. Marks, *Chem. Rev.*, 1994, **94**, 195.
10. L. T. Cheng, W. Tam, S. R. Marder, A. E. Stiegman, G. Rikken and C. W. Spangler, *J. Phys. Chem.*, 1991, **95**, 10643.
11. S. Eisler, A. D. Slepkov, E. Elliott, T. Luu, R. McDonald, F. A. Hegmann and R. R. Tykwinski, *J. Am. Chem. Soc.*, 2005, **127**, 2666.
12. Y. Kang, C. Seward, D. Song and S. Wang, *Inorg. Chem.*, 2003, **42**, 2789.
13. R. M. Ward, *Diethynylrhodacyclopentadienes: A New Class of Luminescent Organometallics*, Ph.D. Thesis, Durham University, 2007.
14. C. Glaser, *Ber. Dtsch. Chem. Ges.*, 1869, **2**, 422.
15. P. Siemsen, R. C. Livingston and F. Diederich, *Angew. Chem.*, 2000, **39**, 2632.
16. G. Eglinton and R. Galbraith, *J. Chem. Soc.*, 1959, 889.
17. A. S. Hay, *J. Org. Chem.*, 1962, **27**, 3320.
18. Q. Liu and D. J. Burton, *Tetrahedron Lett.*, 1997, **38**, 4371.
19. J. A. Marsden, J. J. Miller and M. M. Haley, *Angew. Chem. Int. Ed.*, 2004, **43**, 1694.
20. W. Chodkiewicz and P. Cadiot, *C. R. Hebd. Seances Acad. Sci.*, 1955, **241**, 1055.
21. G. Eglinton and W. McCrae, *Adv. Org. Chem.*, 1963, **4**, 225.
22. E. Negishi, X. Zeng, Z. Tan, M. Qian, Q. Hu and Z. Huang, *Palladium- or Nickel-Catalyzed Cross-Coupling With Organometals Containing Zinc, Aluminum and Ziconium: The Negishi Coupling* in *Metal-catalyzed Cross Coupling Reactions*, eds. A. de Meijere and F. Diederich, Wiley-VCH Verlag GmbH & Co. KGaA, Weinheim, 2nd edn., 2004, vol. 2, pp. 815.
23. N. Miyaura and A. Suzuki, *J. Chem. Soc., Chem. Commun.*, 1979, 866.
24. N. Miyaura, T. Yanagi and A. Suzuki, *Synth. Commun.*, 1981, **11**, 513.
25. E. Negishi and A. de Meijere, *Handbook of Organopalladium Chemistry for Organic Synthesis*, 1st edn., John Wiley & Sons, Inc., New York, 2002.
26. A. Suzuki, *Overview of the Suzuki Protocol with B* in *Handbook of Organopalladium Chemistry for Organic Synthesis*, ed. E. Negishi, John Wiley & Sons, Inc., New York, 2002, vol. 1, p. 249.

27. E. Negishi, A. O. King and N. Okukado, *J. Org. Chem.*, 1977, **42**, 1821.
28. A. O. King, N. Okukado and E. Negishi, *J. Chem. Soc., Chem. Commun.*, 1977, 683.
29. D. Milstein and J. K. Stille, *J. Am. Chem. Soc.*, 1978, **100**, 3636.
30. D. Milstein and J. K. Stille, *J. Am. Chem. Soc.*, 1979, **101**, 4992.
31. K. Sonogashira, Y. Tohda and N. Hagihara, *Tetrahedron Lett.*, 1975, **50**, 4467.
32. P. Nguyen, Z. Yuan, L. Agocs, G. Lesley and T. B. Marder, *Inorg. Chim. Acta*, 1994, **220**, 289.
33. A. S. Batsanov, J. C. Collings, I. J. S. Fairlamb, J. P. Holland, J. A. K. Howard, Z. Lin, T. B. Marder, A. C. Parsons, R. W. Ward and J. Zhu, *J. Org. Chem.*, 2005, **70**, 703.
34. P. Fitton and E. A. Rick, *J. Organomet. Chem.*, 1971, **28**, 287.
35. K. C. Lam, T. B. Marder and Z. Lin, *Organometallic*, 2007, **26**, 758.
36. E. Negishi and L. Anastasia, *Chem. Rev.*, 2003, **103**, 1979.
37. W. Shi, Y. Luo, X. Luo, L. Chao, H. Zhang, J. Wang and A. Lei, *J. Am. Chem. Soc.*, 2008, **130**, 14713.
38. E. A. Bercot and T. Rovis, *J. Am. Chem. Soc.*, 2001, **124**, 174.
39. J. B. Johnson, E. A. Bercot, J. M. Rowley, G. W. Coates and T. Rovis, *J. Am. Chem. Soc.*, 2007, **129**, 2718.
40. I. J. S. Fairlamb and A. F. Lee, *Organometallics*, 2007, **26**, 4087.
41. M. Alami and F. Ferri, *Tetrahedron Lett.*, 1996, **37**, 2763.
42. A. L. K. Shi Shun, E. T. Chernick, S. Eisler and R. R. Tykwinski, *J. Org. Chem.*, 2003, **68**, 1339.
43. L. Liu, W.-Y. Wong, S.-Y. Poon and K.-W. Cheah, *J. Inorg. Organomet. Polym. Mater.*, 2005, **15**, 555.
44. Z. Yuan, G. Stringer, I. R. Jobe, D. Kreller, K. Scott, L. Koch, N. J. Taylor and T. B. Marder, *J. Organomet. Chem.*, 1993, **452**, 115.
45. A. S. Kende and C. A. Smith, *J. Org. Chem.*, 1988, **53**, 2655.
46. K. West, C. Wang, A. S. Batsanov and M. R. Bryce, *J. Org. Chem.*, 2006, **71**, 8541.
47. Y. Matano, M. Nakashima and H. Imahori, *Angew. Chem. Int. Ed.*, 2009, **48**, 4002.
48. C. Eaborn and D. R. M. Walton, *J. Organomet. Chem.*, 1965, **4**, 217.
49. M. R. Al-Haddad, *Synthesis of Substituted Phenylene-ethynylene-based Conjugated Rods*, M.Sc. Thesis, Durham University, 2006.
50. M. Erdélyi and A. Gogoll, *J. Org. Chem.*, 2001, **66**, 4165.
51. S. Takahashi, Y. Kuroyama, K. Sonogashira and N. Hagihara, *Synthesis*, 1980, **8**, 627.
52. W. B. Austin, N. Bilow, W. J. Kelleghan and K. S. Y. Lau, *J. Org. Chem.*, 1981, **46**, 2280.
53. S. Thorand and N. Krause, *J. Org. Chem.*, 1998, **63**, 8551.
54. R. Oliver and D. R. M. Walton, *Tetrahedron Lett.*, 1972, **13**, 5209.
55. A. Mori, M. S. M. Ahmed, A. Sekiguchi, K. Masui and T. Koike, *Chem. Lett.*, 2002, **31**, 756.
56. A. Köllhofer and H. Plenio, *Adv. Synth. Catal.*, 2005, **347**, 1295.
57. M. I. Al-Hassan, *J. Organomet. Chem.*, 1990, **395**, 227.

58. R. P. Hsung, J. R. Babcock, C. E. D. Chidsey and L. R. Sita, *Tetrahedron Lett.*, 1995, **36**, 4525.
59. P. Stefano, F. Maurizio and A. Angelo, *Angew. Chem. Int. Ed.*, 2005, **44**, 5675.
60. N. A. Bumagin, A. B. Ponomarev and I. P. Beletskaya, *Synthesis*, 1984, **9**, 728.
61. M. M. Otto, *J. Am. Chem. Soc.*, 1934, **56**, 1393.
62. D. A. Dawso and W. F. Reynolds, *Can. J. Chem.*, 1975, **53**, 373.
63. A. E. Stiegman, E. Graham, K. J. Perry, L. R. Khundkar, L. T. Cheng and J. W. Perry, *J. Am. Chem. Soc.*, 2002, **113**, 7658.
64. W. Shen and S. A. Thomas, *Org. Lett.*, 2000, **2**, 2857.
65. S. V. Damle, D. Seomoon and P. H. Lee, *J. Org. Chem.*, 2003, **68**, 7085.
66. J.-H. Li, Y. Liang and Y.-X. Xie, *J. Org. Chem.*, 2005, **70**, 4393.
67. K. Vipan, C. Alex and C. Kelly, *Eur. J. Org. Chem.*, 2008, **2008**, 43.
68. J. J. Mayerle, T. C. Clarke and K. Bredfeldt, *Acta Cryst.*, 1979, **B35**, 1519.
69. C. H. Oh and V. R. Reddy, *Tetrahedron Lett.*, 2004, **45**, 5221.
70. S. Fomine, L. Fomina and T. Ogawa, *J. Mol. Struct.: THEOCHEM*, 2001, **540**, 123.
71. K. Ikegashira, Y. Nishihara, K. Hirabayashi, A. Mori and T. Hiyama, *Chem. Commun.*, 1997, 1039.
72. S. Anderson, R. T. Aplin, T. D. W. Claridge, T. Goodson III, A. C. Maciel, G. Rumbles, J. F. Ryan and H. L. Anderson, *J. Chem. Soc., Perkin Trans. 1*, 1998, 2383.
73. J. G. Rodríguez, J. L. Tejedor, T. La Parra and C. Díaz, *Tetrahedron*, 2006, **62**, 3355.
74. S. Goeb and R. Ziessel, *Org. Lett.*, 2007, **9**, 737.
75. R. Vadnais, M.-A. Beaudoin, A. Beaudoin, B. Heinrich and A. Soldera, *Liq. Cryst.*, 2008, **35**, 357.
76. O. Mongin, L. Porrès, L. Moreaux, J. Mertz and M. Blanchard-Desce, *Org. Lett.*, 2002, **4**, 719.
77. L. Porrès, O. Mongin, C. Katan, M. Charlot, T. Pons, J. Mertz and M. Blanchard-Desce, *Org. Lett.*, 2003, **6**, 47.
78. T. Boris, J. J. Wolff, R. Frank, O. Thomas, G. Rolf, G. Mark and W. Rüdiger, *Chem. Eur. J.* , 2004, **10**, 1227.
79. G. Eglinton and W. McCrae, *J. Chem. Soc.*, 1963, 2295.
80. Z. Xuejun, L. Hongyan, Y. Lingfeng, T. Yu and P. H. Richard *Adv. Synth. Catal.*, 2006, **348**, 2437.

Chapter 3

The synthesis, characterisation and investigation of the photophysical properties of 2,5-bis(arylethynyl)rhodacyclopentadienes

3.1 Introduction

Metallacyclopentadiene complexes, especially with 2,2'-bipyridine (bpy) ligands, have been extensively studied over the last few decades because of their interesting photophysical properties such as strong spin-orbit coupling (SOC), extremely fast intersystem crossing (ISC) rates and microsecond lifetimes, which make the complexes potential candidates for various applications such as probes for biological-labelling[1] and two-photon absorption materials.[2-5] More recently, [Ir(ppy)$_3$] has been applied in organic light emitting diode devices (OLEDs), due to its highly efficient triplet state emission.[6]

In 2001, Marder and Rourke et al. reported an example of a new type of luminescent metallacyclopentadiene complex, namely a 2,5-bis(*p*-tolylethynyl)-3,4-bis(*p*-tolyl) rhodacyclopentadiene, the structure of which is shown in **Figure 3.1**.[7]

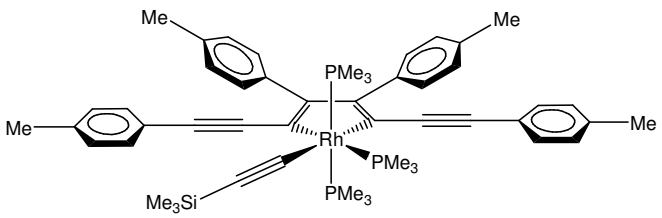

Figure 3.1: The structure of 2,5-bis(*p*-tolylethynyl)-3,4-bis(*p*-tolyl)rhodacyclopentadiene.

The photophysical properties of this and related complexes were investigated further by Ward in his Ph.D. study,[8] in which he varied the R substituents at the *para*-positions of the phenyl rings, and also used different kinds of ligands on the Rh centre (**Figure 3.2**). The ligands that were studied by Ward included trimethylsilylethynyl- (TMSE), methyl- (Me-), chloro- (Cl-), 4-*N*,*N*-dimethylaminophenylethynyl (Me_2N-C_6H_4-C≡C-) and 4-*N*,*N*-diphenylaminophenylbutadiynyl (Ph_2N-C_6H_4-C≡C-C≡C-). The reasons for using the

Me_2N-C_6H_4-C≡C- and Ph_2N-C_6H_4-C≡C-C≡C- ligands was to extend the conjugation length of the alkynyl ligand and also to attempt to maximise the co-planarity between the phenyl ring at the 2-position of the rhodacycle ring and the phenyl ring of the alkynyl ligand, which can subsequently increase the π-interaction of the conjugated alkynyl ligand with the rhodacycle ring. For the TMSE-based rhodacyclopentadienes, Ward investigated the effect of different R substituents including NO_2, CN, CO_2Me, CF_3, H, Me, OMe, SMe and NMe_2 on the photophysical properties.

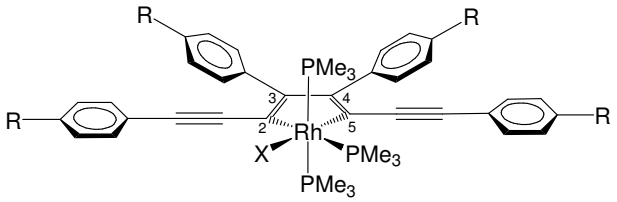

X = TMSE; R = NO_2, CN, CO_2Me, CF_3, H, Me, OMe, SMe, CCTMS
X = Me_2N-C_6H_4-CC; R = CO_2Me, CF_3, H, Me, OMe,
X = Ph_2N-C_6H_4-CC-CC; R = Me
X = Me; R = CO_2Me, CF_3, H, Me, OMe
X = Cl; R = CF_3

Figure 3.2: Rhodacyclopentadienes with different R substituents and X ligands that have been studied by Ward.[8]

The photophysical results of Ward can be summarised as follows:

(i) the room temperature emissions of rhodacyclopentadienes originate from singlet excited states, which have nanosecond lifetimes;

(ii) the λ_{max} values in absorption and emission are bathochromically shifted for both electron donating and withdrawing R-substituents; the electron withdrawing groups have a greater effect than the electron donating groups;

(iii) changing the X ligand has little effect on the overall absorption and emission wavelengths. The alkynyl-rhodacyclopentadienes e.g. TMSE-, Me_2N-C_6H_4-C≡C-

and Ph_2N-C_6H_4-C≡C-C≡C- have similar λ_{max} values in absorption and emission; and

(iv) rhodacyclopentadienes bearing the TMSE- ligand have higher quantum yields than those with other ligands.

Comparing the emission lifetimes of the rhodacyclopentadienes (type **a**, **Figure 3.3**) to the other luminescent metallacyclopentadienes (type **b**, **Figure 3.3**), the nanosecond fluorescence lifetimes of the rhodacyclopentadienes are an unusual photophysical property.

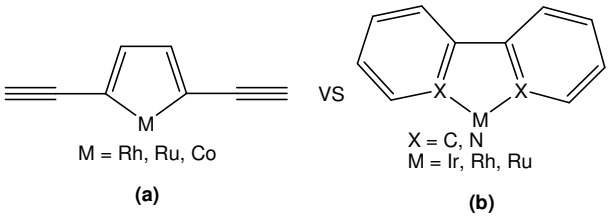

Figure 3.3: Comparison of the structures of rhodacyclopentadienes to other luminescent metallacyclopentadienes.

Indeed, most luminescent metallacyclopentadienes do not fluoresce because of a strong spin-orbit coupling (SOC) effect from the metal centre, which causes extremely fast intersystem crossing (ISC) to convert the singlet excited states to triplet excited states. Therefore, the singlet excited state lifetimes of most of the luminescent metallacyclopentadienes should be on the femto- to picosecond timescale.

Che et al. reported the luminescent properties of a $Au^{(I)}$ complex $[TEE][Au(PCy_3)]_4$ ($[TEE]H_4$ = tetraethynylethene, **Figure 3.4**). Interestingly, despite the fact that the TEE ligand is directly bonded to the Au centres, this $Au^{(I)}$ complex also exhibits a strong

fluorescent emission at λ_{max} = 412 nm (Φ = 0.22, τ < 50 ns), which can be confirmed from its short lifetime and small Stokes shift (1040 cm^{-1}). No phosphorescence was observed even at 77 K, and the group believed that its T_1 state must be very close in energy to the ground state, which leads to a very low Φ_p value.[9]

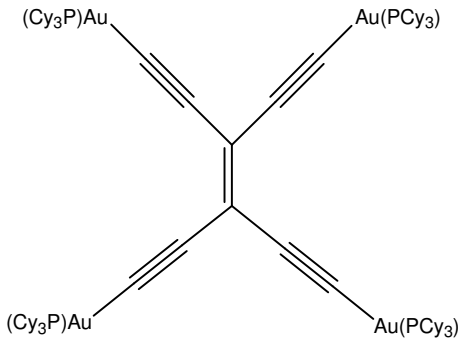

Figure 3.4: The structure of [TEE][$Au(PCy_3)$]$_4$.

Besides the $Au^{(I)}$ complex, another heavy atom complex, [$Pt^{(0)}(binap)_2$] (binap = 2,2'-bis(diphenylphosphino)-1,1'binaphthyl), has also been reported regarding its interesting fluorescent properties.[10] Two kinds of fluorescence were observed at room temperature, (i) prompt fluorescence with a lifetime of 3.2 ps and Φ_f = 1.56 x 10^{-4} and (ii) delayed-fluorescence with a lifetime of 1.25 μs and Φ_f = 0.12. The reason that the emission with lifetime of 1.25 μs was assigned as delayed-fluorescence is because the Φ_f value decreases when the temperature decreases. This is due to the fact that the ^{1}MLCT and ^{3}MLCT states are very close in energy (1200 cm^{-1}), therefore, the ^{3}MLCT state can return back to the ^{1}MLCT state and fluoresce at ambient temperature. At low temperatures, the delayed-fluorescence was then replaced by phosphorescence with a lifetime of 1.2 μs. Importantly, the authors also pointed out that the ISC rate is dependent on the effectiveness of the SOC but not the value of the SOC constant of the heavy atom.[10]

In the rhodacyclopentadiene systems, Φ_f values of up to 0.18 can be achieved (TMSE-rhodacyclopentadiene, R = NO_2, which has a lifetime of 1.2 ns).[8] Preliminary results of TD-DFT calculations that have been carried out on a TMSE-rhodacyclopentadiene suggest that the main $S_0 \rightarrow S_1$ transition is mainly HOMO to LUMO. The calculations also reveal that the Rh centre makes some contribution to the HOMO, but very little contribution to the LUMO (**Figure 3.5**). In this case, the Rh-participation should be able to generate triplet excited states in the rhodacyclopentadienes. In order to investigate the SOC effect from the Rh centre, which facilitates the ISC process, rhodacyclopentadienes with TMSE-, Me- and Cl- ligands have been investigated with regard to the quantum yields of triplet excited state generation (Φ_Δ) using singlet oxygen sensitisation experiments, which were carried out by Dr. Andreas Steffen from our group, and the results are shown in **Table 3.1**.

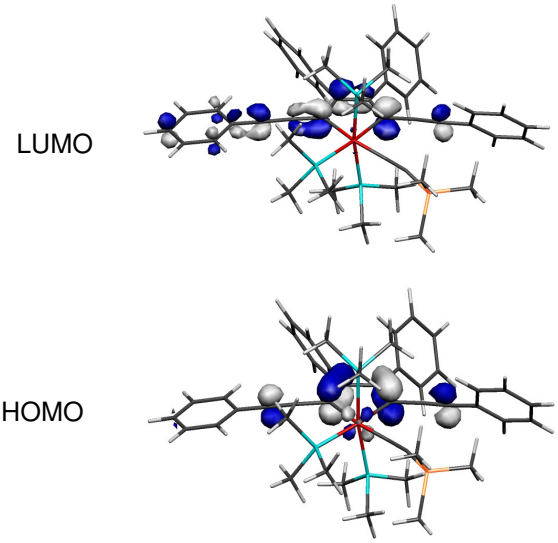

Figure 3.5: HOMO-LUMO diagrams for the TMSE-rhodacyclopentadiene with phenyl groups.

Table 3.1: Quantum yields of fluorescence (Φ_f) and triplet excited state generation (Φ_Δ) of TMSE-, Me- and Cl-rhodacyclopentadienes. Lifetimes (τ_f), fluorescence rate (k_f) and ISC rate (k_Δ) for TMSE-rhodacyclopentadienes.

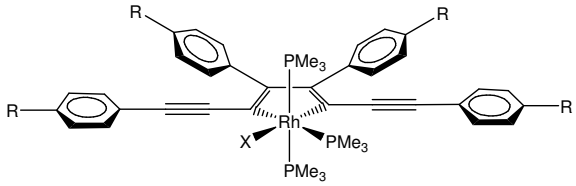

X	R	Φ_f	Φ_Δ	τ_f (ns)	k_f (x 10^8 s^{-1})*	k_Δ (x 10^8 s^{-1})*
TMSE-	H	0.15	0.57	0.87	1.72	6.55
	SMe	0.10	0.50	0.55	1.81	9.09
	CO_2Me	0.16	0.45	0.98	1.63	4.59
Me-	H	0.003	0.68	-	-	-
	CO_2Me	0.003	0.38	-	-	-
Cl-	H	0.003	0.65	-	-	-
	OMe	0.004	0.62	-	-	-
	CO_2Me	0.22	0.55	-	-	-

*$k_f = \Phi_f / \tau_f$ and $k_\Delta = \Phi_\Delta / \tau_f$

The principle of the singlet oxygen sensitisation experiment is to use triplet oxygen molecules to quench the molecules in the triplet excited states, and form singlet oxygen molecules. The number of singlet oxygen molecules formed corresponds to the number of molecules originally in the triplet excited states. Thus, the quantum yields of the emission from singlet oxygen molecules are related to the quantum yields of triplet excited state generation in the rhodacyclopentadienes. The results in **Table 3.1** show that the quantum yields of triplet excited state formation in rhodacyclopentadienes are higher than those of fluorescence. This indicates that ISC in rhodacyclopentadienes is more efficient than the fluorescence processes. Indirectly, the results also reveal that Rh centres possibly participate in the frontier orbitals of the excited states. The rhodacyclopentadienes with Me- and Cl- ligands seem to have a generally higher SOC influence than those with

TMSE- (except the Me-rhodacyclopentadiene with R = CO_2Me). Nevertheless, the results in **Table 3.1** also show that non-radiative decay processes, such as internal conversion (IC), are very effective in the Me- and Cl- rhodacyclopentadienes; therefore, low Φ_f values were observed (except for the Cl-rhodacyclopentadiene with R = CO_2Me).

In TMSE-rhodacyclopentadienes, the k_Δ values are much smaller compared to typical luminescent organometallic complexes ($k_\Delta \approx 10^{12}$ s^{-1}). Since the k_f values are close to the k_Δ values, the fluorescent processes are competitive with ISC; therefore, fluorescence is observed.

To date, the photophysical properties of type **a** metallacyclopentadienes in **Figure 3.3** have been investigated only briefly by Ward, although the photophysical properties of structurally related analogues with main group elements (EC_4), such as phospholes,[11] siloles,[12] and thiophenes[13] have been reported in depth. In general, most of the EC_4 analogues fluoresce in the visible region (λ_{max} = 380 – 540 nm) with $\pi \rightarrow \pi^*$ transitions. For example, the λ_{max} values of the absorption in 2,5-bis(*p*-R-arylethynyl)thiophenes were recorded in the range of 350 and 387 nm, which are assigned to $\pi \rightarrow \pi^*$ transitions, while the λ_{max} values of emission were in the range 382 and 435 nm, depending on the substituent R at the phenyl rings. The quantum yields range from 0.19 - 0.33 with lifetimes of 0.21 - 0.40 ns.[13]

Indeed, type **a** metallacyclopentadienes are more well-known for their catalytic function in [2+2+2] cycloadditions of alkynes to form benzene derivatives (**Figure 3.6**).[14-16] As shown in **Figure 3.6**, a metallacyclopentadiene **ii** is produced when the metal (M) reacts with two equivalents of alkyne. The coordination of the third alkyne to the metal centre in the metallacyclopentadiene can lead to the formation of π-complex **iii**. It

is then converted to complex **v**, either through direct (Diels-Alder) cycloaddition, or by insertion and then reductive elimination from an intermediate seven-membered metallacycle **iv**. By adding another alkyne to complex **v**, π-complex **vi** is formed, and then a benzene derivative is eliminated after another alkyne binds to the metal centre to regenerate complex **i**.[15]

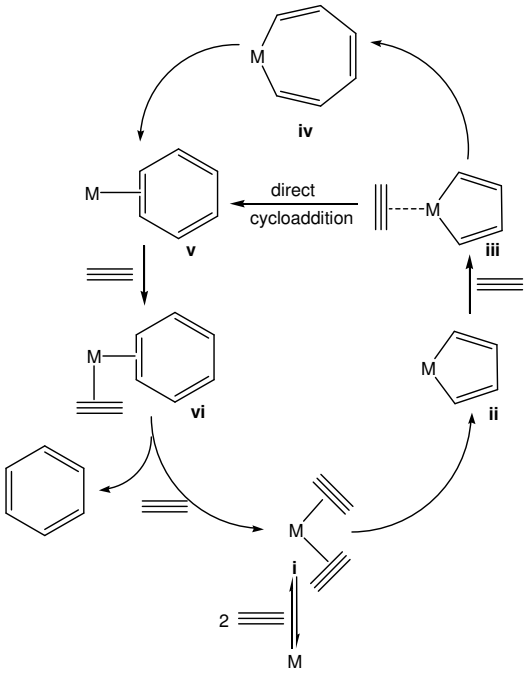

Figure 3.6: Catalytic cycle for the cyclotrimerisation of acetylene to benzene.[15]

In term of synthesis, the preparation of the type **a** metallacyclopentadienes in **Figure 3.3** is not straightforward. This is due to the regioselectivity problems that can lead to the formation of three different isomeric products (**Figure 3.7.a**, **b**, and **c**), as has been reported by Nishihara et al. in 1995.[17]

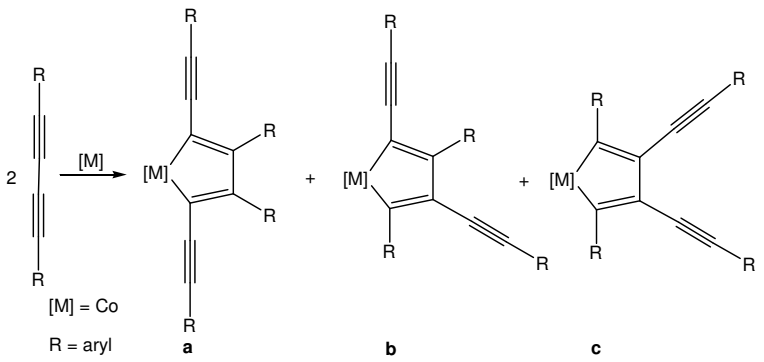

Figure 3.7: Formation of three regioisomers from the coupling of symmetrical buta-1,3-diynes at a transition metal centre.[17]

Hill and co-workers reported the formation of a ruthenacyclopentadiene by refluxing $[Ru(CO)_2(PPh_3)_3]$ (**Figure 3.8.a**) in the presence of excess diphenylbutadiyne in toluene.[18] They observed an intermediate π-complex (**Figure 3.8.b**), before formation of the ruthenacyclopentadiene (**Figure 3.8.c**).

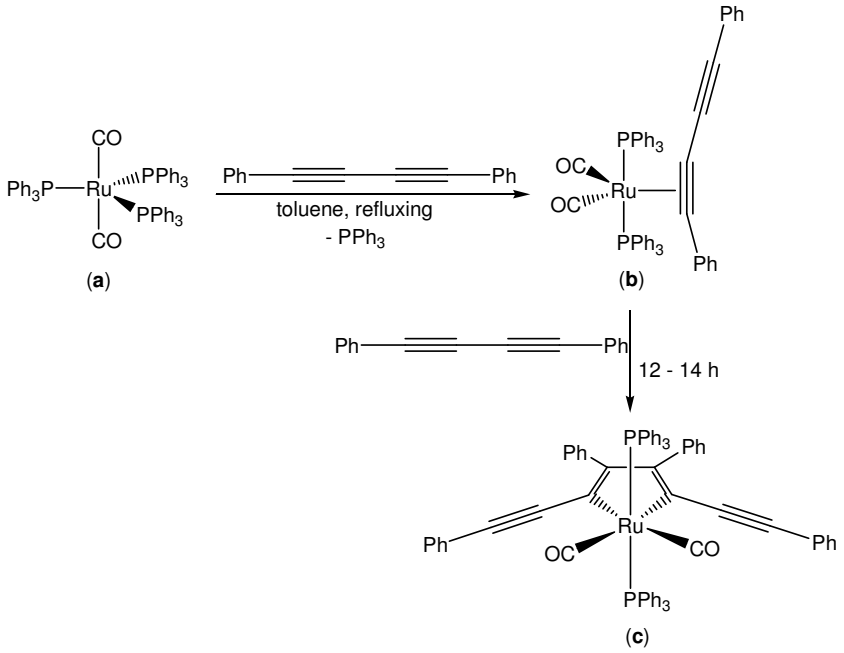

Figure 3.8: The formation of a ruthenacyclopentadiene.

The reaction in **Figure 3.8** was very slow (12 – 14 h), even under reflux conditions. Interestingly, when xylene was used as the solvent, the reaction was complete after 10 minutes at reflux.[18] In his report, Hill noted that the 2,5-bis(arylethynyl) rhodacyclopentadiene synthesis published by Marder and Rourke et al. in 2001 (**Figure 3.1**)[7] is the only example of metallacycle formation by reductive coupling of butadiynes at room temperature without any regioselectivity problems.[18]

3.1.1 Objectives and outline of synthetic routes

The main objective of this project was to explore, as well as to understand, the unusual photophysical behaviour of the rhodacyclopentadienes, e.g., long-lived singlet excited states and high-intensity fluorescence, and lack of phosphorescence. These unusual photophysical properties may be due to the small Rh contribution to the frontier orbitals of the excited states. In that case, the SOC effect from the Rh centre might not sufficient to facilitate a fast ISC to convert all of the singlet excited states to triplet excited states, and thus appreciable amounts of fluorescence are observed. In order to test this hypothesis, many photophysical experiments (e.g. low-temperature lifetime measurement and singlet oxygen sensitisation) were carried out.

Apart from the photophysical experiments, several series of rhodacyclopentadienes with different types of ligand were synthesised. The first type was designed based on the suggestions from Ward's thesis,[8] in which the rhodacyclopentadienes were synthesised by reacting two equivalents of a 1,4-bis(*p*-R-phenyl)buta-1,3-diyne with one equivalent of [RhX(PMe_3)$_4$], [where X = 4-[4-(*N*,*N*-di-*n*-hexylamino)phenylethynyl]phenylethynyl-

(DHAPEPE-) or trimethylsilylethynyl- (TMSE-)], as shown in **Figure 3.9**. The reason for preparing the DHAPEPE-rhodacyclopentadienes was to investigate the effect of an extended phenylene-ethynylene as a σ-donor at the X position on the photophysical properties of rhodacyclopentadienes. Hexyl groups were employed to improve solubility.

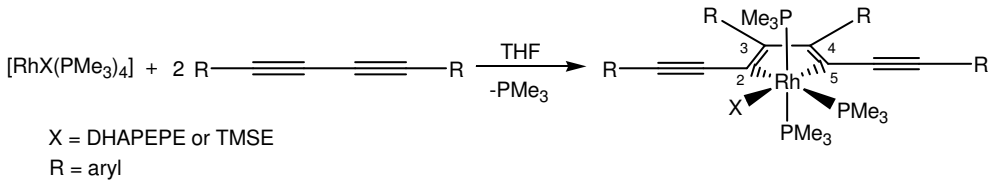

Figure 3.9: Synthetic route to the first type of rhodacyclopentadienes.

In addition, extended phenylene-ethynylene moieties were employed at the R positions. The two extended phenylene-ethynylenes with R groups employed were: i) R = C≡C-(C_6H_4-*p*-CO_2-*n*-C_8H_{17}) as an electron withdrawing group; and ii) R = C≡C-[C_6H_4-*p*-N(*n*-C_6H_{13})$_2$] as an electron donating group. The reason for preparing these two rhodacyclopentadienes was to observe the effect of extended phenylene-ethynylenes at the R-positions on the photophysical properties of the rhodacyclopentadienes by comparing them to their shorter analogues, and also to observe whether any liquid crystal phase behaviour might be present. The absorption and emission spectra were expected to be red-shifted as the conjugation length increases in the extended phenylene-ethynylene analogues.

The calculation results from **Figure 3.5** show that the two phenyl rings at the 3- and 4-positions of the rhodacycle ring do not have any contribution in the HOMO-LUMO transitions. Indeed, the two phenyl rings may act as quenchers by assisting in the loss of excitation energy through rotation, and subsequently reduce the emission efficiency. Therefore, more rigid rhodacyclopentadienes, which have a cyclohexyl loop instead of

two phenyl rings at the 3- and 4-positions of the rhodacycle ring have been designed. These rhodacyclopentadienes were synthesised by reacting one equivalent of the appropriate 1,12-bis(*p*-R-phenyl)-dodeca-1,3,9,11-tetrayne with one equivalent of [RhX(PMe_3)$_4$] (X = TMSE and Me), as shown in **Figure 3.10**.

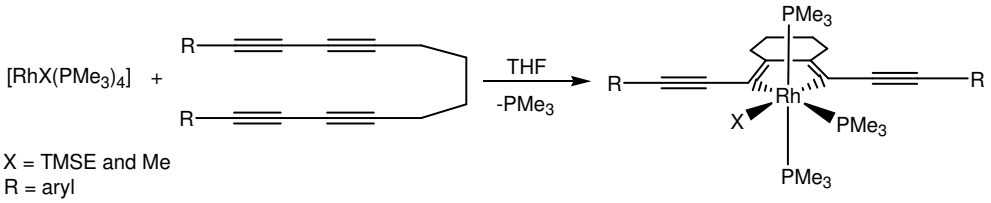

Figure 3.10: Synthetic route to the second type of rhodacyclopentadienes.

The singlet oxygen sensitisation experiment results from **Table 3.1** showed that the rhodacyclopentadienes with σ-donor ligands such as Me- and Cl- generally have slightly higher Φ_Δ values compared to TMSE-rhodacyclopentadiene, which might be due to increased Rh-participation in the frontier orbitals. To explore this further, σ- and π-donor ligands [e.g. acetylacetonato, (acac-)] were used in order to increase the Rh contribution to the frontier orbitals further by destabilising the Rh d-orbitals. Faster ISC was expected from this type of rhodacyclopentadiene, which would generate triplet excited states more efficiently. This third type of rhodacyclopentadiene was synthesised by reacting one equivalent of [RhMe(PMe_3)$_4$] with one equivalent of acetylacetone (acac-), followed by reaction with one equivalent of the appropriate 1,12-bis(*p*-R-phenyl)dodeca-1,3,9,11-tetrayne to form bis(trimethylphosphine)-η^2-acetylacetonato-rhodacyclopentadienes (**Figure 3.11**).

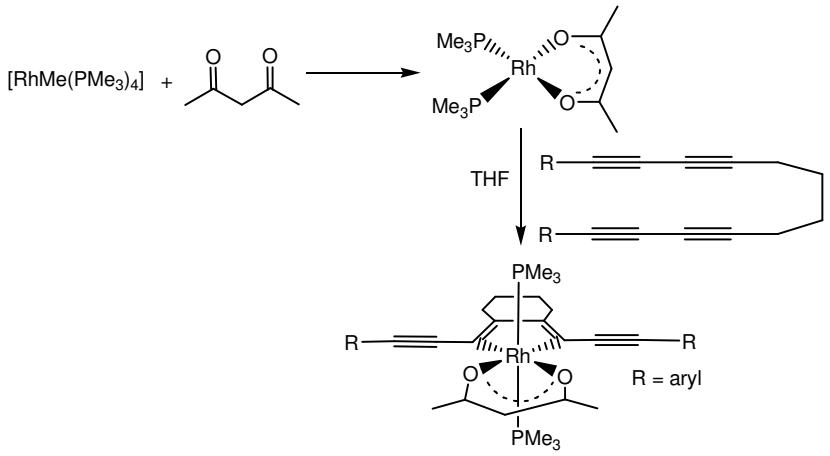

Figure 3.11: Synthetic route to the third type of rhodacyclopentadiene.

3.2 Results and discussion

3.2.1 Synthesis and characterisation of tetrakis(trimethylphosphine)methyl rhodium, [RhMe(PMe$_3$)$_4$]

The synthetic route to the precursor, [RhMe(PMe$_3$)$_4$], is shown in **Figure 3.12**. $RhCl_3 \cdot 3H_2O$ was reacted with 1,5-cyclooctadiene (COD) under nitrogen for 3 h to produce $[RhCl(COD)]_2$ dimer. Alternatively, $[RhCl_3 \cdot 3H_2O]$ can also be reacted with cyclooctene (COE) to produce $[RhCl(COE)_2]_2$ dimer. Both $[RhCl(COD)]_2$ and $[RhCl(COE)_2]_2$ dimers can be used to synthesise $[Rh(PMe_3)_4]Cl$ by reaction with excess trimethylphosphine (PMe_3) to give the product in over 80% yield.

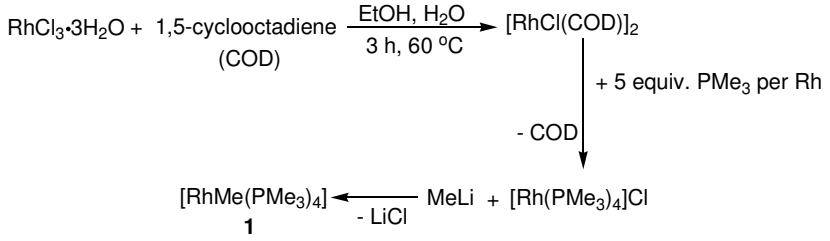

Figure 3.12: The preparation of [RhMe(PMe$_3$)$_4$].

The preparation of [RhMe(PMe_3)$_4$] from [Rh(PMe_3)$_4$]Cl was based on the method described by Price et al. with some modifications.[19] In a nitrogen-filled glovebox, LiMe was added dropwise to a solution of [Rh(PMe_3)$_4$]Cl in THF. The solution colour changed from orange to yellow indicating that [RhMe(PMe_3)$_4$] was forming in the reaction. After LiCl was filtered off and the solvent was removed, [RhMe(PMe_3)$_4$] (**1**) was obtained as a yellow solid in high yield (> 80%).

3.2.2 4-[4-(*N*,*N*-di-*n*-hexylamino)phenylethynyl]phenylethynylrhodacyclopenta-dienes (DHAPEPE-rhodacyclopentadienes)

3.2.2.1 Synthesis and characterisation

The 4-[4-(*N*,*N*-di-*n*-hexylamino)phenylethynyl]phenylethynyl-based rhodacyclopenta-dienes (DHAPEPE-rhodacyclopentadienes) were first prepared and studied by van Leeuwen in her M. Chem. fourth-year project.[20] Some of the DHAPEPE-rhodacyclopentadienes were resynthesised in this work in order to complete the data collection for this series of rhodacyclopentadienes.

Firstly, [RhMe(PMe_3)$_4$] (**1**) was reacted with one equivalent of 4-(4-ethynylphenylethynyl)-*N*,*N*-di-n-hexylaniline (EPEDHA) to form a rhodium complex [Rh(DHAPEPE)(PMe_3)$_4$] (**2**), which was subsequently reacted with two equivalents of the appropriate 1,4-bis(*p*-R-phenyl)buta-1,3-diyne in THF forming the DHAPEPE-rhodacyclopentadienes (R = H, **3(a)**; R = OMe, **3(b)**; R = CF_3, **3(c)**; R = CO_2Me, **3(d)**; **Figure 3.13**).

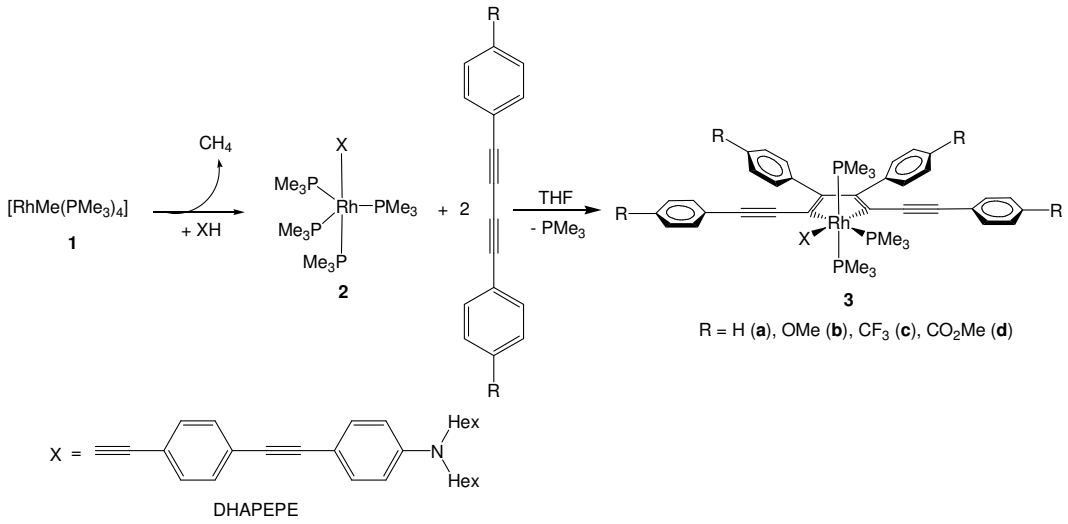

Figure 3.13: Syntheses of the DHAPEPE-rhodacyclopentadienes.

However, care must be taken to add an accurate amount of the EPEDHA to [RhMe(PMe_3)$_4$]. Adding excess EPEDHA (> 1 equivalent), or adding it too quickly to [RhMe(PMe_3)$_4$], leads to the formation of *mer*,*trans*-[RhH(-C≡C-R)$_2$(PMe_3)$_3$] (**Figure 3.14**), a process which has been reported by Marder et al.[21-23]

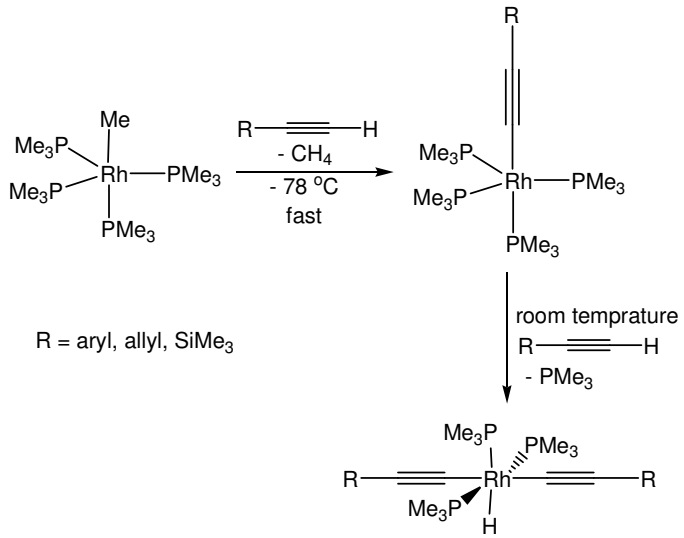

Figure 3.14: Formation of *mer*,*trans*-[RhH(-C≡C-R)$_2$(PMe_3)$_3$] by adding excess RC≡CH to [RhMe(PMe_3)$_4$].[21-23]

After adding two equivalents of the appropriately substituted 1,4-bis(*p*-R-phenyl)buta-1,3-diyne to [Rh(DHAPEPE)(PMe_3)$_4$], the volatiles (i.e. solvent and dissociated PMe_3) were removed *in vacuo* and the flask was refilled with fresh THF. This process was repeated at least three times in order to remove the dissociated PMe_3 from [Rh(DHAPEPE)(PMe_3)$_4$]. The reactions were monitored by *in situ* $^{31}P\{^1H\}$ NMR spectroscopy, and the rate of reaction was found to depend on the R substituent on the 1,4-bis(*p*-R-phenyl)buta-1,3-diyne. For example, the buta-1,3-diyne with the electron donating OMe groups reacted more slowly compared to those with electron withdrawing substituents, such as CO_2Me. This may be due to the fact that the electron donating property of OMe leads to weaker back-bonding from Rh to the C≡C bonds of the buta-1,3-diyne and subsequently slows down the reductive coupling process of butadiyne. The reactions took about 15 - 48 h to complete at room temperature. An intermediate π-complex can be observed in the $^{31}P\{^1H\}$ NMR spectrum (**Figure 3.15**) if the reaction is not complete.

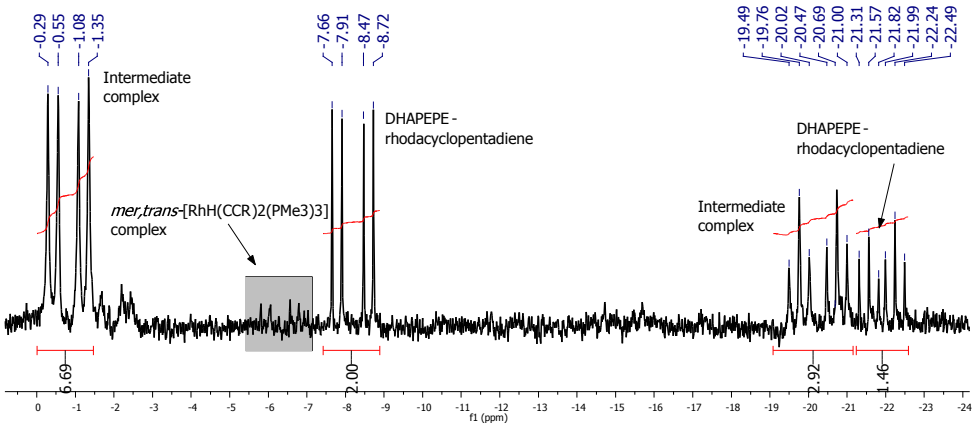

Figure 3.15: $^{31}P\{^1H\}$ NMR spectrum (122 MHz, C_6D_6) of **3(b)** after 3 h reaction.

The presence of the intermediate π-complex in the reaction **3(b)** was confirmed by comparing the $^{31}P\{^{1}H\}$ NMR signals to those of a structurally related Rh π-complex (**Figure 3.16**) from the reaction of $[Rh(C{\equiv}C\text{-}SiMe_3)(PMe_3)_4]$ with (*p*-CF_3-C_6H_4)-C≡C-(*p*-C_6H_4-CF_3) reported by Marder and Rourke et al.[23] The $^{31}P\{^{1}H\}$ NMR spectrum in **Figure 3.15** was obtained *in situ* after 3 h reaction, and the signals of the π-intermediate complex appear as a doublet of doublets at -0.82 ppm and a doublet of triplets at -20.25 ppm, in a ratio of 2:1. This implies that there are two equivalent phosphorus atoms mutually *trans* to each other and one unique phosphorus atom. Based on the value of the Rh to phosphorus coupling constant ($J_{Rh\text{-}P}$) of ca. 96 Hz for the doublet of doublets and 118 Hz for the doublet of triplets, the unique phosphorus is subjected to a weaker *trans*-influence than the other two phosphorus atoms. Therefore, the structure of the intermediate π-complex is believed to be similar to the one reported by Marder and Rourke et al.[23] In addition, the magnitudes of the $J_{Rh\text{-}P}$ values (118 Hz for the doublet of triplets) clearly indicate that the intermediate complex contains $Rh^{(I)}$ rather than $Rh^{(III)}$.

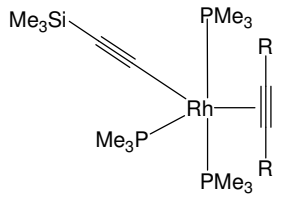

Figure 3.16: The structure of the intermediate complex that was reported by Marder and Rourke et al.[23]

In **Figure 3.15**, a small doublet of doublets was found at -6.28 ppm ($J_{Rh\text{-}P}$ = 92 Hz, $J_{P\text{-}P}$ = 26 Hz), which is assigned to the *mer,trans*-$[RhH(\text{-}C{\equiv}C\text{-}R)_2(PMe_3)_3]$ complex [R =

C_6H_4-C≡C-C_6H_4-*p*-N(*n*-$C_6H_{13})_2$].[23] As mentioned before, the formation of this complex was probably due to adding the alkynyl ligand too quickly into the [RhMe$(PMe_3)_4$] solution.

The reaction was continuously stirred until the doublet of doublets at -0.82 ppm, as well as the doublet of triplets at -20.25 ppm, disappeared in the $^{31}P\{^1H\}$ NMR spectrum, indicating that the reaction had gone to completion [48 h for **3(b)**]. The volatiles were removed *in vacuo* and the product was washed with hexane. The crude product was purified by several recrystallisations from THF and hexane or C_6D_6 and hexane in order to obtain high-purity samples for photophysical studies. The purity of the compounds was determined by elemental analysis (EA), $^{31}P\{^1H\}$, ^1H NMR and mass spectroscopy. The isolated yields for pure compounds **3(a)**, **3(b)**, **3(c)** and **3(d)** are shown in **Table 3.2**, and the $^{31}P\{^1H\}$ NMR spectrum of **3(a)** is shown in **Figure 3.17**.

Table 3.2: Isolated yields of **3(a)**, **3(b)**, **3(c)** and **3(d)**.

Compound	R Group	Yield (%)
3(a)	H	85
3(b)	OMe	64
3(c)	CF_3	81
3(d)	CO_2Me	51

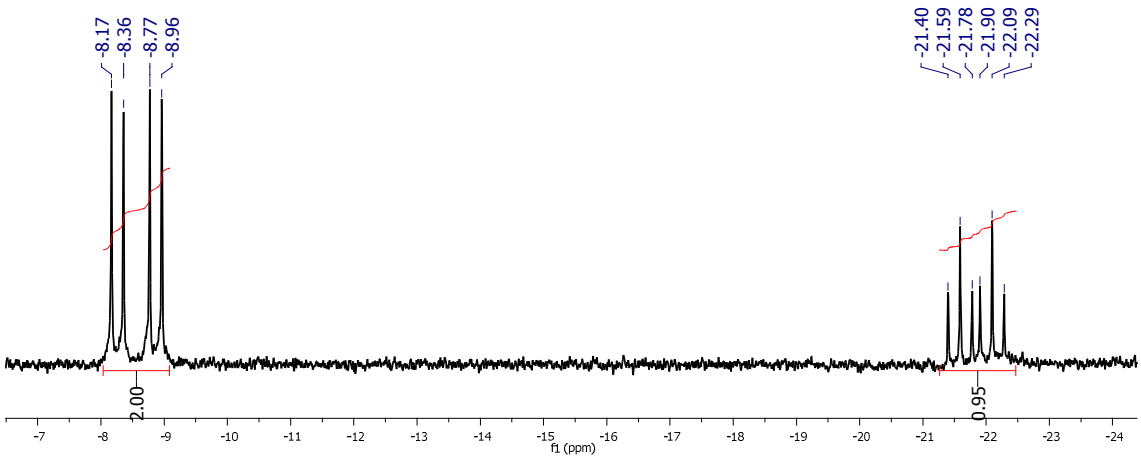

Figure 3.17: $^{31}P\{^{1}H\}$ NMR spectrum (162 MHz, C_6D_6) of **3(a)**.

Based on the $^{31}P\{^{1}H\}$ NMR patterns in **Figure 3.17**, the doublet of doublets and associated doublet of triplets in a ratio of 2:1 indicate that there are two equivalent phosphorus atoms and one unique phosphorus atom. The $J_{Rh\text{-}P}$ values of ca. 98 Hz for the doublet of doublets and 81 Hz for the doublet of triplets show that the unique phosphorus atom is incurring a stronger *trans*-influence than the two equivalent ones. This clearly implies that the unique phosphorus atom is *trans* to the rhodacycle α-carbon and is located in the rhodacycle plane, while the other two are located at axial positions, as seen in **Figure 3.13**.

The ^{1}H NMR spectrum of **3(a)** is shown in **Figure 3.18**. The twenty-eight aromatic protons from the phenyl rings give rise to signals in the region of 7.65 – 6.50 ppm, which confirms that there are six different phenyl rings present. The doublet ($J_{P\text{-}H}$ = 8 Hz) at 1.36 ppm belongs to the PMe_3 ligand which is *trans* to the α-carbon of the rhodacycle ring, whereas the virtual triplet at 1.30 ppm is assigned to the two mutually *trans* PMe_3 ligands which are located in the axial positions.

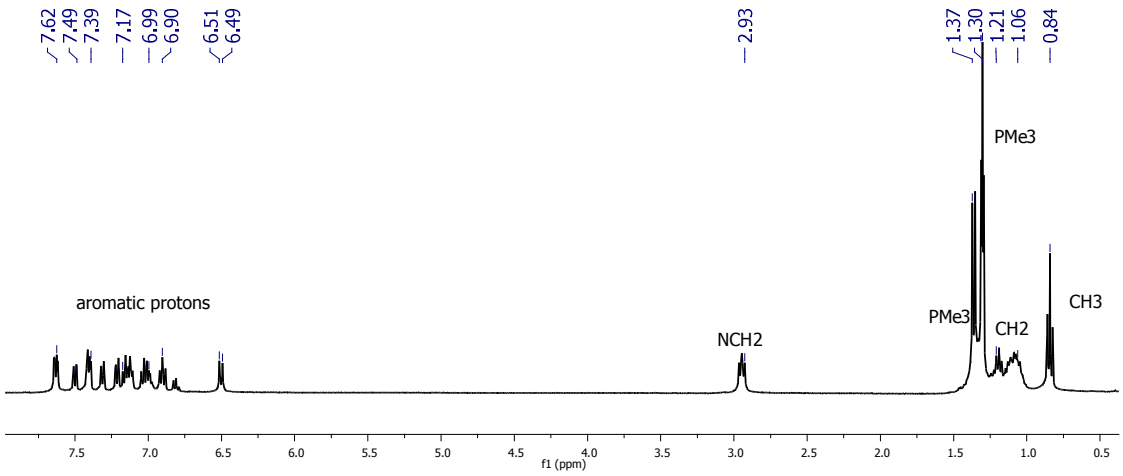

Figure 3.18: ^{1}H NMR spectrum (500 MHz, C_6D_6) of **3(a)**.

Interestingly, the chemical shifts of the NCH_2CH_2 signal in the ^{1}H NMR spectra from the DHAPEPE fragment are significantly influenced by the R groups on the phenyl substituents the rhodacycle ring. The chemical shift of this proton signal is 1.22 ppm for R = H and OMe, whereas for R = CF_3 and CO_2Me, this signal is shifted to lower field at 1.38 and 1.40 ppm, respectively. This indicates that the electronic effect of the R groups can pass through the Rh centre and reach the end of the alkynyl ligand.

The IR spectra of the complexes show four signals to be present in the region between 2000 and 2200 cm^{-1}, which indicates that there are four allowed C≡C stretching modes present in each complex. An additional strong band at 1721 cm^{-1} can be observed in the IR spectrum of **3(d)**, which is assigned to the C=O stretches from the CO_2Me groups.

3.2.2.2 Photophysical studies

The photophysical data for the DHAPEPE-rhodacyclopentadienes **3(a)**, **3(c)** and **3(d)** are given in **Table 3.3**, and the absorption and emission spectra of these complexes are shown in **Figure 3.19**.

Table 3.3: Summary of the photophysical data for **3(a)**, **3(c)** and **3(d)**.

Compound	λ_{max} ABS (nm)	ε (M^{-1} cm^{-1})	λ_{max} EM (nm)	Stokes shift (cm^{-1})	Φ_f	τ_f (ns)
3(a), R = H	454	27000	497	1900	0.04	0.26 (82%) 1.38 (18%)
3(c), R = CF_3	465	31000	510	1900	0.04	0.18 (82%) 1.55 (18%)
3(d), R = CO_2Me	484	26000	535	2010	0.14	0.55 (85%) 1.43 (15%)

Note: All of the data (except ε) above were recorded in degassed toluene solution at room temperature. ε values were recorded in non-degassed toluene solution.
No data were recorded for **3(b)** due to sample decomposition in low concentration solutions.

The progressional spacings in the emission spectra (**Figure 3.19**) are in the range of 1320 – 1290 cm^{-1}. The absorption and emission maxima (λ_{max}) for those DHAPEPE-rhodacyclopentadienes with electron withdrawing substituents such as R = CF_3 [**3(c)**] and CO_2Me [**3(d)**] are red-shifted compared to those of **3(a)**. This can be rationalised by the fact that the rhodacyclopentadienes with these electron withdrawing groups have a smaller energy gap between the excited and ground states. However, comparing the λ_{max} values of absorption and emission between the DHAPEPE- and the TMSE-rhodacyclopentadienes reported by Ward[8] (**Table 1.5**, **Chapter 1**), the extended phenylene-ethynylene alkynyl ligand in the DHAPEPE-rhodacyclopentadienes did not impart any bathochromic effect.

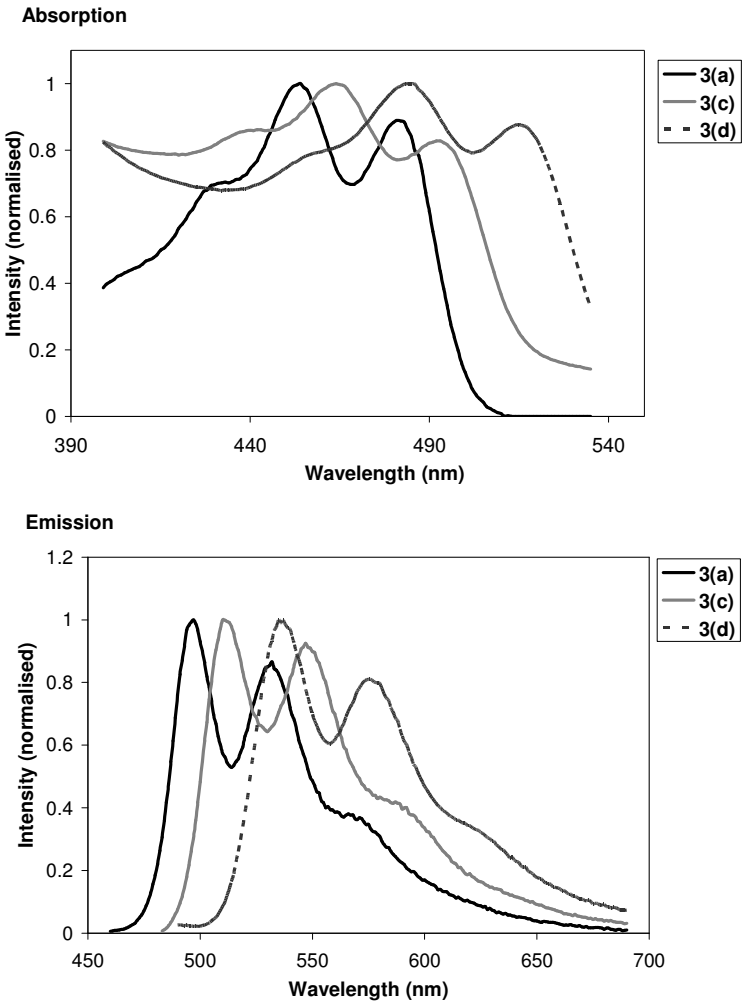

Figure 3.19: Absorption (top) and emission (bottom) spectra of **3(a)**, **3(c)** and **3(d)**.

All of the lifetimes of the DHAPEPE-rhodacyclopentadienes are on the nanosecond timescale. These results are parallel to the results from Ward,[8] and confirm that the emissions arise from fluorescence, i.e., they originate from singlet excited states. As mentioned before, the fluorescence emission from the DHAPEPE-rhodacyclopentadienes is an unusual photophysical property because fluorescence is rarely observed in metallacyclopentadiene complexes, especially those containing Rh. In most cases, Rh complexes do not fluoresce, but phosphoresce at 77 K in a rigid glass with micro- to

millisecond lifetimes. The dominant phosphorescent emissions are mainly from ligand-centred $^3\pi \rightarrow \pi^*$ transitions with small amounts of metal contributions.[24-27]

The DHAPEPE-rhodacyclopentadienes were observed to have two fluorescence lifetime (τ_f) components compared to one for the TMSE-series in **Table 1.5**. This may be due to partial decomposition of the DHAPEPE-rhodacyclopentadienes when they were prepared in low-concentration (10^{-6} M) solutions. Fast decomposition was noticed for the more electron rich compound, **3(b)**, when it was prepared for lifetime measurement: 30 minutes after preparation, the emission colour was found to have changed from yellow to blue, even in degassed solution, which indicated that decomposition had occurred. However, the fact that two lifetime components occur in essentially identical ratios for all three compounds, which should have different stabilities, suggests that an alternative process might be responsible such as a second localised transition.

The Φ_f values of the DHAPEPE-series are relatively low compared to the TMSE-rhodacyclopentadienes in **Table 1.5**, which are in the range of $\Phi_f = 0.03 – 0.18$. This may be due to the excitation energy lost through the long alkynyl ligand, which increases the quenching possibilities from C-H stretching motions and poor rigidity in the hexyl chains. For example, the Φ_f values for TMSE-rhodacyclopentadienes with R = H and CF_3 in Ward's study[8] were reported as 0.15 and 0.08, respectively, but for the DHAPEPE-rhodacyclopentadienes with the same R-substituents, the Φ_f values are 0.04. However, the Φ_f values for the rhodacyclopentadienes with R = CO_2Me are very similar: 0.14 (for the DHAPEPE-rhodacyclopentadiene) and 0.16 (for the TMSE-analogue).

The fluorescence rate constant (k_f) can be calculated from the formula $k_f = \Phi_f/\tau_f$; thus, the k_f values in DHAPEPE-rhodacyclopentadienes **3(a)**, **3(c)** and **3(d)** must be in the

range of 0.26 – 2.54 x 10^8 s^{-1}. If it is assumed, and this is unlikely, that no IC from the S_1 state is occurring, the Φ_Δ values for **3(a)** and **3(c)** would be 0.96. As the rate constant of ISC (k_Δ) is calculated from the formula $k_\Delta = \Phi_\Delta/\tau_f$, the k_Δ values of these three DHAPEPE-rhodacyclopentadienes can be up to 5 x 10^9 s^{-1} [for **3(c)**]. This value is still over two orders of magnitude slower than the ISC rates of typical organometallic complexes, which are in the range of 10^{12} s^{-1}. This explains why significant fluorescence can occur in the DHAPEPE-rhodacyclopentadienes.

3.2.3 Me-rhodacyclopentadiene with NMe_2 groups at the *para*-position of the phenyl rings

3.2.3.1 Synthesis and characterisation

The synthesis of a Me-rhodacyclopentadiene bearing -NMe_2 groups at the *para*-positions of the phenyl rings (**Figure 3.20**) is much more difficult than those with other *para*-substituents because 1,4-bis(*p*-*N*,*N*-dimethylaminophenyl)butadiyne contains strong electron donor substituents, which significantly affect the back-bonding from the Rh centre to the C≡C bonds and slows down the reaction. In this case, the reaction needs to be heated in order for it to reach completion at a reasonable rate. However, the optimum synthesis conditions were not found by Ward.[8] In a continuation of Ward's work, one of the objectives in the early part of this project was to ascertain the optimum synthesis conditions for this rhodacyclopentadiene.

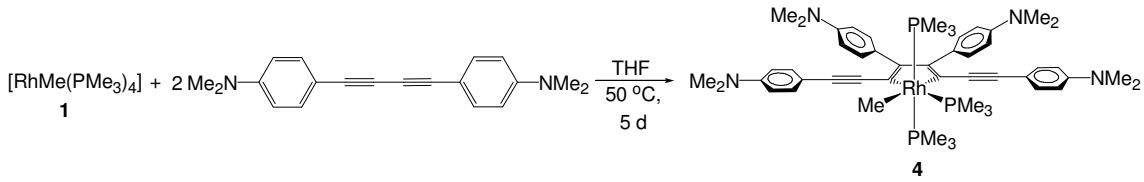

Figure 3.20: Synthetic route to a Me-rhodacyclopentadiene with NMe_2 groups at the *para*-positions of the phenyl rings.

In the synthesis of **4**, two equivalents of 1,4-bis(*p*-*N*,*N*-dimethylaminophenyl)butadiyne were added to $[RhMe(PMe_3)_4]$ in degassed THF solution, the volatiles (e.g. THF and PMe_3) were removed *in vacuo* and the flask was refilled with fresh THF. This process was repeated three times. Then, the reaction was heated at 50 °C for five days under nitrogen condition, and the reaction progress was monitored *in situ* using $^{31}P\{^1H\}$ NMR spectroscopy. It is worth noting that the reaction time is temperature-dependent: at 45 °C, the reaction took about six weeks to complete; but surprisingly, it can be completed within five days at 50 °C, although there is only a 5 °C difference in temperature.

When the reaction was complete, the solvent was removed *in vacuo*, and the crude product was crystallised via slow diffusion of hexane vapour into a concentrated toluene solution in order to obtain high-purity product with EA results within the acceptable range. In the mass spectrum [electrospray (ES), positive ion mode], the major signal occurred at $m/z = 907$, which is associated with the fragment $[M^+ - CH_3]$.

The $^{31}P\{^1H\}$ NMR spectrum of **4** is similar to those shown in **Figure 3.17**, which indicates that the PMe_3 ligands in **4** are at similar positions to those in **3(a) - 3(d)**. The $J_{Rh\text{-}P}$ values (dd, 106 Hz; dt, 89 Hz) are higher than those in **3(a)** - **3(d)**, which confirms that the Me- group is a stronger donor ligand that increases the electron density at the Rh

centre. In the ^{1}H NMR spectrum, the protons from this Me- ligand appear as a doublet of quartets (dq) at 0.15 ppm ($^{2}J_{Rh-H}$ = 2 Hz, $^{3}J_{P-H}$ = 7 Hz) because they are coupled with the Rh centre and three PMe_3 ligands. The coupling to Rh is smaller than the couplings to P, and therefore a doublet of quartets is observed. Four singlets for the protons of the NMe_2 groups were observed in the 2.50 – 2.36 ppm region, which confirms that they are in four different environments. Similarly, for the aromatic protons, there are eight sets of doublets from four different phenyl rings, which appear in the 7.68 – 6.43 ppm region.

In the IR spectrum, a band appears at 2121 cm^{-1} which is assigned to a C≡C stretching mode of the two ethynyl moieties at the 2- and 5-positions of the rhodacycle ring.

3.2.3.2 Crystallographic data for 4

The crystallographic data for **4** are listed in **Table 3.4**. Me-rhodacyclopentadiene **4** crystallises in the triclinic space group $P\bar{1}$ and the molecular structure is shown in **Figure 3.21**.

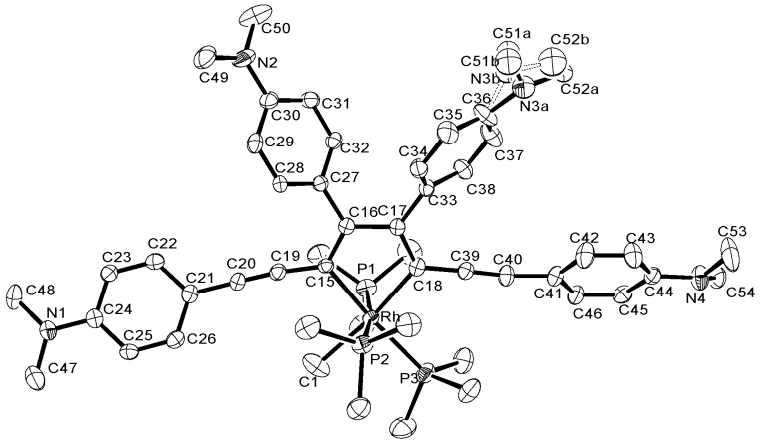

Figure 3.21: Molecular structure of **4**, with thermal ellipsoids plotted at 50% probability (hydrogen atoms, H_2O and C_7H_8 molecules are omitted for clarity).

Table 3.4: Crystallographic data for **4**.

Compound	**4**
Empirical formula	$0.85(C_{50}H_{70}N_4P_3Rh),0.15(C_{49}H_{67}ClN_4P_3Rh)\cdot 0.5(C_7H_8)\cdot 0.5(H_2O)$
Formula weight	981.06
Temperature (K)	120(2)
Crystal system	Triclinic
Space group	$P\bar{1}$
a (Å)	9.6364(6)
b (Å)	15.4817(10)
c (Å)	18.2839(14)
α (º)	99.844(14)
β (º)	101.008(13)
γ (º)	102.875(15)
Volume ($Å^3$)	2544.4(3)
Z	2
Density (calculated) (Mg/m^3)	1.280
Absorption coefficient (mm^{-1})	0.478
Crystal size (mm^3)	0.13 x 0.09 x 0.05
Θ range for data collection (º)	2.23 to 29.98
Reflection collected	15803
Independent reflections	8950
Data / Restraints / Parameters	8950 / 6 / 583
Final R indices [I>2σ(I)]	$R1 = 0.0491$ $wR2 = 0.0986$
R indices (all data)	$R1 = 0.0901$ $wR2 = 0.1104$

In compound **4**, the bond length of Rh-C1 [2.201(4) Å] is slightly longer than Rh-C15 [2.087(4) Å] and Rh-C18 [2.078(4) Å], because C1 is sp^3-hybridised, whereas C15 and C18 are sp^2-hybridised. The bond lengths of Rh-P1 [2.3049(13) Å] and Rh-P2 [2.3088(13) Å] are shorter than Rh-P3 [2.3544(13) Å], which indicates that the α-carbon has a stronger *trans*-influence than the PMe_3 ligand. The two NMe_2- phenyl rings at C16 and C17 are twisted suggesting the presence of unfavourable steric interactions, which

prevent a co-planar arrangement of these two phenyl rings. The C-C≡C-C moiety at C15 is slightly more distorted from linearity than the one at C18, by comparison of the bond angles of C15-C19-C20 [173.9(5)°] and C18-C39-C40 [176.6(5)°]. The NMe_2 group at C36 is disordered between positions **a** and **b** with equal occupancies. In addition, the methyl ligand, -C1H_3, at the Rh centre is partially refined as a chlorine (Cl) atom with a 0.15 probability. The Cl incorporation probably arises from LiCl, which was formed during the [RhMe(PMe_3)$_4$] synthesis. Indeed, this problem was also found in the molecular structures of the other Me-rhodacyclopentadienes (e.g. Ward's Me-rhodacyclopentadienes). However, the Cl contamination is believed very small because other spectroscopic data such as mass spectra, and $^{31}P\{^1H\}$ and ^1H NMR spectra did not detect the presence of any Cl-rhodacyclopentadienes. In addition, it is also possible that it is Br rather than Cl which is present, arising from LiBr in the MeLi used. In this case, even less Br would be required to account in the extra electron density peak. It is also likely that the halide is enriched in the crystals due to lower solubility of the halide complex.

3.2.3.3 Photophysical studies

Photophysical data for **4** are presented in **Table 3.5**, and the absorption and emission spectra are shown in **Figure 3.22**.

Table 3.5: Summary of the photophysical data of **4**.

λ_{max} ABS (nm)	ε (mol^{-1} cm^{-1} dm^3)	λ_{max} EM (nm)	Stokes shift (cm^{-1})
474	40000	523	2000

Note: all of the data above (except ε) were measured in degassed toluene at room temperature. ε value was recorded in non-degassed toluene solutions.

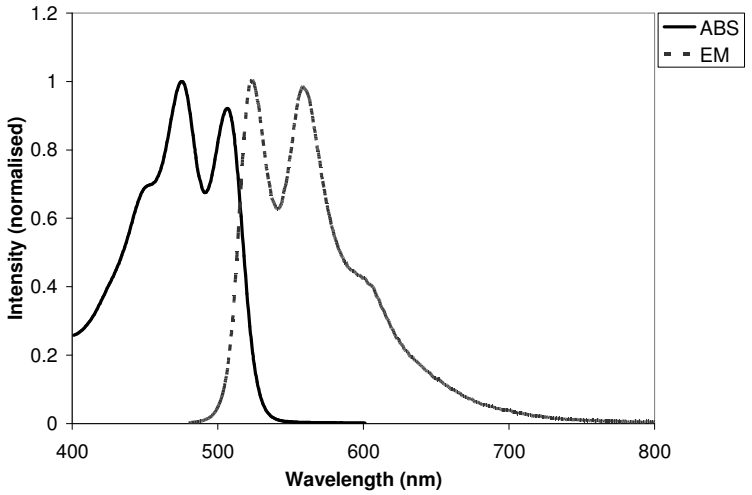

Figure 3.22: Absorption and emission spectra of **4**.

Me-rhodacyclopentadiene **4** exhibits a yellow emission at λ_{max} = 523 nm. Similar to **3(a)**, **3(c)** and **3(d)**, **4** also has a small Stokes shift (ca. 2000 cm^{-1}), which indicates that the emission originates from the singlet excited states. The progressional spacings of ca. 1250 cm^{-1} in the emission spectrum are probably due to a stretching mode of the π-system in the structure.

3.2.4 Trimethylsilylethynyl- (TMSE-) rhodacyclopentadienes containing extended phenylene-ethynylene groups

3.2.4.1 Synthesis and characterisation

From the photophysical results of the DHAPEPE-rhodacyclopentadienes, we know that the extended phenylene-ethynylene alkynyl ligand on the Rh centre does not impart any bathochromic effects on the absorption and emission λ_{max} values. In addition, the extended alkynyl ligand decreases the Φ values compared to shorter alkynyl ligands such as TMSE-. Two TMSE-rhodacyclopentadienes containing extended phenylene-ethynylene moieties at the 2- and 5-positions of the rhodacycle ring were thus synthesised (**Figure 3.23**). The reason for including these extended moieties was to study their effects on the photophysical properties of the rhodacyclopentadienes by comparison to the simple TMSE-rhodacyclopentadienes reported by Ward.[8] Another reason was to see whether these two systems might display liquid crystal phase behaviour.

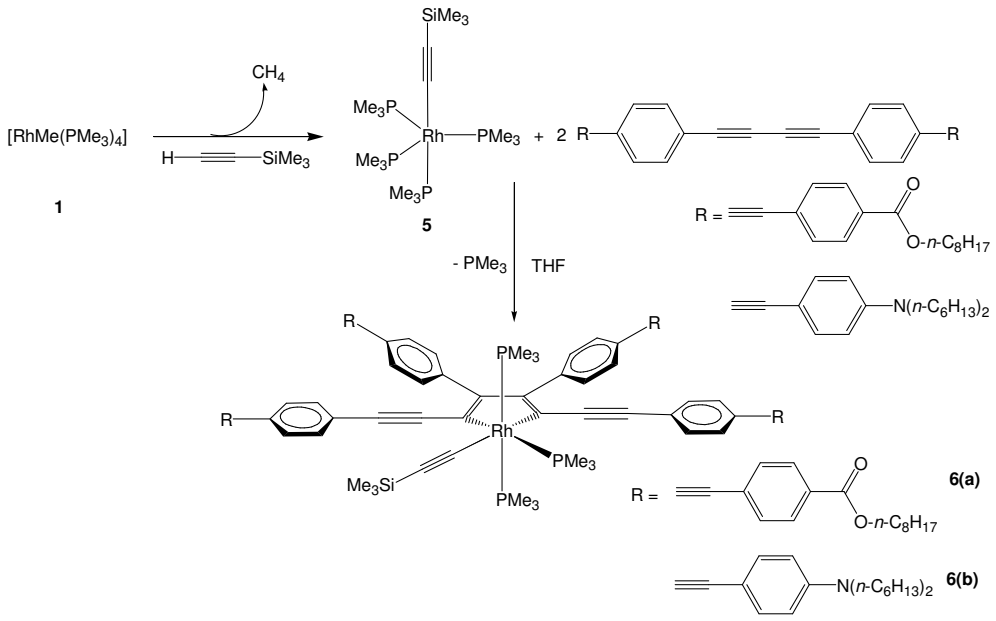

Figure 3.23: Synthetic route to TMSE-rhodacyclopentadienes containing extended phenylene-ethynylene moieties at the 2- and 5-positions of the rhodacycle ring.

About 1.2 equivalents of trimethylsilylacetylene (TMSA) in THF solution were added dropwise to a stirred solution of [RhMe(PMe_3)$_4$] in THF to give **5**. Then two equivalents of the appropriate extended bis(*p*-R-phenylethynyl)diarylbutadiyne with different R substituents [R = C≡C-C_6H_4-*p*-CO_2-*n*-C_8H_{17} and C≡C-C_6H_4-*p*-N(*n*-C_6H_{13})$_2$, the syntheses of which have already been discussed in **Chapter 2**] were added, respectively, to solutions of **5**, and the volatiles were repeatedly removed *in vacuo* and fresh solvent was added at least three times, to form the respective **6(a)** and **6(b)** [R = C≡C-C_6H_4-*p*-CO_2-*n*-C_8H_{17}, **6(a)**; R = C≡C-C_6H_4-*p*-N(*n*-C_6H_{13})$_2$, **6(b)**]. The colour of the solutions changed from yellow to dark red indicating that the rhodacyclopentadienes were forming in the reaction.

The progress of both reactions was monitored *in situ* using $^{31}P\{^1H\}$ NMR spectroscopy, and similar NMR spectra to those shown **Figure 3.17** were obtained when the reactions were complete. The pattern of a doublet of doublets associated with a doublet of triplets (in a 2:1 ratio) indicates that there are two phosphine environments. The $J_{Rh\text{-}P}$ values of ca. 97 Hz for the doublet of doublets and 82 Hz for the doublet of triplets, which are similar to the DHAPEPE-rhodacyclopentadienes, indicate that one phosphine is located in the plane of the rhodacycle, while the other two phosphines are located at mutually-*trans* axial positions.

At room temperature, the volatility of TMSA can result in some loss of the reagent and thus some unreacted [RhMe(PMe_3)$_4$] remaining in the solution following reaction with the alkyne. When two equivalents of butadiyne are then added to the solution, two kinds of rhodacyclopentadiene will be formed, namely TMSE-based and Me-based

rhodacyclopentadienes, which reduces the isolated yields of the desired product. This is a common problem when synthesising the TMSE-rhodacyclopentadienes.

3.2.4.2 Photophysical studies

The absorption and emission spectra of **6(a)** and **6(b)** are shown in **Figure 3.24**, and a summary of the photophysical data for **6(a)** and **6(b)** is given in **Table 3.6**.

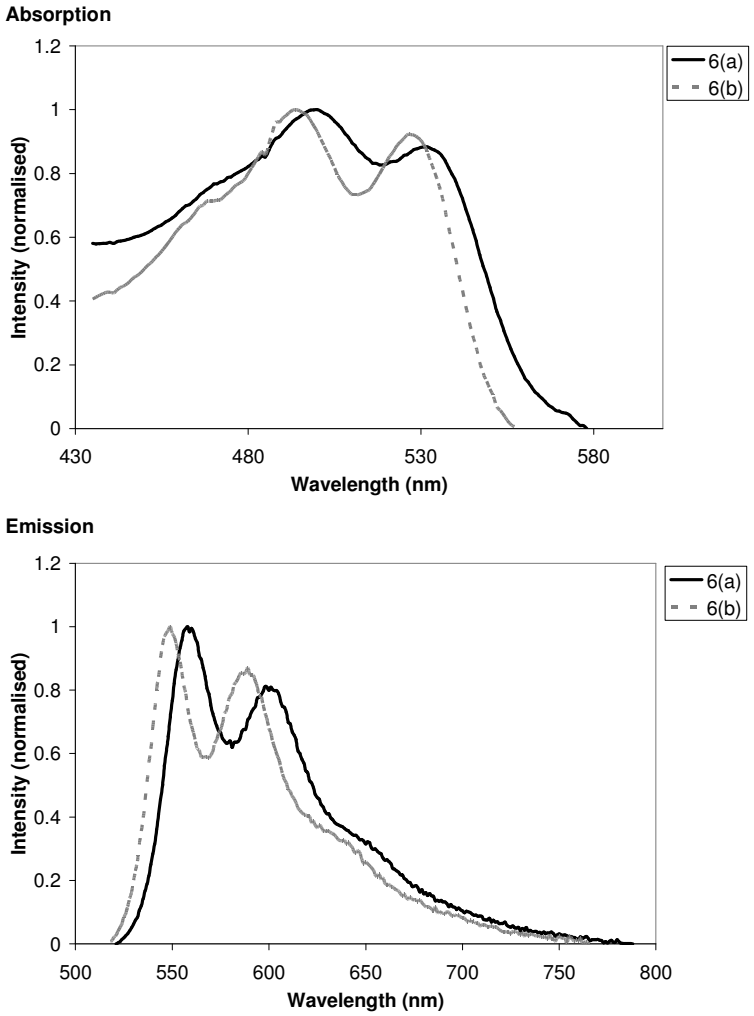

Figure 3.24: Absorption (top) and emission (bottom) spectra of **6(a)** and **6(b)**.

Table 3.6: Summary of the photophysical data of **6(a)** and **6(b)**, and comparison of the photophysical data between **6(a)** and **6(b)**, and the simple TMSE-rhodacyclopentadiene (R = CO_2Me) reported by Ward.[8]

Compounds, R	**λ_{max} ABS (nm)**	**ε (M^{-1} cm^{-1})**	**λ_{max} EM (nm)**	**Stokes shift (cm^{-1})**	**Φ**	**τ (ns)**
6(a), R = C≡C-C_6H_4-*p*-CO_2-*n*-C_8H_{17}	500	40000	556	2010	0.02	0.096 (47%) 0.856 (53%)
6(b), R = C≡C-C_6H_4-*p*-N(*n*-C_6H_{13})$_2$	494	48000	549	2030	0.01	0.059 (27%) 1.640 (73%)
R = CO_2Me	485	21000	536	1960	0.16	0.98

Note: All data above (except ε) were recorded in degassed toluene solution at room temperature. ε values were recorded in non-degassed toluene solution.

From the results in **Figure 3.24**, the λ_{max} values for absorption and emission of the rhodacyclopentadiene with the electron withdrawing substituent, namely R = C≡C-C_6H_4-*p*-CO_2-*n*-C_8H_{17} [**6(a)**], are slightly red-shifted compared to that with the electron donating substituent, R = C≡C-C_6H_4-*p*-N(*n*-C_6H_{13})$_2$, [**6(b)**]. This indicates that the energy gap between the excited and ground states in the compound containing the electron withdrawing substituent is smaller than that in the compound with the electron donating substituent. The small Stokes shifts (~2000 cm^{-1}) and the nanosecond lifetimes of these two rhodacyclopentadienes imply that the emissions are from fluorescence, which occurs from singlet excited states.

The Φ_f values for these two rhodacyclopentadienes are only 0.02 [**6(a)**] and 0.01 [**6(b)**]. These low Φ_f values are possibly due to external quenching processes, such as energy transfer from the excited molecules to solvent molecules, and the increased molecular vibrations and rotations when the molecular size increases.[28] On the other hand, they are also possibly due to the flexibility of the long alkyl chains in **6(a)** and **6(b)**. In addition,

the low Φ_f values in **6(a)** and **6(b)** might be also due to efficient ISC leading to non-radiative triplet excited states.

A comparison of the photophysical data between the extended phenylene-ethynylene-rhodacyclopentadiene and its shorter analogue with R = CO_2Me is also given in **Table 3.6**. The λ_{max} values of **6(a)** and **6(b)** in both absorption and emission showed bathochromic shifts compared to the simple TMSE-rhodacyclopentadiene. These bathochromic shifts are due to the increase in the conjugation lengths of the extended phenylene-ethynylene moieties that consequently reduces the HOMO-LUMO gap, which is assumed to dominate the transition (**Figure 3.5**).

A smaller energy gap between the HOMO and LUMO can increase the Frank-Condon factors because of increasing overlap between the ground and excited states, leading to more effective IC processes. Thus, the Φ values of both **6(a)** and **6(b)** are lower than the simple TMSE-rhodacyclopentadienes.

The extinction coefficient values (ε) of both **6(a)** and **6(b)** are greater than those of the simple TMSE-rhodacyclopentadienes. This is consistent with the result of Ward,[8] who found that the extended bis(arylethynyl)diarylbutadiynes themselves have greater ε values than the shorter butadiyne analogues (see the **Introduction** section in **Chapter 2**).

Neither **6(a)** nor **6(b)** shows any liquid crystal phases when they were analysed by a transmission polarised light microscope, fitted with a temperature-controlled hot-stage. The melting points of **6(a)** and **6(b)** are 102 – 104 and 112 – 113 °C, respectively. Both compounds melted directly into isotropic liquids. One possible reason for the lack of liquid crystal phases in both compounds may be that the alkyl chains are not sufficiently long.

3.2.5 Second-generation TMSE-rhodacyclopentadienes

The preliminary results of DFT calculations (**Figure 3.5**) show that the two phenyl rings at the 3- and 4-positions of the rhodacycle ring are not involved in the frontier orbitals; indeed, they are suspected to act as luminescence quenchers because both rings can rotate and lead to loss of excitation energy. Therefore, second-generation rhodacyclopentadienes with a more rigid structure have been designed by attaching a cyclohexyl loop at the 3- and 4-positions of the rhodacycle ring in order to eliminate the quenching possibilities from the two phenyl rings at these two positions.

3.2.5.1 Synthesis and characterisation

The synthesis of the second-generation TMSE-rhodacyclopentadienes (**Figure 3.25**) is similar to the synthesis of the first-generation TMSE-rhodacyclopentadienes.[8] The only difference is the use of 1,12-(*p*-R-phenyl)dodeca-1,3,9,11-tetraynes, the syntheses of which have been discussed in **Chapter 2**, rather than using 1,4-di(*p*-R-phenyl)buta-1,3-diynes.

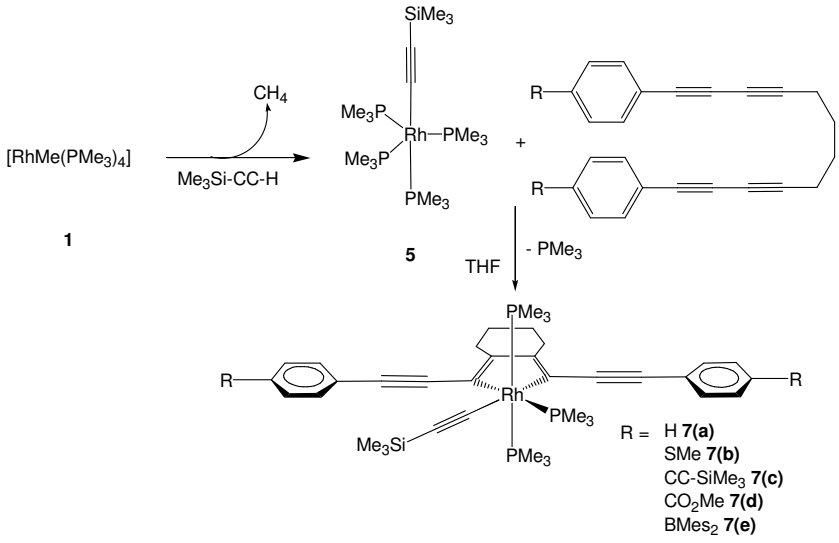

Figure 3.25: Synthetic route to the second-generation TMSE-rhodacyclopentadienes.

One equivalent of the appropriate 1,12-(*p*-R-phenyl)dodeca-1,3,9,11-tetrayne was added to the [Rh(C≡C-SiMe$_3$)(PMe$_3$)$_4$] in THF solution and the reactions were stirred at room temperature for 15 h to give the respective second-generation TMSE-rhodacyclopentadienes [R = H, **7(a)**; R = SMe, **7(b)**; R = C≡C-SiMe$_3$, **7(c)**; R = CO$_2$Me, **7(d)**; R = BMes$_2$ (Mes = mesityl), **7(e)**]. As the reaction progressed, the solvent was repeatedly removed *in vacuo* and the flask was refilled with fresh THF in order to remove the dissociated PMe$_3$. The solution colour changed from yellow to yellow-brown, with strong yellow-green luminescence observed for **7(a)**. Upon completion, the ^{31}P{^{1}H} NMR spectra were similar to those shown in **Figure 3.17**. As expected, the J_{Rh-P} value of the doublets of doublets is ca. 90 Hz and for the doublets of triplets is ca. 83 Hz. In their ^{1}H NMR spectra [e.g. **7(d)** in **Figure 3.26**], two additional multiplets appear at 2.85 and 1.62 ppm, indicating the presence of the -CH$_2$-CH$_2$- moiety from the cyclohexyl ring.

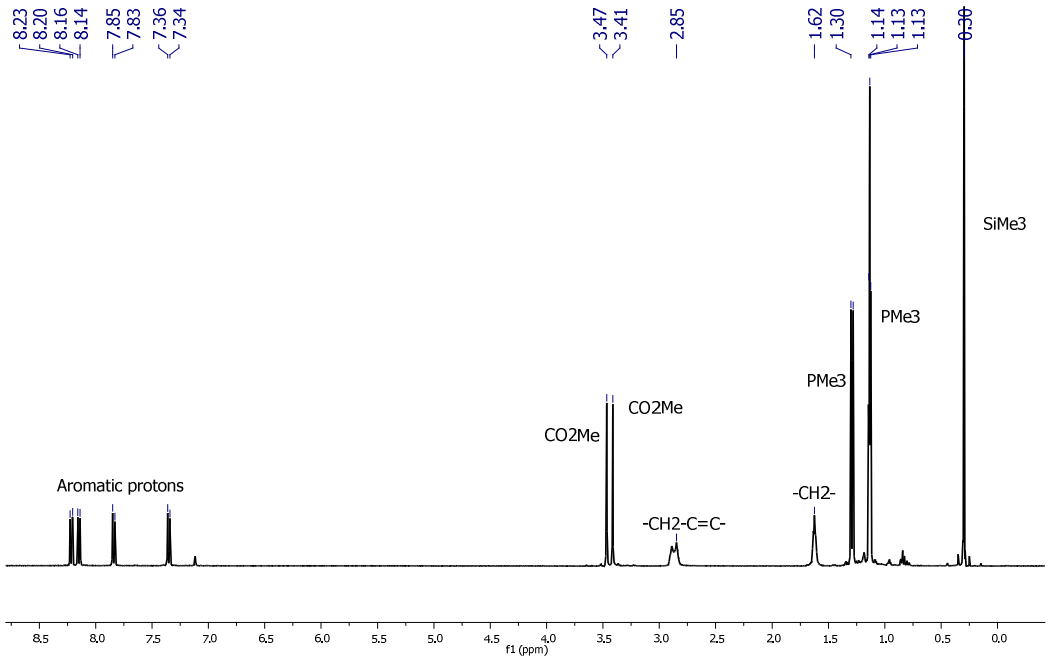

Figure 3.26: ^{1}H NMR spectrum (400 MHz, C$_6$D$_6$) of **7(d)**.

Two different proton environments are observed for the CO_2Me groups. This is due to the fact that two different ligands, C≡C-$SiMe_3$ and PMe_3, are located in the equatorial plane of rhodacyclopentadiene. For the same reason, there are also two sets of signal for aromatic protons in the spectrum, which represent the presence of two different phenyl ring environments in the rhodacyclopentadiene.

TMSE-rhodacyclopentadiene **7(f)** [R = C≡CH] was synthesised from **7(c)** by deprotecting the *para*-substituted trimethylsilyl (TMS) groups on the phenyl rings (**Figure 3.27**). Compound **7(c)** was stirred with four equivalents of nBu_4NF (TBAF, 1M solution in THF) in degassed THF at room temperature for 15 h. Once the reaction was complete, the solvent was removed *in vacuo*, and the residual solid was dissolved in CH_2Cl_2 and then washed with water, in order to remove the TBAF. Interestingly, the TMS group of the TMSE ligand was not affected by the deprotection conditions. The growth of single crystals of the compound was attempted via slow diffusion of a layer of hexane into a concentrated solution in degassed THF. Unfortunately, a black solid was found at the bottom of the vial, indicating that some decomposition during the recrystallisation attempt. However, re-dissolving in C_6D_6 and subsequent filtration allowed the recovery of a sample which was pure by $^{31}P\{^1H\}$ NMR and elemental analysis.

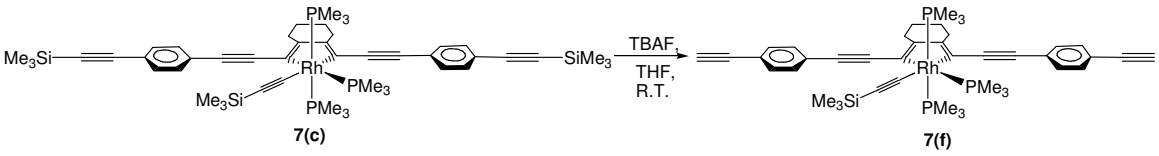

Figure 3.27: Deprotection of the TMS groups at the *para*-positions of the phenyl rings.

3.2.5.2 Crystallographic data for 7(a), 7(b) and 7(d)

The crystallographic data for **7(a), 7(b)** and **7(d)** are listed in **Table 3.7**. Molecular structures of **7(a)**, **7(b)** and **7(d)** were obtained from single-crystal X-ray diffraction data.

Table 3.7: Crystallographic data for **7(a)**, **7(b)** and **7(d)**.

Compound	**7(a)**	**7(b)**	**7(d)**
Empirical formula	$C_{38}H_{54}P_3RhSi$	$C_{40}H_{58}P_3RhS_2Si$	$C_{42}H_{58}O_4P_3RhSi{\cdot}C_6H_{14}$
Formula weight	734.72	826.89	936.97
Temperature (K)	120(2)	120(2)	120(2)
Crystal system	Monoclinic	Triclinic	Monoclinic
Space group	$P2_1/c$	$P\bar{1}$	$P2_1/c$
a (Å)	9.1905(9)	10.404(1)	9.513(3)
b (Å)	27.141(3)	11.562(1)	18.154(6)
c (Å)	15.4133(16)	20.121(2)	28.872(8)
α (º)	90.00	76.48(2)	90.00
β (º)	94.39(1)	89.22(2)	95.16(2)
γ (º)	90.00	64.46(2)	90.00
Volume ($Å^3$)	3833.5(7)	2112.6(4)	4966(3)
Z	4	2	4
Density (calculated) (Mg/m^3)	1.273	1.300	1.253
Absorption coefficient (mm^{-1})	0.626	0.671	0.50
Crystal size (mm^3)	0.29 x 0.18 x 0.16	0.40 x 0.20 x 0.06	0.25 x 0.10 x 0.05
Θ range for data collection (º)	2.61 to 29.98	2.18 to 29.97	2.24 to 29.62
Reflections collected	39036	30305	43458
Independent reflections	10880	11813	8743
Data / Restraints / Parameters	10880 / 0 / 412	11813 / 0 / 452	8743 / 0 / 532
Final R indices [I>2σ (I)]	$R1 = 0.0316$ $wR2 = 0.0665$	$R1 = 0.0291$ $wR2 = 0.0678$	$R1 = 0.0907$ $wR2 = 0.1599$
R indices (all data)	$R1 = 0.0436$ $wR2 = 0.0701$	$R1 = 0.0378$ $wR2 = 0.0713$	$R1 = 0.1115$ $wR2 = 0.1656$

Orange monoclinic (space group $P2_1/c$) single crystals of **7(a)** formed in a 5 mm diameter glass tube by slow diffusion of a layer of hexane into a concentrated C_6D_6 solution. The molecular structure of **7(a)** is shown in **Figure 3.28**, and selected bond lengths and angles are listed in **Table 3.8**.

Table 3.8: List of selected bond lengths (Å) and angles (°) for **7(a)**, **7(b)** and **7(d)**.

	7(a)	**7(b)**	**7(d)**
Rh-P1	2.3153(5)	2.3163(7)	Disorder
Rh-P2	2.3160(5)	2.3111(7)	Disorder
Rh-P3	2.3606(5)	2.3608(5)	Disorder
Rh-C1	2.0479(18)	2.0458(19)	Disorder
Rh-C15	2.0806(17)	2.0857(16)	Disorder
Rh-C18	2.0993(17)	2.1010(18)	Disorder
C1≡C2	1.218(2)	1.210(2)	1.207(9)
C19≡C20	1.206(2)	1.208(2)	1.203(9)
C31≡C32	1.205(3)	1.207(2)	1.217(8)
C15=C16	1.365(2)	1.368(2)	1.371(9)
C17=C18	1.374(2)	1.371(2)	1.360(10)
C16-C17	1.447(2)	1.447(2)	1.429(8)
C16-C27	1.516(2)	1.515(2)	1.494(10)
C27-C28	1.523(3)	1.523(3)	1.504(12)
C28-C29	1.526(3)	1.523(3)	1.526(10)
C29-C30	1.521(3)	1.524(2)	1.509(11)
C17-C30	1.514(2)	1.508(2)	1.508(10)
P1-Rh-P2	169.571(18)	170.535(16)	Disorder
C1-Rh-C18	173.81(7)	173.47(6)	Disorder
P3-Rh-C15	173.00(5)	172.85(5)	Disorder

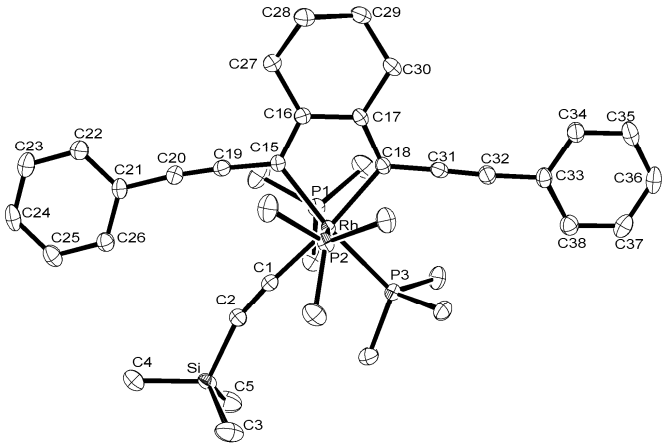

Figure 3.28: Molecular structure of **7(a)**, the hydrogen atoms are omitted for clarity (thermal ellipsoids drawn at 50% probability).

Compound **7(b)** was recrystallised via slow vapour diffusion of hexane into a concentrated solution of **7(b)** in degassed THF. Orange crystals grew at the bottom of the vial overnight. They crystallised in the triclinic space group $P\bar{1}$. The molecular structure of **7(b)** is shown in **Figure 3.29**, and selected bond lengths and angles are listed in **Table 3.8**.

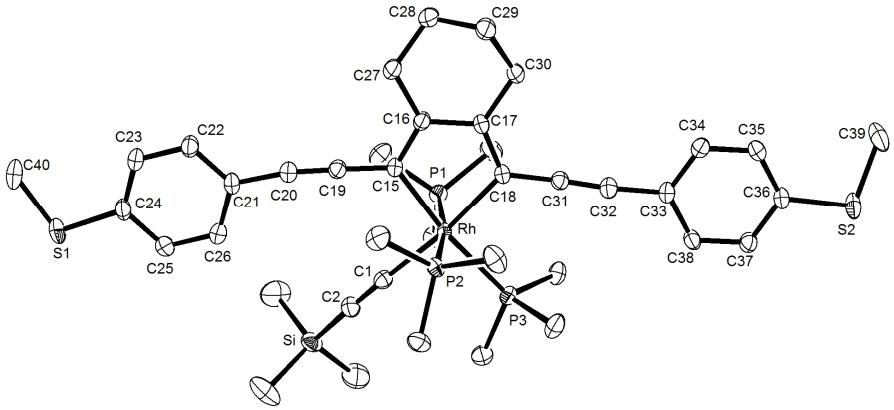

Figure 3.29: Molecular structure of **7(b)**, the hydrogen atoms are omitted for clarity (thermal ellipsoids drawn at 50% probability).

Compound **7(d)** was recrystallised by slow vapour diffusion of hexane into a concentrated solution of **7(d)** in degassed THF. Red crystals of **7(d)** grew in the vial at room temperature overnight. The molecular structure of **7(d)** is shown in **Figure 3.30** and selected bond lengths are listed in **Table 3.8**. An *n*-hexane molecule of crystallisation is disordered between two positions partially overlapping with one another. One of the CO_2Me groups was found to be disordered between two opposite orientations. In addition, the Rh centre is also disordered giving alternative positions for Rh, P1, P3, C6, C7, C12, C13 and C14 with their attached hydrogens. The occupancies were refined to 0.434(5) for the minor component and 0.566(5) for the major component.

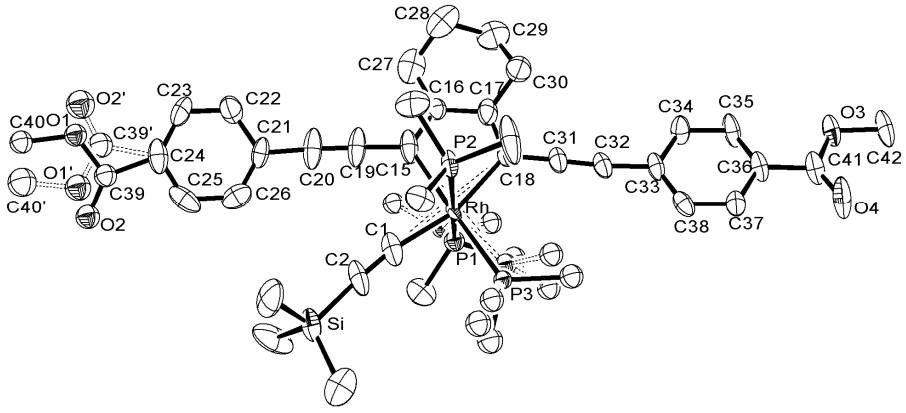

Figure 3.30: Molecular structure of **7(d)**. Thermal ellipsoids are drawn at the 50% probability level (hydrogen atoms and the *n*-hexane molecule are omitted for clarity).

In general, the bond lengths of Rh-C1 [2.0458(19) - 2.0479(18) Å] are slightly shorter than Rh-C15 [2.0806(17) – 2.0857(16) Å] and Rh-C18 [2.0993(17) – 2.1010(18) Å], which is due the fact that C1 is sp-hybridised, whereas C15 and C18 are sp^2-hybridised. The C≡C bond lengths of the TMSE ligands [C1-C2, 1.207(9) – 1.218(2) Å] are similar to the C≡C bond lengths at the 2- and 5-positions of the rhodacycles [1.203(9) – 1.208(2)

and 1.205(3) – 1.217(8) Å]. Comparing the bond lengths of Rh-C15 to Rh-C18, the latter are ca. 0.02 Å longer, which indicates that the TMSE ligand has a slightly stronger *trans*-influence than PMe_3. The Rh-P1 and Rh-P2 bond lengths are almost the same [2.3153(5) – 2.3163(7) and 2.3160(5) – 2.3111(7) Å, respectively]. However, the Rh-P3 bond lengths are longer than the Rh-P1 and Rh-P2 bond lengths [2.3606(5) – 2.3608(5) Å], which is in agreement with the Rh-P coupling constants observed by $^{31}P\{^{1}H\}$ NMR spectroscopy. Thus, the coupling constants for the doublets of doublets for P1 and P2 ($J_{Rh\text{-}P}$ = 98 – 99 Hz) are always greater than for the doublets of triplets for P3 ($J_{Rh\text{-}P}$ = 83 – 84 Hz). This indicates that the *trans*-influence of the α-carbon of the rhodacycle is stronger than that of a PMe_3 group. The C=C bond lengths of C15-C16 and C17-C18 are 1.365(2) – 1.371(9) and 1.374(2) – 1.360(10) Å, respectively. However, the C-C single bond lengths of C16-C17 [1.447(2) – 1.429(8) Å] are slightly shorter than the typical C-C single bond length. This is because C16 and C17 are sp^2 hybridised carbons. For similar reasons, the bond lengths of C16-C27 and C17-C30 are slightly shorter (ca. 0.012 – 0.032 Å) than the other single bonds in the cyclohexyl ring because C16 and C17 are sp^2-hybridised carbons and the others are sp^3-hybridised carbons.

3.2.5.3 Photophysical studies

The second-generation TMSE-rhodacyclopentadienes (**Table 3.9**) showed a significant increase in the Φ values compared to the first-generation TMSE-rhodacyclopentadienes (**Table 3.10**). For example, the Φ value of **7(a)** are 0.33, but its first-generation analogue (**Table 3.10**), has a Φ value of 0.15. Moreover, the second-generation TMSE-rhodacyclopentadienes with R = CO_2Me and $BMes_2$, respectively, have the highest Φ

values [Φ = 0.69 for both **7(d)** and **7(e)**] of any rhodacyclopentadiene synthesised thus far. Indeed, these values are comparable to some of the best organic fluorophores. This proves that the two phenyl rings at the 3- and 4-positions in the rhodacycle ring act as quenchers. The λ_{max} values of absorption and emission of the second-generation TMSE-rhodacyclopentadienes are also shifted to the lower energy region compared to the first-generation ones (12 nm for absorption and 24 nm for emission for the compound with R = CO_2Me). The absorption and emission spectra of **7(a) – (f)** are shown in **Figure 3.31**.

Table 3.9: Summary of the photophysical data for **7(a)** – **(f)**.

Compound	λ_{max} ABS (nm)	ε (mol^{-1} cm^{-1} dm^3)	λ_{max} EM (nm)	Stokes shift (cm^{-1})	Φ	τ (ns)
7(a), R = H	456	30000	501	2000	0.33	1.2
7(b), R = SMe	467	41000	518	2100	0.34	1.8
7(c), R = C≡CTMS	491	47000	550	2200	-*	-*
7(d), R = CO_2Me	497	44000	560	2300	0.69	3.0
7(e), R = $BMes_2$	532	48000	606	2400	0.69	2.6
7(f), R = C≡CH	484	31000	542	2200	-*	-*

Note: All of the data above (except ε) were recorded in degassed toluene solutions at room temperature. ε values were recorded in non-degassed toluene solutions.
* The Φ and τ values of **7(c)** and **7(f)** have not been recorded yet.

Table 3.10: The photophysical data for the first-generation TMSE-rhodacyclopentadienes in toluene solution at room temperature.[8]

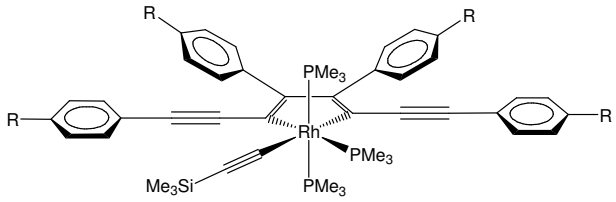

substituent	λ_{max} ABS (nm)	ε (mol^{-1} cm^{-1} dm^3)	λ_{max} EM (nm)	Stokes shift (cm^{-1})	Φ	τ (ns)
R = H	453	26000	496	1910	0.15	0.87
R = SMe	468	35000	515	1950	0.10	0.55
R = CO_2Me	485	21000	536	1960	0.16	0.98

From the results in **Table 3.9**, it can be seen that both electron donating and withdrawing substituents at the *para*-positions of the phenyl rings cause bathochromic shifts. However, electron accepting substituents have a greater influence on the bathochromic shift than electron donating ones: the stronger the electron accepting ability, the greater the bathochromic shift. Therefore, the largest Stokes shift was observed in **7(e)** because the $BMes_2$ substituent is a very strong electron accepting group. The electron accepting substituents stabilise the LUMO to a greater extent than the HOMO, whereas the electron donating substituents destabilise the HOMO to a greater extent than the LUMO. As a result, both types of substituents are able to decrease the HOMO-LUMO energy gap, as previously reported for related 2,5-bis(arylethynyl)thiophenes.[13]

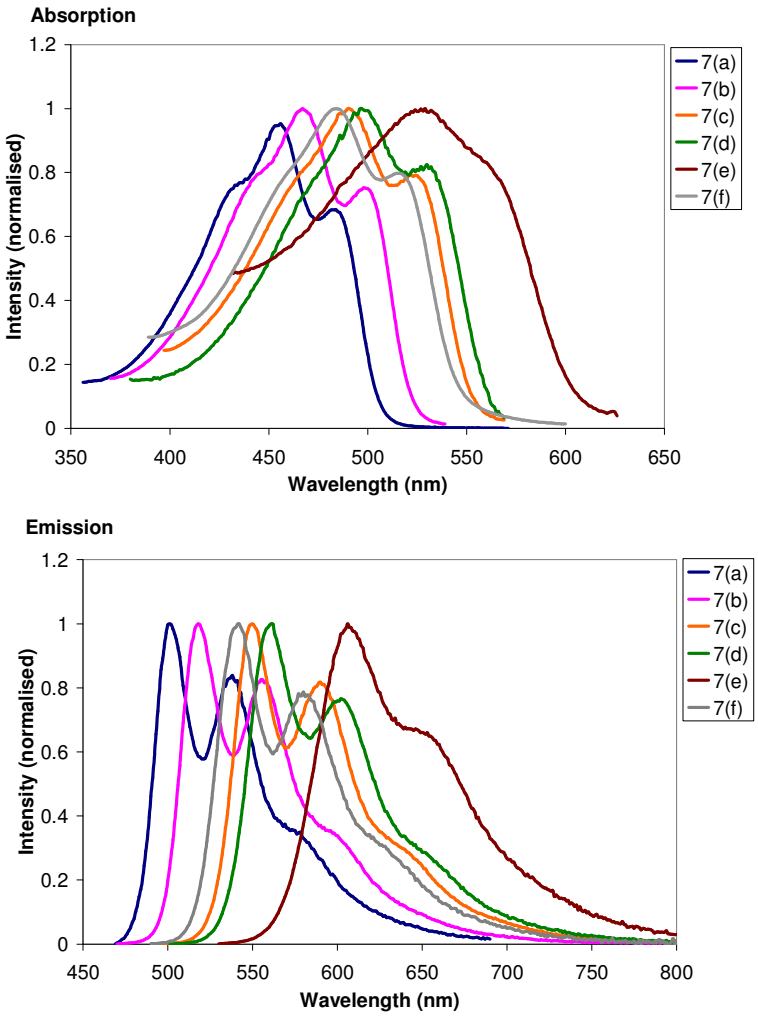

Figure 3.31: Absorption (top) and emission (bottom) spectra of **7(a)** – **(f)**.

The absorption and emission spectra of **7(a)** are shown in **Figure 3.32**. The small Stokes shifts (ca. 2000 cm^{-1}) and the nanosecond lifetimes suggest that the emission occurs from the singlet excited state. Unprecedented Φ_f values for metallacyclopentadienes of up to 0.69 have been achieved for **7(d)** and **7(e)** with lifetimes of 3.0 and 2.6 ns, respectively.

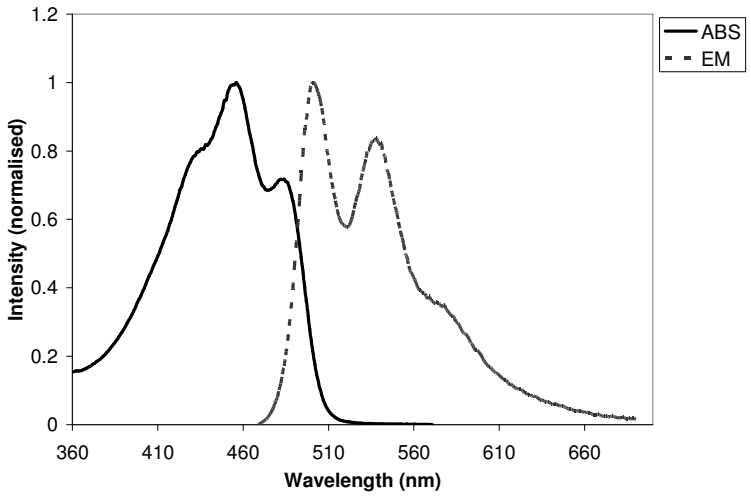

Figure 3.32: Absorption and emission spectra of **7(a)**.

Singlet oxygen sensitisation experiments[29] on **7(a)**, **7(b)** and **7(d)** have been conducted by Dr. Andreas Steffen in order to determine the quantum yields of triplet excited state generation (Φ_Δ) as shown in **Table 3.11**. For **7(a)**, the Φ_Δ value was ca. 0.65. This indicates that the singlet excited state is decaying effectively only by fluorescence and ISC to the triplet excited state, with no $S_1 \rightarrow S_0$ internal conversion (IC) [as Φ_Δ (0.65) + Φ_f (0.33) $\approx$ 1.00]. For **7(b)** and **7(d)**, the sums of $\Phi_\Delta + \Phi_f$ are less than unity (0.74 and 0.95, respectively) indicating that some IC is taking place. Nevertheless, the k_f and k_Δ values of **7(a)**, **7(b)** and **7(d)** are close to each other ($k_f \approx k_\Delta \approx 10^8$ s^{-1}), which allows fluorescence to occur to an appreciable extent in the TMSE-rhodacyclopentadienes. Although ISC to the triplet excited states was confirmed in the TMSE-rhodacyclopentadienes, no phosphorescence was observed between 400 – 1000 nm at room temperature in these rhodacyclopentadienes.

Table 3.11: The Φ_Δ, τ_0, k_f and k_Δ formation of **7(a)**, **7(b)** and **7(d)**.

Compound	Φ_Δ*	$\tau_0^{\#}$ (ns)	k_f [10^8 s^{-1}]	k_Δ [10^8 s^{-1}]
7(a)	0.65	3.6	2.75	5.42
7(b)	0.40	5.3	1.89	2.22
7(d)	0.26	4.3	2.30	0.87

*Quantum yield for $^1O_2$ formation in O_2-saturated toluene solution.
$^{\#}\tau_0$ is the natural lifetime calculated from the equation $\tau_0 = \tau_f/\Phi_f$.

A low-temperature lifetime measurement on **7(a)** was carried out by Dr. Andrew Beeby from the Department of Chemistry, Durham University. The idea behind the low-temperature experiment is to slow down all vibrational relaxation modes and non-radiative processes in an excited molecule by freezing the sample in an *iso*-pentane/Et_2O/EtOH glass at 77 K. Thus, emission (i.e. fluorescence and phosphorescence) should be the only means of the decay to the ground state, and the lifetime from low temperature experiment should be the pure natural radiative lifetime (τ_0). The calculated τ_0 value for **7(a)** is 3.6 ns, close to the experimental value (τ_f = 3.2 ns at 77 K). This means that the Φ_Δ value for **7(a)** at 77 K must be significantly less than 0.65. The fact that τ_0 occurs on the nanosecond timescale in **7(a)** confirms that only fluorescence rather than phosphorescence occurs at 77 K (within the wavelength of 400 – 1000 nm). This observation is different from other luminescent rhodium complexes; for example, at 77 K, $[Rh(bpy)_3]^{3+}$ emits at 448 nm with a lifetime of 2.2 ms in a rigid glass, whereas no emission occurs at room temperature.[24]

The fact that no phosphorescence was observed at 77 K in TMSE-rhodacyclopentadienes can be explained by two possibilities: (i) the triplet excited states are not populated at 77 K, or (ii) the lowest triplet excited (T_1) state is close in energy to

the ground state (i.e. emission occurs at $\lambda > 1000$ nm); therefore, the emission was not detected in the experiment.

Preliminary TD-DFT calculations for **7(d)** (**Figure 3.33**) by Prof. Marder show that the energy gap between S_1 and S_0 states is 2.24 eV [554 nm; recorded λ_{max} emission for **7(d)** = 560 nm], the S_1 state is only slightly below the T_2 state by ca. 0.07 eV, but above the T_1 state ca. 1.10 eV. The energy gap between T_1 and S_0 states is ca. 1.14 eV (1087 nm). Thus, ISC from S_1 to T_1 is very slow ($k_\Delta = 10^8$ s^{-1}), which may be due to the large energy gap (1.10 eV) between them. However, the S_1 state may thermally populate the T_2 state at room temperature because of the very small energy gap (0.07 eV) between them. This calculations also indicate that any possible phosphorescence would not have been observed either at room or low-temperature experiment, because emission at ca. 1100 nm would be out of the range of the wavelengths that we measured.

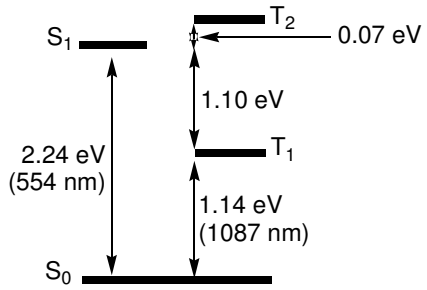

Figure 3.33: The energy levels diagram of S_0, S_1, T_1 and T_2 states of **7(d)**.

Comparing the photophysical properties of **7(a) – (f)** to those of the structurally related 2,5-bis(arylethynyl)thiophenes[13] (Φ_f = 0.2 - 0.3, τ_f = 0.2 - 0.3 ns), the rhodacyclopentadienes exhibit higher Φ_f values and longer lifetimes than the bis(arylethynyl)thiophenes despite the fact that the spin-orbit coupling (SOC) constant of Rh (1200 cm^{-1}) is more than three times higher than that of sulphur (380 cm^{-1}). In

addition, the greater λ_{max} values in both the absorption and emission spectra of **7(a) – (f)** than those of their thiophene- based analogues clearly indicate that the Rh centre is participating in the transitions. This strongly implies that the effectiveness of SOC from the Rh in the ISC from the S_1 to T_1 state is less than that in most luminescent organometallic complexes. Therefore, the fluorescence rate is competitive to the ISC rate ($k_f \approx k_\Delta \approx 10^8$ s^{-1}). It is generally thought that the SOC constant from the metal centre is the main factor which facilitates the ISC ($S_1 \rightarrow T_1$ state) in organometallic complexes: the greater the SOC, the more efficient the ISC is. However, in the case of rhodacyclopentadienes, despite the fact that the Rh has a large SOC coefficient, **7(a)**, **7(b)**, **7(d)** and **7(e)** are still able to exhibit high-intensity fluorescent emissions with nanosecond lifetimes. This brings us to another issue, i.e., how effective the SOC of the Rh is in influencing the ISC from the S_1 to the T_1 state, or, in other words, how much the Rh-centre participates in the excited states.

The emission solvatochromism for **7(e)** (**Figure 3.34**) implies significant charge transfer (CT) in the excited state. In polar solvents (e.g. MeCN), the emission λ_{max} values are shifted to lower energy than in less polar solvents. In addition, the structureless emission spectrum shows that there is a significant interaction between the excited **7(e)** molecules and the polar solvent molecules. As a result, the emission from **7(e)** is quenched by Coulombic interactions in polar solvents.

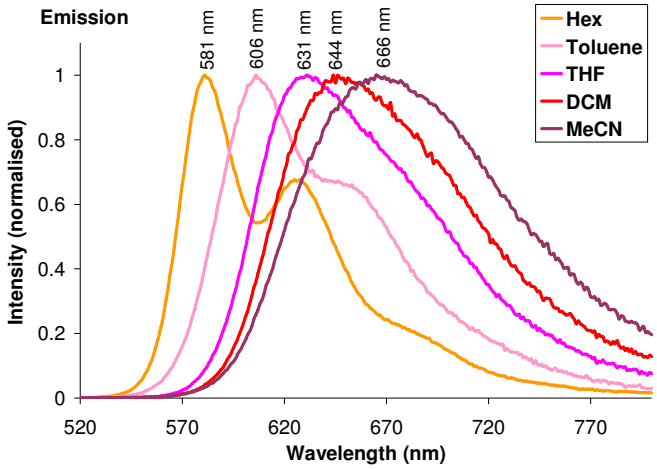

Figure 3.34: Emission solvatochromism spectra of **7(e)**.

In collaboration with Prof. Michael George from the School of Chemistry at the University of Nottingham, time-resolved infrared (TRIR) absorption measurements have been carried out for **7(a)** in DCM in order to obtain additional information about the excited states. In TRIR experiments, a strong IR-active band (e.g. ester C=O, C≡N or C≡C) is selected for observation at several time intervals in the range of 11 – 3000 ps after the molecule has been excited. In **7(a)**, a particular IR band (2128 cm^{-1}), which belongs to a C≡C stretch of the alkynyl moieties at the 2- and 5-positions of the rhodacycle ring, was investigated. The changes in intensity vs. time, on the picosecond (ps) timescale, over which the molecule was excited and then decayed to the ground state, were recorded in different TRIR spectra (**Figure 3.35**). After 10 ps, the TRIR spectrum shows that the band at 2128 cm^{-1} was bleached, and another band at 2008 cm^{-1}, which is putatively assigned to the S_1 state, was observed. This band decays at the same rate [τ = 1.6 (± 0.6) ns] as a new IR band at 1941 cm^{-1} appears, which is believed to arise from the T_1 state. The decay rate is in close agreement with the fluorescence lifetime of **7(a)** in

Table 3.9, which is about 1.2 ns. Moreover, the IR frequency is reduced from 2128 to 1941 cm^{-1} which indicates decreasing C≡C triple bond character in the putative triplet excited state.

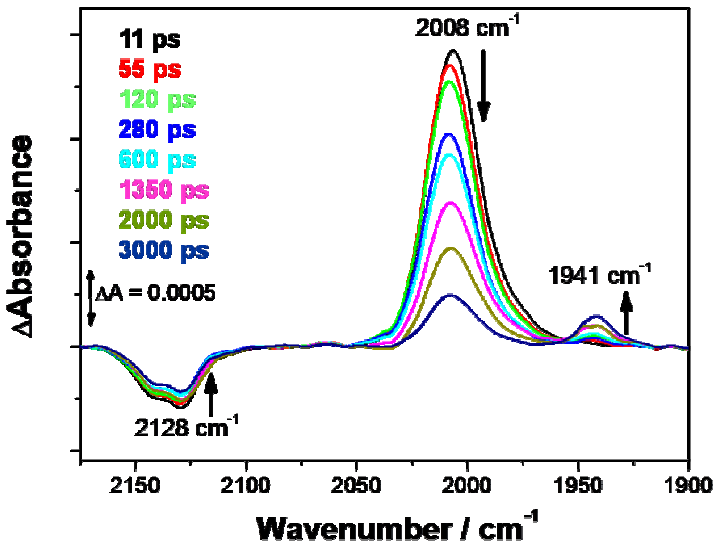

Figure 3.35: Pico-second (ps)-TRIR spectra of **7(a)**.

Based on the results presented in **Figures 3.35** and **3.36**, it can be surmised that about 35% of the ground state is reformed at the same rate as the S_1 state decays, and another 65% is formed from the decay of a state postulated to be a T_1 state. This is consistent with the result from the singlet oxygen sensitisation experiment in **Table 3.11**, which stated that the Φ_Δ for **7(a)** is 65%.

The state associated with the band at 1941 cm^{-1} (believed to be the T_1 state) decays to the ground state with τ = 55 ns in a concentrated degassed solution (10^{-3} M). The short lifetime of the T_1 state lifetime is probably due to a small energy gap between the triplet excited state and the ground state, facilitating a non-radiative process.

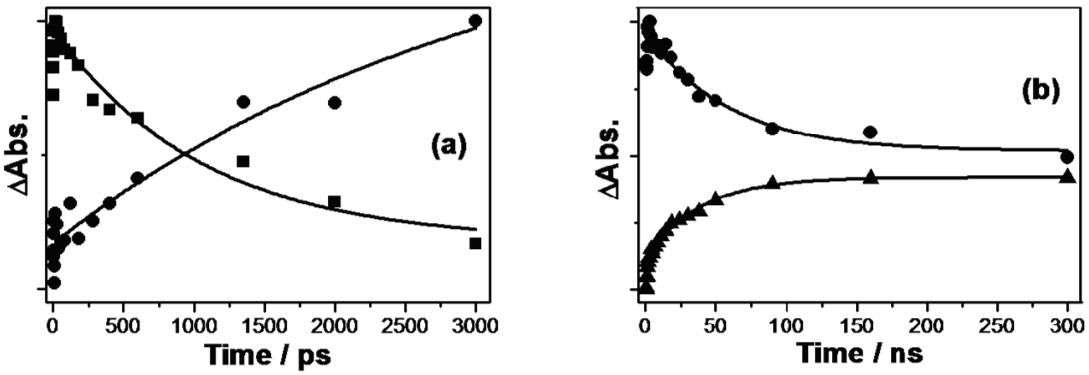

Figure 3.36: Kinetic traces: **(a)** the decay of the S_1 state at 2008 cm^{-1} (■) and the growth of the T_1 state at 1941 cm^{-1} (•); **(b)** the decay of T_1 state at 1941 cm^{-1} (•) and the recovery of the ground state bleach at 2128 cm^{-1} (▲).

3.2.6 Second-generation Me-rhodacyclopentadienes

3.2.6.1 Synthesis and characterisation

The second-generation of TMSE-rhodacyclopentadienes has proved that the removal of the two phenyl rings at the 3- and 4-positions of the rhodacycle ring significantly increases the Φ values of the rhodacyclopentadienes. In addition, the singlet oxygen sensitisation experiment results from **Table 3.1** (for the first-generation TMSE- and Me-rhodacyclopentadienes) also show that strong σ-donors such as Me- ligand tend to have higher Φ_Δ values compared to TMSE- ones. This may be due to the increase in metal contribution to the frontier orbitals, which could impact on k_Δ. In order to investigate further the function of the in-plane donor ligand set, second-generation Me-rhodacyclopentadienes have been synthesised.

The synthesis of Me-rhodacyclopentadienes (**Figure 3.37**) is much easier than for the TMSE-rhodacyclopentadienes. One equivalent of the appropriate 1,3,9,11-dodecatetrayne in degassed THF solution was added to the [RhMe(PMe_3)$_4$] solution, and the reaction was stirred for 4 – 15 h at room temperature to obtain the Me-rhodacyclopentadienes [R = H, **8(a)**; R = SMe, **8(b)**; R = CO_2Me, **8(c)**].

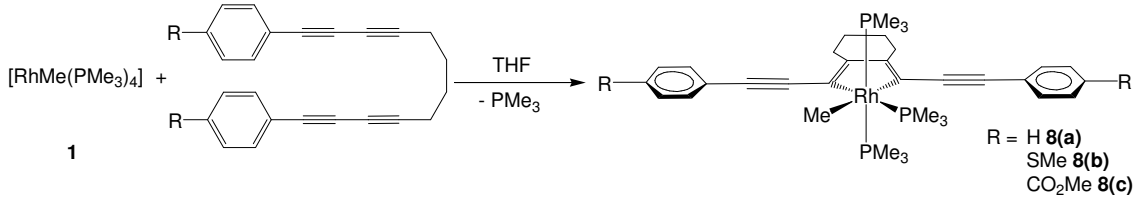

Figure 3.37: Synthetic route to the second-generation Me-rhodacyclopentadienes.

Upon completion of the reactions, the $^{31}P\{^1H\}$ NMR spectra of the Me rhodacyclopentadienes were found to be similar to those shown in **Figure 3.17**. As expected, the $J_{Rh\text{-}P}$ values for the doublets of doublets are ca. 106 Hz, and for the doublets of triplets are ca. 90 Hz, which are slightly higher than those of the DHAPEPE- and TMSE-rhodacyclopentadienes, showing a higher electron density at the Rh centre due to the strong σ-donor nature of the Me- ligand. The ^1H NMR spectrum of **8(c)** (**Figure 3.38**) shows the appearance of an approximate doublet of quartets at -0.08 ppm ($^2J_{Rh\text{-}H}$ = 2 Hz, $^3J_{P\text{-}H}$ = 7 Hz), which indicates that the Me- group is present on the Rh. In addition, the two multiplets at 2.95 and 1.69 ppm indicate the presence of the -CH_2-CH_2- moiety from the cyclohexyl loop.

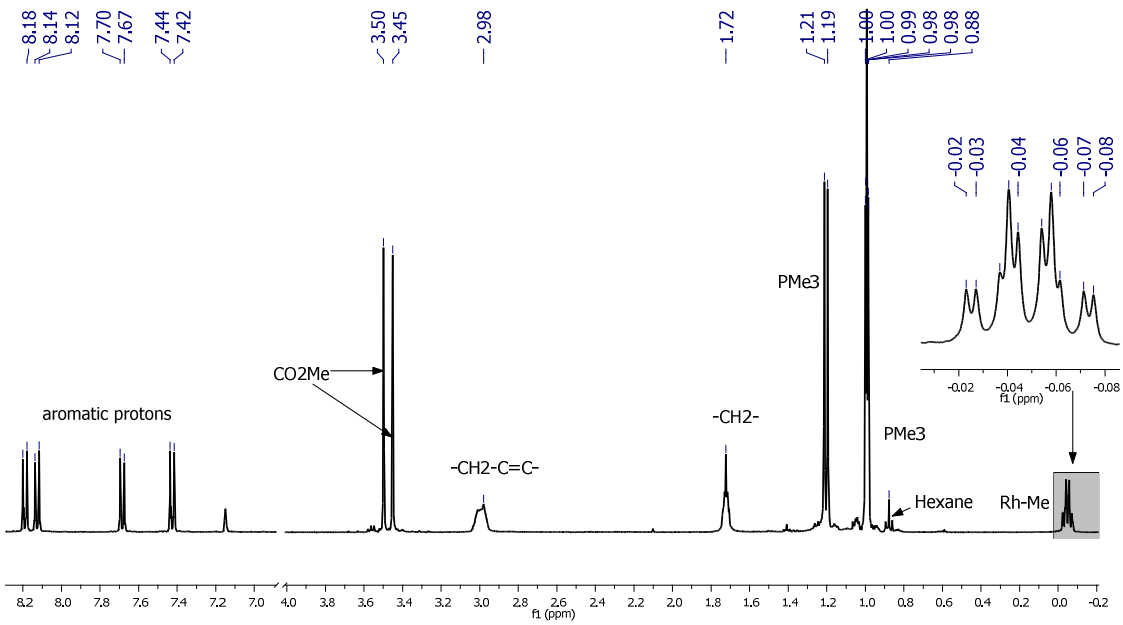

Figure 3.38: ^{1}H NMR (400 MHz, C_6D_6) spectrum of **8(c)**.

3.2.6.2 Photophysical studies

A summary of the photophysical data for **8(a)** – **(c)** is shown in **Table 3.12**. Unlike the TMSE-rhodacyclopentadienes, the second-generation Me-rhodacyclopentadienes appear to exhibit very weak emission, but no quantum yields have yet been measured (**Figure 3.39**). These results are similar to the first-generation Me-rhodacyclopentadienes, for which the Φ_f values are only about 0.003 for the compounds where the *para*-substituents at the phenyl rings are H and CO_2Me (**Table 3.1**). Weak emission from the Me-rhodacyclopentadienes is due to effective IC processes taking place in the excited states or the singlet excited states undergoing ISC to triplet excited states, or both.

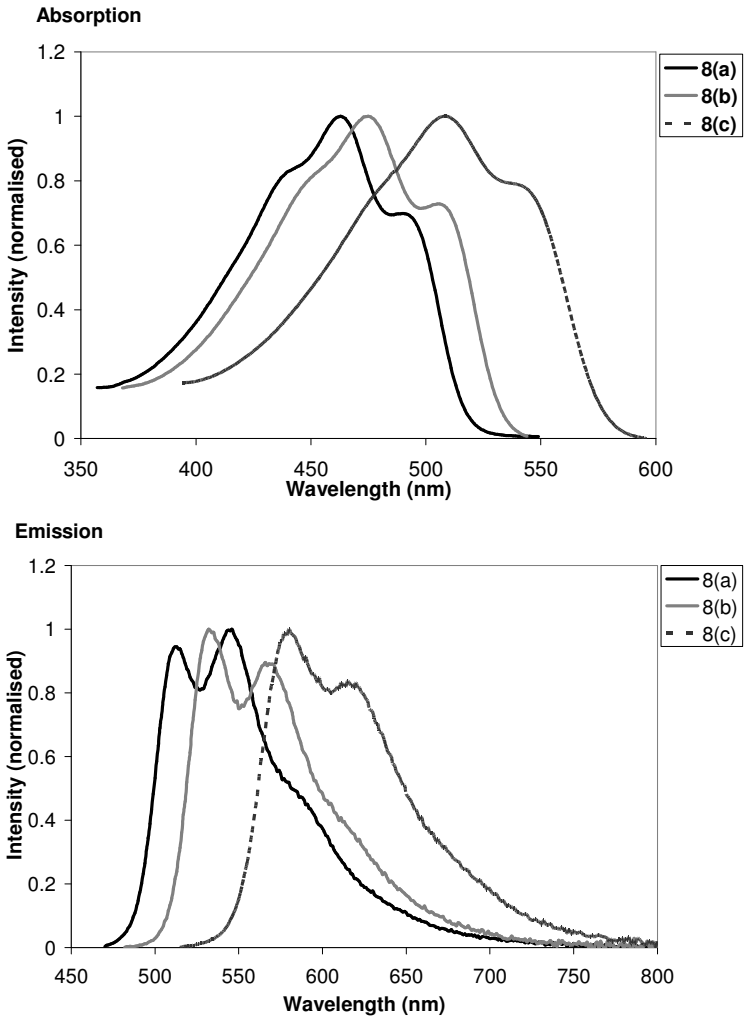

Figure 3.39: Absorption (top) and emission (bottom) spectra of **8(a) – (c)**.

Table 3.12: Summary of the photophysical data of **8(a) – (c)**.

Compound	λ_{max} ABS (nm)	ε (mol^{-1} cm^{-1} dm^3)	λ_{max} EM (nm)	Stokes shift (cm^{-1})
8(a), R = H	463	34000	512	2100
8(b), R = SMe	475	39000	532	2300
8(c), R = CO_2Me	509	27000	580	2400

Note: All of the data above (except ε) were obtained in degassed toluene solution at room temperature. ε values were recorded in non-degassed toluene solutions.

Comparing their absorption and emission spectra to those of the TMSE-rhodacyclopentadienes, the λ_{max} values of absorption and emission of the Me-rhodacyclopentadienes are slightly shifted to the lower energy region by 10 - 12 nm, supporting the fact that the Me ligand is a stronger electron donating group than the acetylide ligand. This also indicates that the Rh centre is involved in the transitions, because changing the ligand can influence the λ_{max} values in both absorption and emission. However, the small Stokes shift (ca. 2400 cm^{-1}) indicates that the emissions originate from S_1 states.

3.2.7 Discovery of *trans*-[bis(trimethylphosphine)-μ-η^2-succinato-2,5-bis(*p*-*N*,*N*-dimethylaminophenylethynyl)-3,4-(*p*-*N*,*N*-dimethylaminophenyl)rhodacyclo-penta-2,4-diene] dimer [9(b)]

3.2.7.1 Synthesis and characterisation

Compound **9(b)** was discovered by accident in the process of synthesising **4**. When preparing **4**, the reaction needs to be heated at 50 °C in a Young's tube in order to complete the reaction in a reasonable time period. We suspected that a small amount of succinic acid, presumably formed by hydrolysis of NBS used in a previous reaction, was present in the Young's tube, which reacted with **4** at 50 °C to form **9(b)**. During the recrystallisation process, undertaken with the aim of obtaining crystals of **4**, compound **9(b)** crystallised and was analysed by X-ray diffraction; thus, this compound was discovered. The intentional formation of **9(b)** was investigated by adding one equivalent of succinic acid to a toluene solution of **4** and monitoring the progress of the reaction by

$^{31}P\{^{1}H\}$ NMR spectroscopy (**Figure 3.40**). After stirring for 15 h at room temperature and then removal of the solvent, a doublet of doublets at -8.63 ppm (J_{Rh-P} = 108 Hz, J_{P-P} = 31 Hz) and a doublet of triplets at -20.74 ppm (J_{Rh-P} = 89 Hz, J_{P-P} = 31 Hz) were observed to be the major peaks in an NMR spectrum in C_6D_6. These were assigned to an η^1-succinato-rhodacyclopentadiene dimer, **9(a)**. Small peaks were also observed for **4** and **9(b)**, a doublet at -1.23 ppm (J_{Rh-P} = 117 Hz) being assigned to the latter.

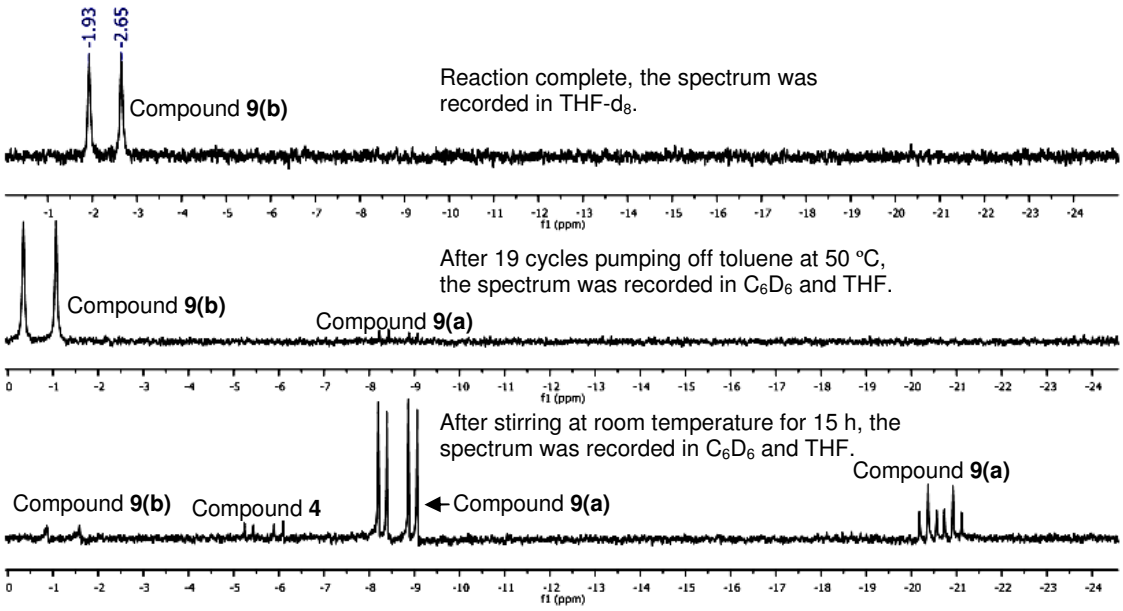

Figure 3.40: $^{31}P\{^{1}H\}$ NMR (162 MHz) spectra of the conversion of **9(a)** to **9(b)**.

The reaction was driven to form the η^2-succinato complex **9(b)** by heating at 50 °C for 15 minutes, followed by removal of the volatiles (solvent and dissociated PMe_3) and refilling with the fresh solvent. This process was repeated ca. 20 times until all of the **9(a)** was converted to **9(b)**.

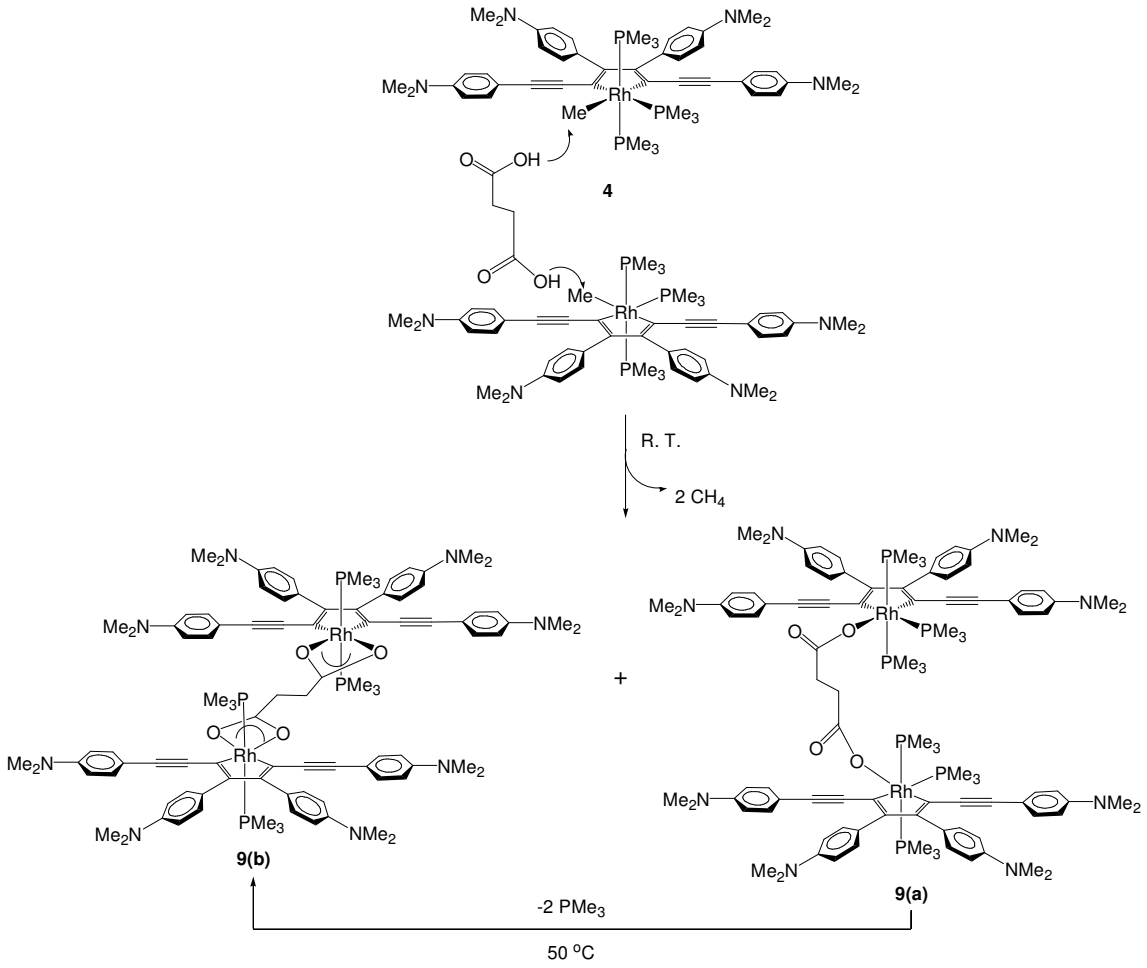

Figure 3.41: Formation of **9(b)** from **4** and succinic acid.

The doublet in the top spectrum in **Figure 3.40** is slightly shifted to -2.29 ppm compared to the ones below; the lower spectra were recorded in a mixture of C_6D_6 and THF, whereas the upper spectrum is in pure THF-d_8 in which **9(b)** is more soluble. It is worth noting that chlorinated solvents such as chloroform ($CHCl_3$) can lead to the decomposition of both **9(a)** and **9(b)**. This problem was noticed when the reaction was monitored using $^{31}P\{^1H\}$ NMR spectroscopy in $CDCl_3$.

An ESI$^+$ mass spectrum of **9(b)** shows signals at m/z = 890 and 904, which are assigned to $[M + 2H]^{2+}$ and $[M^+/2 + CH_2]$, respectively. The m/z = 890 peak is probably due to doubly protonated and charged **9(b)**, and therefore, appears at M/2.

3.2.7.2 Crystallographic data for 9(b)

The crystallographic data for **9(b)** are listed in **Table 3.13**. Crystals of **9(b)** were grown in a 5 mm diameter glass tube by slow diffusion of a layer of hexane into a C_6D_6 solution.

Compound **9(b)** crystallised in the triclinic space group $P\bar{1}$ and its molecular structure is shown in **Figure 3.42**.

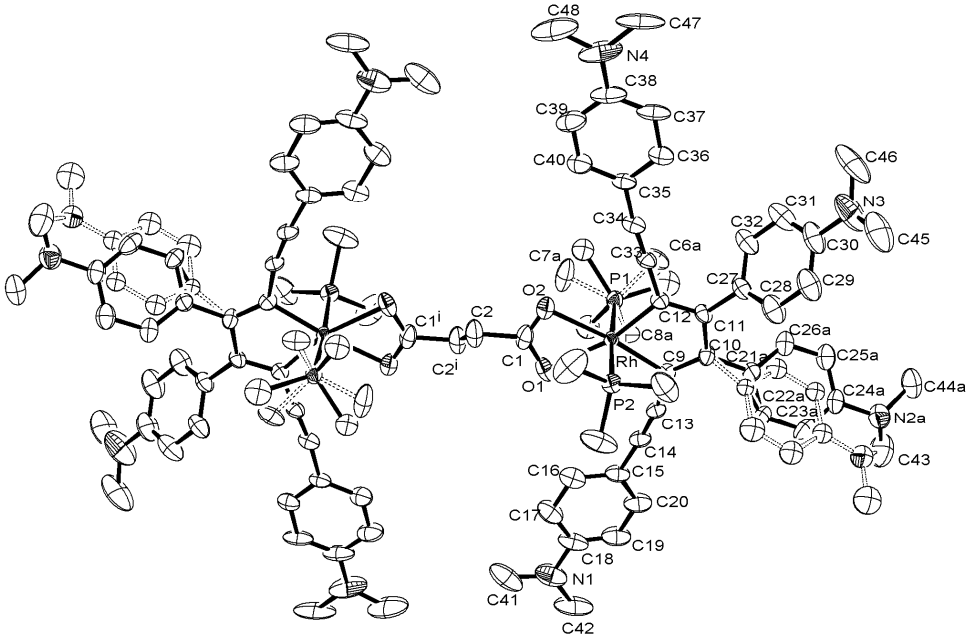

Figure 3.42: Molecular structure of **9(b)** with thermal ellipsoids plotted at 50% probability (hydrogen atoms and C_6D_6 molecules are omitted for clarity).

Table 3.13: Crystallographic data for **9(b)**.

Compound	**9(b)**
Empirical formula	$C_{96}H_{120}N_8O_4P_4Rh_2 \cdot 3(C_6D_6)$
Formula weight	2014.02
Temperature (K)	120(2)
Crystal system	Triclinic
Space group	$P\bar{1}$
a (Å)	9.5957(7)
b (Å)	12.7868(9)
c (Å)	22.5429(16)
α (º)	88.381(11)
β (º)	79.043(10)
γ (º)	82.887(10)
Volume (Å^3)	2694.6(3)
Z	1
Density (calculated) (Mg/m^3)	1.241
Absorption coefficient (mm^{-1})	0.419
Crystal size (mm^3)	0.29 x 0.07 x 0.04
Θ range for data collection (º)	2.45 to 24.99
Reflection collected	21250
Independent reflections	9505
Data / Restraints / Parameters	9505 / 6 / 647
Final R indices [I>2σ(I)]	$R1 = 0.0750$ $wR2 = 0.1566$
R indices (all data)	$R1 = 0.1178$ $wR2 = 0.1752$

The centres of the molecules in **9(b)** are co-incident with crystallographic inversion centres. The Rh-O1 and Rh-O2 bond lengths are 2.300(4) and 2.233(4) Å, respectively (which is significantly different but probably due to crystal packing forces), whereas the Rh-C9 and Rh-C12 bond lengths are 2.011(6) and 1.979(6) Å. The C1-C2 and C2-C2^i bond lengths of are 1.519(9) and 1.478(14) Å, respectively. The O1-Rh-O2 bond angle is 57.64(17)°, which is relatively close to related bond angles that were reported in the

literature (60.2(1)° for [Rh(η^2-O_2CMe)(P*i*Pr$_3$)$_2$], 58.9(3)° for [RhCp*(η^1-O_2CPh)(η^2-O_2CPh)] and 58.5(2)° for [Rh(η^2-O_2CMe)(ppy)$_2$]).[30-32] The C-C≡C-C moiety at C9 is more distorted from linearity than the one at C12 by comparison of the bond angle of C9-C13-C14 [168.8(7)°] to that of C12-C33-C34 [176.7(7)°]. The P1Me$_3$ ligand is rotationally disordered: C6, C7 and C8 with attached hydrogens are distributed between positions **a** and **b** in a 2:1 ratio. In addition, the dimethylaminophenyl group at C10 is disordered between positions **a** and **b** in a 4:1 ratio.

3.2.7.3 Photophysical studies

Photophysical data for **9(b)** are presented in **Table 3.14**, whereas absorption and emission spectra are shown in **Figure 3.43**. Compound **9(b)** is barely soluble in toluene, benzene and THF; however, chlorinated solvents, such as $CHCl_3$, can lead to its decomposition. For these reasons, its extinction coefficient was not measured.

Table 3.14: Summary of the photophysical data of **9(b)**.

λ_{max} ABS (nm)	ε (mol^{-1} cm^{-1} dm^3)	λ_{max} EM (nm)	Stokes shift (cm^{-1})
486	-	578	3300

Note: The absorption and emission spectra were measured in degassed toluene at room temperature.
- No data was recorded due to the poor solubility of **9(b)** in toluene, benzene and THF.

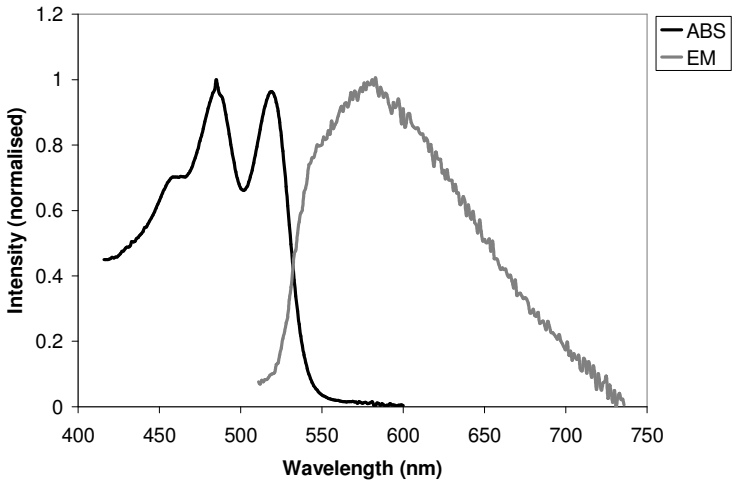

Figure 3.43: Absorption and emission spectra of **9(b)** in toluene.

The λ_{max} values for absorption and emission of **9(b)** show bathochromic shifts compared to **4** (12 nm in absorption and 55 nm in emission). Indeed, the emission from **9(b)** is very weak with a broad signal at λ_{max} = 578 nm. There are no differences in the emission spectra between degassed and non-degassed solutions at room temperature, which indicates that the emission at room temperature does not originate from the triplet excited states. The weak emission is possibly due to the π-donor succinato ligand destabilises the Rh d-orbitals in **9(b)**, facilitating a metal-centred (MC) transition, which is a well-known non-radiative transition. However, this is purely speculative at present.

3.2.8 Benzoato-rhodacyclopentadienes

3.2.8.1 Synthesis and characterisation

The discovery of **9(b)** initiated the idea of synthesising a new series of rhodacyclopentadienes bearing σ- and π-donor ligands such as η^2-benzoato (**Figure**

1.43.a) and acetylacetonato (acac-) (**Figure 1.43.b**), in order to examine the hypothesis that strong σ- and π-donor ligands can increase the Rh character of the frontier orbitals, and consequently enhance the ISC rates in the rhodacyclopentadienes.

Apart from using the synthetic route as described in **Section 3.2.7**, the benzoato-rhodacyclopentadienes were also synthesised using the route shown in **Figure 3.44**. In all cases, the benzoic acid was dried in the oven for a week before use. One equivalent of benzoic acid in THF solution was added to [$RhMe(PMe_3)_4$] in THF solution, then the volatiles (e.g. THF and dissociated PMe_3) were removed *in vacuo* and the flask was refilled with fresh solvent. This removal and refilling of solvent was repeated three times before the reaction was stirred at room temperature for 1 h in order to produce [$Rh(\eta^1$-$O_2CPh)(PMe_3)_3$], **10**.

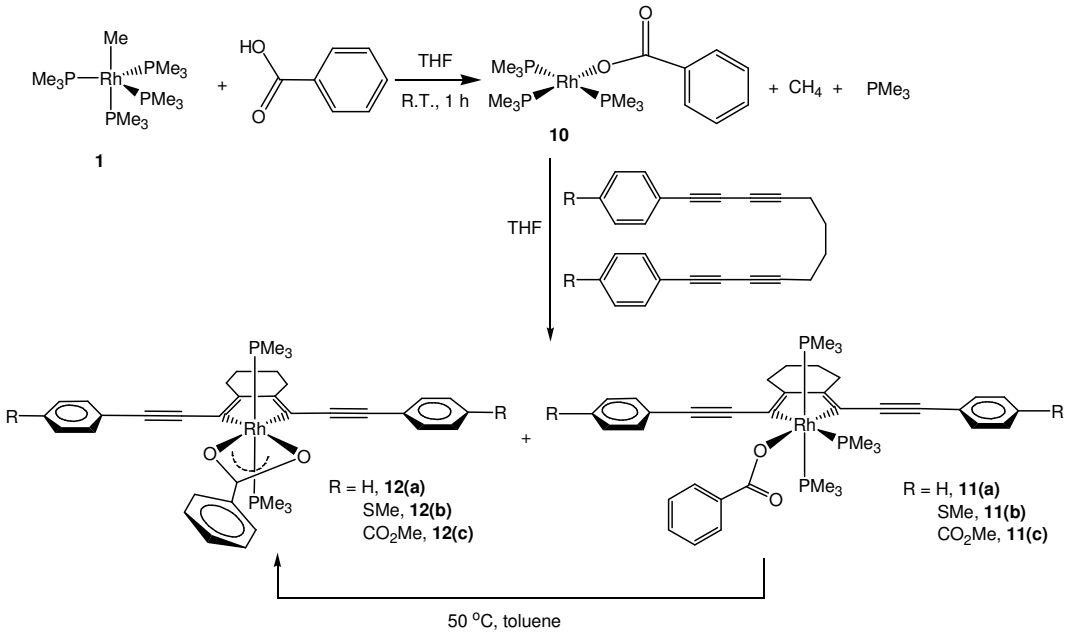

Figure 3.44: Synthetic route to η^2-benzoato-rhodacyclopentadienes.

At room temperature, it was found that the original broad signal at -24.0 ppm in $^{31}P\{^{1}H\}$ NMR spectrum of [RhMe(PMe_3)$_4$] was shifted to lower field at -6.5 ppm, which implies that [RhMe(PMe_3)$_4$] has been converted to **10**. The dynamics may be due to the presence of traces of PMe_3 or the formation of a pseudo five-coordinate species via an η^1-η^2- transformation of the benzoato ligand. At 203 K (**Figure 3.45**), a doublet of triplets ($J_{Rh\text{-}P}$ = 168 Hz, $J_{P\text{-}P}$ = 48 Hz) associated a with doublet of doublets ($J_{Rh\text{-}P}$ = 139 Hz, $J_{P\text{-}P}$ = 48 Hz) at 3.85 and -9.55 ppm, respectively, in a ratio of 1:2 are observed in the $^{31}P\{^{1}H\}$ NMR spectrum of **10**. This shows that two of the PMe_3 ligands are in a different environment than the third one. The molecular structure of **10** in the solid state was confirmed by X-ray diffraction analysis, which showed that the complex is square planar.

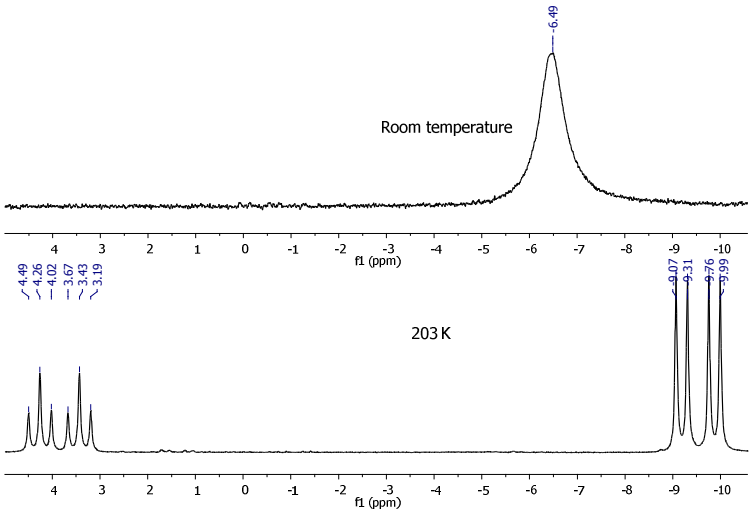

Figure 3.45: $^{31}P\{^{1}H\}$ NMR spectra of **10** at room temperature (top, 162 MHz, C_6D_6) and 203 K (bottom, 202 MHz, 10% C_6D_6 in THF).

Rhodium complex **10** was synthesised by Darensbourg et al. in 1987, via reaction of [RhPh(PMe_3)$_3$] with CO_2 to form [Rh(η^2-O_2CPh)(PMe_3)$_2$] (**Figure 3.46**).[33] The group monitored the reaction progress using IR spectroscopy, and reported that **10**, an

intermediate en route to [Rh(η^2-O_2CPh)(PMe_3)$_2$], is unstable in the absence of a CO_2 atmosphere. Upon removal of CO_2, **10** can revert to [RhPh(PMe_3)$_3$].[33] However, the rhodium complex **10** that was synthesised in this work was found to be stable in an N_2 atmosphere, without CO_2 being present.

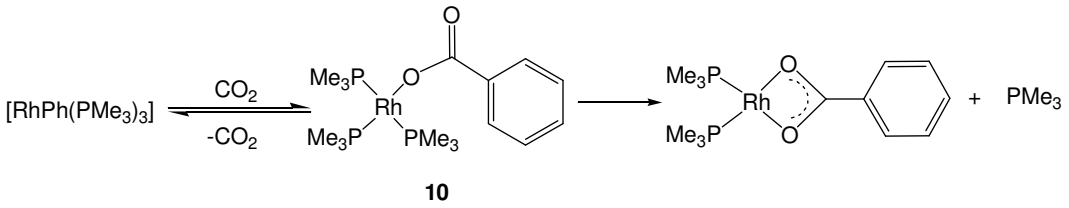

Figure 3.46: Synthesis of [Rh(η^2-O_2CPh)(PMe_3)$_2$] by Darensbourg and co-workers.[33]

It is worth noting that Darensbourg et al. also attempted to synthesise **10** by reaction of [Rh(PMe_3)$_4$]Cl with AgO_2CPh, but this was unsuccessful because of a redox process involving $Ag^{(I)}$ and $Rh^{(I)}$.[33] Our attempt to synthesise **10** by reaction of [(PMe_3)$_4$Rh]Cl with NaO_2CPh in degassed water at 60 °C was also unsuccessful.

In order to prove that this reaction can be further applied to other carboxylic acids, a similar reaction was also carried out with succinic acid (**Figure 3.47**). Analogously to **10**, a di-rhodium complex **13** was obtained, and its molecular structure was also confirmed by X-ray crystallography. Moreover, the $^{31}P\{^1H\}$ NMR spectrum of **13** at 203 K also displays a doublet of triplets at 3.41 ppm ($J_{Rh\text{-}P}$ = 168 Hz, $J_{P\text{-}P}$ = 45 Hz) and a doublet of doublets at -9.41 ppm ($J_{Rh\text{-}P}$ = 143 Hz, $J_{P\text{-}P}$ = 45 Hz) in a ratio of 1:2.

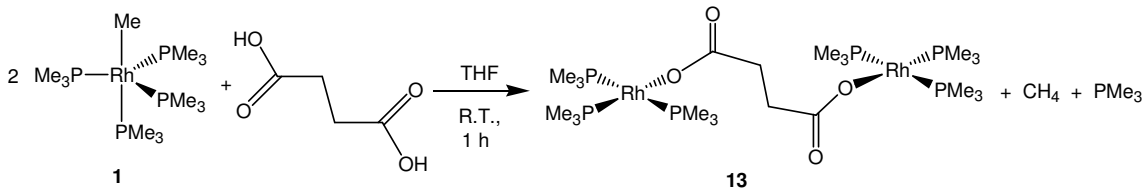

Figure 3.47: Synthesis of the di-rhodium complex **13** using succinic acid.

After confirmation of the structure of **10**, it was reacted with one equivalent of the appropriate 1,12-bis(*p*-R-phenyl)dodeca-1,3,9,11-tetrayne in THF at room temperature for 15 h. After removal of the solvent, $^{31}P\{^{1}H\}$ NMR spectroscopy in C_6D_6 revealed a doublet of doublets and doublet of triplets to be the major peaks. These were assigned to η^1-benzoato-rhodacyclopentadienes with R = H, **11(a)**; R = SMe, **11(b)**; and R = CO_2Me, **11(c)**. Minor doublets were assigned to η^2-benzoato-rhodacyclopentadienes with R = H, **12(a)**; R = SMe, **12(b)**; and R = CO_2Me, **12(c)**. For example, for the reaction with 1,12-bis(phenyl)dodeca-1,3,9,11-tetrayne, the doublet of doublets and doublet of triplets at -7.52 ppm (J_{Rh-P} = 107 Hz, J_{P-P} = 31 Hz) and -18.86 ppm (J_{Rh-P} = 91 Hz, J_{P-P} = 31 Hz), respectively are assigned to **11(a)**, whereas the doublet at -1.04 ppm (J_{Rh-P} = 115 Hz) is assigned to **12(a)** (**Figure 3.48**).

The η^1-benzoato-products were able to be separated from the η^2-benzoato-products in pure form by repeated recrystallisations from THF/hexane mixtures. After this, the residues from the recrystallisations were driven to form the η^2-benzoato products by dissolving them in toluene and heating at 50 °C for 15 minutes, followed by removal of the volatiles (toluene and dissociated PMe_3) and refilling with fresh toluene. This process was repeated ca. 11 times until the η^1-benzoato-rhodacyclopentadienes were completely converted to their η^2-benzoato-analogues. The progress of this for **12(a)** is shown in **Figure 3.48**.

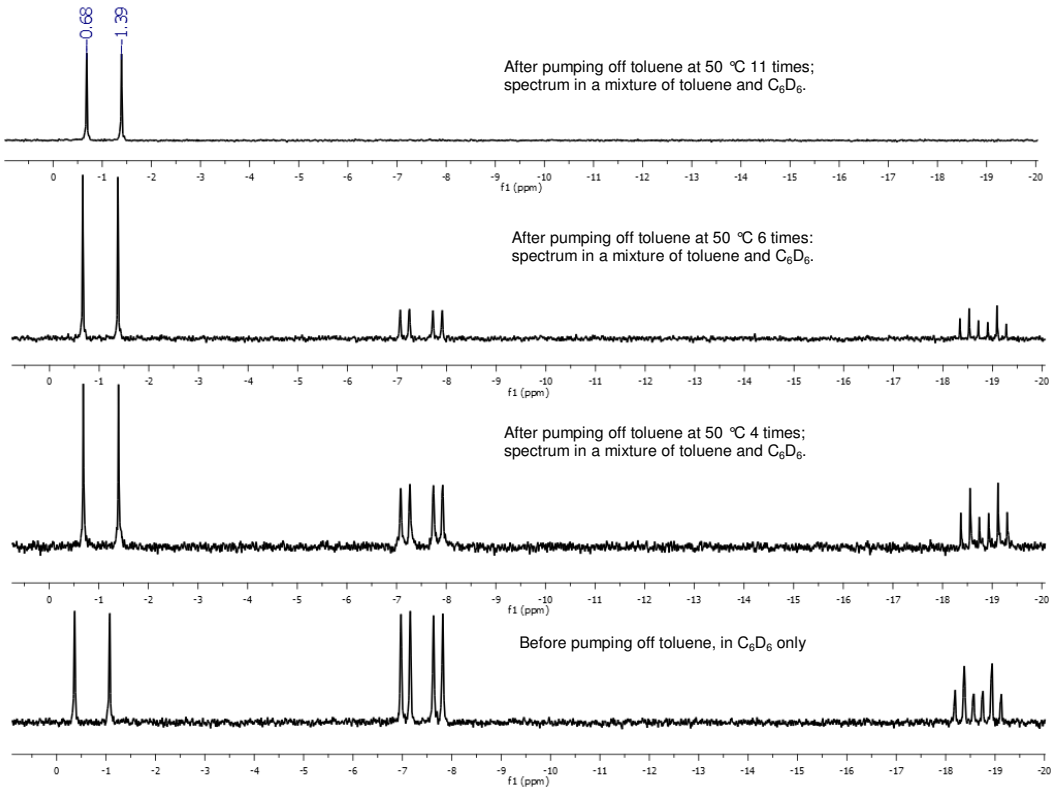

Figure 3.48: $^{31}P\{^{1}H\}$ NMR (162 MHz) spectra in the conversion of **11(a) → 12(a)**.

Comparing the $^{31}P\{^{1}H\}$ NMR spectra of the η^1-benzoato-rhodacyclopentadienes to those of the TMSE-rhodacyclopentadienes, it can be concluded that the positions of the PMe_3 ligands in the η^1-benzoato-rhodacyclopentadienes are similar to those in the TMSE-rhodacyclopentadienes. However, the $J_{Rh\text{-}P}$ values for the η^1-benzoato-rhodacyclopentadienes are larger than those of the TMSE-ones (dd, $J_{Rh\text{-}P}$ = 106 – 107 Hz; dt, $J_{Rh\text{-}P}$ = 91 Hz), which indicates that the benzoato- ligand is a stronger donor ligand, similar to the Me- ligand. The appearance of a doublet in the $^{31}P\{^{1}H\}$ NMR spectrum of **12(a)** indicates that the two PMe_3 ligands are in the same environment; hence, they are located at the axial positions.

The ^{1}H NMR spectrum of **12(a)** (**Figure 3.49**) shows only one multiplet for CH_2-C=C at 2.85 ppm revealing that **12(a)** is a symmetrical compound, which has been confirmed by X-ray crystallography.

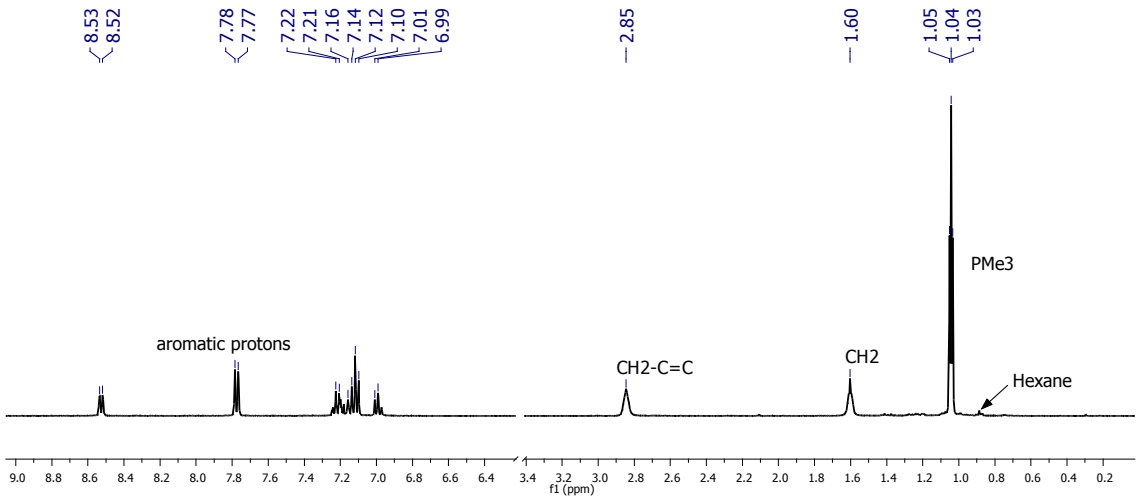

Figure 3.49: ^{1}H NMR spectrum (400 MHz, C_6D_6) of **12(a)**.

3.2.8.2 Crystallographic data for **10**, **11(a)**, **11(c)**, **12(a)** and **13**

The X-ray crystallographic data for **10**, **11(a)**, **11(c)** **12(a)** and **13** are listed in **Table 3.15**. Crystals of **10** and **13** were grown in a Young's tube via slow diffusion of hexane into concentrated C_6D_6 solutions. Rhodium complex **10** crystallises in the hexagonal space group $P6_3/m$, whereas the di-rhodium complex **13** adopts the monoclinic space group $P2_1$. The molecular structures of **10** and **13** are shown in **Figures 3.50** and **3.51**, respectively.

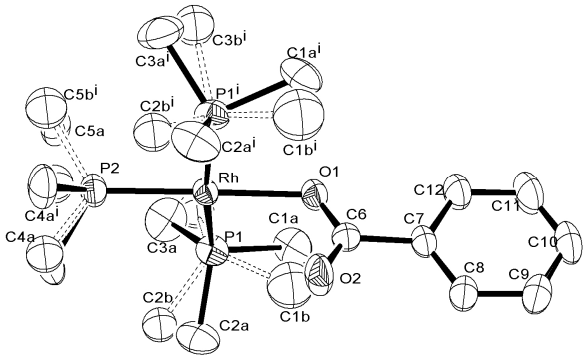

Figure 3.50: Molecular structure of **10**. Hydrogen, C6^i, O2^i atoms and C_6D_6 molecule are omitted for clarity (thermal ellipsoids are shown at 50% probability).

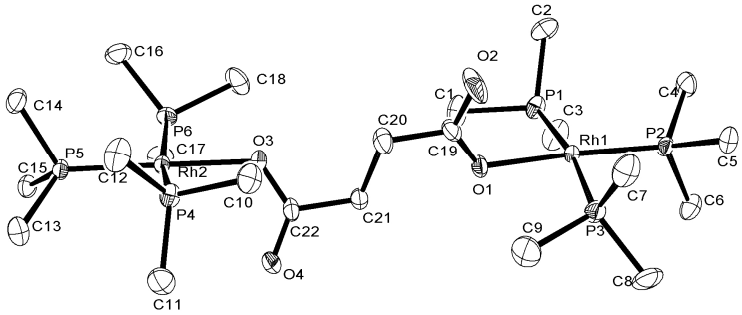

Figure 3.51: Molecular structure of **13**. Hydrogen atoms and C_6D_6 molecule are omitted for clarity (thermal ellipsoids are shown at 50% probability).

Table 3.15: Crystallographic data for **10**, **13**, **11(a)**, **11(c)** and **12(a)**.

Compound	**10**	**13**	**11(a)**	**11(c)**	**12(a)**
Empirical formula	$C_{16}H_{32}O_2P_3Rh{\cdot}C_6D_6$	$C_{22}H_{58}O_4P_6Rh_2{\cdot}C_6D_6$	$C_{40}H_{50}O_2P_3Rh{\cdot}CH_2Cl_2$	$C_{44}H_{54}O_6P_3Rh{\cdot}C_6H_{14}$	$C_{37}H_{42}O_2P_2Rh$
Formula weight	508.33	862.47	843.55	960.86	683.56
Temperature (K)	120(2)	120(2)	120(2)	120(2)	120(2)
Crystal system	Hexagonal	Monoclinic	Orthorhombic	Monoclinic	Monoclinic
Space group	$P6_3/m$	$P2_1$	$Pbca$	$P2_1/c$	$P2_1/c$
a (Å)	17.5052(2)	9.7664(3)	8.9317(6)	9.0388(3)	20.1880(18)
b (Å)	17.5052(2)	11.2945(4)	23.2239(18)	18.7389(7)	9.1185(9)
c (Å)	13.6195(2)	19.2319(7)	38.962(2)	28.9001(10)	18.6726(18)
α (°)	90.00	90.00	90.00	90.00	90.00
β (°)	90.00	102.438(13)	90.00	93.48(1)	92.056(9)
γ (°)	120.00	90.00	90.00	90.00	90.00
Volume (Å^3)	3614.31(8)	2071.61(12)	8081.8(9)	4886.0(3)	3435.1(6)
Z	6	2	8	4	4
Density (calculated) (Mg/m^3)	1.401	1.383	1.387	1.306	1.322
Absorption coefficient (mm^{-1})	0.919	1.055	0.707	0.494	0.620
Crystal size (mm^3)	0.50 x 0.35 x 0.25	0.25 x 0.15 x 0.02	0.25 x 0.14 x 0.04	0.13 x 0.07 x 0.04	0.50 x 0.22 x 0.03
Θ range for data collection (°)	2.33 to 32.16	2.7 to 29.9	2.50 to 29.94	2.26 to 22.84	2.18 to 29.54
Reflections collected	50188	28244	126368	52305	24951
Independent reflections	3660	11961	9742	8603	7113
Data / Restraints / Parameters	3660 / 6 / 147	11961 / 1 / 398	9742 / 10 / 476	8603 / 0 / 535	7113 / 15 / 406
Final R indices [I>2σ(I)]	$R1$ = 0.0282 $wR2$ = 0.0708	$R1$ = 0.0305 $wR2$ = 0.0586	$R1$ = 0.0375 $wR2$ = 0.0866	$R1$ = 0.0594 $wR2$ = 0.1118	$R1$ = 0.0458 $wR2$ = 0.1032
R indices (all data)	$R1$ = 0.0324 $wR2$ = 0.0731	$R1$ = 0.0419 $wR2$ = 0.0629	$R1$ = 0.0455 $wR2$ = 0.0914	$R1$ = 0.1629 $wR2$ = 0.1420	$R1$ = 0.0699 $wR2$ = 0.1152

In **10**, the Rh-P1 bond length of 2.3002(5) Å is substantially longer than the Rh-P2 bond length of Rh-P2 [2.1935(7) Å]. This confirms that the PMe_3 ligand has a stronger *trans*-influence than the oxygen atom. The O1-C6 and O2-C6 bond lengths are 1.261(3) and 1.232(3) Å, respectively, which are significantly different. The Rh-O1 bond length is 2.1339(16) Å. The bond angles of P1-Rh-P2 and O1-Rh-P1 are 93.255(14) and 86.802(14)°, respectively, revealing that the geometry of **10** is distorted square planar. The larger than 90º P1-Rh-P2 bond angle in **10** is parallel to its large $J_{P\text{-}P}$ value (48 Hz) in the $^{31}P\{^{1}H\}$ NMR, consistent with the correlation between bond angles and coupling constants which were described by Karplus fifty years ago.[34, 35] All of the PMe_3 ligands are rotationally disordered: C1, C2, C3, C4 and C5 with attached hydrogens [and their symmetrical equivalents] occupy positions **a** (0.85 occupancy) and **b** (0.15 occupancy). The phenyl group and O1 lie on a mirror plane (together with the Rh and P2 atoms), but C6 and O2 are disordered between two positions related by this plane with equal occupancies.

In **13**, the Rh1-P1 and Rh1-P3 bond lengths are 2.2958(8) and 2.2941(8) Å, respectively (which are identical within experimental error), whereas the Rh1-P2 bond length is 2.1984(8) Å. This result is consistent with those in **10**, which further confirms that the PMe_3 ligand has a stronger *trans*-influence than the η^1-succinato oxygen atom. The Rh1-O1 and Rh2-O3 bond lengths are statistically identical [2.119(2) and 2.114(2) Å, respectively], and are shorter than the Rh-O1 bond length in **10** [2.1339(16) Å]. Similar to **10**, the P1-Rh1-P2 bond angle is larger than 90°, which can be observed from the large $J_{P\text{-}P}$ value (45 Hz) in its $^{31}P\{^{1}H\}$ NMR spectrum. The P1-Rh1-P2, P1-Rh1-O1, P2-Rh1-P3 and P3-Rh-O1 bond angles are 94.15(3), 85.34(7), 94.35(3) and 85.94(7)°,

respectively, whereas the P5-Rh2-P6, O3-Rh2-P6, P5-Rh2-P4 and O3-Rh2-P4 bond angles are 93.72(3), 84.64(7), 93.83(3) and 88.14(7)°, respectively, confirming that the geometry of **13** is distorted square planar. The C19-C20 and C20-21 bond lengths are 1.519(4) and 1.512(4) Å, respectively, which are typical for single $C(sp^3)$-$C(sp^3)$ bonds.

Crystals of **11(a)** and **11(c)** were grown via slow vapour diffusion of hexane into their respective concentrated THF solutions. Rhodacyclopentadiene **11(a)** crystallised in the orthorhombic space group *Pbca*, whereas **11(c)** crystallised in the monoclinic space group $P2_1/c$. The molecular structures of **11(a)** and **11(c)** are shown in **Figures 3.52** and **3.53**, respectively. The crystallographic data are listed in **Table 3.15**.

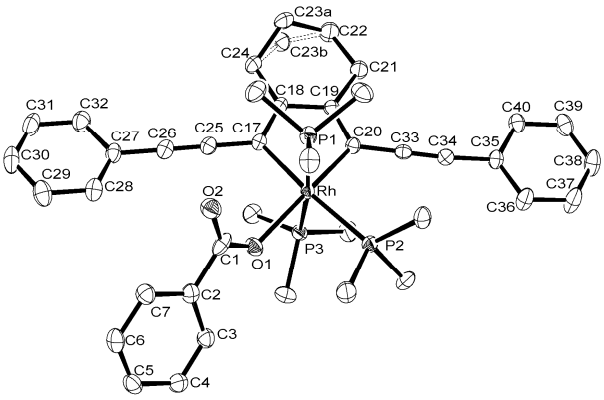

Figure 3.52: Molecular structure of **11(a)**. Hydrogen atoms and the CH_2Cl_2 molecule are omitted for clarity (thermal ellipsoids are shown at 50% probability).

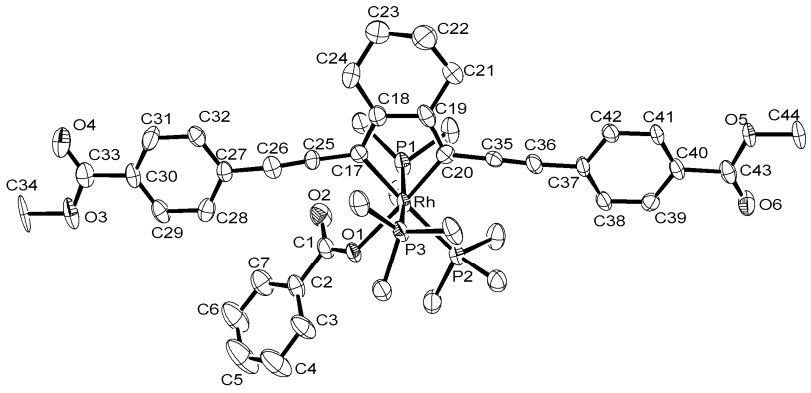

Figure 3.53: Molecular structure of **11(c)**. Hydrogen atoms and the C_6H_{14} molecule are omitted for clarity (thermal ellipsoids are shown at 50% probability).

In **11(a)** and **11(c)**, the Rh-P1 bond lengths of 2.3614(6) - 2.359(2) Å are slightly shorter than those of Rh-P2 [2.3739(6) - 2.378(2) Å], but the Rh-P3 bond lengths [2.3235(6) - 2.3215(19) Å] are much shorter than those of Rh-P2. The Rh-O1 bond lengths in **11(a)** and **11(c)** [2.1992(17) - 2.195(4) Å] are also significantly longer than those in **10** and **13**, because there is no α-carbon from the rhodacycle ring in **10** and **13**. Similarly, the shorter Rh-C20 bond lengths [2.033(2) - 2.012(7) Å] compared to Rh-C17 [2.071(2) - 2.063(7) Å] also confirm that the PMe_3 ligands have a stronger *trans*-influence compared to the oxygen atom in the η^1-benzoato- ligand.

The C=C C19-C20 and C17-C18 bond lengths are 1.376(3) - 1.350(9) and 1.369(3) - 1.356(9) Å, but the C18-C19 bond lengths of 1.446(3) - 1.441(9) Å are shorter than a typical C-C single bond length [1.52 Å]. This is due to the fact that they are both sp^2-hybridised, with the possibility of increased the double bond character in C18-C19. The C23 atom in **11(a)** is disordered between two positions, namely position **a** (0.75 occupancy) and **b** (0.25 occupancy).

In **11(a)**, The C-C≡C-C moiety at C17 is distorted from linearity to roughly the same degree as the analogous one at C20. The C17-C25-C26 and C25-C26-C27 bond angles are 178.3(3) and 175.8(3)°, whereas the C20-C33-C34 and C33-C34-C35 bond angles are 178.1(3) and 175.1(3)°. However, in **11(c)**, the former is distorted slightly more than the latter: C17-C25-C26 [177.1(8)°] and C25-C26-C27 [173.5(8)°] versus C20-C35-C36 [178.5(8)°] and C35-C36-C37 [176.1(8)°].

Single crystals of **12(a)** were obtained via slow vapour diffusion of hexane into a concentrated THF solution. It crystallised in the monoclinic space group $P2_1/c$. The molecular structure of **12(a)** is shown in **Figure 3.54**, and its crystallographic data are listed in **Table 3.15**. The C1-O1 [1.281(5) Å] and C1-O2 [1.291(5) Å] bond lengths are identical within experimental error, which indicates that the electrons are delocalised in the O1-C1-O2 fragment. In addition, the Rh-O1 and Rh-O2 bond lengths are also identical [2.240(2) and 2.241(3) Å, respectively]. The O1-Rh-O2 bond angle is 59.88(10)°, which is similar to the one reported by Werner et al.[30] (60.2(1)° for [Rh(η^2-O_2CMe)(P*i*Pr$_3$)$_2$]) but slightly larger than those reported by Matsumoto and Yoshida[31] (58.5(2)° for [Rh(η^2-O_2CMe)(ppy)$_2$]) and Merola et al.[32] (58.9(3)° for [RhCp*(η^1-O_2CPh)(η^2-O_2CPh)]). The Rh-Cα bond lengths in **12(a)** (Rh-C16 [2.017(4) Å] and Rh-C23 [2.019(3) Å]) are generally shorter than those in **11(a)** [2.033(2) - 2.071(2) Å] and **11(b)** [2.012(7) – 2.063(7) Å]. The C-C≡C-C moiety at C16 is distorted from linearity slightly more than the one at C23 by comparing the bond angles of C16-C15-C14 [171.8(4)°] and C15-C14-C32 [176.9(5)°] to C23-C24-C25 [173.8(4)°] and C24-25-26 [177.4(4)°]. The two PMe_3 ligands are disordered: the P1Me_3 ligand is disordered between positions **a** and **b** with equal occupancies, whereas at the P2Me_3 ligand, all of the

methyl groups are disordered between positions **a** and **b** with occupancies of 0.85 and 0.15, respectively. In addition, the C19 and C20 atoms in the cyclohexyl ring are also disordered between positions **a** and **b** with equal occupancies.

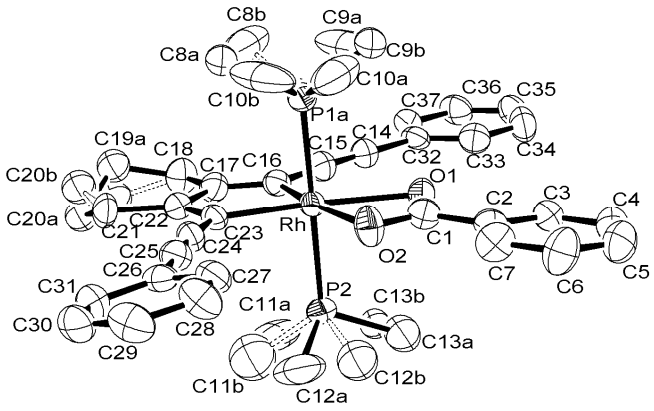

Figure 3.54: Molecular structure of **12(a)**. Disorder is shown but hydrogen atoms are omitted for clarity (thermal ellipsoids are shown at 50% probability).

3.2.8.3 Photophysical studies

Table 3.16 shows a summary of the photophysical data of **11(a)** – **(c)** and **12(a)** – **(c)**. The absorption and emission spectra of **11(a)** – **(c)** and **12(a)** – **(c)** are shown in **Figures 3.55** and **3.56**, respectively.

Both electron withdrawing and donating substituents lead to a bathochromic shift on the λ_{max} values of absorption and emission for both the η^1- and η^2-benzoato-rhodacyclopentadienes. The rhodacyclopentadienes with the electron withdrawing R = CO_2Me substituent absorb and emit at lower wavelengths than those with the electron donating substituent, R = SMe. In addition, the λ_{max} values are shifted to longer wavelengths upon conversion of the η^1-benzoato-rhodacyclopentadienes to their η^2-

benzoato analogues. In the absorption spectra, the smallest bathochromic shift is ca. 8 nm, but in the emission spectra, the smallest bathochromic shift is only 5 nm.

Table 3.16: Summary photophysical data for **11(a)** – **(c)** and **12(a)** – **(c)**.

Compound	λ_{max} ABS (nm)	ε (mol^{-1} cm^{-1} dm^3)	λ_{max} EM (nm)	Stokes shift (cm^{-1})	Φ	τ (ns)
11(a), R = H	465	19000	520	2300	-	-
11(b), R = SMe	477	19000	533	2500	-	-
11(c), R = CO_2Me	503	19000	570	2300	0.07	1.4
12(a), R = H	474	20000	525	2000	0.007	-
12(b), R = SMe	485	23000	543	2200	0.004	-
12(c), R = CO_2Me	512	22000	575	2100	0.03	2.4 (56%) 0.6 (29%) 0.1 (15%)

Note: All of the data (except ε) were recorded in degassed toluene solution at room temperature. ε values were recorded in non-degassed toluene solution.
- No data recorded due to the low emission efficiency.

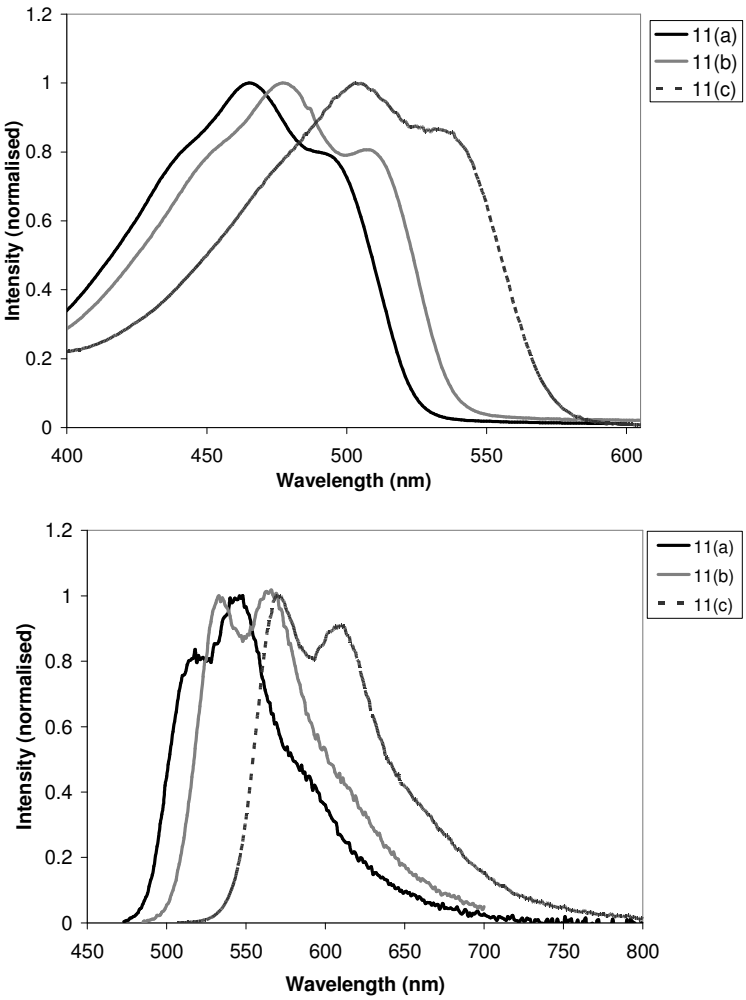

Figure 3.55: Absorption (top) and emission (bottom) spectra of **11(a)** – **(c)** in toluene.

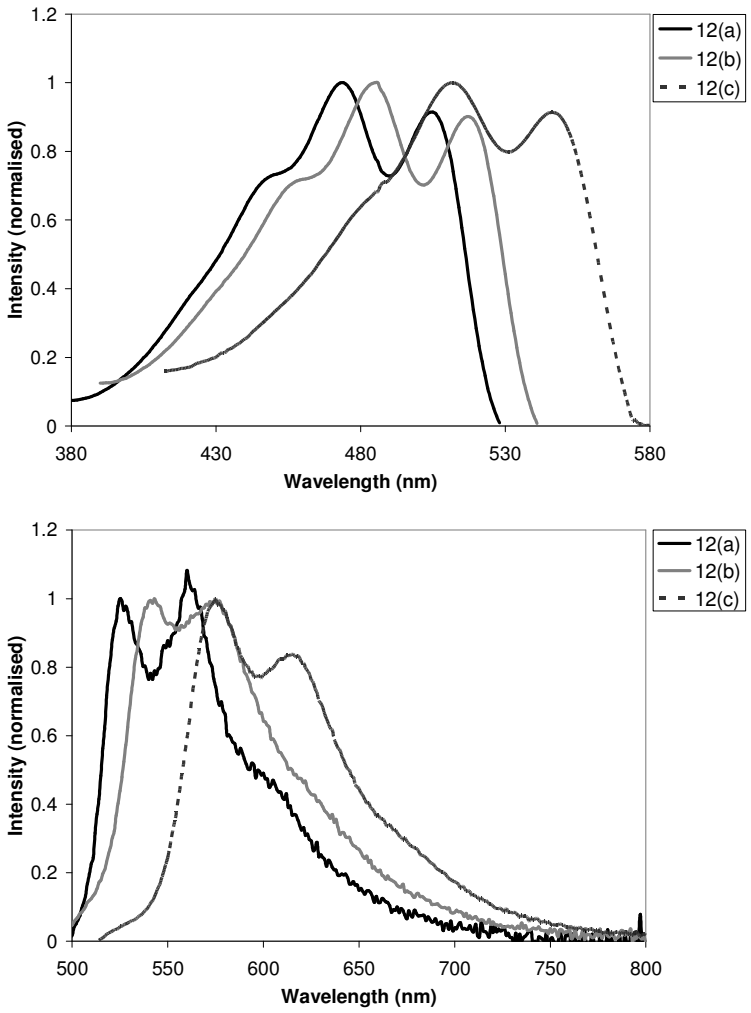

Figure 3.56: Absorption (top) and emission (bottom) spectra of **12(a)** – **(c)** in toluene.

Based on **Figures 3.55** and **3.56**, the emission spectra of **11(a)**, **11(b)**, **12(a)** and **12(b)** are not smooth (they contain significant amounts of noise), which is due to the weak emissions from these four compounds, and the few photons generated by these four compounds are not sufficient for the lifetime measurements. The CO_2Me-substituted benzoato-rhodacyclopentadienes have stronger emissions compared to those with H- and SMe-substituted analogues. The Φ values are 0.07 and 0.03 for the CO_2Me-substituented η^1- and η^2-benzoato-rhodacyclopentadienes, respectively. The lifetime of **11(c)** is 1.4 ns;

however, there are three lifetime components in **12(c)**, which are 2.4 (56%), 0.6 (29%) and 0.1 ns (15%). Of the three lifetime components, the one of 2.4 ns is more likely to be the real lifetime of **12(c)**, whereas the other two are probably due to impurities such as decomposition components from **12(c)**, when it is in low-concentration solutions. Again, the nanosecond lifetimes and small Stokes shifts (~2000 cm^{-1}) for **11(c)** and **12(c)** indicate that the emissions originated from singlet excited states.

The k_f values for **11(c)** and **12(c)** are 5.00 x 10^7 and 1.25 x 10^7 s^{-1}, respectively, which are relatively smaller than those in TMSE-rhodacyclopentadienes (k_f values for **7(a)**, **7(b)** and **7(d)**: 2.75 – 1.89 x 10^8 s^{-1}). This indicates that the non-radiative processes such as IC and ISC in benzoato-rhodacyclopentadienes are more efficient than the radiative ones. Non-radiative decay mechanisms could include rotations of the phenyl ring in the benzoato- ligand. On the other hand, the high-lying Rh filled d-orbitals could facilitate non-emissive MC d → d* transitions, which could also be a possible reason for the low Φ_f values in the η^2-benzoato-rhodacyclopentadienes.

Absorption and emission spectra of **12(c)** were also recorded in non-degassed toluene solution at room temperature (**Figure 3.57**). The emission spectrum is the same as that in degassed solution (**Figure 3.56**) indicating that the emission is from fluorescence rather than phosphorescence.

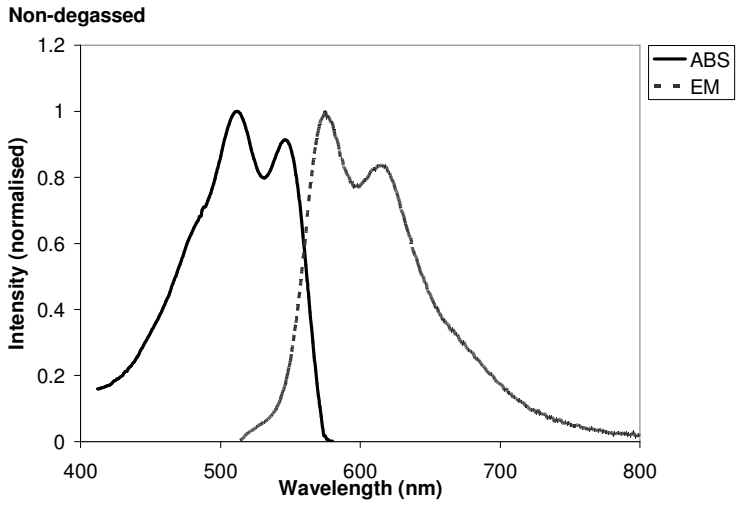

Figure 3.57: Absorption and emission spectra of **12(c)** in non-degassed toluene solution.

Comparing their photophysical data to their *N*,*N*-diethyldithiocarbamato-rhodacyclopentadiene analogues, which were synthesised by Dr. Andreas Steffen (**Table 3.17**),[36] reveals that the λ_{max} values in both absorption and emission for the *N*,*N*-diethyldithiocarbamato-rhodacyclopentadienes with R = H and SMe are similar to those of **12(a)** and **12(b)**. However, for the *N*,*N*-diethyldithiocarbamato-rhodacyclopentadiene with R = CO_2Me, the λ_{max} values in absorption and emission are shifted to lower energy by 6 and 11 nm, respectively, compared to **12(c)**. Moreover, the Φ_f values of the *N*,*N*-diethyldithiocarbamato-rhodacyclopentadienes are significantly higher than those in η^2-benzoato-analogues.

Table 3.17: Summary of the photophysical data for dithiocarbamato-rhodacyclopentadienes.[36]

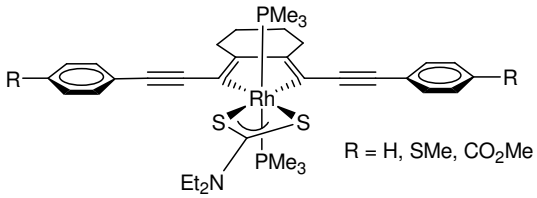

Compound	λ_{max} ABS (nm)	ε (mol^{-1} cm^{-1} dm^3)	λ_{max} EM (nm)	Stokes shift (cm^{-1})	Φ	τ (ns)
R = H	476	24000	526	2000	0.07	1.0 (13%) 0.4 (87%)
R = SMe	487	21000	541	2000	0.16	1.1 (72%) 0.7(28%)
R = CO_2Me	518	19000	586	2200	0.46	2.5

Compared to the TMSE-rhodacyclopentadienes [**7(a)**, **7(b)** and **7(d)**], the emissions of **12(a)** – **(c)** and the dithiocarbamato-rhodacyclopentadienes are significantly red-shifted but with lower Φ values. The implication here is that the Rh centre must be involved in the transitions since the photophysical properties of the rhodacyclopentadienes can be altered by changing the ligand sphere. Again, no phosphorescence was observed for the dithiocarbamato-rhodacyclopentadienes at 77 K, although the Rh participates to a certain extent in the transitions of the rhodacyclopentadienes.[36]

3.2.9 Acetylacetonato- (acac-) rhodacyclopentadienes

3.2.9.1 Synthesis and characterisation

The acetylacetonato- (acac-) ligand has been used in cyclometallated iridium complexes in order to tune their emission colours and Φ_p values.[37] In this work, the acac- ligand was

attached to rhodacyclopentadienes in order to increase the metal character in the frontier orbitals by destabilising the Rh filled d-orbitals. Although the benzoato- and *N*,*N*-diethyldithiocarbamato- ligands have been examined for this purpose, the nanosecond lifetimes and the small Stokes shifts (about 2000 cm^{-1}) implied that the emissions were purely from the singlet excited states. This is supported by the results from the low-temperature lifetime measurements for the *N*,*N*-diethyldithiocarbamato- analogues, in which no phosphorescence was observed at 77 K. Moreover, the emissions were quenched in **11(a)**, **11(b)**, **12(a)** and **12(b)**, which implies that the benzoato- ligand is not generally interesting for photophysical studies of rhodacyclopentadienes.

To synthesise the acac-rhodacyclopentadienes (**Figure 3.58**), acetylacetone was added to a [$RhMe(PMe_3)_4$] solution in degassed THF. The reaction was stirred for 1 h and the volatiles were removed *in vacuo* and refilled with fresh solvent three times in order to remove the methane and two equivalents of PMe_3 to afford the [$Rh(acac)(PMe_3)_2$] complex, **14**.

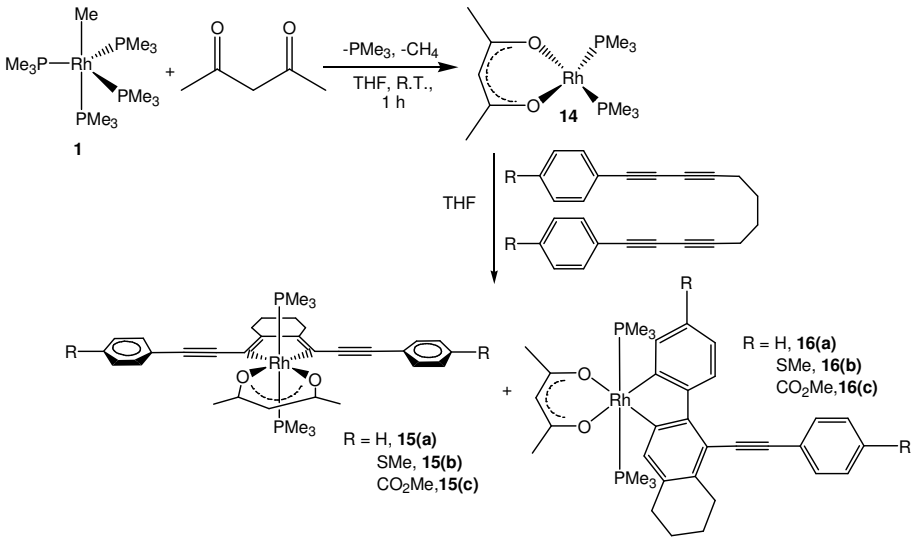

Figure 3.58: Synthetic route to acac-rhodacyclopentadienes and their biphenyl-rhodacyclopentadiene by-products.

The reaction of $[Rh(PMe_3)_4]Cl$ with Na(acac) in degassed water was also attempted as a potential route to **14**, but was not successful as only starting materials were observed in the *in situ* $^{31}P\{^1H\}$ NMR spectrum of the reaction. Interestingly, the reaction between $[RhMe(PMe_3)_4]$ and acetylacetone in degassed THF provides a clean, easy and fast route with quantitative conversion to give **14** in good isolated yield (86%). Similar to **10**, the $^{31}P\{^1H\}$ NMR spectrum of **14** at room temperature shows a broad signal at 6.92 ppm. At 203 K, a doublet appears at 5.78 ppm with $J_{Rh\text{-}P}$ = 185 Hz indicating that there is only one type of PMe_3 present in the structure and the Rh oxidation state is +1. The square planar structure with two PMe_3 ligands and a chelating acac-ligand was confirmed by X-ray diffraction analysis.

After confirming the structure of **14**, it was reacted with one equivalent of the appropriate 1,12-bis(*p*-R-phenyl)dodeca-1,3,9,11-tetrayne at 50 °C to form acac-rhodacyclopentadienes [R = H, **15(a)**; R = SMe, **15(b)**; R = CO_2Me, **15(c)**] and their respective isomeric products [R = H, **16(a)**; R = SMe, **16(b)**; R = CO_2Me, **16(c)**]. The formation of the isomeric species was observed in the *in situ* $^{31}P\{^1H\}$ NMR spectra (**Figure 3.59**).

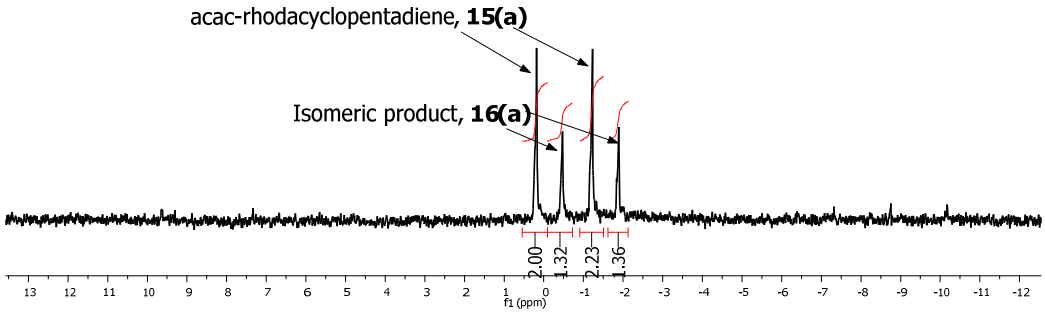

Figure 3.59: *In situ* $^{31}P\{^1H\}$ NMR spectrum (81 MHz, C_6D_6) of **15(a)** and the isomeric product, **16(a)**.

The ratios of the isomers to simple acac-rhodacyclopentadiene are dependent on the R group. For example, for **15(a)** [R = H], the ratio of isomeric product **16(a)** to acac-rhodacyclopentadiene is ca. 1 : 2 (**Figure 3.59**), whereas for **15(c)** [R =CO_2Me], the ratio of **16(c)** : **15(c)** is 1 : 1. The reaction times are also dependent on the R groups. For example, for R = CO_2Me, the reaction was complete after 3 days, whereas for R = H, the reaction took about 16 days to complete. The pure acac-rhodacyclopentadienes **15(a)** - **(c)** were able to be separated from the mixtures by washing the residues with hexane, as the isomeric products are soluble in hexane. Single crystals of the biphenyl-based rhodacyclopentadiene **16(c)** grew in the hexane solution and were analysed by X-ray diffraction, which confirmed its structure. The ^{1}H NMR spectrum of isolated **16(c)** is shown in **Figure 3.60**. A doublet and a broad singlet appear at the extreme low field chemical shifts at 9.53 (J = 8 Hz) and 9.11 ppm. A singlet from an aromatic proton overlaps with a doublet at 8.05 ppm; therefore, the proton integration for this signal is 3. Unlike other rhodacyclopentadienes, the CH_2-C=C and CH_2 signals from the cyclohexyl moiety in **16(c)** are well resolved, which show triplets for CH_2C=C at 3.24 and 2.91 ppm (J = 8 Hz), and quintets for CH_2 at 1.79 and 1.69 ppm (J = 8 Hz).

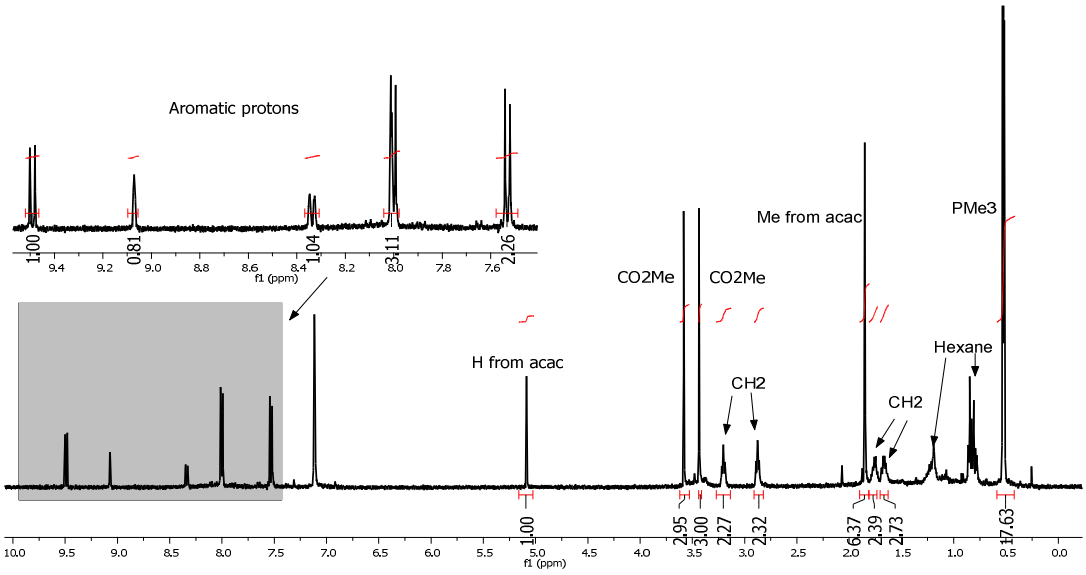

Figure 3.60: ^{1}H NMR (400 MHz, C_6D_6) of **16(c)**.

It is likely that the isomeric products **16(a)** and **16(b)** from reactions **15(a)** and **15(b)** are analogous to **16(c)**, because the chemical shifts and coupling constants of **16(a)** and **16(b)** in the $^{31}P\{^{1}H\}$ NMR spectra are similar to those in **16(c)**. The biphenyl-based rhodacyclopentadiene **16(c)** is the first example of an isomeric by-product to be observed in our rhodacyclopentadiene syntheses since our first report in 2001.[7]

3.2.9.2 Crystallographic data for 14, 15(b), 15(c) and 16(c)

The X-ray crystallographic data for **14**, **15(b)**, **15(c)** and **16(c)** are listed in **Table 3.18**. Rhodium complex **14** was recrystallised via slow diffusion of a layer of hexane into a THF solution in a Young's tube. It crystallised in the tetragonal space group $P42_1c$. The molecular structure of **14** is shown in **Figure 3.61**.

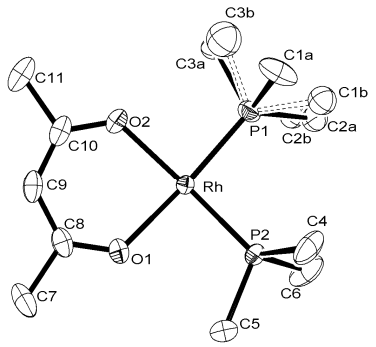

Figure 3.61: Molecular structure of **14**. Hydrogen atoms are omitted for clarity (thermal ellipsoids are shown at 50% probability).

The C10-C9 [1.383(3) Å] and C9-C8 [1.399(3) Å] bond lengths are shorter than typical C-C single bond lengths, which indicates that the electrons are delocalised in the acac-moiety, and have partial C=C bond character. The C10-C9-C8 bond angle is 126.12(15)°, which supports C9 being an sp^2-hybridised carbon. The Rh-P1 and Rh-P2 bond lengths are identical within experimental error [2.1953(5) and 2.1950(5) Å, respectively]. Similarly, the Rh-O1 and Rh-O2 bond lengths are also identical within experimental error [2.0850(11) and 2.0868(10) Å, respectively]. The P1-Rh-P2 [94.716(15)°], P2-Rh-O1 [89.52(3)°], P1-Rh-O2 [87.98(3)°] and O1-Rh-O2 [88.02(4)°] bond angles are all close to 90°, which indicates that the geometry of the Rh is distorted square planar. The $P1Me_3$ ligand is rotationally disordered between two orientations, **a** and **b**, with occupancies refined to 0.747(4) and 0.253(4), respectively.

Table 3.18: Crystallographic data for **14**, **15(b)**, **15(c)** and **16(c)**.

Compound	**14**	**15(b)**	**15(c)**	**16(c)**
Empirical formula	$C_{11}H_{25}O_2P_2Rh$	$C_{37}H_{47}O_2P_2RhS_2$	$C_{39}H_{47}O_6P_2Rh$	$C_{39}H_{47}O_6P_2Rh$
Formula weight	354.16	752.72	776.62	776.62
Temperature (K)	120(2)	120(2)	120(2)	120(2)
Crystal system	Tetragonal	Triclinic	Triclinic	Monoclinic
Space group	$P42_1c$	$P\bar{1}$	$P\bar{1}$	$P2_1/c$
a (Å)	18.090(2)	9.7099(8)	9.8978(8)	14.2755(19)
b (Å)	18.090(2)	9.7832(8)	10.0553(8)	24.309(3)
c (Å)	10.1741(14)	20.0082(17)	19.9344(16)	10.5470(14)
α (º)	90.00	97.636(7)	102.462(6)	90.00
β (º)	90.00	103.479(7)	99.966(6)	99.423(8)
γ (º)	90.00	96.458(7)	98.427(6)	90.00
Volume (Å^3)	3329.6(8)	1811.5(3)	1872.8(3)	3610.6(8)
Z	8	2	2	4
Density (calculated) (Mg/m^3)	1.413	1.380	1.377	1.429
Absorption coefficient (mm^{-1})	1.205	0.706	0.586	0.607
Crystal size (mm^3)	0.45 x 0.40 x 0.32	0.26 x 0.20 x 0.04	0.20 x 0.14 x 0.10	0.27 x 0.25 x 0.17
Θ range for data collection (º)	2.30 to 29.99	2.21 to 29.95	2.58 to 29.83	2.58 to 29.96
Reflections collected	33857	25937	18559	42397
Independent reflections	4820	10123	10253	10309
Data / Restraints / Parameters	4820 / 0 / 180	10123 / 0 / 431	10253 / 0 / 469	10309 / 0 / 453
Final R indices [I>2σ(I)]	R_1 = 0.0152 wR_2 = 0.0360	R_1 = 0.0343 wR_2 = 0.0727	R_1 = 0.0455 wR_2 = 0.0922	R_1 = 0.0307 wR_2 = 0.0678
R indices (all data)	R_1 = 0.0161 wR_2 = 0.0363	R_1 = 0.0447 wR_2 = 0.0763	R_1 = 0.0686 wR_2 = 0.1008	R_1 = 0.0386 wR_2 = 0.0707

Single crystals of **15(b)** and **15(c)** were obtained via slow vapour diffusion from hexane into concentrated THF solutions. Both compounds crystallised in the triclinic space group $P\bar{1}$. The molecular structures of **15(b)** and **15(c)** are shown in **Figures 3.62** and **3.63**, respectively.

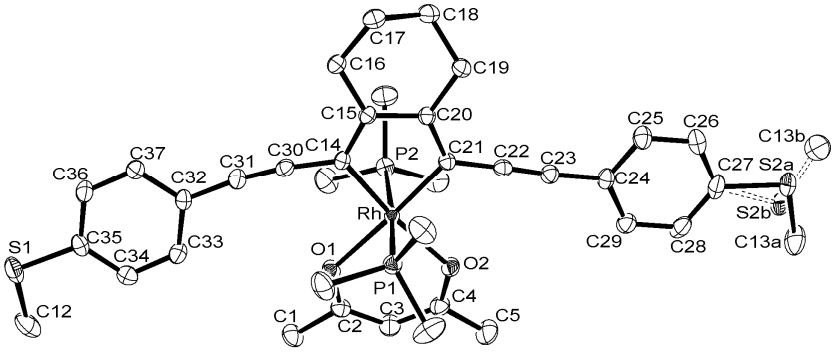

Figure 3.62: Molecular structure of **15(b)**. Hydrogen atoms are omitted for clarity (thermal ellipsoids are shown at 50% probability).

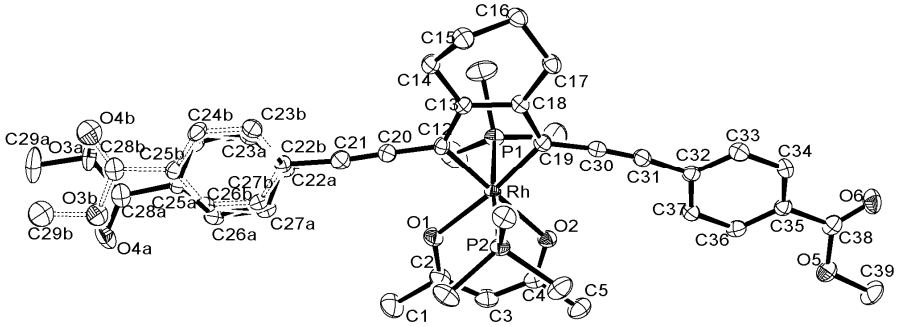

Figure 3.63: Molecular structure of **15(c)**. Hydrogen atoms are omitted for clarity (thermal ellipsoids are shown at 50% probability).

In both compounds, the Rh-O1 and Rh-O2 bond lengths are 2.1513(14) – 2.1279(18) and 2.1383(14) - 2.1567(17) Å, respectively. The Rh-Cα bond lengths of both compounds are in the range 2.0120(19) – 2.0234(19) Å, which is similar to that of **12(a)** [2.017(4) - 2.019(3) Å]. The O1-Rh-O2 bond angles are 88.52(6) – 88.34(5)°, which are slightly larger than the one in **14** [88.02(4)°]. Similarly to **14**, the C2-C3 [1.401(3) - 1.400(4) Å] and C3-C4 [1.406(3) - 1.400(4) Å] bond lengths in both **15(b)** and **15(c)** are also shorter than typical C-C single bond length, which indicates that the electrons are delocalised in the acac- moiety. Moreover, the C2-C3-C4 bond angles of 127.7(2) - 127.8(3)° support

C3 being sp^2-hybridised in both compounds. The P1-Rh-P2 bond angle in **15(c)** [173.91(3)°] deviates more from linearity than the one in **15(b)** [175.63(2)°].

In **15(b)**, the Rh-C14 and Rh-C21 bond lengths are 2.0234(19) and 2.0120(19) Å, respectively, and the C14-Rh-C21 bond angle is 79.37(8)°. The C-C≡C-C moiety at C14 is distorted more from linearity than the one at C21, which can be observed from the comparison of the C14-C30-C31 [173.5(2)°] and C30-C31-C32 [172.3(2)°] bond angles to C21-C22-C23 [178.0(2)°] and C22-C23-C24 [175.6(2)°]. One of the SMe groups is disordered between two opposite orientations, with occupancies of 0.643(5) for orientation **a** and 0.357(5) for orientation **b**.

In **15(c)**, the Rh-C12 and Rh-C19 bond lengths are 2.012(2) and 2.020(3) Å, respectively, and the C12-Rh-C19 bond angle is 79.07(10)°. The C-C≡C-C moiety at C19 is distorted much more from linearity than the one at C12 by comparison of the C19-C30-C31 [173.2(3)°] and C30-C31-C32 [170.2(3)°] bond angles to C12-C20-C21 [178.9(3)°] and C20-C21-C22a [178.2(5)°] or C20-C21-C22b [174.2(7)°]. One of the benzene rings (and its CO_2Me group) is disordered between two orientations (**a** and **b**) differing by an in-plane tilt and a 180°-rotation around the C21-C28 bond, with occupancies refined to 0.704(6) and 0.296(6), respectively.

Biphenyl-rhodacyclopentadiene **16(c)** crystallises in the monoclinic space group $P2_1/c$ from a concentrated hexane solution. The molecular structure of **16(c)** is shown in **Figure 3.64**. The Rh-O1 and Rh-O2 bond lengths are 2.1540(12) and 2.1529(12) Å (identical within experimental error), respectively. The Rh-Cα bond lengths, namely, Rh-C12 and Rh-C19 are 1.9914(16) and 2.0062(12) Å, respectively, and these two bonds are slightly shorter (ca. 0.014 – 0.020 Å) than those in **15(b)** and **15(c)**. This may be because the

electron delocalisation in the rhodacycle ring in **16(c)** is slightly greater than that in **15(b)** and **15(c)**. Moreover, the C12-C17 and C18-C19 bond lengths are 1.424(2) and 1.419(2) Å, respectively, and the C17-C18 [1.477(2) Å] bond length is shorter than the typical $C(sp^3)$-$C(sp^3)$ bond length [1.52 Å], since they are both sp^2-hybridised carbons. The geometry at the Rh centre is distorted octahedral, because the C12-Rh-C19 [80.75(7)°] and O1-Rh-O2 [88.93(5)°] bond angles are smaller than 90°. The C21-C36, C36-C37, C37-C38, C38-C39 and C22-C39 bond lengths are in the range 1.519(3) – 1.529(3) Å, which are typical $C(sp^3)$-$C(sp^3)$ bond lengths.

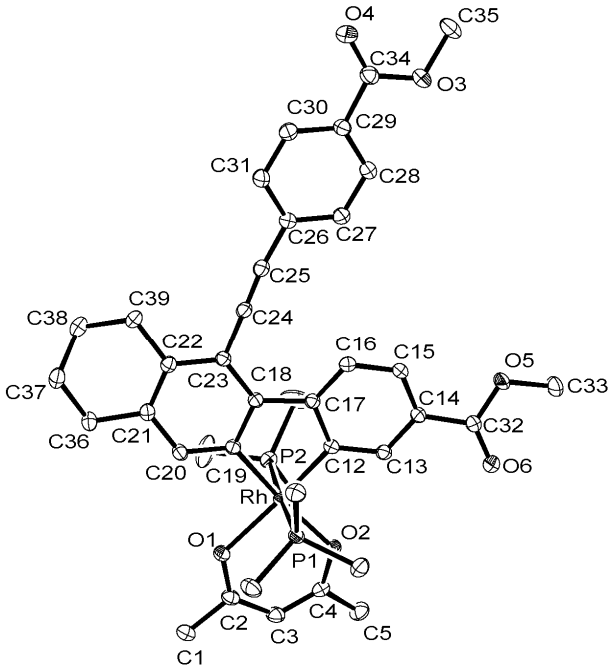

Figure 3.64: Molecular structure of **16(c)**. Hydrogen atoms are omitted for clarity (thermal ellipsoids are shown at 50% probability).

3.2.9.3 Photophysical studies

Table 3.19 gives a summary of the photophysical data obtained for **15(a)**, **15(b)** and **15(c)**, and their absorption and emission spectra are shown in **Figure 3.65**. As expected,

the λ_{max} values of both absorption and emission spectra for the complex containing electron withdrawing substituent (R = CO_2Me) are also more red-shifted compared to that containing the electron donating substituent (R = SMe). The λ_{max} values of absorption and emission for the acac-rhodacyclopentadienes are close to those of the η^2-benzoato-rhodacyclopentadienes [**12(a)**, **12(b)** and **12(c)**]. This indicates that the acac- ligand, as a strong σ- and π-donor to the Rh centre, is able to reduce the energy gap between the excited states and the ground state of rhodacyclopentadienes.

Table 3.19: The summary of the photophysical data for **15(a) - (c)**.

Compound	**λ_{max} ABS (nm)**	**ε (mol^{-1} cm^{-1} dm^3)**	**λ_{max} EM (nm)**	**Stokes shift (cm^{-1})**	**Φ**	**τ (ns)**
15(a), R = H	470	16000	520	2000	0.04	3.4 (6%) 1.0 (10%) 0.2 (84%)
15(b), R = SMe	481	23000	534	2100	0.13	2.0 (25%) 0.5 (75%)
15(c), R = CO_2Me	514	34000	579	2200	0.50	2.5

Note: All of the data above (except ε) were recorded at room temperature in degassed toluene solution. ε values were recorded in non-degassed toluene solutions.

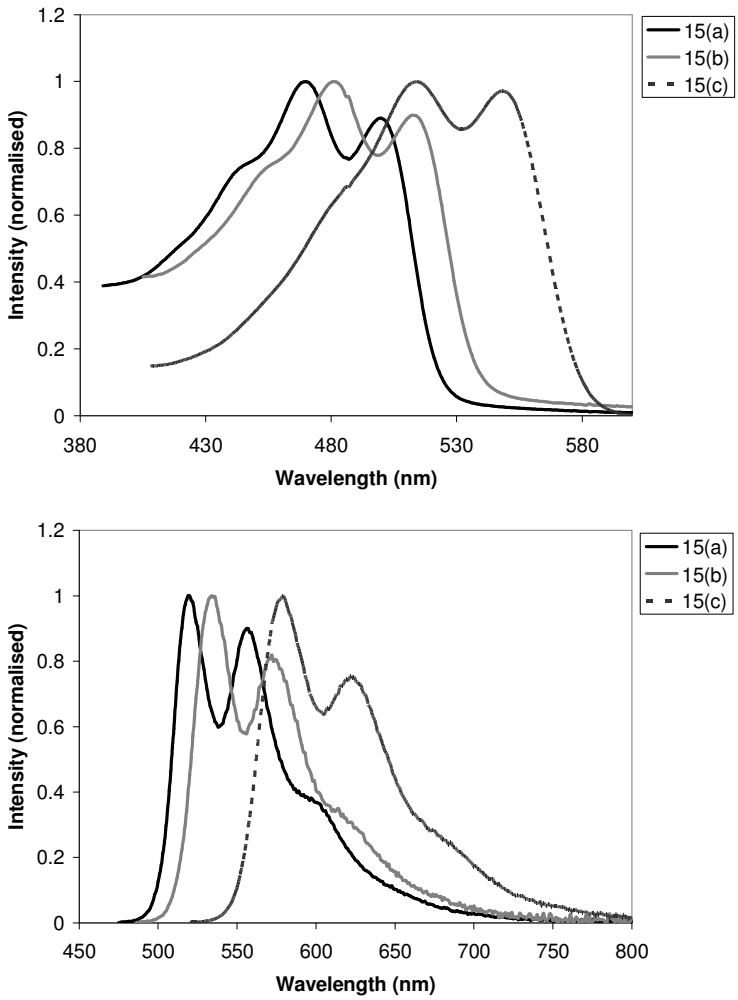

Figure 3.65: Absorption (top) and emission (bottom) spectra of **15(a)** – **(c)** in toluene.

The Φ values of the acac-rhodacyclopentadienes are higher than those for the η^2-benzoato-rhodacyclopentadienes, which may be because the acac- ligand is more rigid than the benzoato- ligand. Acac-rhodacyclopentadiene **15(a)** (R = H) gave the lowest Φ value (Φ = 0.04), whereas **15(c)** (R = CO_2Me) gave the highest Φ value (Φ = 0.50). Again, the nanosecond lifetimes and small Stokes shifts (ca. 2000 cm^{-1}) in the acac-rhodacyclopentadienes confirm that the emissions occur from the singlet excited states, and no phosphorescence was observed at room temperature between 400 – 800 nm. One

of the possible explanations for this lack of phosphorescence is that the triplet excited states lie close in energy to the ground state, increasing the Frank-Condon factors.

3.2.9.4 Photophysical studies of 16(c)

The photophysical information from isolated **16(c)** is very important to compare with the other rhodacyclopentadienes that have been reported so far. **Table 3.20** shows the photophysical data for **16(c)**, its absorption and emission spectra in non-degassed and degassed solutions are shown in **Figure 3.66**, and the excitation spectrum is shown in **Figure 3.67**.

Table 3.20: Summary of the photophysical data for **16(c)**.

λ ABS (nm)	**ε (mol^{-1} cm^{-1} dm^3)**	**λ EM (nm)**	**Stokes shift (cm^{-1})**	**Φ**	**τ @ 394 nm (ns)**	**τ @ 544 nm (μs)**
330	28000	394	4600	0.03 (Φ_f)	3.0 (31%)	237.6
372	24000	416			0.6 (69%)	
410 (sh)	9000	544	11920	0.05(Φ_p)		
		587				

Note: The data above (except ε) were recorded in degassed toluene at room temperature. ε values were recorded in non-degassed toluene solution.

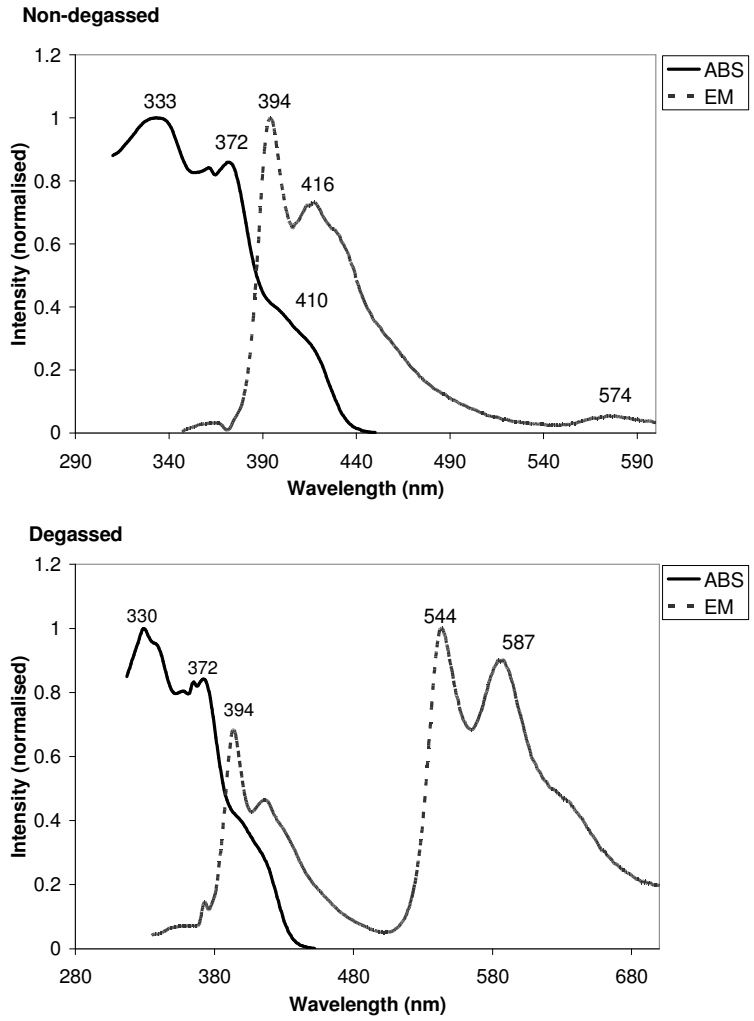

Figure 3.66: Absorption and emission spectra of **16(c)** in non-degassed (top) and degassed toluene solutions (bottom).

In the non-degassed toluene solution, a fluorescent emission at 394 nm and a weak broad emission band at 574 nm were observed in the spectrum. After the sample was fully degassed, a strong emission was found with λ_{max} at 544 nm. This emission only appears as a weak broad band in the non-degassed solution; therefore, this must be phosphorescent emission that occurs from the triplet excited states because it was

quenched by the triplet oxygen molecules through the process of triplet-triplet annihilation.

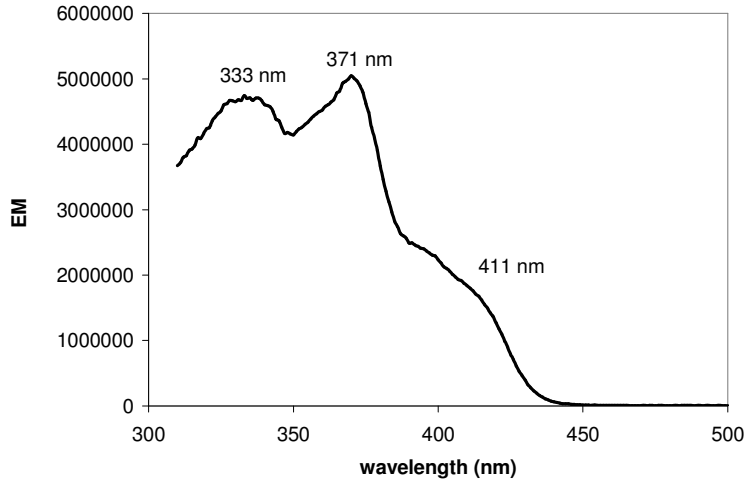

Figure 3.67: Excitation spectrum of **16(c)** with the emission wavelength at 544 nm.

The dual fluorescent and phosphorescent emissions in emission spectrum of the degassed solution are possibly due to the presence of two chromophores in the structure. The emission at 394 nm is due to the organic chromophore, while the emission at 544 nm is possibly due to the biphenyl-rhodacyclopentadiene moiety.

Two lifetime components were recorded for **16(c)**: the one on the nanosecond timescale was assigned to the emission at 394 nm, while the other one on the 200 microsecond timescale belongs to the emission at 544 nm. The long-lived emission lifetime (237 μs at room temperature) indicates that the emission at 544 nm is possibly due to triplet state ligand-centred (LC) $\pi \rightarrow \pi^*$ transitions. The long-lived emission lifetime at room temperature is unusual in cyclometallated $Rh^{(III)}$ complexes. For example, as mentioned before, $[Rh(bpy)_3]^{3+}$ was reported as non-emissive at room temperature.[24] Similarly to $[Rh(bpy)_3]^{3+}$, $[Rh(ppy)_2(bpy)]^{+}$ was also non-emissive at room temperature in EtOH or

MeOH. However, an emission was observed at 77 K, which was assigned to a $\pi \rightarrow \pi^*$ transition with a lifetime of 177 μs.[38] Moreover, Lo et al.[39] reported their cyclometallated $Rh^{(III)}$ diimine complexes e.g. $[Rh(pba)_2(bpy)]Cl$ (Hpba = 4-(2-pyridyl)benzaldehyde; bpy = 2,2'-bipyridine) have the room temperature phosphorescence lifetimes of 4.2 – 8.7 μs. The room temperature lifetime of **16(c)** is at least twenty-five times longer than those reported by Lo et al.

In typical phosphorescent rhodium complexes containing cyclometallating ligands, the emissions are usually weak especially at room temperature (Φ_p = 0.001 – 0.03),[39-41] but the Φ_p value at room temperature for **16(c)** is 0.05.

Compound **16(c)** is the only rhodacyclopentadiene that we have found to phosphorescence at room temperature in this work. The photophysical properties of **16(c)** have proven that Rh participates in the excited states, as it shows phosphorescent emission. Compared to the other rhodacyclopentadienes in this work, the difference between **16(c)** and the others is in the rhodacycle ring: namely that **16(c)** contains a biphenyl moiety, where as the others have cyclohexyl loops or phenyl rings. It is possible that the electron delocalisation in the rhodacycle ring in **16(c)** is more effective than that in the others. This can be supported by inspection of the Rh-Cα bond lengths which are shorter in **16(c)** [1.9914(16) – 2.0062(16) Å] than in **15(b)** [2.012(19) – 2.0234(19) Å] and **15(c)** [2.012(2) – 2.020(3) Å]. The effectiveness of the electron delocalisation in the rhodacycle ring is a possible factor, which might determine the amount of Rh participation in the excited states.

3.3 Summary and conclusion

Twenty-six rhodacyclopentadienes with different types of ligands were synthesised and characterised. Many of their structures have also been confirmed from single-crystal X-ray diffraction data. The photophysical data for these rhodacyclopentadienes were collected and the general results are as follows:

(i) nanosecond lifetimes and small Stokes shifts (ca. 2000 cm^{-1}) indicate that the emissions originate from the singlet excited states;

(ii) no phosphorescence was observed at room temperature in the 400 – 800 nm range in any of the rhodacyclopentadienes [except **16(c)**], despite the fact that the Rh centres are involved in the transitions;

(iii) both electron withdrawing and donating R substituents shift the λ_{max} values of absorption and emission bathochromically;

(iv) those with electron withdrawing R substituents absorb and emit at lower energies and with higher Φ values than those with electron donating R substituents; and

(v) the use of TMSE as the σ-donor ligand to the Rh centre gives the highest Φ values compared to the other ligands.

Extended phenylene-ethynylene moieties were applied as the R substituents [namely -C≡C-C_6H_4-CO_2(*n*-C_8H_{17}) and -C≡C-C_6H_4-N(*n*-C_6H_{13})$_2$], and the σ-donor ligand (DHAPEPE-). Both types of rhodacyclopentadienes exhibited a decrease of Φ_f values, which is possibly due to the poor rigidity of the long alkyl chains. However, the use of extended phenylene-ethynylene as the R substituents in rhodacyclopentadienes shifts the absorption and emission maxima bathochromically.

Replacement of the two phenyl rings at the 3- and 4-positions of the rhodacycle by a cyclohexyl ring can greatly improve the Φ_f values of the TMSE-rhodacyclopentadienes. The TMSE-rhodacyclopentadiene with R = H [**7(a)**] has been investigated further by singlet oxygen experiments, low-temperature lifetime measurements, and time resolved-infrared (TRIR) experiments. The results from these experiments showed that the singlet excited state decays effectively only by fluorescence and ISC to a triplet excited state, with no $S_1 \rightarrow S_0$ internal conversion [since Φ_Δ (0.65) + Φ_f (0.33) ≈ 1.00]. This is because the fluorescence rate is competitive with the intersystem crossing (ISC) rate as both rates are of the order of 10^8 s^{-1}. The TRIR results showed **7(a)** has a short-lived triplet excited state lifetime, which is ca. 55 ns. Based on the results of preliminary TD-DFT calculations that have been performed for **7(d)**, the T_1 state is low in energy, which results in appreciably large Frank-Condon factors. Therefore, non-radiative processes are believed to dominate the deactivation of the T_1 state, which result in a short triplet state lifetime.

Benzoato- and acac- ligands were introduced to the Rh centre in an attempt to increase the rate of ISC by raising the Rh filled d-orbitals, and consequently increasing the Rh character in the frontier orbitals. The λ_{max} values in absorption and emission of both η^2-benzoato- and acac-rhodacyclopentadienes are very similar. The significant bathochromic shifts of the λ_{max} values in absorption and emission of η^2-benzoato- and acac-rhodacyclopentadienes relative to those rhodacyclopentadienes with other ligands such as TMSE- and DHAPEPE- indicate that the energy gaps between the excited and ground states are smaller than those in their TMSE- and DHAPEPE- analogues.

The first example of biphenyl-rhodacyclopentadiene formation in our rhodacyclopentadiene syntheses was observed in the preparation of acac-rhodacyclopentadienes. The biphenyl-rhodacyclopentadiene **16(c)** shows phosphorescent emission with a λ_{max} value of 544 nm in degassed solution. The long-lived phosphorescence lifetime (237 μs) confirms that the phosphorescence arises from ^{3}LC $\pi \rightarrow \pi^*$ transitions. The Φ values for **16(c)** are 0.03 for fluorescence and 0.05 for phosphorescence at room temperature.

In conclusion, we have reported different series of rhodacyclopentadienes, which exhibit long-lived fluorescence and slow ISC rates ($k_\Delta \approx k_f \approx 10^8$ s^{-1}, especially TMSE-rhodacyclopentadienes), although the Rh centre is involved to a certain extent in the transitions, which is confirmed by the shifts in λ_{max} values when different ligands are placed on the Rh centres. This indicates that the efficiency of ISC in an organometallic complex is not only dependent on what type of metal is present, but is also dependent on how efficient the SOC effect from the metal is. The results from the singlet oxygen sensitisation and TRIR experiments showed that the triplet excited states are present in the rhodacyclopentadienes, but no phosphorescence [except for **16(c)**] was observed at room temperature in the 400 – 800 nm range. A potential reason for this is the T_1 states lie close in energy to the ground states, which causes a significant overlap between the triplet excited states and upper vibrational levels of the ground states. As a result, the triplet excited states decay via non-emissive processes which are more efficient than emission of a photon (i.e. phosphorescence).

3.4 Experimental

3.4.1 General

All rhodacyclopentadiene syntheses and purifications were performed in a nitrogen-filled Innovative Technology Inc. glovebox unless otherwise noted. [$RhCl_3 \cdot 3H_2O$] was purchased from Precious Metals Online, Australia, and used without further purification. 1,12-bis(*p*-trimethylsilylethynylphenyl)dodeca-1,3,9,11-tetrayne was supplied by Liu Chao from the Green Catalyst Institute, Wuhan University, China. HPLC grade solvents (Fisher Scientific and J.T. Baker) were nitrogen saturated and were dried and deoxygenated using an Innovative Technology Inc. Pure-Solv 400 Solvent Purification System, and further deoxygenated using the freeze-pump-thaw method. C_6D_6 was purchased from Cambridge Isotope Laboratories and dried over sodium granules for 72 h, deoxygenated using the freeze-pump-thaw method and vacuum transferred to a sealed vessel.

All NMR spectra recorded at ambient temperature, were obtained using Varian Mercury 400 (^{1}H: 400 MHz, ^{31}P{^{1}H}: 162 MHz, ^{19}F{^{1}H}: 376 MHz), Bruker Avance 400 (^{1}H: 400 MHz, ^{31}P{^{1}H}: 162 MHz), Varian Inova 500 (^{1}H: 500 MHz, ^{31}P{^{1}H}: 202 MHz) or Varian DD-700 (^{1}H: 700 MHz) spectrometers. The ^{31}P{^{1}H} NMR spectra of **1**, **10**, **13** and **14** at 196 – 203 K were recorded using a Varian Inova 500 spectrometer. ^{1}H NMR chemical shifts are reported relative to TMS and were referenced via residual proton resonances of the appropriate deuterated solvent (C_6D_6: 7.15 ppm), whereas the ^{31}P{^{1}H} NMR spectra were referenced externally to H_3PO_4 (85%) at 0 ppm.

Elemental analyses were obtained using an Exeter Analytical Inc. CE-440 elemental analyzer in the Department of Chemistry at Durham University. Mass spectrometric

determinations were obtained using either a MALDI ToF Applied Biosystems Voyager-DE STR mass spectrometer or by ES using a Thermo-Finnigan LTQ FT spectrometer operating in positive ion mode. The samples for elemental analysis and mass spectrometric determinations were prepared in the glovebox. IR spectra were recorded as KBr disks using a Perkin-Elmer Spectrum 100 series FT-IR spectrometer.

The crystallographic data collections and structure solutions were carried out by Dr. Andrei S. Batsanov, the Department of Chemistry, Durham University, using a Bruker three-circle diffractometer with a CCD area detector. The structures were solved by direct methods and refined by full-matrix least squares against F^2 of all data, using SHELXTL software.

3.4.2 Photophysical studies

UV-Vis and fluorescence spectra were recorded in HPLC toluene which was degassed via the freeze-pump-thaw method. All of the UV-Vis absorption spectra and extinction coefficients were measured on a Hewlett-Packard 8453 diode array spectrophotometer using standard 1 cm width quartz cells. Emission spectra were obtained on a Horiba Jobin-Yvon Fluoromax-3 spectrophotometer. The emission spectra were fully corrected using the manufacturer's correction curves for the spectral response of the emission optical components.

Low temperature emission, quantum yield and fluorescence lifetime measurements were recorded using the instruments located in Dr. Andrew Beeby's laboratory, in the Department of Chemistry, Durham University. The low temperature emission spectrum

of **7(a)** was recorded by Dr. Andrew Beeby in an *iso*-pentane/Et_2O/EtOH glass at 77 K. The quantum yield and lifetime measurements as well as the singlet oxygen sensitisation experiments were carried out by Dr. Andreas Steffen from our group. Quantum yields for samples with absorbance at the maximum typically below 0.2 were determined using a Horiba Jobin-Yvon Fluorolog 3-22 Tau-3 spectrophotometer. The method of quantum yield calculation followed that described in the literature.[42]

Fluorescence lifetimes were measured by time-correlated single-photon counting (TCSPC) using a pulsed diode laser 396 nm providing a 1 MHz train of pulses of < 100 ps. The fluorescence emission was collected at right angles to the excitation source, with the emission wavelength selected using a monochromator and detected by a single-photon avalanche diode (SPAD). The instrument response function was measured using a dilute LUDOX® suspension as the scattering sample, setting the monochromator at the emission wavelength of the laser, giving an instrument response function (IRF) of 200 ps at 396 nm. The resulting intensity decay was a convolution of the fluorescence decay with the IRF, and iterative reconvolution of the IRF with a decay function and non-linear least-squares analysis were used to analyse the convoluted data.[43, 44]

Singlet oxygen sensitisation experiments for **7(a)**, **7(b)** and **7(d)** in aerated solutions were also performed in Dr. Andrew Beeby's laboratory. The quantum yields of singlet oxygen formation were determined relative to perinaphthanone in toluene (Φ_Δ = 1.0) using a method described by Nonell and Braslavsky.[29] The samples and the reference compounds were analysed in the same solvent because of the strong dependence of the radiative and non-radiative rate constants for deactivation of the triplet states on the solvent. The singlet oxygen emission was detected at 1269 nm from solutions in a 1 cm

path length quartz cuvette after being excited at 355 nm by a Q-switched Nd:YAG laser (Spectra Physics, Quanta Ray GCR-150-10) with a 10 Hz repetition rate. The emission was collected at 90° to the excitation beam by a liquid nitrogen cooled germanium photodiode (North Coast E0-817P) after passing through an interference filter centred at 1270 nm. The photodiode output was amplified and AC coupled to a digital oscilloscope which digitised and averaged the transients. The averaged data were then analysed using the Microsoft Excel package.

Time-resolved infrared (TRIR) measurements for **7(a)** were performed in Prof. Michael George's laboratory, School of Chemistry in the University of Nottingham. The concentration of **7(a)** was approximately 10^{-3} M in all the TRIR experiments. A brief explanation of the measurement technique was reported in the supporting information in reference 36.

3.4.3. Preparation of tetrakis(trimethylphosphine)methylrhodium

Rhodium cyclooctadiene chloride dimer[45]

$[RhCl_3 \cdot 3H_2O]$ (10.00 g, 37.98 mmol) was added to a 500 mL round bottom flask which had been evacuated and refilled 3 times with N_2. Degassed spectroscopic grade ethanol (120 mL) and degassed distilled water (50 mL) were transferred to the flask via cannula and the solution was stirred rapidly. 1,5-Cyclooctadiene (COD, in liquid form, density = 0.882 g/mL) (10 mL, 81.53 mmol) was added dropwise to the solution via dropping funnel and the reaction was heated at 60 °C for 24 h under N_2. The product, $[RhCl(COD)]_2$, was precipitated as a yellow solid, and was collected by filtration, washed

with degassed EtOH (20 mL), followed by degassed Et_2O (30 mL), dried *in vacuo* and stored under N_2. Yield: 17.60 g, 94%. ^1H NMR (400 MHz, C_6D_6) δ: 4.27 (s, 4H, olefin COD), 2.02 (m, 4H, CH_2, COD), 1.26 (m, 4H, CH_2, COD).

[Tetrakis(trimethylphosphine)rhodium]chloride, $[Rh(PMe_3)_4]Cl$[19]

$[RhCl(COD)]_2$ (3.215 g, 6.53 mmol) was added under N_2 to degassed THF (100 mL) in a 500 mL round bottom flask and the solution was stirred rapidly. PMe_3 (6.73 mL, 65.30 mmol) was dissolved in THF (20 mL) and added dropwise to the solution using a dropping funnel. The reaction was heated at 60 °C for 3 h. An orange precipitate, $[Rh(PMe_3)_4]Cl$, formed as addition continued and the solution turned yellow. The product, $[Rh(PMe_3)_4]Cl$, was collected by filtration, washed with degassed Et_2O (50 mL), dried *in vacuo* and stored under N_2. Yield: 2.60 g, 90%. ^1H NMR (400 MHz, D_2O) δ: 1.34 (s, 36H, PMe_3). $^{31}P\{^1H\}$ NMR (162 MHz, D_2O) δ: -15.46 (d, $J_{Rh\text{-}P}$ = 125 Hz, 4P).

1 – Tetrakis(trimethylphosphine)methylrhodium, $[RhMe(PMe_3)_4]$[19]

In a nitrogen-filled glovebox, $[Rh(PMe_3)_4]Cl$ (2.50 g, 5.65 mmol) was added to a flask that contained 50 mL of degassed THF and the suspension was stirred rapidly. MeLi (1.6 M in Et_2O, 4.59 mL, 7.34 mmol) diluted with ca. 5 mL of degassed Et_2O was added dropwise to the solution using a dropping funnel. The reaction was stirred for 3 h; the solution turned yellow and white LiCl precipitated. The solution was filtered through a small bed of celite and the solvent was removed *in vacuo* to give $[RhMe(PMe_3)_4]$ as a yellow crystalline solid. Yield: 2.01 g, 84%. ^1H NMR (400 MHz, C_6D_6) δ: 1.16 (s, 36H, PMe_3), 0.01 (d, J = 4 Hz, 3H, CH_3). $^{31}P\{^1H\}$ NMR (202 MHz, 196 K, 10% C_6D_6 in THF)

δ: -0.52 (dq, J_{Rh-P} = 105 Hz, J_{P-P} = 40 Hz, 1P), -22.68 (dd, J_{Rh-P} =158 Hz, J_{P-P} = 40 Hz, 3P). Anal. Calcd. for $C_{13}H_{39}P_4Rh$: C, 36.98; H, 9.31. Found: C, 37.30; H, 9.12%.

3.4.4 Preparation of 4-[*p*-(*N*,*N*-di-*n*-hexylamino)phenylethynyl]phenylethynylrhoda-cyclopentadienes

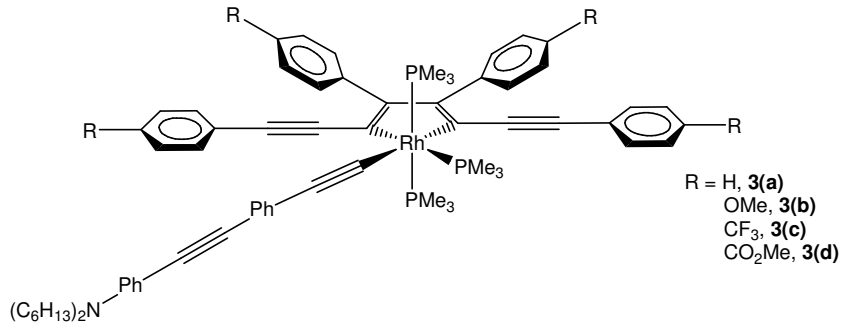

3(a) - *mer*,*cis*-[tris(trimethylphosphine)-4-[*p*-(*N*,*N*-di-*n*-hexylamino)phenylethynyl] phenylethynyl-2,5-bis(phenylethynyl)-3,4-bis(phenyl)rhodacyclopenta-2,4-diene][20]

The compound 4-(4-ethynylphenylethynyl)-*N*,*N*-di-*n*-hexylaniline (EPEDHA) (0.0181 g, 0.047 mmol) in THF (1 mL) was added dropwise to a 28 mL vial that contained a stirred solution of [RhMe(PMe_3)$_4$] (0.0198 g, 0.047 mmol) in THF (1 mL), and the resulting solution was stirred for 15 min. A solution of 1,4-diphenylbuta-1,3-diyne (0.0190 g, 0.094 mmol) in THF (1 mL) was added, the solution was stirred for 5 min and the solvent was removed *in vacuo*. THF (2 mL) was added to the vial, the solution was stirred for 5 min and the solvent was removed *in vacuo* again. This cycle was repeated one more time and then THF (2 mL) was added and the solution was stirred for 24 h. The solvent was removed *in vacuo* and the compound was washed with hexane, and dried *in vacuo* yielding crude **3(a)**, which was recrystallised from C_6D_6 and hexane to give a yellow solid. Yield: 0.045 g, 85%. ^{1}H NMR (500 MHz, C_6D_6) δ: 7.67 (d, *J* = 8 Hz, 2H,

CH_{arom}), 7.66 (d, *J* = 8 Hz, 2H, CH_{arom}), 7.54 (d, *J* = 8 Hz, 2H, CH_{arom}), 7.44 (d, *J* = 8 Hz, 2H, CH_{arom}), 7.43 (d, *J* = 8 Hz, 2H, CH_{arom}), 7.34 (d, *J* = 8 Hz, 2H, CH_{arom}), 7.24 (d, *J* = 8 Hz, 2H, CH_{arom}), 7.19 (t, *J* = 8 Hz, 2H, CH_{arom}), 7.17 (t, *J* = 8 Hz, 2H, CH_{arom}), 7.06 (t, *J* = 8 Hz, 3H, CH_{arom}), 7.02 (m, 1H, CH_{arom}), 6.93 (t, *J* = 8 Hz, 3H, CH_{arom}), 6.84 (t, *J* = 8 Hz, 1H, CH_{arom}), 6.53 (d, *J* = 8 Hz, 2H, CH_{arom}), 2.98 (t, *J* = 7 Hz, 4H, $N(CH_2)_2$), 1.39 (d, J_{P-H} = 8 Hz, 9H, PMe_3 *trans* to Cα), 1.34 (vt, J_{P-H} = 4 Hz, 18H, PMe_3 *trans* to PMe_3), 1.22 (quint, *J* = 7 Hz, 4H, $N(CH_2C\mathit{H}_2)_2$), 1.13 (m, 12H, 2 x C_3H_6), 0.88 (t, *J* = 7 Hz, 6H, 2 x CH_3). $^{31}P\{^1H\}$ NMR (81 MHz, C_6D_6) δ: -9.07 (dd, J_{Rh-P} = 98 Hz, J_{P-P} = 31 Hz, 2P), -21.95 (dt, J_{Rh-P} = 83 Hz, J_{P-P} = 31 Hz, 1P). Anal. Calcd. for $C_{69}H_{81}NP_3Rh$: C, 73.98; H, 7.29; N, 1.25. Found: C, 73.44; H, 7.18; N, 1.55%. MS (ES^+) *m/z*: 1119 [M^+]. IR (KBr) $\upsilon_{C\equiv C}$ = 2205, 2159, 2132, 2088 cm^{-1}.

3(b) - *mer*,*cis*-[tris(trimethylphosphine)-4-[*p*-(*N*,*N*-di-*n*-hexylamino)phenylethynyl] phenylethynyl-2,5-bis(*p*-methoxyphenylethynyl)-3,4-bis(*p*-methoxyphenyl)rhodacyclo-penta-2,4-diene][20]

EPEDHA (0.0181 g, 0.047 mmol) in THF (1 mL) was added dropwise to a 28 mL vial that contained a stirred solution of [$RhMe(PMe_3)_4$] (0.0198 g, 0.047 mmol) in THF (1 mL), and the resulting solution was stirred for 15 min. A solution of 1,4-bis(*p*-methoxyphenyl)buta-1,3-diyne (0.0247 g, 0.094 mmol) in THF (1 mL) was added, the solution was stirred for 5 min, and then the solvent was removed *in vacuo*. THF (2 mL) was added to the vial, the solution was stirred for 5 min and the solvent was removed *in vacuo* again. This cycle was repeated one more time, and then THF (2 mL) was added and the solution was stirred for 48 h. The solvent was removed *in vacuo* and the

compound was washed with hexane, and dried *in vacuo* yielding crude **3(b)**, which was purified via recrystallisation from C_6D_6 and hexane to give a yellow solid. Yield: 0.037 g, 64%. ^{1}H NMR (400 MHz, C_6D_6) δ: 7.68 (d, *J* = 8 Hz, 2H, CH_{arom}), 7.63 (d, *J* = 8 Hz, 2H, CH_{arom}), 7.55 (d, *J* = 8 Hz, 2H, CH_{arom}) 7.50 (d, *J* = 8 Hz, 2H, CH_{arom}), 7.46 (d, *J* = 8 Hz, 2H, CH_{arom}), 7.37 (d, *J* = 8 Hz, 2H, CH_{arom}), 7.26 (d, *J* = 8 Hz, 2H, CH_{arom}), 6.86 (d, *J* = 8 Hz, 2H, CH_{arom}), 6.84 (d, *J* = 8 Hz, 2H, CH_{arom}), 6.69 (d, *J* = 8 Hz, 2H, CH_{arom}), 6.59 (d, *J* = 8 Hz, 2H, CH_{arom}), 6.53 (d, *J* = 8 Hz, 2H, CH_{arom}), 3.28 (s, 3H, OCH_3), 3.27 (s, 3H, OCH_3), 3.22 (s, 3H, OCH_3), 3.13 (s, 3H, OCH_3), 2.98 (t, *J* = 7 Hz, 4H, $N(CH_2)_2$), 1.46 (d, J_{P-H} = 7 Hz, 9H, PMe_3 *trans* to Cα), 1.40 (vt, J_{P-H} = 3 Hz, 18H, PMe_3 *trans* to PMe_3), 1.22 (quint, *J* = 8 Hz, 4H, $N(CH_2C\mathit{H}_2)_2$), 1.11 (m, 12H, 2 x C_3H_6), 0.88 (t, *J* = 7 Hz, 6H, 2 x CH_3). ^{31}P{^{1}H} NMR (162 MHz, C_6D_6) δ: -8.19 (dd, J_{Rh-P} = 99 Hz, J_{P-P} = 31 Hz, 2P), -21.90 (dt, J_{Rh-P} = 82 Hz, J_{P-P} = 31 Hz, 1P). Anal. Calcd. for $C_{73}H_{89}NO_4P_3Rh$: C, 70.69; H, 7.23; N, 1.13. Found: C, 70.98; H, 7.04; N, 0.93%. MS (ES^+) *m/z*: 1239 [M^+]. IR (KBr) $\upsilon_{C\equiv C}$ = 2204, 2160, 2132, 2085 cm^{-1}.

3(c) - *mer*,*cis*-[tris(trimethylphosphine)-4-[*p*-(*N*,*N*-di-*n*-hexylamino)phenylethynyl] phenylethynyl-2,5-bis(4-trifluoromethylphenylethynyl)-3,4-bis(4-trifluoromethylphenyl)-rhodacyclopenta-2,4-diene][20]

EPEDHA (0.0181 g, 0.047 mmol) in THF (1 mL) was added dropwise to a 28 mL vial that contained a stirred solution of [$RhMe(PMe_3)_4$] (0.0198 g, 0.047 mmol) in THF (1 mL), and the resulting solution was stirred for 15 min. A solution of 1,4-bis(4-trifluoromethylphenyl)buta-1,3-diyne (0.0318 g, 0.094 mmol) in THF (1 mL) was added, the solution was stirred for 5 min and the solvent was removed *in vacuo*. THF (2 mL)

was added to the vial, the solution was stirred for 5 min and the solvent was removed *in vacuo* again. This cycle was repeated one more time and then THF (2 mL) was added and the solution was stirred for 15 h. The solvent was removed *in vacuo* to give crude **3(c)**, which was further purified by dissolving it in THF (1 mL) and layering this with hexane (ca. 10 mL) to recrystallise the compound as a yellow solid. Yield: 0.053 g, 81%. ^{1}H NMR (400 MHz, C_6D_6) δ: 7.64 (d, *J* = 8 Hz, 2H, CH_{arom}), 7.63 (d, *J* = 8 Hz, 2H, CH_{arom}), 7.39 (d, *J* = 8 Hz, 2H, CH_{arom}), 7.35 (d, *J* = 8 Hz, 2H, CH_{arom}), 7.34 (d, *J* = 8 Hz, 2H, CH_{arom}), 7.28 (d, *J* = 8 Hz, 2H, CH_{arom}), 7.25 (d, *J* = 8 Hz, 2H, CH_{arom}), 7.23 (d, *J* = 8 Hz, 2H, CH_{arom}), 7.16 (d, *J* = 8 Hz, 2H, CH_{arom}), 7.12 (d, *J* = 8 Hz, 2H, CH_{arom}), 6.96 (d, *J* = 8 Hz, 2H, CH_{arom}), 6.53 (d, *J* = 9 Hz, 2H, CH_{arom}), 2.98 (t, *J* = 7 Hz, 4H, $N(CH_2)_2$), 1.38 (quint, *J* = 8 Hz, 4H, $N(CH_2C\mathit{H}_2)_2$), 1.32 (d, $J_{P\text{-}H}$ = 8 Hz, 9H, PMe_3 *trans* to Cα), 1.28 (vt, $J_{P\text{-}H}$ = 3 Hz, 18H, PMe_3 *trans* to PMe_3), 1.12 (m, 12H, 2 x C_3H_6), 0.88 (t, *J* = 7 Hz, 6H, 2 x CH_3), ^{31}P{^{1}H} NMR (162 MHz, C_6D_6) δ: -8.98 (dd, $J_{Rh\text{-}P}$ = 96 Hz, $J_{P\text{-}P}$ = 31 Hz, 2P), -21.58 (dt, $J_{Rh\text{-}P}$ = 82 Hz, $J_{P\text{-}P}$ = 31 Hz, 1P). ^{19}F{^{1}H} NMR (376 MHz, C_6D_6) δ: -62.29 (s, 3F), -62.31 (s, 3F), -62.61 (s, 3F), -62.68 (s, 3F). Anal. Calcd. for $C_{73}H_{77}F_{12}NP_3Rh$: C, 62.98; H, 5.57; N, 1.01. Found: C, 62.70; H, 5.68; N, 1.25%. MS (ES^+) *m/z*: 1391 [M^+]. IR (KBr): $\upsilon_{C\equiv C}$ = 2205, 2165, 2136, 2091, υ_{arom} = 1520 cm^{-1}.

3(d) - *mer*,*cis*-[tris(trimethylphosphine)-4-[*p*-(*N*,*N*-di-*n*-hexylamino)phenylethynyl]-phenylethynyl-2,5-bis(*p*-carbomethoxyphenyl)-3,4-bis(*p*-carbomethoxyphenyl)rhoda-cyclopenta-2,4-diene][20]

EPEDHA (0.0181 g, 0.047 mmol) in THF (1 mL) was added dropwise to a 28 mL vial that contained a stirred solution of [$RhMe(PMe_3)_4$] (0.0198 g, 0.047 mmol) in THF (1

mL) and the resulting solution was stirred for 15 min. A solution of 1,4-bis(*p*-carbomethoxyphenyl)buta-1,3-diyne (0.0299 g, 0.094 mmol) in THF (1 mL) was added, the solution was stirred for 5 min and then the solvent was removed *in vacuo*. THF (2 mL) was added to the vial, the solution was stirred for 5 min and the solvent was removed *in vacuo* again. This cycle was repeated one more time and then, THF (2 mL) was added and the solution was stirred for 15 h. The solvent was removed *in vacuo* and the compound was washed with hexane, and dried *in vacuo* yielding **3(d)**, which was recrystallised from C_6D_6 and hexane. Yield: 0.032 g, 50%. ^{1}H NMR (400 MHz, C_6D_6) δ: 8.18 (d, *J* = 8 Hz, 2H, CH_{arom}), 8.15 (d, *J* = 8 Hz, 2H, CH_{arom}), 8.01 (d, *J* = 8 Hz, 2H, CH_{arom}) 7.93 (d, *J* = 8 Hz, 2H, CH_{arom}), 7.65 (d, *J* = 8 Hz, 2H, CH_{arom}), 7.64 (d, *J* = 8 Hz, 2H, CH_{arom}), 7.49 (d, *J* = 8 Hz, 2H, CH_{arom}), 7.38 (d, *J* = 8 Hz, 2H, CH_{arom}), 7.36 (d, *J* = 8 Hz, 2H, CH_{arom}), 7.29 (d, *J* = 8 Hz, 2H, CH_{arom}), 7.18 (d, *J* = 8 Hz, 2H, CH_{arom}), 6.55 (d, *J* = 8 Hz, 2H, CH_{arom}), 3.45 (s, 3H, $COOCH_3$), 3.44 (s, 3H, $COOCH_3$), 3.43 (s, 3H, $COOCH_3$), 3.35 (s, 3H, $COOCH_3$), 3.00 (t, *J* = 7 Hz, 4H, $N(CH_2)_2$), 1.40 (quint, *J* = 8 Hz, 4H, $N(CH_2C\mathit{H}_2)_2$), 1.32 (d, $J_{P\text{-}H}$ = 8 Hz, 9H, PMe_3 *trans* to Cα), 1.26 (vt, $J_{P\text{-}H}$ = 4 Hz, 18H, PMe_3 *trans* to PMe_3), 1.19 (m, 12H, 2 x C_3H_6), 0.88 (t, *J* = 7 Hz, 6H, 2 x CH_3). ^{31}P{^{1}H} NMR (162 MHz, C_6D_6) δ: -9.02 (dd, $J_{Rh\text{-}P}$ = 99 Hz, $J_{P\text{-}P}$ = 31 Hz, 2P), -22.75 (dt, $J_{Rh\text{-}P}$ = 81 Hz, $J_{P\text{-}P}$ = 31 Hz, 1P). Anal. Calcd. for $C_{77}H_{89}NO_8P_3Rh$: C, 68.39; H, 6.63; N, 1.04. Found: C, 68.00; H, 6.51; N, 1.28%. MS (ES^+) *m/z*: 1352 [M^+]. IR (KBr) $\upsilon_{C\equiv C}$ = 2204, 2162, 2134, 2091, $\upsilon_{ester(C=O)}$ = 1721 cm^{-1}.

3.4.5 Preparation of *mer,cis*-[tris(trimethylphosphine)methyl-2,5-bis(*p*-di-*N*,*N*-methylaminophenylethynyl)-3,4-(*p*-di-*N*,*N*-methylaminophenyl)rhodacyclo-penta-2,4-diene] (4)

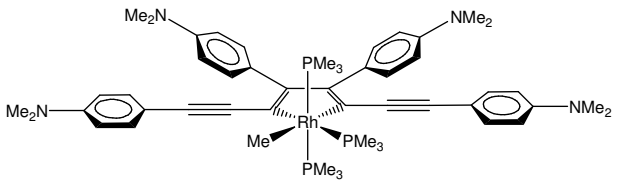

In a N_2-filled glovebox, 1,4-bis(*p*-di-*N*,*N*-methylaminophenyl)buta-1,3-diyne (0.0283 g, 0.098 mmol) and [RhMe(PMe_3)$_4$] (0.0207 g, 0.049 mmol) were added to THF (3 mL) in a Young's tube. The resulting solution was stirred for 15 min and the solvent was removed *in vacuo*. THF (3 mL) was added, the solution was stirred for 15 min, and the solvent was removed *in vacuo* again. This cycle was repeated one more time, and then THF (3 mL) was added. The Young's tube was removed from the glovebox and heated at 50 °C for 5 d. The reaction progress was monitored *in situ* by $^{31}P\{^1H\}$ NMR spectroscopy until complete conversion to **4** was observed. The THF solvent was removed *in vacuo* and hexane (1 mL) was added to the residue and then removed *in vacuo*. This process was repeated two times in order to remove completely any residual THF. The hexane was removed *in vacuo* yielding **4** as a yellow solid, which was purified via recrystallisation from toluene and hexane. Yield: 0.029 g 64%. ^1H NMR (400 MHz, C_6D_6) δ: 7.68 (d, J = 8 Hz, 2H, CH_{arom}), 7.59 (d, J = 8 Hz, 2H, CH_{arom}), 7.52 (d, J = 8 Hz, 2H, CH_{arom}), 7.39 (d, J = 8 Hz, 2H, CH_{arom}), 6.67 (d, J = 8 Hz, 2H, CH_{arom}), 6.66 (d, J = 8 Hz, 2H, CH_{arom}), 6.50 (d, J = 8 Hz, 2H, CH_{arom}), 6.43 (d, J = 8 Hz, 2H, CH_{arom}), 2.50 (s, 6H, $N(CH_3)_2$), 2.48 (s, 6H, $N(CH_3)_2$), 2.41 (s, 6H, $N(CH_3)_2$), 2.36 (s, 6H, $N(CH_3)_2$), 1.43 (d, $J_{P\text{-}H}$ = 8 Hz, 9H, PMe_3 *trans* to Cα), 1.25 (vt, $J_{P\text{-}H}$ = 3 Hz, 18H, PMe_3 *trans* to PMe_3), 0.15 (dq, $^2J_{Rh\text{-}H}$ = 2 Hz, $^3J_{P\text{-}H}$ = 8 Hz, 3H, CH_3-Rh). $^{31}P\{^1H\}$ NMR (162 MHz, C_6D_6) δ: -5.66 (dd, $J_{Rh\text{-}P}$ =

106 Hz, $J_{P\text{-}P}$ = 33 Hz, 2P), -18.39 (dt, $J_{Rh\text{-}P}$ = 89 Hz, $J_{P\text{-}P}$ = 33 Hz, 1P). Anal. Calcd. for $C_{50}H_{70}N_4P_3Rh$: C, 65.07; H, 7.64; N, 6.07. Found: C, 65.09; H, 7.59; N, 5.98%. MS (ES^+) *m/z* = 907 [M^+ - CH_3]. IR (KBr) $\upsilon_{C\text{-}H}$ = 2903, 2793, $\upsilon_{C\equiv C}$ = 2121, υ_{Ar} = 1516, 1441 cm^{-1}.

3.4.6 Preparation of TMSE-rhodacyclopentadienes containing extended phenylene-ethynylene groups

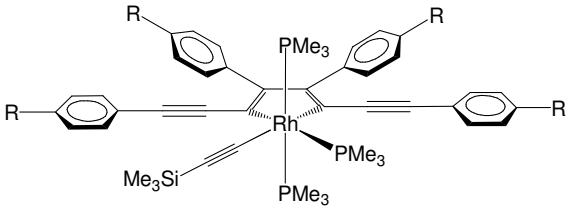

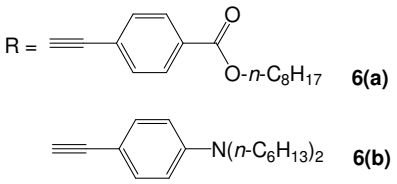

6(a) - *mer*,*cis*-[tris(trimethylphosphine)trimethylsilylethynyl-2,5-bis[4-(4-ethynyl-phenylethynyl)-benzoic acid *n*-octyl ester]-3,4-bis(4-phenylethynylbenzoic acid *n*-octyl ester)rhodacyclopenta-2,4-diene]

Trimethylacetylene (TMSA, 8 μL, 0.058 mmol) in THF (1 mL) was added dropwise to a 28 mL vial that contained a stirred solution of [$RhMe(PMe_3)_4$] (0.0207 g, 0.049 mmol) in THF (1 mL) and the resulting solution was stirred for 5 min to give the **5** in THF solution. A solution of 4,4'-bis-(4-carbo-*n*-octyloxylphenylethynyl)diphenyl-buta-1,3-diyne (0.0701 g, 0.098 mmol) in THF (2 mL) was then added and the reaction was stirred for 5 min, and then the solvent was removed *in vacuo*. THF (2 mL) was added again, the solution was stirred for 5 min and the solvent was removed *in vacuo* again. This cycle was repeated one more time, and then THF (3 mL) was added and the solution was stirred for 15 h at room temperature. The solvent was removed *in vacuo* and the compound was washed with hexane, and dried *in vacuo* yielding **6(a)** as a dark red solid. Yield: 0.068 g,

75%. ^{1}H NMR (400 MHz, C_6D_6) δ: 8.03 (d, *J* = 8 Hz, 4H, CH_{arom}), 8.00 (d, *J* = 8 Hz, 4H, CH_{arom}), 7.67 (d, *J* = 8 Hz, 2H, CH_{arom}), 7.56 (d, *J* = 8 Hz, 2H, CH_{arom}), 7.52 (d, *J* = 8 Hz, 2H, CH_{arom}), 7.46 (d, *J* = 8 Hz, 2H, CH_{arom}), 7.38 (d, *J* = 8 Hz, 4H, CH_{arom}) 7.35 (d, *J* = 8 Hz, 4H, CH_{arom}), 7.32 (d, *J* = 8 Hz, 4H, CH_{arom}), 7.22 (d, *J* = 8 Hz, 2H, CH_{arom}), 7.15 (d, *J* = 8 Hz, 2H, CH_{arom}), 4.13 (t, *J* = 8 Hz, 8H, OCH_2), 1.47 (m, 8H, OCH_2CH_2), 1.36 (d, J_{P-H} = 8 Hz, 9H, PMe_3 *trans* to Cα), 1.28 (vt, J_{P-H} = 3 Hz, 18H, PMe_3 *trans* to PMe_3), 1.19 (m, 40H, CH_2), 0.84 (t, *J* = 7 Hz, 12H, 4 x CH_3), 0.32 (s, 9H, $Si(CH_3)_3$). ^{31}P{^{1}H} NMR (162 MHz, C_6D_6) δ: -9.19 (dd, J_{Rh-P} = 97 Hz, J_{P-P} = 31 Hz, 2P), -22.93 (dt, J_{Rh-P} = 82 Hz, J_{P-P} = 31 Hz, 1P). Anal. Calcd. for $C_{114}H_{136}O_8P_3RhSi$: C, 73.68; H, 7.38. Found: C, 73.82; H, 7.41%. MS (ES^+) *m/z*: 1858 [M^+]. IR (KBr) υ_{C-H} = 2952, 2923, 2853, $\upsilon_{C\equiv C}$ = 2211, 2128, 2022, $\upsilon_{ester(C=O)}$ = 1716, υ_{Ar} = 1594 cm^{-1}.

6(b) – *mer*,*cis*-[tris(trimethylphosphine)trimethylsilylethynyl-2,5-bis[4-(4-di-*N*,*N*-*n*-hexylaminophenylethynyl)phenylethynyl]-3,4-bis[4-(4-di-*n*-hexylaminophenyl)ethynyl-phenyl)]rhodacyclopenta-2,4-diene]

TMSA (8 μL, 0.058 mmol) in THF (1 mL) was added dropwise to a 28 mL vial that contained a stirred solution of [$RhMe(PMe_3)_4$] (0.0207 g, 0.049 mmol) in THF (1 mL) and the resulting solution was stirred for 5 min to give the **5** in THF solution. A solution of 4,4'-bis-(4-di-*N*,*N*-*n*-hexylaminophenylethynyl)diphenylbuta-1,3-diyne (0.0754 g, 0.098 mmol) in THF (3 mL) was added and the reaction was stirred for 5 min and then the solvent was removed *in vacuo*. THF (3 mL) was added, the solution was stirred for 5 min and the solvent was removed *in vacuo* again. This cycle was repeated one more time, and then THF (3 mL) was added and the solution was stirred for 15 h at room

temperature. The solvent was removed *in vacuo*, washed with hexane, and dried *in vacuo* yielding **6(b)** as a red solid. Yield: 0.057 g, 59%. ^{1}H NMR (400 MHz, C_6D_6) δ: 7.68 (d, *J* = 8 Hz, 2H, CH_{arom}), 7.63 (d, *J* = 8 Hz, 2H, CH_{arom}), 7.60 (d, *J* = 8Hz, 2H, CH_{arom}), 7.59 (d, *J* = 8 Hz, 4H, CH_{arom}), 7.55 (d, *J* = 8 Hz, 2H, CH_{arom}), 7.52 (d, *J* = 8 Hz, 2H, CH_{arom}), 7.50 (d, *J* = 8 Hz, 2H, CH_{arom}), 7.42 (d, *J* = 8 Hz, 2H, CH_{arom}), 7.33 (d, *J* = 8 Hz, 2H, CH_{arom}) 7.23 (d, *J* = 8 Hz, 2H, CH_{arom}), 7.15 (d, *J* = 8 Hz, 2H, CH_{arom}), 6.52 (d, *J* = 8 Hz, 4H, CH_{arom}), 6.49 (d, *J* = 8 Hz, 4H, CH_{arom}), 2.95 (t, *J* = 8 Hz, 16H, 4 x $N(CH_2)_2$), 1.38 (d, $J_{P\text{-}H}$ = 8 Hz, 9H, PMe_3 *trans* to C-α), 1.28 (vt, $J_{P\text{-}H}$ = 3 Hz, 18H, PMe_3 *trans* to PMe_3), 1.23 (quint, 16H, 4 x $N(CH_2CH_2)_2$), 1.11 (m, 48H, CH_2), 0.88 (t, *J* = 3 Hz, 24H, 8 x CH_3), 0.34 (s, 9H, $Si(CH_3)_3$). ^{31}P{^{1}H} NMR (81 MHz, C_6D_6) δ: -9.06 (dd, $J_{Rh\text{-}P}$ = 98 Hz, $J_{P\text{-}P}$ = 31 Hz, 2P), -23.11 (dt, $J_{Rh\text{-}P}$ = 82 Hz, $J_{P\text{-}P}$ = 31 Hz, 1P). Anal. Calcd. for $C_{126}H_{172}N_4P_3RhSi$: C, 76.95; H, 8.82; N, 2.85. Found: C, 76.64; H, 8.71; N, 3.19%. MS (ES^+) *m/z*: 1965 [M^+]. IR (KBr) $\upsilon_{C\text{-}H}$ = 2952, 2923, 2853, $\upsilon_{C\equiv C}$ = 2202, 2130, 2020, υ_{Ar} = 1607 cm^{-1}.

3.4.7 Preparation of second-generation TMSE-rhodacyclopentadienes

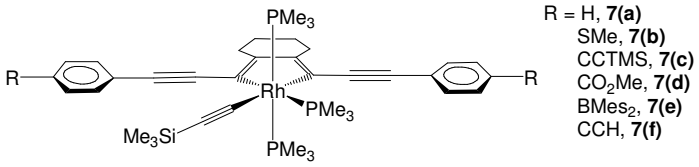

7(a) – *mer*,*cis*-[tris(trimethylphosphine)trimethylsilylethynyl-2,5-bis(phenylethynyl)-3,4-μ-tetramethylenerhodacyclopenta-2,4-diene]

TMSA (8 μL, 0.058 mmol) in THF (1 mL) was added dropwise to a 28 mL vial that contained a stirred solution of [$RhMe(PMe_3)_4$] (0.0207 g, 0.049 mmol) in THF (1 mL)

and the resulting solution was stirred for 5 min. A solution of 1,12-diphenyldodeca-1,3,9,11-tetrayne (0.0150 g, 0.049 mmol) in THF (1 mL) was added and the reaction was stirred for 5 min, and then the solvent was removed *in vacuo*. THF (2 mL) was added, the solution was stirred for 5 min and the solvent was removed *in vacuo* again. This cycle was repeated one more time and then, THF (2 mL) was added and the solution was stirred for 15 h at room temperature. The THF solvent was removed *in vacuo* and hexane (1 mL) was added to the residue and removed *in vacuo*; this process was repeated two more times in order to remove completely the residual THF. The hexane was removed *in vacuo* giving the product **7(a)** as a yellow solid, which was recrystallised from C_6D_6 and hexane. Yield: 0.021 g, 58%. ^{1}H NMR (500 MHz, C_6D_6) δ: 7.86 (d, J = 8 Hz, 2H, CH_{arom}), 7.41 (d, J = 8 Hz, 2H, CH_{arom}), 7.18 (t, J = 8 Hz, 2H, CH_{arom}), 7.13 (t, J = 8 Hz, 3H, CH_{arom}), 7.00 (t, J = 8 Hz, 1H, CH_{arom}), 2.93 (m, 4H, CH_2-C=C), 1.65 (m, 4H, CH_2), 1.36 (d, J_{P-H} = 8 Hz, 9H, PMe_3 *trans* to Cα), 1.20 (vt, J = 3 Hz, 18H, PMe_3 *trans* to PMe_3), 0.33 (s, 9H; $Si(CH_3)_3$). $^{31}P\{^1H\}$ NMR (162 MHz, C_6D_6) δ: -7.85 (dd, J_{Rh-P} = 99 Hz, J_{P-P} = 31 Hz, 2P, PMe_3), -22.52 (dt, J_{Rh-P} = 83 Hz, J_{P-P} = 31 Hz, 1P, PMe_3). Anal. Calcd. for $C_{38}H_{54}P_3RhSi$: C, 62.12; H, 7.41. Found: C, 62.36; H, 7.25%. MS (MALDI$^+$) *m/z* = 734 [M^+], 658 [M^+ - PMe_3]. IR (KBr) $\upsilon_{C\equiv C}$ = 2124, 2010, υ_{Ar} = 1590, 1418 cm^{-1}.

7(b) – *mer*,*cis*-[tris(trimethylphosphine)trimethylsilylethynyl-2,5-bis(*p*-methylthio phenylethynyl)-3,4-μ-tetramethylenerhodacyclopenta-2,4-diene]

TMSA (8 μL, 0.058 mmol) in THF (1 mL) was added dropwise to a 28 mL vial that contained a stirred solution of [$RhMe(PMe_3)_4$] (0.0207 g, 0.049 mmol) in THF (1 mL) and the resulting solution was stirred for 5 min. A solution of 1,12-bis(*p*-

methylthiophenyl)dodeca-1,3,9,11-tetrayne (0.0195 g, 0.049 mmol) in THF (1 mL) was added, the reaction was stirred for 5 min and then the solvent was removed *in vacuo*. THF (2 mL) was added, the solution was stirred for 5 min and the solvent was removed *in vacuo* again. This cycle was repeated one more time and then, THF (2 mL) was added and the solution was stirred for 15 h at room temperature. The THF solvent was removed *in vacuo*, hexane (1 mL) was added to the residue and removed *in vacuo*, and this process was repeated two more times in order to remove completely the residual THF. The hexane was removed *in vacuo* giving **7(b)** as an orange solid, which was recrystallised from THF and hexane. Yield: 0.024 g, 59%. ^{1}H NMR (400 MHz, C_6D_6) δ: 7.81 (d, J = 8 Hz, 2H, CH_{arom}), 7.33 (d, J = 8 Hz, 2H, CH_{arom}), 7.22 (d, J = 8 Hz, 2H, CH_{arom}), 7.12 (d, J = 8 Hz, 2H, CH_{arom}), 2.98 (m, 2H, CH_2-C=C), 2.95 (m, 2H, CH_2-C=C), 1.97 (s, 3H, SCH_3), 1.94 (s, 3H, SCH_3), 1.69 (m, 4H, CH_2), 1.40 (d, $J_{P\text{-}H}$ = 8 Hz, 9H, PMe_3 *trans* to Cα), 1.23 (vt, $J_{P\text{-}H}$ = 3 Hz, 18H, PMe_3 *trans* to PMe_3), 0.37 (s, 9H, $Si(CH_3)_3$). $^{31}P\{^{1}H\}$ NMR (162 MHz, C_6D_6) δ: -7.86 (dd, $J_{Rh\text{-}P}$ = 99 Hz, $J_{P\text{-}P}$ = 31 Hz, 2P), -22.41 (dt, $J_{Rh\text{-}P}$ = 84 Hz, $J_{P\text{-}P}$ = 31 Hz, 1P). Anal. Calcd. for $C_{40}H_{58}P_3RhS_2Si$: C, 58.10; H, 7.07. Found: C, 58.51; H, 7.02%. MS (MALDI$^+$) *m/z* = 826 [M^+]. IR (KBr) $\upsilon_{C\equiv C}$ = 2124, 2011, υ_{Ar} = 1558, 1487 cm^{-1}.

7(c) – *mer*,*cis*-[tris(trimethylphosphine)trimethylsilylethynyl-2,5-bis(*p*-trimethylsilyl ethynylphenylethynyl)-3,4-μ-tetramethylenerhodacyclopenta-2,4-diene]

TMSA (17.5 μL, 0.123 mmol) in THF (1 mL) was added dropwise to a 28 mL vial that contained a stirred solution of [$RhMe(PMe_3)_4$] (0.0498 g, 0.118 mmol) in THF (2 mL) and the resulting solution was stirred for 5 min. A solution of 1,12-bis(*p*-

trimethylsilylethynylphenyl)dodeca-1,3,9,11-tetrayne (0.0589 g, 0.118 mmol) in THF (2 mL) was added, the reaction was stirred for 5 min and then the solvent was removed *in vacuo*. THF (2 mL) was added, the solution was stirred for 5 min and the solvent was removed *in vacuo* again. This cycle was repeated one more time and then, THF (2 mL) was added and the solution was stirred for 15 h at room temperature. The THF solvent was removed *in vacuo*, hexane (2 mL) was added to the residue and removed *in vacuo*, and this process was repeated two more times in order to remove completely the residual THF. The hexane was removed *in vacuo* giving **7(c)** as an orange solid, which was purified via recrystallisation from THF and hexane. Yield: 0.043 g, 39%. ^{1}H NMR (400 MHz, C_6D_6) δ: 7.69 (d, J = 8 Hz, 2H, CH_{arom}), 7.52 (d, J = 8 Hz, 2H, CH_{arom}), 7.48 (d, J = 8 Hz, 2H, CH_{arom}), 7.21 (d, J = 8 Hz, 2H, CH_{arom}), 2.87 (m, 2H, CH_2-C=C), 2.82 (m, 2H, CH_2-C=C), 1.61 (m, 4H, CH_2), 1.26 (d, $J_{P\text{-}H}$ = 8 Hz, 9H, PMe_3 *trans* to Cα), 1.11 (vt, $J_{P\text{-}H}$ = 3 Hz, 18H, PMe_3 *trans* to PMe_3), 0.25 (s, 9H, $Si(CH_3)_3$), 0.21 (s, 9H, $Si(CH_3)_3$), 0.19 (s, 9H, $Si(CH_3)_3$). ^{31}P{^{1}H} NMR (162 MHz, C_6D_6) δ: -8.02 (dd, $J_{Rh\text{-}P}$ = 99 Hz, $J_{P\text{-}P}$ = 31 Hz, 2P), -22.51 (dt, $J_{Rh\text{-}P}$ = 83 Hz, $J_{P\text{-}P}$ = 31 Hz, 1P). Anal. Calcd. for $C_{48}H_{70}P_3RhSi_3$: C, 62.18; H, 7.61. Found: C, 61.61; H, 7.55%. MS (ES^+) *m/z* = 926 [M^+]. IR (KBr) $\upsilon_{C\text{-}H}$ = 2952, 2907, $\upsilon_{C\equiv C}$ = 2125, 2019, υ_{Ar} = 1592, 1491 cm^{-1}.

7(d) – *mer*,*cis*-[tris(trimethylphosphine)trimethylsilylethynyl-2,5-bis(*p*-carbomethoxy phenylethynyl)-3,4-μ-tetramethylenerhodacyclopenta-2,4-diene]

TMSA (8 μL, 0.058 mmol) in THF (1 mL) was added dropwise to a 28 mL vial that contained a stirred solution of [$RhMe(PMe_3)_4$] (0.0207 g, 0.049 mmol) in THF (1 mL) and the resulting solution was stirred for 5 min. A solution of 1,12-bis(*p*-

carbomethoxyphenyl)dodeca-1,3,9,11-tetrayne (0.0207 g, 0.049 mmol) in THF (1 mL) was added, the reaction was stirred for 5 min and then the solvent was removed *in vacuo*. THF (2 mL) was added, the solution was stirred for 5 min and the solvent was removed *in vacuo* again. This cycle was repeated one more time, and then THF (2 mL) was added and the solution was stirred for 15 h at room temperature. The THF solvent was removed *in vacuo*, hexane (1 mL) was added to the residue and removed *in vacuo*, and this process was repeated two more times in order to remove completely the residual THF. The hexane was removed *in vacuo* giving **7(d)** as a red solid, which was purified by recrystallisation from THF and hexane. Yield: 0.026 g, 62%. ^{1}H NMR (400 MHz, C_6D_6) δ: 8.25 (d, J = 8 Hz, 2H, CH_{arom}), 8.18 (d, J = 8 Hz, 2H, CH_{arom}), 7.87 (d, J = 8 Hz, 2H, CH_{arom}), 7.38 (d, J = 8 Hz, 2H, CH_{arom}), 3.50 (s, 3H, CO_2CH_3), 3.45 (s, 3H, CO_2CH_3), 2.92 (m, 2H, CH_2-C=C), 2.88 (m, 2H, CH_2-C=C), 1.66 (m, 4H, CH_2), 1.32 (d, $J_{P\text{-}H}$ = 8 Hz, 9H, PMe_3 *trans* to Cα), 1.17 (vt, $J_{P\text{-}H}$ = 3 Hz, 18H, PMe_3 *trans* to PMe_3), 0.33 (s, 9H, $Si(CH_3)_3$). ^{31}P{^{1}H} NMR (162 MHz, C_6D_6) δ: -8.05 (dd, $J_{Rh\text{-}P}$ = 98 Hz, $J_{P\text{-}P}$ = 31 Hz, 2P), -22.41 (dt, $J_{Rh\text{-}P}$ = 83 Hz, $J_{P\text{-}P}$ = 31 Hz, 1P). Anal. Calcd. for $C_{42}H_{58}O_4P_3RhSi$: C, 59.29; H, 6.87. Found: C, 59.53; H, 6.96%. MS (MALDI^{+}) *m/z* = 850 [M^{+}]. IR (KBr) $\upsilon_{C\equiv C}$ = 2121, 2018, $\upsilon_{ester(C=O)}$ = 1718, υ_{Ar} = 1596, 1435 cm^{-1}.

7(e) – *mer*,*cis*-[tris(trimethylphosphine)trimethylsilylethynyl-2,5-bis(*p*-dimesitylboryl phenylethynyl)-3,4-μ-tetramethylenerhodacyclopenta-2,4-diene]

TMSA (8 μL, 0.058 mmol) in THF (1 mL) was added dropwise to a 28 mL vial that contained a stirred solution of [$RhMe(PMe_3)_4$] (0.0207 g, 0.049 mmol) in THF (1 mL) and the resulting solution was stirred for 5 min. A solution of 1,12-bis(*p*-dimesitylboryl

phenyl)dodeca-1,3,9,11-tetrayne (0.0393 g, 0.049 mmol) in THF (1 mL) was added and the reaction was stirred for 5 min and then the solvent was removed *in vacuo*. THF (2 mL) was added, the solution was stirred for 5 min and the solvent was removed *in vacuo* again. This cycle was repeated one more time and then, THF (2 mL) was added and the solution was stirred for 15 h at room temperature. The THF solvent was removed *in vacuo*, hexane (1 mL) was added to the residue and removed *in vacuo*, and this process was repeated two more times in order to remove completely the residual THF. The hexane was removed *in vacuo* giving **7(e)** as a maroon solid, which was purified by washing with hexane (3 x 1 mL). Yield: 0.024 g, 40%. ^{1}H NMR (400 MHz, C_6D_6) δ: 7.88 (d, J = 8 Hz, 2H, CH_{arom}), 7.79 (d, J = 8 Hz, 2H, CH_{arom}), 7.70 (d, J = 8 Hz, 2H, CH_{arom}), 7.43 (d, J = 8 Hz, 2H, CH_{arom}), 6.82 (s, 4H, CH_{arom}), 6.79 (s, 4H, CH_{arom}), 2.91 (m, 4H, CH_2-C≡C), 2.20 (s, 12H, Ar-CH_3), 2.18 (s, 24H, Ar-CH_3), 1.63 (m, 4H, CH_2), 1.37 (d, $J_{P\text{-}H}$ = 8 Hz, 9H, PMe_3 *trans* to Cα), 1.17 (vt, $J_{P\text{-}H}$ = 3 Hz, 18H, PMe_3 *trans* to PMe_3), 0.28 (s, 9H, $Si(CH_3)_3$). ^{31}P{^{1}H} NMR (162 MHz, C_6D_6) δ: -8.06 (dd, $J_{Rh\text{-}P}$ = 98 Hz, $J_{P\text{-}P}$ = 31 Hz, 2P), -22.43 (dt, $J_{Rh\text{-}P}$ = 83 Hz, $J_{P\text{-}P}$ = 31 Hz, 1P). Anal. Calcd. for $C_{74}H_{96}B_2P_3RhSi$: C, 72.20; H, 7.86. Found: C, 71.85; H, 8.01%. MS (ES^+) *m/z* = 1230 [M^+]. IR (KBr) $\upsilon_{C\equiv C}$ = 2122, 2044, υ_{Ar} = 1586, 1420 cm^{-1}.

7(f) – *mer*,*cis*-[tris(trimethylphosphine)trimethylsilylethynyl-2,5-bis(*p*-ethynylphenyl ethynyl)-3,4-μ-tetramethylenerhodacyclopenta-2,4-diene]

A 1.0 M THF solution of (n-Bu_4N)F (0.172 mL, 0.172 mmol) was added to a rapidly stirred solution of **7(c)** (0.0399 g, 0.043 mmol) in THF (3 mL). The solution was stirred for 15 h at room temperature and then the solvent was removed *in vacuo*. The residual

solid was dissolved in CH_2Cl_2 (5 mL) and then the solution was washed with water (5 x 10 mL). The organic layer was separated and dried over $MgSO_4$. The solvent was removed *in vacuo* to give the product as an orange solid. Yield: 0.016 g, 48%, ^{1}H NMR (400 MHz, C_6D_6) δ: 7.69 (d, J = 8 Hz, 2H, CH_{arom}), 7.47 (d, J = 8 Hz, 2H, CH_{arom}), 7.40 (d, J = 8 Hz, 2H, CH_{arom}), 7.19 (d, J = 8 Hz, 2H, CH_{arom}), 2.88 (m, 2H, CH_2-C=C), 2.84 (m, 2H, CH_2-C=C), 2.79 (s, 1H, C≡CH), 2.74 (s, 1H, C≡CH), 1.62 (m, 4H, CH_2), 1.27 (d, J_{P-H} = 8 Hz, 9H, PMe_3 *trans* to Cα), 1.13 (vt, J_{P-H} = 4 Hz, 18H, PMe_3 *trans* to PMe_3), 0.28 (s, 9H, $Si(CH_3)_3$). $^{31}P\{^1H\}$ NMR (162 MHz, C_6D_6) δ: -8.01 (dd, J_{Rh-P} = 98 Hz, J_{P-P} = 31 Hz, 2P), -22.48 (dt, J_{Rh-P} = 84 Hz, J_{P-P} = 31 Hz, 1P). Anal. Calcd. for $C_{42}H_{54}P_3RhSi$: C, 64.44; H, 6.95. Found: C, 64.97; H, 7.19%. MS (ES^+) *m/z* = 782 [M^+]. IR (KBr) υ_{C-H} = 2907, $\upsilon_{C\equiv C}$ = 2124, 2012, υ_{Ar} = 1594, 1492 cm^{-1}.

3.4.8 Preparation of second-generation Me-rhodacyclopentadienes

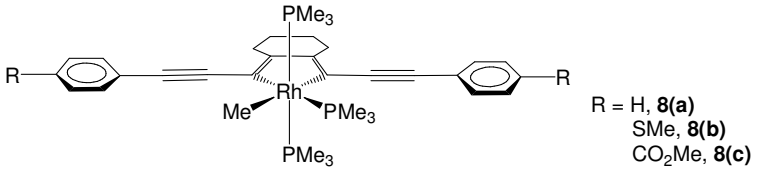

8(a) – *mer*,*cis*-[tris(trimethylphosphine)methyl-2,5-bis(phenylethynyl)-3,4-μ-tetramethylenerhodacyclopenta-2,4-diene]

1,12-biphenyldodeca-1,3,9,11-tetrayne (0.0150 g, 0.049 mmol) in THF (1 mL) was added to a stirred solution of [$RhMe(PMe_3)_4$] (0.0207 g, 0.049 mmol) in THF (1 mL). The reaction was stirred for 5 min and the solvent was removed *in vacuo*. THF (2 mL) was added, the solution was stirred for 5 min and the solvent was removed *in vacuo*

again. This cycle was repeated one more time and then, THF (2 mL) was added and the solution was stirred for 4 h at room temperature. The THF solvent was removed *in vacuo*, hexane (1 mL) was added to the residue and removed *in vacuo*, and this process was repeated two more times in order to remove completely the residual THF. The hexane was removed *in vacuo* giving **8(a)** as a yellow-orange solid, which was purified by recrystallisation from THF and hexane. Yield: 0.025 g, 78%. ^{1}H NMR (400 MHz, C_6D_6) δ: 7.71 (d, J = 8 Hz, 2H, CH_{arom}), 7.45 (d, J = 8 Hz, 2H, CH_{arom}), 7.12 (t, J = 8 Hz, 2H, CH_{arom}), 7.07 (t, J = 8 Hz, 2H, CH_{arom}), 6.98 (t, J = 8 Hz, 1H, CH_{arom}), 6.94 (t, J = 8 Hz, 1H, CH_{arom}), 3.02 (m, 4H, CH_2-C=C), 1.71 (m, 4H, CH_2), 1.23 (d, J_{P-H} = 7 Hz, 9H, PMe_3 *trans* to Cα), 1.02 (vt, J_{P-H} = 3 Hz, 18H, PMe_3 *trans* to PMe_3), -0.05 (dq, $^{2}J_{Rh-H}$ = 2 Hz, $^{3}J_{P-H}$ = 8 Hz, 3H, CH_3-Rh). ^{31}P{^{1}H} NMR (162 MHz, C_6D_6) δ: -5.12 (dd, J_{Rh-P} = 106 Hz, J_{P-P} = 33 Hz, 2P), -17.87 (dt, J_{Rh-P} = 90 Hz, J_{P-P} = 33 Hz, 1P). Anal. Calcd. for $C_{34}H_{48}P_3Rh$: C, 62.58; H, 7.41. Found: C, 62.20; H, 7.39%. MS (ES^+) m/z = 637 [M^+ - CH_3]. IR (KBr) υ_{C-H} = 2907, $\upsilon_{C\equiv C}$ = 2114, υ_{Ar} = 1586, 1416 cm^{-1}.

8(b) – *mer*,*cis*-[tris(trimethylphosphine)methyl-2,5-bis(*p*-methylthiophenylethynyl)-3,4-μ-tetramethylenerhodacyclopenta-2,4-diene]

1,12-bis(*p*-methylthiophenyl)dodeca-1,3,9,11-tetrayne (0.0195 g, 0.049 mmol) in THF (1 mL) solution was added to a stirred solution of [$RhMe(PMe_3)_4$] (0.0207 g, 0.049 mmol) in THF (1 mL). The reaction was stirred for 5 min and the solvent was removed *in vacuo*. THF (2 mL) was added, the solution was stirred for 5 min and the solvent was removed *in vacuo* again. This cycle was repeated one more time and then, THF (2 mL) was added and the solution was stirred for 15 h at room temperature. The THF solvent

was removed *in vacuo*, hexane (1 mL) was added to the residue and removed *in vacuo*, and this process was repeated two more times in order to remove completely the residual THF. The hexane was removed *in vacuo* giving **8(b)** as an orange solid, which was purified by recrystallisation from THF and hexane. Yield: 0.029 g, 80%. ^{1}H NMR (400 MHz, C_6D_6) δ: 7.63 (d, J = 8 Hz, 2H, CH_{arom}), 7.38 (d, J = 8 Hz, 2H, CH_{arom}), 7.14 (d, J = 8 Hz, 2H, CH_{arom}), 7.07 (d, J = 8 Hz, 2H, CH_{arom}), 3.05 (m, 4H, CH_2-C=C), 1.98 (s, 3H, SCH_3), 1.93 (s, 3H, SCH_3), 1.75 (m, 4H, CH_2), 1.28 (d, $J_{P\text{-}H}$ = 7 Hz, 9H, PMe_3 *trans* to Cα), 1.06 (vt, $J_{P\text{-}H}$ = 3 Hz, 18H, PMe_3 *trans* to PMe_3), 0.01 (dq, $^{2}J_{Rh\text{-}H}$ = 2 Hz, $^{2}J_{P\text{-}H}$ = 8 Hz, 3H, CH_3-Rh). ^{31}P{^{1}H} NMR (162 MHz, C_6D_6) δ: -5.14 (dd, $J_{Rh\text{-}P}$ = 106 Hz, $J_{P\text{-}P}$ = 33 Hz, 2P), -17.82 (dt, $J_{Rh\text{-}P}$ = 90 Hz, $J_{P\text{-}P}$ = 33 Hz, 1P). Anal. Calcd. for $C_{36}H_{52}P_3RhS_2$: C, 58.06; H, 7.04. Found: C, 58.16; H, 7.05%. MS (ES^+) *m/z* = 744 [M^+]. IR (KBr) $\upsilon_{C\text{-}H}$ = 2909, $\upsilon_{C\equiv C}$ = 2117, υ_{Ar} = 1581, 1428 cm^{-1}.

8(c) – *mer*,*cis*-[tris(trimethylphosphine)methyl-2,5-bis(*p*-carbomethoxyphenylethynyl)-3,4-μ-tetramethylenerhodacyclopenta-2,4-diene]

1,12-bis(*p*-carbomethoxyphenyl)dodeca-1,3,9,11-tetrayne (0.0207 g, 0.049 mmol) in THF (1 mL) solution was added to a stirred solution of [$RhMe(PMe_3)_4$] (0.0207 g, 0.049 mmol) in THF (1 mL). Then, the reaction was stirred for 5 min and the solvent was removed *in vacuo*. THF (2 mL) was added, the solution was stirred for 5 min and the solvent was removed *in vacuo* again. This cycle was repeated one more time and then, THF (2 mL) was added and the solution was stirred for 15 h at room temperature. The THF solvent was removed *in vacuo*, hexane (1 mL) was added to the residue and removed *in vacuo*, and this process was repeated two more times in order to remove

completely the residual THF. The hexane was removed *in vacuo* giving **8(c)** as a dark-red solid, which was purified by recrystallisation from THF and hexane. Yield: 0.030 g, 80%. ^{1}H NMR (400 MHz, C_6D_6) δ: 8.19 (d, J = 8 Hz, 2H, CH_{arom}), 8.13 (d, J = 8 Hz, 2H, CH_{arom}), 7.69 (d, J = 8 Hz, 2H, CH_{arom}), 7.43 (d, J = 8 Hz, 2H, CH_{arom}), 3.50 (s, 3H, CO_2CH_3), 3.45 (s, 3H, CO_2CH_3), 2.98 (m, 4H, CH_2-C=C), 1.72 (m, 4H, CH_2), 1.20 (d, J_{P-H} = 8 Hz, 9H, PMe_3 *trans* to Cα), 0.99 (vt, J_{P-H} = 3 Hz, 18H, PMe_3 *trans* to PMe_3), -0.05 (dq, $^{2}J_{Rh-H}$ = 2 Hz, $^{3}J_{P-H}$ = 8 Hz, 3H, CH_3-Rh). ^{31}P{^{1}H} NMR (162 MHz, C_6D_6) δ: -5.49 (dd, J_{Rh-P} = 105 Hz, J_{P-P} = 33 Hz, 2P), -17.95 (dt, J_{Rh-P} = 90 Hz, J_{P-P} = 33 Hz, 1P). Anal. Calcd. for $C_{38}H_{52}O_4P_3Rh$: C, 59.38; H, 6.82. Found: C, 59.37; H, 6.80%. MS (ES^+) *m/z* = 752 [M^+ - CH_3]. IR (KBr) υ_{C-H} = 2912, $\upsilon_{C\equiv C}$ = 2112, $\upsilon_{ester(C=O)}$ = 1712, υ_{Ar} = 1593, 1432 cm^{-1}.

3.4.9 Preparation of *trans*-[bis(trimethylphosphine)-μ-η^2-succinato-2,5-bis(*p*-di-*N*,*N*-methylaminophenylethynyl)-3,4-(*p*-di-*N*,*N*-methylaminophenyl)rhodacyclo-penta-2,4-diene] dimer [9(b)]

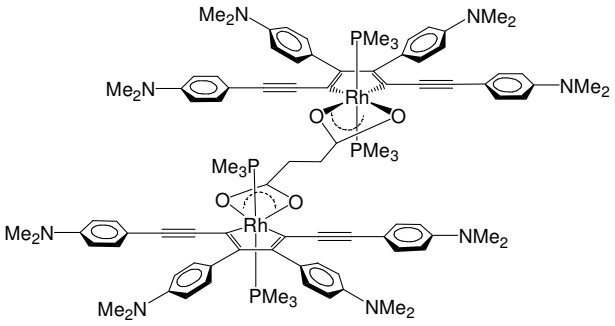

In a N_2 filled glovebox, succinic acid (0.0013 g, 0.011 mmol) was added into a stirred toluene solution of **4** (0.0203 g, 0.022 mmol) in a Young's tube. The Young's tube was then removed from the glovebox and heated at 50 °C. The progress of the reaction was

monitored by $^{31}P\{^{1}H\}$ NMR spectroscopy using C_6D_6/THF, and the solvent was removed *in vacuo* and refilled repeatedly until the *in situ* $^{31}P\{^{1}H\}$ NMR spectrum showed full conversion to **9(b)**. The solvent was removed *in vacuo*, hexane (1 mL) was added to the residue and removed *in vacuo*, and this process was repeated five more times in order to remove completely the residual toluene. Then, the hexane was removed *in vacuo* to give a yellow-orange solid. Yield: 0.0162 g, 84%. ^{1}H NMR (700 MHz, THF-d_8) δ: 7.28 (d, J = 8 Hz, 8H, CH_{arom}), 7.03 (d, J = 8 Hz, 8H, CH_{arom}), 6.62 (d, J = 8 Hz, 8H, CH_{arom}), 6.52 (d, J = 8 Hz, 8H, CH_{arom}), 2.92 (s, 24H, 4 x $N(CH_3)_2$), 2.87 (s, 28H, 4 x $N(CH_3)_2$ and 2 x CH_2), 1.25 (br, s, 36H, 4 x PMe_3). $^{31}P\{^{1}H\}$ NMR (162 MHz, THF-d_8) δ: -2.29 (d, $J_{Rh\text{-}P}$ = 116 Hz, 4P). Anal. Calcd. for $C_{96}H_{120}N_8O_4P_4Rh_2$: C, 64.79; H, 6.80; N, 6.30. Found: C, 63.61; H, 6.65; N, 6.29%. MS (ES^+) *m/z* = 890 $[M + 2H]^{2+}$, 904 $[M^+/2 + CH_2]$. IR (KBr) $\upsilon_{C\text{-}H}$ = 2904, $\upsilon_{C\equiv C}$ = 2131, υ_{Ar} = 1519, 1442 cm^{-1}.

3.4.10 Preparation of a η^1-benzoato-rhodium$^{(I)}$ complex and μ-η^1-succinato rhodium$^{(I)}$ dimer

10 – Tris(trimethylphosphine)-η^1-benzoato-rhodium$^{(I)}$

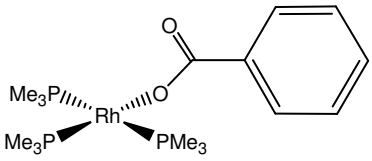

Benzoic acid (0.0116 g, 0.095 mmol) in a THF solution (1 mL) was added into a stirred solution of $[RhMe(PMe_3)_4]$ (0.0401 g, 0.095 mmol) in THF (1 mL), and the resulting solution was stirred at room temperature for 5 min, after which the solvent was removed *in vacuo*. THF (2 mL) was added, the solution was stirred for 2 min and the solvent was

removed *in vacuo* again. This cycle was repeated one more time, and then THF (2 mL) was added. The reaction was stirred at room temperature for 1 h, after which the solvent was removed *in vacuo* to give **10** as a yellow solid. The product was recrystallised in a Young's tube via slow diffusion of a layer of hexane into a concentrated THF solution of **10**. Yield: 0.038 g, 88%. ^{1}H NMR (400 MHz, C_6D_6) δ: 8.63 (d, J = 8 Hz, 2H, CH_{arom}), 7.32 (t, J = 8 Hz, 2H, CH_{arom}), 7.22 (t, J = 8 Hz, 1H, CH_{arom}), 1.11 (br, s, 18H, PMe_3 *trans* to PMe_3), 1.01 (br, s, 9H, PMe_3 *trans* to OCOPh). ^{31}P{^{1}H} NMR (202 MHz, 203 K, 10% C_6D_6 in THF) δ: 3.85 (dt, $J_{Rh\text{-}P}$ = 168 Hz, $J_{P\text{-}P}$ = 48 Hz, 1P), -9.55 (dd, $J_{Rh\text{-}P}$ =139 Hz, $J_{P\text{-}P}$ = 48 Hz, 2P).

13 – Tris(trimethylphosphine)-μ-η^{1}-succinato-rhodium$^{(I)}$ dimer

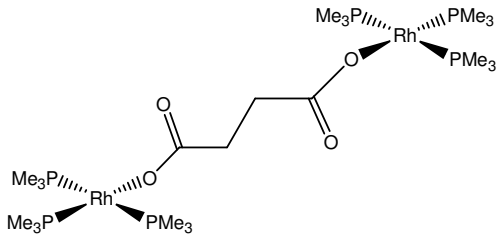

Succinic acid (0.0057 g, 0.048 mmol) in THF (1 mL) was added to a stirred solution of [RhMe(PMe_3)$_4$] (0.0405 g, 0.096 mmol) in THF (1 mL), and the resulting solution was stirred at room temperature for 5 min, after which the solvent was removed *in vacuo*. THF (2 mL) was added, the solution was stirred for 2 min and the solvent was removed *in vacuo* again. This cycle was repeated one more time, and then THF (2 mL) was added. The reaction was stirred at room temperature for 1 h, after which the solvent was removed *in vacuo* to give **13** as a yellow solid. The product was recrystallised in a Young's tube via slow diffusion of a layer of hexane into a concentrated THF solution of **13**. Yield: 0.035 g, 94%. ^{1}H NMR (200 MHz, C_6D_6) δ: 3.21 (br, s, 4H, 2 x CH_2), 1.12 (br,

s, 54H, 6 x PMe_3). $^{31}P\{^1H\}$ NMR (202 MHz, 203 K, 10% C_6D_6 in THF) δ: 3.41 (dt, $J_{Rh\text{-}P}$ = 168 Hz, $J_{P\text{-}P}$ = 45 Hz, 2P), -9.41 (dd, $J_{Rh\text{-}P}$ =143 Hz, $J_{P\text{-}P}$ = 45 Hz, 4P).

3.4.11 Preparation of η^1- and η^2-benzoato-rhodacyclopentadienes

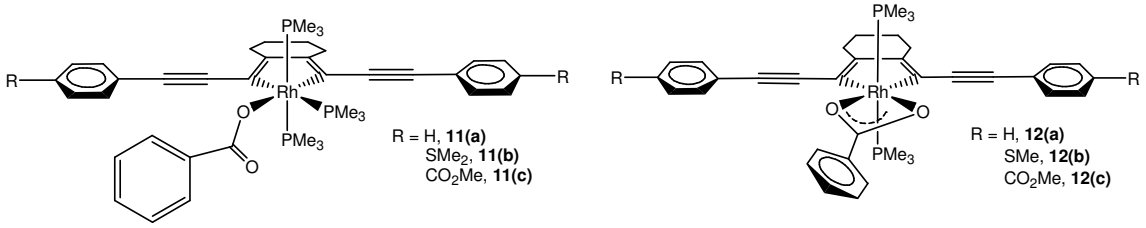

11(a) – *mer*,*cis*-[tris(trimethylphosphine)-η^1-benzoato-2,5-bis(phenylethynyl)-3,4-μ-tetramethylenerhodacyclopenta-2,4-diene]

The compound 1,12-diphenyldodeca-1,3,9,11-tetrayne (0.0291 g, 0.095 mmol) in THF was added to a stirred THF solution of **10** (0.0430 g, 0.095 mmol), which was obtained via *in situ* reaction of benzoic acid (0.0116 g, 0.095 mmol) and [$RhMe(PMe_3)_4$] (0.0401 g, 0.095 mmol). The resulting solution was stirred for 15 h at room temperature to give a mixture of the η^1-compound **11(a)** and η^2-compound **12(a)**. Compound **11(a)** was isolated in pure form via several recrystallisations from THF and hexane. Yield: 0.014 g, 19%. ^1H NMR (400 MHz, C_6D_6) δ: 8.55 (d, J = 8 Hz, 2H, CH_{arom}), 7.41 (d, J = 8 Hz, 2H, CH_{arom}), 7.38 (d, J = 8 Hz, 2H, CH_{arom}), 7.27 (t, J = 8 Hz, 2H, CH_{arom}), 7.22 (t, J = 8 Hz, 2H, CH_{arom}), 7.11 (t, J = 8 Hz, 2H, CH_{arom}), 6.96 (m, 3H, CH_{arom}), 2.93 (m, 2H, C=C-CH_2), 2.79 (m, 2H, C=C-CH_2), 1.63 (m, 4H, CH_2), 1.36 (d, $J_{P\text{-}H}$ = 8 Hz, 9H, PMe_3 *trans* to Cα), 1.27 (vt, $J_{P\text{-}H}$ = 4 Hz, 18H, PMe_3 *trans* to PMe_3). $^{31}P\{^1H\}$ NMR (162 MHz, C_6D_6) δ: -7.52 (dd, $J_{Rh\text{-}P}$ = 107 Hz, $J_{P\text{-}P}$ = 31 Hz, 2P), -18.86 (dt, $J_{Rh\text{-}P}$ = 91 Hz, $J_{P\text{-}P}$ = 31 Hz, 1P).

Anal. Calcd. for $C_{40}H_{50}P_3O_2Rh$: C, 63.33; H, 6.64. Found: C, 63.60; H, 6.48%. MS (ES^+) *m/z* = 759 [M + H^+]. IR (KBr) $\upsilon_{C\text{-}H}$ = 2909, 2850, $\upsilon_{C\equiv C}$ = 2135, $\upsilon_{C=O}$ = 1601, υ_{Ar} = 1566, 1485 cm^{-1}.

12(a) - *trans*-[bis(trimethylphosphine)-η^2-benzoato-2,5-bis(phenylethynyl)-3,4-μ-tetramethylenerhodacyclopenta-2,4-diene]

In a N_2 filled glovebox, the remaining mixture of **11(a)** and **12(a)** was added to toluene (3 mL) in a Young's tube, which was then sealed, removed from the glovebox and heated at 50 °C. The reaction progress was monitored *in situ* by $^{31}P\{^1H\}$ NMR spectroscopy and the toluene was removed *in vacuo* and refilled repeatedly until the *in situ* $^{31}P\{^1H\}$ NMR spectrum showed complete conversion to **12(a)**. The product was washed with hexane (5 x 1 mL) to give **12(a)** as a yellow-orange solid. Yield: 0.049 g, 76%. ^1H NMR (400 MHz, C_6D_6) δ: 8.52 (d, *J* = 8 Hz, 2H, CH_{arom}), 7.77 (d, *J* = 8 Hz, 4H, CH_{arom}), 7.20 (t, *J* = 8 Hz, 2H, CH_{arom}), 7.15 (t, *J* = 8 Hz, 2H, CH_{arom}), 7.09 (t, *J* = 8 Hz, 4H, CH_{arom}), 6.98 (t, *J* = 8 Hz, 1H, CH_{arom}), 2.85 (m, 4H, C≡C-CH_2), 1.60 (m, 4H, CH_2), 1.04 (vt, $J_{P\text{-}H}$ = 4 Hz, 18H, 2 x PMe_3). $^{31}P\{^1H\}$ NMR (162 MHz, C_6D_6) δ: -1.04 (d, $J_{Rh\text{-}P}$ = 115 Hz, 2P). Anal. Calcd. for $C_{37}H_{41}O_2P_2Rh$: C, 65.11; H, 6.05. Found: C, 64.96; H, 6.09%. MS ($MALDI^+$) *m/z* = 682 [M^+], 561 [M^+ - O_2CPh]. IR (KBr) $\upsilon_{C\text{-}H}$ = 2907, $\upsilon_{C\equiv C}$ = 2137, υ_{Ar} = 1594 cm^{-1}.

11(b) – *mer*,*cis*-[tris(trimethylphosphine)-η^1-benzoato-2,5-bis(*p*-methylthio-phenylethynyl)-3,4-μ-tetramethylenerhodacyclopenta-2,4-diene]

The compound 1,12-bis(*p*-methylthiophenyl)dodeca-1,3,9,11-tetrayne (0.0379 g, 0.095 mmol) in THF was added to a stirred THF solution of **10** (0.0430 g, 0.095 mmol), which

was obtained via *in situ* reaction of benzoic acid (0.0116 g, 0.095 mmol) and [RhMe(PMe_3)$_4$] (0.0401 g, 0.095 mmol). The resulting solution was stirred for 15 h at room temperature to give a mixture of η^1-compound **11(b)** and η^2-compound **12(b)**. Compound **11(b)** was isolated in pure form via several recrystallisations from THF and hexane. Yield: 0.012 g, 15%. ^{1}H NMR (400 MHz, C_6D_6) δ: 8.55 (d, *J* = 8 Hz, 2H, CH_{arom}), 7.29 (d, *J* = 8 Hz, 2H, CH_{arom}), 7.27 (m, 4H, CH_{arom}), 7.20 (t, *J* = 8 Hz, 1H, CH_{arom}), 7.07 (d, *J* = 8 Hz, 2H, CH_{arom}), 6.92 (d, *J* = 8 Hz, 2H, CH_{arom}), 2.94 (m, 2H, C=C-CH_2), 2.80 (m, 2H, C=C-CH_2), 1.94 (s, 3H, SCH_3), 1.87 (s, 3H, SCH_3), 1.64 (m, 4H, CH_2), 1.37 (d, $J_{P\text{-}H}$ = 8 Hz, 9H, PMe_3 *trans* to Cα), 1.29 (vt, $J_{P\text{-}H}$ = 4 Hz, 18H, PMe_3 *trans* to PMe_3). ^{31}P{^{1}H} NMR (162 MHz, C_6D_6) δ: -7.50 (dd, $J_{Rh\text{-}P}$ = 106 Hz, $J_{P\text{-}P}$ = 30 Hz, 2P), -18.77 (dt, $J_{Rh\text{-}P}$ = 91 Hz, $J_{P\text{-}P}$ = 30 Hz, 1P). Anal. Calcd. for $C_{42}H_{54}O_2P_3RhS_2$: C, 59.29; H, 6.40. Found: C, 59.08; H, 6.37%. MS (ES^+) *m/z* = 729 [M^+ - O_2CPh]. IR (KBr) $\upsilon_{C\text{-}H}$ = 2909, 2850, $\upsilon_{C\equiv C}$ = 2132, $\upsilon_{C=O}$ = 1609, υ_{Ar} = 1571, 1486 cm^{-1}.

12(b) - *trans*-[bis(trimethylphosphine)-η^2-benzoato-2,5-bis(*p*-methylthiophenylethynyl)-3,4-μ-tetramethylenerhodacyclopenta-2,4-diene]

In a N_2 filled glovebox, the remaining mixture of **11(b)** and **12(b)** was added to toluene (3 mL) in a Young's tube, which was then sealed, removed from the glovebox and heated at 50 °C. The reaction progress was monitored *in situ* by ^{31}P{^{1}H} NMR spectroscopy, and the toluene was removed *in vacuo* and refilled repeatedly until the *in situ* ^{31}P{^{1}H} NMR spectrum showed complete conversion to **12(b)**. The product was washed with hexane (5 x 1 mL) to give **12(b)** as an orange solid. Yield: 0.058 g, 79%. ^{1}H NMR (700 MHz, C_6D_6) δ: 8.51 (d, *J* = 8 Hz, 2H, CH_{arom}), 7.64 (d, *J* = 8 Hz, 4H, CH_{arom}), 7.22 (t, *J* = 8 Hz,

2H, CH_{arom}), 7.17 (t, J = 8 Hz, 1H, CH_{arom}), 7.05 (d, J = 8 Hz, 4H, CH_{arom}), 2.83 (m, 4H, C=C-CH_2), 1.90 (s, 6H, 2 x SCH_3), 1.61 (m, 4H, CH_2), 1.05 (vt, J_{P-H} = 4 Hz, 18H, 2 x PMe_3). $^{31}P\{^1H\}$ NMR (162 MHz, C_6D_6) δ: -0.91 (d, J_{Rh-P} = 115 Hz, 2P). Anal. Calcd. for $C_{39}H_{45}O_2P_2RhS_2$: C, 60.46; H, 5.85. Found: C, 60.27; H, 5.95%. MS ($MALDI^+$) *m/z* = 774 [M^+], 653 [M^+ - O_2CPh]. IR (KBr) υ_{C-H} = 2905, $\upsilon_{C\equiv C}$ = 2134, υ_{Ar} = 1591 cm^{-1}.

11(c) – *mer*,*cis*-[tris(trimethylphosphine)-η^1-benzoato-2,5-bis(*p*-carbomethoxyphenyl ethynyl)-3,4-μ-tetramethylenerhodacyclopenta-2,4-diene]

The compound 1,12-bis(carbomethoxyphenyl)dodeca-1,3,9,11-tetrayne (0.0401 g, 0.095 mmol) in THF solution was added to a stirred THF solution of compound **10** (0.0430 g, 0.095 mmol), which was obtained via *in situ* reaction of benzoic acid (0.0116 g, 0.095 mmol) and [$RhMe(PMe_3)_4$] (0.0401 g, 0.095 mmol). The resulting solution was stirred for 15 h at room temperature to give a mixture of η^1-compound **11(c)** and η^2-compound **12(c)**. Compound **11(c)** was isolated in pure form via several recrystallisations from THF and hexane. Yield: 0.013 g, 16%. ^1H NMR (400 MHz, C_6D_6) δ: 8.50 (d, J = 8 Hz, 2H, CH_{arom}), 8.14 (d, J = 8 Hz, 2H, CH_{arom}), 7.97 (d, J = 8 Hz, 2H, CH_{arom}), 7.35 (d, J = 8 Hz, 2H, CH_{arom}), 7.31 (d, J = 8 Hz, 2H, CH_{arom}), 7.26 (t, J = 8 Hz, 2H, CH_{arom}), 7.18 (t, J = 8, 1H, CH_{arom}), 3.49 (s, 3H, CO_2CH_3), 3.41 (s, 3H, CO_2CH_3), 2.88 (m, 2H, C=C-CH_2), 2.75 (m, 2H, C=C-CH_2), 1.61 (m, 4H, CH_2), 1.30 (d, J_{P-H} = 8 Hz, 9H, PMe_3 *trans* to Cα), 1.24 (vt, J_{P-H} = 4 Hz, 18H, PMe_3 *trans* to PMe_3). $^{31}P\{^1H\}$ NMR (162 MHz, C_6D_6) δ: -7.74 (dd, J_{Rh-P} = 106 Hz, J_{P-P} = 31 Hz, 2P), -18.82 (dt, J_{Rh-P} = 91 Hz, J_{P-P} = 31 Hz, 1P). Anal. Calcd. for $C_{44}H_{54}O_6P_3Rh$: C, 60.42; H, 6.22. Found: C, 60.25; H, 6.20%. MS (ES^+)

m/z = 874 [M^+]. IR (KBr) υ_{C-H} = 2912, $\upsilon_{C\equiv C}$ = 2129, $\upsilon_{ester(C=O)}$ = 1718, $\upsilon_{C=O}$ = 1598, υ_{Ar} = 1570, 1432 cm^{-1}.

12(c) - *trans*-[bis(trimethylphosphine)-η^2-benzoato-2,5-bis(*p*-carbomethoxy-phenylethynyl)-3,4-μ-tetramethylenerhodacyclopenta-2,4-diene]

In a N_2 filled glovebox, the remaining mixture of **11(c)** and **12(c)** was added to toluene (3 mL) in a Young's tube, which was then sealed, removed from the glovebox and heated at 50 °C. The reaction progress was monitored *in situ* by $^{31}P\{^1H\}$ NMR spectroscopy, and the toluene was removed *in vacuo* and refilled repeatedly until the *in situ* $^{31}P\{^1H\}$ NMR spectrum showed complete conversion to **12(c)**. The product was washed with hexane (5 x 1 mL) to give **12(c)** as a dark-red solid. Yield: 0.052 g, 69%. ^1H NMR (700 MHz, C_6D_6) δ: 8.48 (d, *J* = 8 Hz, 2H, CH_{arom}), 8.12 (d, *J* = 8 Hz, 4H, CH_{arom}), 7.71 (d, *J* = 8 Hz, 4H, CH_{arom}), 7.21 (t, *J* = 8 Hz, 2H, CH_{arom}), 7.18 (t, *J* = 8 Hz, 1H, CH_{arom}), 3.46 (s, 6H, 2 x CO_2CH_3), 2.80 (m, 4H, C=C-CH_2), 1.58 (m, 4H, CH_2), 0.99 (vt, J_{P-H} = 4 Hz, 18H, 2 x PMe_3). $^{31}P\{^1H\}$ NMR (162 MHz, C_6D_6) δ: -1.15 (d, J_{Rh-P} = 114 Hz, 2P). Anal. Calcd. for $C_{41}H_{45}O_6P_2Rh$: C, 61.66; H, 5.68. Found: C, 61.61; H, 5.79%. MS (MALDI$^+$) *m/z* = 798 [M^+], 677 [M^+ - O_2CPh]. IR (KBr) υ_{C-H} = 2905, $\upsilon_{C\equiv C}$ = 2128, $\upsilon_{ester(C=O)}$ = 1717, υ_{Ar} = 1594 cm^{-1}.

3.4.12 Preparation of bis(trimethylphosphine)-η^2-acetylacetonato-rhodium$^{(I)}$ (14)

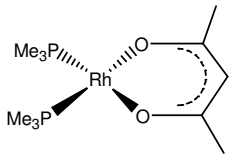

Acetylacetone (0.0095 g, 0.095 mmol) in THF (1 mL) was added to a stirred solution of [RhMe(PMe_3)$_4$] (0.0401 g, 0.095 mmol) in THF (1 mL), and the resulting solution was stirred at room temperature for 5 min, after which the solvent was removed *in vacuo*. THF (2 mL) was added, the solution was stirred for 2 min and the solvent was removed *in vacuo* again. This cycle was repeated one more time, and then THF (2 mL) was added. The reaction was stirred at room temperature for 1 h, after which the solvent was removed *in vacuo* to give **14** as a yellow solid. The product was recrystallised in a Young's tube via slow diffusion of a layer of hexane into a concentrated THF solution of **14**. Yield: 0.029 g, 86%. ^{1}H NMR (400 MHz, C_6D_6) δ: 5.36 (s, 1H, acac-CH), 1.83 (s, 6H, acac-CH_3), 1.13 (s, 18H, 2 x PMe_3). ^{31}P{^{1}H} NMR (202 MHz, 203 K, 10% C_6D_6 in THF) δ: 5.78 (d, $J_{Rh\text{-}P}$ = 185 Hz, 2P). Anal. Calcd. for $C_{11}H_{25}P_2O_2Rh$: C, 37.30; H, 7.11. Found: C, 37.10; H, 7.38%. MS (ES$^+$) m/z = 354 [M$^+$].

3.4.13 Preparation of acetylacetonato-rhodacyclopentadienes

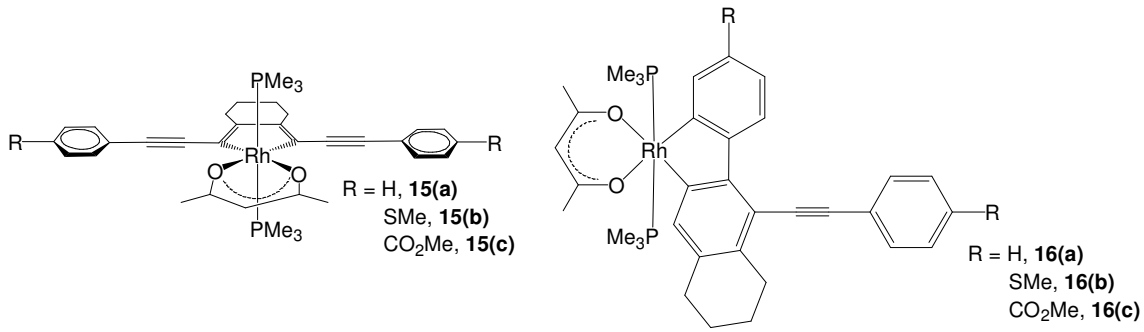

15(a) - *trans*-[bis(trimethylphosphine)-η^2-acetylacetonato-2,5-bis(phenylethynyl)-3,4-μ-tetramethylenerhodacyclopenta-2,4-diene]

In a N_2 filled glove box, 1,12-diphenyldodeca-1,3,9,11-tetrayne (0.0291 g, 0.095 mmol) in THF was added to a stirred THF solution of **14** (0.0337 g, 0.095 mmol), which was obtained via *in situ* reaction of acetylacetone (0.0095 g, 0.095 mmol) and [RhMe(PMe_3)$_4$] (0.0401 g, 0.095 mmol). The resulting solution was transferred into a Young's tube, which was then sealed and removed from the glovebox. The reaction was heated for 16 d at 50 °C to give a mixture of **15(a)** and its isomeric biphenyl-rhodacyclopentadiene **16(a)**. Compound **15(a)** was isolated by washing the mixture with hexane (5 x 1 mL) as **16(a)** was soluble in hexane. The remaining **15(a)** was isolated as a yellow-orange solid. Yield: 0.034 g, 54%. ^{1}H NMR (400 MHz, C_6D_6) δ: 7.74 (d, J = 8 Hz, 4H, CH_{arom}), 7.13 (t, J = 8 Hz, 4H, CH_{arom}), 6.99 (t, J = 8 Hz, 2H, CH_{arom}), 5.15 (s, 1H, acac-CH), 2.96 (m, 4H, C=C-CH_2), 1.95 (s, 6H, acac-CH_3), 1.68 (m, 4H, CH_2), 0.94 (vt, J_{P-H} = 4 Hz, 18H, 2 x PMe_3). ^{31}P{^{1}H} NMR (162 MHz, C_6D_6) δ: -0.46 (d, J_{Rh-P} = 114 Hz, 2P). Anal. Calcd. for $C_{35}H_{43}O_2P_2Rh$: C, 63.64; H, 6.56. Found: C, 63.80; H, 6.46%. MS (ES^+) m/z = 660 [M^+], 561 [M^+ - acac]. IR (KBr) υ_{C-H} = 2908, $\upsilon_{C\equiv C}$ = 2139, υ_{Ar} = 1588, 1426 cm^{-1}.

16(a): ^{31}P{^{1}H} NMR (81 MHz, C_6D_6) δ: -1.18 (d, J_{Rh-P} = 115 Hz, 2P).

15(b) - *trans*-[bis(trimethylphosphine)-η^2-acetylacetonato-2,5-bis(*p*-methylthiophenyl ethynyl)-3,4-μ-tetramethylenerhodacyclopenta-2,4-diene]

In a N_2 filled glove box, 1,12-bis(methylthiophenyl)dodeca-1,3,9,11-tetrayne (0.0379 g, 0.095 mmol) in THF was added to a stirred THF solution of **14** (0.0337 g, 0.095 mmol), which was obtained via *in situ* reaction of acetylacetone (0.0095 g, 0.095 mmol) and [$RhMe(PMe_3)_4$] (0.0401 g, 0.095 mmol). The resulting solution was transferred into a Young's tube, which was then sealed and removed from the glovebox. The reaction was heated for 7 d at 50 °C to give a mixture of **15(b)** and its isomeric biphenyl-rhodacyclopentadiene **16(b)**. Compound **15(b)** was isolated by washing the mixture with hexane (5 x 1 mL) as **16(b)** is soluble in hexane. Compound **15(b)** was recrystallised from THF and hexane and isolated as an orange solid. Yield: 0.024 g, 34%. ^{1}H NMR (400 MHz, C_6D_6) δ: 7.62 (d, J = 8 Hz, 4H, CH_{arom}), 7.08 (d, J = 8 Hz, 4H, CH_{arom}), 5.17 (s, 1H, acac-CH), 2.96 (m, 4H, C=C-CH_2), 1.97 (s, 6H, acac-CH_3), 1.93 (s, 6H, 2 x SCH_3), 1.69 (m, 4H, CH_2), 0.96 (vt, J_{P-H} = 4 Hz, 18H, 2 x PMe_3). $^{31}P\{^1H\}$ NMR (162 MHz, C_6D_6) δ: -0.41 (d, J_{Rh-P} = 114 Hz, 2P). Anal. Calcd. for $C_{37}H_{47}O_2P_2RhS_2$: C, 59.04; H, 6.29. Found: C, 59.60; H, 6.08%. MS (ES^+) *m/z* = 752 [M^+], 676 [M^+ - PMe_3], 653 [M^+ - acac]. IR (KBr) υ_{C-H} = 2910, $\upsilon_{C\equiv C}$ = 2137, υ_{Ar} = 1585, 1427 cm^{-1}.

16(b): $^{31}P\{^1H\}$ NMR (162 MHz, C_6D_6) δ: -1.15 (d, J_{Rh-P} = 115 Hz, 2P).

15(c) - *trans*-[bis(trimethylphosphine)-η^2-acetylacetonato-2,5-bis(*p*-carbomethoxyphenyl ethynyl)-3,4-μ-tetramethylenerhodacyclopenta-2,4-diene]

In a N_2 filled glove box, 1,12-bis(carbomethoxyphenyl)dodeca-1,3,9,11-tetrayne (0.0401 g, 0.095 mmol) in THF was added to a stirred THF solution of **14** (0.0337 g,

0.095 mmol), which was obtained via *in situ* reaction of acetylacetone (0.0095 g, 0.095 mmol) and [RhMe(PMe_3)$_4$] (0.0401 g, 0.095 mmol). The resulting solution was transferred into a Young's tube, which was then sealed and removed from the glovebox. The reaction was heated for 3 d at 50 °C to give a mixture of **15(c)** and its isomeric biphenyl-rhodacyclopentadiene **16(c)**. Compound **15(c)** was isolated by washing the mixture with hexane (5 x 1 mL) as **16(c)** is soluble in hexane. Compound **15(c)** was recrystallised from THF and hexane to give a dark-red solid. Yield: 0.015 g, 20%. ^{1}H NMR (700 MHz, C_6D_6) δ: 8.13 (d, J = 8 Hz, 4H, CH_{arom}), 7.68 (d, J = 8 Hz, 4H, CH_{arom}), 5.13 (s, 1H, acac-CH), 3.47 (s, 6H, 2 x CO_2CH_3), 2.91 (m, 4H, C=C-CH_2), 1.91 (s, 6H, acac-CH_3), 1.66 (m, 4H, CH_2), 0.88 (vt, J_{P-H} = 4 Hz, 18H, 2 x PMe_3). ^{31}P{^{1}H} NMR (162 MHz, C_6D_6) δ: -0.56 (d, J_{Rh-P} = 113 Hz, 2P). Anal. Calcd. for $C_{39}H_{47}O_6P_2Rh$: C, 60.31; H, 6.10. Found: C, 60.15; H, 6.10%. MS (ES^+) *m/z* = 776 [M^+], 700 [M^+ - PMe_3], 677 [M^+ - acac]. IR (KBr) υ_{C-H} = 2908, $\upsilon_{C\equiv C}$ = 2132, $\upsilon_{ester(C=O)}$ = 1718, υ_{Ar} = 1594, 1433 cm^{-1}.

16(c)

Compound **16(c)** was separated from **15(c)** by washing the mixture with hexane as noted above. The hexane filtrate was kept in a vial, and light-red crystals of **16(c)** were formed overnight via slow evaporation. Yield: 0.006 g, 8%. ^{1}H NMR (400 MHz, C_6D_6) δ: 9.53 (d, J = 8 Hz, 1H, CH_{arom}), 9.11 (br, s, 1H, CH_{arom}), 8.37 (br, d, J = 8 Hz, 1H, CH_{arom}), 8.05 (br, s, 1H, CH_{arom}), 8.04 (d, J = 8 Hz, 2H, CH_{arom}), 7.56 (d, J = 8 Hz, 2H, CH_{arom}), 5.12 (s, 1H, acac-CH), 3.62 (s, 3H, CO_2CH_3), 3.47 (s, 3H, CO_2CH_3), 3.24 (t, J = 8 Hz, 2H, C=C-CH_2), 2.91 (t, J = 8 Hz, 2H, C=C-CH_2), 1.88 (s, 6H, acac-CH_3), 1.79 (quint, J = 8 Hz, 2H, CH_2), 1.69 (quint, J = 8 Hz, 2H, CH_2), 0.56 (vt, J_{P-H} = 3 Hz, 18H, 2

x PMe_3). $^{31}P\{^1H\}$ NMR (162 MHz, C_6D_6) δ: -1.16 (d, J_{Rh-P} = 113 Hz, 2P). MS (ES^+) *m/z* = 776 [M^+]. IR (KBr) υ_{C-H} = 2908, $\upsilon_{C\equiv C}$ = 2132, $\upsilon_{ester(C=O)}$ = 1722, υ_{Ar} = 1586, 1433 cm^{-1}.

References

1. K. K.-W. Lo, W.-K. Hui, C.-K. Chung, K. H.-K. Tsang, D. C.-M. Ng, N. Zhu and K.-K. Cheung, *Coord. Chem. Rev.*, 2005, **249**, 1434.
2. T. Le Bouder, L. Viau, J.-P. Guégan, O. Maury and H. Le Bozec, *Eur. J. Org. Chem.*, 2002, 3024.
3. T. Le Bouder, O. Maury, A. Bondon, K. Costuas, E. Amouyal, I. Ledoux, J. Zyss and H. Le Bozec, *J. Am. Chem. Soc.*, 2003, **125**, 12284.
4. H. Le Bozec, T. Le Bouder, O. Maury, A. Bondon, I. Ledoux, S. Deveau and J. Zyss, *Adv. Mater.*, 2001, **13**, 1677.
5. G. S. He, L.-S. Tan, Q. Zheng and P. N. Prasad, *Chem. Rev.*, 2008, **108**, 1245.
6. M. A. Baldo, M. E. Thompson and S. R. Forest, *Nature*, 2000, **403**, 750.
7. J. P. Rourke, A. S. Batsanov, J. A. K. Howard and T. B. Marder, *Chem. Commun.*, 2001, 2626.
8. R. M. Ward, *Diethynylrhodacyclopentadienes: A New Class of Luminescent Organometallics*, Ph.D. Thesis, Durham University, 2007.
9. W. Lu, N. Zhu and C.-M. Che, *J. Organomet. Chem.*, 2003, **670**, 11.
10. Z. A. Siddique, T. Ohno, K. Nozaki and T. Tsubomura, *Inorg. Chem.*, 2004, **43**, 663.
11. Y. Matano, M. Nakashima and H. Imahori, *Angew. Chem. Int. Ed.*, 2009, **48**, 4002.
12. A. J. Boydston, Y. Yin and B. L. Pagenkopf, *J. Am. Chem. Soc.*, 2004, **126**, 3724.
13. J. S. Siddle, R. M. Ward, J. C. Collings, S. R. Rutter, L. Porrès, L. Applegarth, A. Beeby, A. S. Batsanov, A. L. Thompson, J. A. K. Howard, A. Boucekkine, K. Costuas, J.-F. Halet and T. B. Marder, *New J. Chem.*, 2007, **31**, 841.
14. B. R. Galan and T. Rovis, *Angew. Chem. Int. Ed.*, 2009, **48**, 2830.
15. L. Orian, J. N. P. van Stralen and F. M. Bickelhaupt, *Organometallics*, 2007, **26**, 3816.
16. A. Dachs, A. Torrent, A. Pla-Quintana, A. Roglans and A. Jutand, *Organometallics*, 2009, **28**, 6036.
17. T.-i. Shimura, A. Ohkubo, K. Aramaki, H. Uekusa, T. Fujita, S. Ohba and H. Nishihara, *Inorg. Chim. Acta*, 1995, **230**, 215.
18. A. F. Hill, A. D. Rae, M. Schultz and A. C. Willis, *Organometallics*, 2007, **26**, 1325.
19. R. T. Price, R. A. Andersen and E. L. Muetterties, *J. Organomet. Chem.*, 1989, **376**, 407.
20. M. van Leeuwen, *The Synthesis and Properties of Rhodacyclopentadienes*, M. Chem. Fourth-year Project Report, Durham University, 2006.

21. D. Zargarian, P. Chow, N. J. Taylor and T. B. Marder, *J. Chem. Soc., Chem. Commun.*, 1989, 540.
22. P. Chow, D. Zargarian, N. J. Taylor and T. B. Marder, *J. Chem. Soc., Chem. Commun.*, 1989, 1545.
23. J. P. Rourke, G. Stringer, P. Chow, R. J. Deeth, D. S. Yufit, J. A. K. Howard and T. B. Marder, *Organometallics*, 2001, **21**, 429.
24. H. Yersin, W. Humbs and J. Strasser, *Coord. Chem. Rev.*, 1997, **159**, 325.
25. M. A. Bergkamp, R. J. Watts and P. C. Ford, *Inorg. Chem.*, 1981, **20**, 1764.
26. M. G. Colombo, T. C. Brunold, T. Riedener, H. U. Güdel, M. Förtsch and H.-B. Bürgi, *Inorg. Chem.*, 1994, **33**, 545.
27. W. Humbs and H. Yersin, *Inorg. Chem.*, 1996, **35**, 2220.
28. J. S. Wilson, N. Chawdhury, M. R. A. Al-Mandhary, M. Younus, M. S. Khan, P. R. Raithby, A. Köhler and R. H. Friend, *J. Am. Chem. Soc.*, 2001, **123**, 9412.
29. S. Nonell and S. L. Braslavsky, *Time resolved singlet oxygen detection* in *Singlet Oxygen, UV-A and Ozone, Methods in Enzymology*, eds. L. Packer and H. Sies, Academic Press, 2000, vol. 319.
30. H. Werner, M. Schäfer, O. Nürnberg and J. Wolf, *Chem. Ber.*, 1994, **127**, 27.
31. T. Matsumoto and H. Yoshida, *Inorg. Chem. Commun.*, 2001, **4**, 36.
32. P. M. Boyer, C. P. Roy, J. M. Bielski and J. S. Merola, *Inorg. Chim. Acta*, 1996, **245**, 7.
33. D. J. Darensbourg, G. Groetsch, P. Wiegreffe and A. L. Rheingold, *Inorg. Chem.*, 1987, **26**, 3827.
34. M. Karplus, *J. Chem. Phys.*, 1959, **30**, 11.
35. M. Karplus, *J. Am. Chem. Soc.*, 1963, **85**, 2870.
36. A. Steffen, M. G. Tay, A. S. Batsanov, J. A. K. Howard, A. Beeby, K. Q. Vuong, X.-Z. Sun, M. W. George and T. B. Marder, *Angew. Chem. Int. Ed.*, 2010, **49**, 2349.
37. S. Lamansky, P. Djurovich, D. Murphy, F. Abdel-Razzaq, H.-E. Lee, C. Adachi, P. E. Burrows, S. R. Forrest and M. E. Thompson, *J. Am. Chem. Soc.*, 2001, **123**, 4304.
38. Y. Ohsawa, S. Sprouse, K. A. King, M. K. DeArmond, K. W. Hanck and R. J. Watts, *J. Phys. Chem.*, 1987, **91**, 1047.
39. K. K.-W. Lo, C.-K. Li, K.-W. Lau and N. Zhu, *Dalton Trans.*, 2003, 4682.
40. R. C. Evans, P. Douglas and C. J. Winscom, *Coord. Chem. Rev.*, 2006, **250**, 2093.
41. W. L. Su, Y. C. Yu, M. C. Tseng, S. P. Wang and W. L. Huang, *Dalton Trans.*, 2007, 3440.
42. L. Porrès, A. Holland, L.-O. Pålsson, A. P. Monkman, C. Kemp and A. Beeby, *J. Fluorescence*, 2006, **16**, 267.
43. D. V. O. Connor and D. Phillips, *Time Correlated Single Photon Counting*, Academic Press, London, 1984.
44. D. V. O. Connor, W. R. Ware and J. C. Andre, *J. Phys. Chem.*, 1979, **83**, 1333.
45. G. Giordano and R. H. Crabtree, *Inorg. Synth.*, 1990, **28**, 88.

Chapter 4

Suggestions for future work

This project has investigated the effect of different ligands (e.g. DHAPEPE-, TMSE-, η_2-benzoato- and acac-) on the photophysical properties of rhodacyclopentadienes. The TMSE-rhodacyclopentadienes [especially **7(a)**] have been investigated further and found that no phosphorescence was observed either at room temperature or 77 K despite the fact that Rh is covalently bound to the organic chromophore. Moreover, some rhodacyclopentadienes, particularly TMSE-rhodacyclopentadienes, exhibit unexpectedly long-lived singlet excited states, fluorescent rates competitive with intersystem crossing rates ($k_f \approx k_\Delta \approx 10^8$ s^{-1}) and high Φ_f values. On the other hand, the photophysical results for the biphenyl-based rhodacyclopentadiene [**16(c)**, a by-product from the acac-rhodacyclopentadiene synthesis] indicate that the spin-orbit coupling (SOC) effect from the Rh is strong enough to facilitate effective intersystem crossing (ISC) of the singlet excited states to triplet excited states and emit phosphorescence at room temperature. Over the past 50 years, many people have thought that the presence of heavy atoms such as transition metals in the molecule is the main factor to facilitate an effective ISC. However, the photophysical properties of the rhodacyclopentadienes presented in this thesis confirm that the presence of heavy atom is not only the factor required for effective ISC. Indeed, it also depends on how effective the SOC from the heavy atom is in the excited states. Therefore, it will be very interesting to investigate the effectiveness of SOC from heavy atoms in the future, which can be done in two ways:

(i) to study the photophysical properties of other metallacyclopentadienes such as iridacyclopentadienes and platinacyclopentadienes, which are structurally related to the rhodacyclopentadienes;

(ii) to attach two phenyl rings to the cyclohexyl loop of the rhodacycle ring (**Figure 4.1**).

Iridacyclopentadienes are suggested because Ir is in the same group with Rh, but Ir has a three times stronger SOC effect than Rh. Therefore, iridacyclopentadienes are expected to be phosphorescent, and no fluorescence is expected to be observed. For the same reasons, platinacyclopentadienes are also interesting because Pt has much stronger SOC effect than Ir and Rh. (SOC constants: Rh = 1259 cm^{-1}, Ir = 3909 cm^{-1}, Pt = 4481 cm^{-1}).[1]

The proposed molecular structure with two phenyl rings attached to the cyclohexyl loop is shown in **Figure 4.1**. The reason for attaching them is to change the electronic property at the rhodacycle core, which might lead to a increasing of electron delocalisation at the rhodacycle core. Moreover, the presence of the two phenyl rings also increases the rigidity of the rhodacycle; hence the quantum yield values are expected to be increased as well.

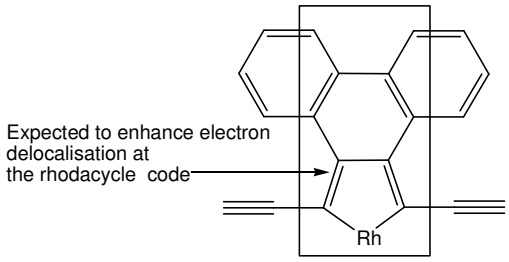

Figure 4.1: Proposed molecular structure of rhodacycle ring with two phenyl rings attached to the cyclohexyl loop.

In addition, we have also demonstrated the deprotection of the C≡C-$SiMe_3$ groups to produce C≡C-H groups in the TMSE-rhodacyclopentadiene as shown in **Figure 3.27**. Interestingly, the TMSE- ligand attached to the Rh centre was not affected by the deprotection conditions. Therefore, the two C≡C-H groups at the terminals can be reacted

with other transition metals such as $Au^{(I)}$, and the changes in the photophysical properties can be investigated. The reason for introducing another metal, such as Au, is to investigate the intra-molecular charge-transfer between Rh and it. In addition, the Au may also increase the SOC effect in the rhodacyclopentadienes, and subsequently may increase the ISC rate.

References:

1. M. Montalti, A. Credi, L. Prodi and M. T. Gandolfi, *Handbook of Photochemistry*, 3rd edn., CRC Taylor & Francis, Boca Raton, 2006.